THE UNIVERSITY OF
WARWICK

University of Warwick institutional repository: http://go.warwick.ac.uk/wrap

A Thesis Submitted for the Degree of PhD at the University of Warwick

http://go.warwick.ac.uk/wrap/71386

This thesis is made available online and is protected by original copyright.

Please scroll down to view the document itself.

Please refer to the repository record for this item for information to help you to cite it. Our policy information is available from the repository home page.

Correlation of N.M.R. and magnetic susceptibility properties in some metallic systems

by

Christopher J. Ford, B.Sc.

A thesis submitted for the degree of
Doctor of Philosophy of the
University of Warwick.

School of Physics,
University of Warwick.

September, 1972.

Memorandum

This dissertation is submitted to the University of Warwick in support of my application for admission to the degree of Doctor of Philosophy. It contains an account of my work carried out at the School of Physics of Warwick University in the period October 1969 to September 1972 under the supervision of Professor E. F. W. Seymour. No part of it has been used previously in a degree thesis submitted to this or any other University. The work described is the result of my own independent research except where specifically acknowledged. The results in the vanadium dioxide system have been published in Phys. kondens. Materie, 14, 111-18, 1972, and those on the dilute lead alloys in J. Phys. F: Metal Physics, 2, 373-85, 1972. It is anticipated that results in the local magnetic moment systems, the tin-cadmium alloys, and the pure metals, will all be published shortly.

C. J. Ford

C. J. Ford

September, 1972.

To my mother and father for their understanding

and encouragement.

Acknowledgements

I would like to thank the following people for the reasons that are mentioned, but also for their friendship and good company. I wish to express my gratitude to my supervisor, Professor E. F. W. Seymour, for his patient guidance and encouragement over the past three years. It is also a pleasure to thank Dr. Dave Brown for many helpful discussions and for aid with the relaxation measurements,and Mr. Barrie Sheffield whose technical assistance proved invaluable. I am grateful to Dr. Graham Styles and Dr. Ian Host, particularly for the use of their computer programs. I appreciate also the brave attempts of Dr. Ray Dupree and Mr. Paul Camwell to explain local moments to me.

Finally, my thanks are due to Professor A. J. Forty for allowing me to use the facilities of the School of Physics, and to the Science Research Council for a maintenance grant.

Abstract

In this investigation, an attempt is made to correlate magnetic susceptibility and nuclear magnetic resonance properties in a wide variety of metallic systems. Such an approach is adopted in order to obtain greater insight into the atomic and electronic structure of these systems. The magnetic susceptibility of several pure metals in the solid and liquid phases is presented and it is shown that in the liquid at least these can be understood in terms of free interacting conduction electrons. Thus, in these metals the spin contribution to the susceptibility (related to the Knight shift) can be confidently estimated. The measured values of the Knight shifts in these pure liquid metals are then compared with those calculated from the susceptibility and the conduction electron wavefunction density at the nucleus, found using a pseudopotential method. It is seen that the temperature variations of the shifts are better explained than their absolute values. In view of the greater success of the prediction of fractional changes the approach is extended to the concentration dependence of the shift upon alloying. Experimental results are presented for the ^{113}Cd and ^{119}Sn resonance shifts and the magnetic susceptibility in tin-cadmium alloys (a system chosen for its simplicity). These shifts are compared with values calculated using either the pseudopotential method or the more limited partial wave analysis. Good agreement is found and the method of correlation is extended to less simple systems. It is used with success to separate spin and orbital contributions to the shift and susceptibility in the transition metal oxide, VO_2, but is of more limited use in heavy metal alloys and in those suspected of liquid atomic ordering or of localised magnetic moment formation.

Contents

Chapter 1

Introduction

The underlying thread of this work is the mutual comparison of the nuclear magnetic resonance (NMR) and magnetic susceptibility properties of metallic systems. It was expected that the study of both together might yield considerable insight into the electronic structure of such systems. This should certainly be true in the simpler liquid phase, where the predictions of the free electron theory may be tested. According to this theory, the conduction electrons form a dense gas. Their wavefunctions are simply described by plane waves, and the Fermi surface is both sharp and spherical in k-space (where k is the wavevector).

However, before discussing predictions of theory and the observations of experiment in detail, it is necessary to expand upon the concepts of magnetic susceptibility and nuclear magnetic resonance, and the various experimentally observable quantities. Particular emphasis must be placed on their behaviour in metals, for although the systems investigated are widely different, all of them are metallic. The information available from combining NMR and susceptibility data in any given system will then be considered. Such discussions have proved valuable for some transition metals (1); the object of the present investigation is to evaluate the method more widely, particularly for non-transition metal systems.

1·1 Magnetic susceptibility

1·1·1 Introduction

The magnetic susceptibility characterises the response of a system to an applied field. A negative susceptibility describes a diamagnetic response, a (small) positive susceptibility, paramagnetism. In a metal there will, in general, be several different contributions

to the susceptibility, some paramagnetic and others diamagnetic. It is possible to consider the total susceptibility as

$$\chi = \chi_i + \chi_e + \chi_n \qquad \text{(in volume units)} \qquad (1\cdot1)$$

where χ_i is the susceptibility of the ion cores, χ_e the conduction electron component and χ_n that due to the nuclei. χ_n is sufficiently small, except under resonant conditions (section 1·2) to be neglected. This simple division into ion core and electronic components becomes more complicated in the presence of s-d hybridisation, when mixing takes place between closely spaced conduction and valence bands. This particular problem will be discussed in section 3·3, for the noble metals, for which it appears to be important. Returning to equation 1·1, the two remaining contributions will be considered in turn.

1·1·2 χ_i

This term is usually a diamagnetic contribution (see, however, section 1·1·4). In the absence of an applied field the orbital angular momentum of a core electron is quenched. The electron orbit could be considered as the path of the cord in a ball of string. Application of a field causes one sense of rotation to be more favoured. The wavefunctions of the electronic state will adjust so that the orbital has a slight circulation in the favourable sense. In accordance with Lenz's law, this has the effect of introducing a diamagnetic field, opposing the applied field.

Angus (2), amongst others, has calculated this contribution for the free ions of the elements, utilising a slightly modified form of Slater's rules (3) for calculating the screening constants for the various core electronic shells. In a few cases, there may be another contribution to the susceptibility, the Van Vleck term, arising from the distortion of the wavefunctions produced by the magnetic field when there exists a degree of covalency. Such a term will be considered in chapter 6.

Despite the fact that improved Hartree-Fock wavefunctions have become available for most ions, the values due to Angus were found, by Dupree and Seymour (4) to give the most acceptable set of χ_es for all the metals for which susceptibility measurements were available in the liquid.

Following this review (4) of the magnetic properties of liquid metals, the values calculated by Angus will be adopted throughout for the ionic contributions in the elements. The values in the alloys will be calculated from the weighted values of the pure metals, according to concentration. The validity of this approach will be discussed in the first alloy chapter.

1·1·3 χ_e

This contribution to the susceptibility may be further expressed as a sum of calculated terms, to be compared with the experimentally derived $\chi - \chi_i$,

$$\chi_e = \chi_p + \chi_d + \chi_o \qquad (1·2)$$

where χ_p is the Pauli spin term, χ_d the Landau diamagnetic part, and χ_o an orbital contribution. The Pauli term arises from the net magnetic moment caused by the differing shifts in the energy distribution of states for electron spins parallel to and antiparallel to the applied field. For free, non-interacting electrons,

$$\chi_{po} = 4\pi\mu_B^{\,2} D(E_f) \qquad (1·3)$$

where μ_B is the Bohr magneton and $D(E_f)$ the density of states at the Fermi level (for both directions of spin together); χ_{po} is normalised to unit volume. However, in a real metal this contribution is modified by three factors: these are the electron-ion, electron-electron and electron-phonon interactions. The last of these has been shown to be negligible by Herring (5). The simplest way of accounting for the electron-ion term (initially assumed zero, then obtained by fitting χ_e with $\chi - \chi_i$) is by use of the effective mass approximation, thus:

$$\chi_{p1} = \chi_{po}\,(m^*/m) \quad . \qquad (1\cdot4)$$

Independently of this, the electron-electron enhancement has been calculated for a free electron gas by a number of authors (Rice (6), Dupree and Geldart (7), amongst others). Dupree and Geldart, whose results appear to give the best agreement with experiment, calculated the enhancement by expanding $\chi_p(k)$ in terms of the screened interaction, making a term by term investigation of the resulting expansion. They obtain an enhancement factor in terms of an electron-electron separation parameter, r_s (defined in equation 1·7). See figure 1·1. Their values of the enhanced Pauli susceptibility, χ_{p2}, are used throughout the present work.

The contribution χ_d, the Landau term, arises from the orbital moment induced in the free electron gas by the applied field. The term, unmodified by electron-ion and electron-electron effects is

$$\chi_{do} = -\tfrac{1}{3}\chi_{po} \qquad (1\cdot5)$$

at all temperatures. The electron-ion effect is obtained in a similar manner to that above, but here,

$$\chi_{d1} = \chi_{do}\,(m/m^*) \quad . \qquad (1\cdot6)$$

Kanazawa and Matsudawa (8) have calculated the effect of the electron-electron enhancement as

$$\chi_{d2}/\chi_{do} = 1 + (8r_s/6\pi)(\ln r_s + 4 + \ln(\S/2\pi)) \qquad (1\cdot7)$$

where $(4/3)\pi r_s^3 = V/N$, $\S^3 = 4/9\pi$, V is the volume, and N is Avogadro's number. This was obtained through the effect of the interactions on the form of the energy-wavenumber relation. Typically, χ_d is increased by 15-20% for most metals. For χ_p and χ_d, the two effects (electron-ion and electron-electron) are for reasons of practicability calculated independently, though it is assumed that the two corrections may be applied together.

The final contribution to the electronic susceptibility is the

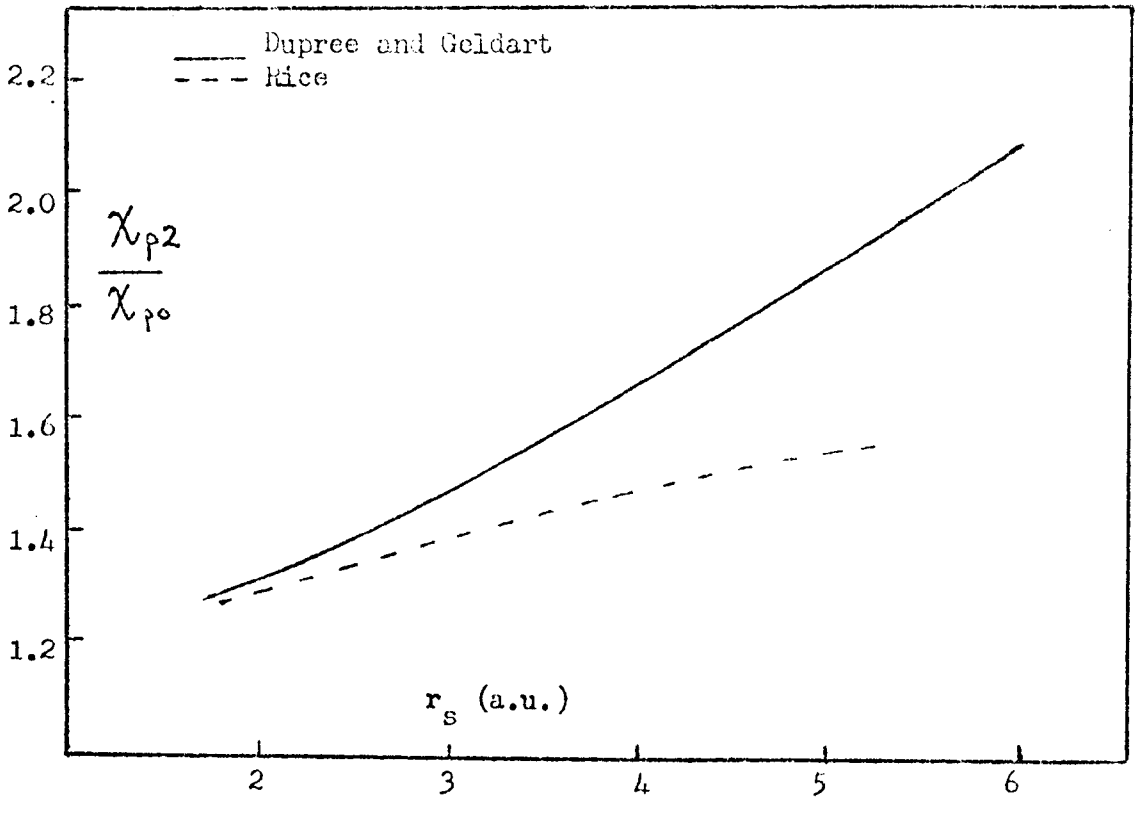

Figure 1.1 Spin susceptibility enhancement factor, (electron-electron effects only).

orbital component, χ_o. In metals, this Kubo-Obata (9) term is the analogue for itinerant electrons of the Van Vleck paramagnetism for bound electrons. It arises from the admixture of higher energy unoccupied levels into the occupied levels, unquenching part of the orbital moment upon application of a magnetic field. This term is zero for free electrons, except in the case of some transition metals and their oxides, where the presence of degenerate unfilled d sub-bands can give rise to an appreciable χ_o. It will be more fully discussed in chapter 6.

1·1·4 Localised moments

The introduction of transition metal impurities into simple metals sometimes results in the formation of localised magnetic moments on the impurity ions. The behaviour of the net susceptibility (χ minus the host metal susceptibility) due to these moments can sometimes be described by a Curie-Weiss law, above the neighbourhood of a critical temperature Θ, where

$$\Delta\chi = \chi_{net} = \frac{C}{T + \Theta}$$, where C is a constant.

However, the behaviour in real systems is often more complicated than simple theory would suggest, and the temperature dependence of $\Delta\chi$ may not be as simply described as this law suggests. In view of the fact that this particular problem will only be investigated in some gallium alloys, a fuller discussion is postponed until chapter 8, where susceptibility results will be considered, along with the behaviour of the host NMR.

1·2 NMR

1·2·1 Introduction

The basic theory of NMR has been adequately described elsewhere (see, for instance, (10) and (11)), and will only be discussed briefly here. A nucleus of spin I and magnetic moment μ interacts with a static

magnetic field, B_o, applied in the z direction. The interaction energy is

$$-\mu.B_o = -\gamma_n h B_o I_z \qquad (1\cdot8)$$

where γ_n is the nuclear gyromagnetic ratio, $2\pi h$ is Planck's constant. Now there will be (2I+1) Zeeman levels, and clearly transitions can occur between these levels, which are spaced $\gamma_n h B_o$ apart. Radiation of angular frequency ω_o must be applied, where

$$\hbar\omega_o = \gamma_n h B_o$$

$$\text{or} \qquad \omega_o = \gamma_n B_o . \qquad (1\cdot9)$$

This is the resonance condition. Net absorption of energy takes place, despite the equality of upward and downward transition probabilities, since the Boltzmann factor ensures that the lower energy level will be more heavily populated. Consequently, there will be a net amount of energy absorbed from the radiofrequency transmission. This process would halt upon equalisation of populations if it were not for the spin-lattice relaxation. The spins in the higher levels release this potential energy to some other system (usually the lattice), repopulating the lower levels. This often exponential process is charecterised by the so-called spin-lattice relaxation time, T_1. The transition is accomplished by local magnetic fields having a component fluctuating at the resonance frequency (and in certain circumstances, twice that frequency). The most important source for metals is usually the contact interaction with the conduction electrons; that is, a mutual spin flipping process occurs between the nucleus and Fermi surface conduction electrons (those for which changes of spin state are possible).

Relaxation also takes place due to the interactions between the nuclear spins themselves. The coherence of the precession of the spins about B_o is destroyed in a time charecterised by the spin-spin relaxation time, T_2. The cause may be the local field due to the neighbouring nuclear spins, giving a spread in ω_o and consequently broadening the NMR line.

Further, a spin flipping process which limits the lifetime of the states and consequently broadens the energy level through the Uncertainty Principle, may occur between identical nuclei. In the presence of thermal motion, the 'random walk' process effectively reduces the value of the local field and the line narrows. For very rapid motion, in liquids for example, the dephasing becomes so slow that the relaxation rate is governed by the lifetime-limiting processes, and T_2 becomes equal to T_1. Under these conditions, the linewidth is given by

$$\Delta\omega = \frac{2}{\sqrt{3}\, T_2} \text{ , for a Lorentzian line.}$$

In metals there will be other contributions to the linewidth, and these will be discussed briefly. The nuclear dipole-dipole interaction, causing varying local fields, gives a contribution which averages to zero for liquids. Indirect interactions of the nuclear magnetic moments with each other via the conduction electrons give rise to further contributions. A pseudo-dipolar term arises because of the existence of a non-s part of the conduction electron wavefunction. A pseudo-exchange term arises through the contact part of the hyperfine interaction. Both of these terms are fully discussed by (11) and are both zero in liquid metals.

For metals with $I > \frac{1}{2}$, a quadrupole moment exists. A quadrupole moment is a measure of the departure of the nuclear charge distribution from spherical symmetry. The moment can give rise to a splitting of the resonance line. When the effects of the quadrupolar interaction as a perturbation are taken to second order, the central component is shifted by an amount proportional to the applied field, and dependent on crystal orientation. In a polycrystalline specimen this gives rise to a broadening. In liquids, the splittings are averaged to zero, but the fluctuating local electric fields can give rise to spin-lattice relaxation. The

contribution which is dominant in liquid metals is that arising from lifetime broadening through the Uncertainty Principle. Here, $T_1=T_2$, and the shorter is the relaxation time, the wider is the line.

1·2·2 The Knight shift and Korringa relation

The resonance of the species in metals is shifted relative to the resonance in a salt. This is usually predominantly due to the contact interaction of the nucleus with the conduction electrons. These are polarised by the applied field which, as explained in the last section, causes a net paramagnetic spin moment interacting with the nuclei to produce a static non-zero average local field at the nuclear site. This contribution to the Knight shift is given, in SI units, by

$$K_s = \frac{\Delta B_o}{B_o} = \frac{2}{3}\chi_p \langle |\psi_k(0)|^2 \rangle_f = \frac{2}{3}\chi_p \Omega P_f \qquad (1\cdot10)$$

where B_o is the applied field for resonance in the metal at a given frequency and ΔB_o is the amount by which the field for resonance in the salt at the same frequency exceeds that in the metal; P_f is the probability density at the nucleus, averaged over the Fermi surface electrons, and Ω is the atomic volume. ($\psi_k(0)$ is the conduction electron wavefunction, at the nucleus.) There are other contributions to the Knight shift which are occasionally more important (chapter 6). Nuclei at non-cubic sites have an anisotropic component to the shift, which gives rise to line broadening for powders. This disappears for liquids, which are isotropic. Two further contributions to K (important in some cases) will now be considered.

K_{cp}: This is the core polarisation contribution. It is an indirect contribution to the contact term (whereas K_s is the direct term). Consider the following: d electrons perturb the core wavefunctions differently, depending on whether the spins are parallel to or antiparallel

to the core spins. The electron density at the nucleus is then not the same for any two paired s electrons, leading to a non-cancellation of the contact interactions. This can result in positive or negative contributions to the total shift.

$\underline{K}_o$: This is an orbital component arising from the orbital moment of the conduction electrons, in an analogous way to the term arising from the spin moment. It is consequently important only in some transition metals and their oxides, where an orbital component of the susceptibility exists.

The orbital and core polarisation contributions are difficult to separate normally. However, a method which may be used with success to separate and distinguish them will be discussed in section 1·3·1. Now, the relaxation rate discussed above, arising from mutual spin flipping of the nucleus and conduction electron may be described by

$$1/T_1 = (64/9)\pi^3\hbar^3 \gamma_e^2 \gamma_n^2 \left[\langle|\psi_k(0)|^2\rangle_f \; D(E_f)\right]^2 kT \qquad (1\cdot11)$$

where γ_e is the electron gyromagnetic ratio, and k is Boltzmann's constant. A full derivation is given in (11). With equation 1·10, this yields

$$T_1 T K_s^2 = (1/16)\left[\chi_p/D(E_f)\right]^2 (1/\pi^3 k \gamma_n^2 \gamma_e^2 \hbar^3) \qquad (1\cdot12)$$

This is the Korringa relation. For a Fermi gas of non-interacting spins, it reduces to

$$T_1 T K_s^2 = (\hbar/4\pi k)(\gamma_e/\gamma_n)^2 \qquad (1\cdot13)$$

Although the contact interaction dominates in most metals, equation 1·13 is not usually satisfied. The discrepancy is attributed to electron-electron interactions which enhance χ_p and also (though differently) affect T_1, since the relaxation process invoves scattering of electrons from one part of the Fermi surface to another (and the expression for T_1 can be re-formulated in terms of the imaginary part of the k-dependent χ_p).

Another possible contribution to the discrepancy could arise when the metal or alloy has a quadrupolar moment. An extra contribution to relaxation then comes from the time-varying electric field gradients produced by diffusing ions. Similarly, there may be orbital and core polarisation contributions, producing local magnetic field components of the required frequency. The behaviour of the Korringa product upon alloying may consequently give information into the processes occuring in the alloy.

1·3 NMR and magnetic susceptibility

There are two distinct approaches to the correlation of Knight shifts and susceptibility discussed here.

1·3·1 Temperature dependence of K and χ

It was mentioned in section 1·2·2 that there is great difficulty in separating the orbital and core polarisation terms in the Knight shift. One way which has been used with success by earlier workers for transition metals (12) and for V_2O_3 (13) is the use of the temperature dependence of K and χ. This process is used in chapter 6, where it will be fully explained. In brief, for a narrow conduction band the spin terms in the susceptibility and the shift can be expected to be appreciably temperature dependent, whereas the orbital parts of both are likely to be virtually temperature-independent.

1·3·2 The contact density term

From equation 1·10 it can be seen that comparison of experimental Knight shifts and experimentally derived χ_p values in metals and alloys yields information about $\Omega|\psi_f|^2$. Clearly, in order to investigate expected and actual behaviour of K, this term must be evaluated.

1·4 Calculation of $\Omega|\psi_f|^2$

Equation 1·10 shows that the specified contribution to K, the

s-state direct term, K_s, is simply related to the product of χ_p and the conduction electron wavefunction density at the nucleus. Two general methods have been adopted for the calculation of the variations in the latter quantity, both of which will now be discussed.

1·4·1 Partial wave analysis for alloys

Upon the introduction of an impurity atom into a pure metal solvent, the electronic structure is perturbed in such a way as to screen out the excess charge of the impurity. This causes electron density oscillations around the impurity which extend for large distances into the metal. The solute is represented by some potential $V(\underline{r})$. The exact forms chosen vary in the particular alloy system discussed, and will be listed in the relevant chapters. The incident and scattered wavefunctions are analysed in terms of spherical wave components, differing essentially by a shifting of phase. These phase shifts, δ_l, which depend of course on $V(\underline{r})$, appear in the expression obtained for the electron density $\rho(\underline{r})$, (14):

$$\frac{\Delta\rho(\underline{r})}{\rho(\underline{r})} = \sum_l (2l+1)\left[\left\{ n_l^2(k_f r) - j_l^2(k_f r) \right\} \sin^2\delta_l - j_l(k_f r) n_l(k_f r) \sin 2\delta_l \right] \qquad (1\cdot14)$$

where n_l and j_l are Spherical Bessel and Neumann functions respectively, and l refers to the angular momentum of the partial wave. The change in the contact density at a nucleus at $\underline{r}=\underline{R}_i$, due to an impurity at the origin, is given by

$$\frac{\Delta(\Omega^P{}_f)}{\Omega^P{}_f} = \frac{\Delta\rho(\underline{R}_i)}{\rho} \qquad (1\cdot15)$$

The average shift for all the solvent nuclei is obtained by integration over all $\underline{R}$

$$\frac{\Delta(\Omega^P{}_f)}{\Omega^P{}_f} = c_y \int \frac{\Delta\rho(\underline{R})}{\rho} P(\underline{r})\, d^3\underline{r} \qquad (1\cdot16)$$

where $P(\underline{r}) = g(r).4\pi\underline{r}^2 n_o$, $g(r)$ is the radial distribution function, n_o the number density of ions, $c=c_y$ is the concentration of solute (y) atoms, and $c_y \ll 1$.

Combining equations 1·14 and 1·16 yields

$$\frac{1}{\Omega P_f}\cdot\frac{d[\Omega P_f]}{dc_y} = \sum_l (A_l \sin^2\delta_l + B_l \sin 2\delta_l) \qquad (1\cdot17)$$

where $$A_l = (2l+1)\int P(\underline{r})\left[n_l^2(k_f r) - j_l^2(k_f r)\right] d^3\underline{r} \quad \text{and}$$

$$B_l = -(2l+1)\int P(\underline{r})\; n_l(k_f r) j_l(k_f r)\; d^3\underline{r} \qquad (1\cdot18)$$

It should be noted that A_l and B_l are independent of the model potential, $V(\underline{r})$, and that the above equations are only valid for low solute concentrations. For the evaluation of A_l and B_l it is necessary to obtain the radial distribution function, $g(r)$, which is in turn defined in terms of the structure factor, $I(K)$. Experimental values of these quantities are not always available for liquids, and so use is often made of the hard sphere structure factors of Ashcroft and Lekner (15). In addition, $g(r)$ for the pure solvent is used as an approximation to the quantity strictly involved, the distribution of solvent atoms around solute atoms. The structure factor, $I(K\sigma)$, is

$$I(K\sigma) = 1 - n_o\, C(K\sigma) \qquad (1\cdot19)$$

where σ is the hard sphere diameter and $C(K\sigma)$ is the direct correlation function in momentum space, given by

$$C(K\sigma) = -4\pi\sigma^3 \int s^2 \frac{\sin sK\sigma}{sK\sigma}\,(t_1 + t_2 s + t_3 s^2)\, ds \qquad (1\cdot20)$$

Here, $$t_1 = \frac{(1+2\eta)^2}{(1-\eta)^4}\,,\quad t_2 = \frac{-6\eta(1+\eta/2)^2}{(1-\eta)^4}\,,\quad t_3 = \frac{1/2\,\eta(1+2\eta)^2}{(1-\eta)^4}, \qquad (1\cdot21)$$

where η, the packing fraction, is given by

$$\eta = (\pi/6)\, n_o \sigma^3 \qquad (1\cdot22)$$

The values of η and σ are obtained from ~~equation 1~~ reference (15). Integration of equation 1·20 gives $C(K\sigma)$ explicitly in terms of t_1, t_2, and t_3, and $K\sigma$. This in turn yields $I(K\sigma)$ from equation 1·19; $g(r)$ is defined as

$$g(r) = 1 + (1/2\pi^2 n_0 r)\int (I(K)-1)\ \sin Kr\ dK \qquad (1\cdot23)$$

where K is the scattering wavevector. The $g(r)$ values calculated in this way are substituted into equations 1·18, and the values of A_1 and B_1 can then be calculated for any host element. These coefficients are evaluated by means of a computer program, fully described by Host (16).

1·4·2 The pseudopotential analysis for metals and alloys

Orthogonalisation of the conduction electron wavefunction to the core wavefunctions results in many oscillations of the conduction electron wavefunction inside the ion. Physically, this corresponds to a high kinetic energy. Furthermore there is a high potential energy, and the two contributions effectively almost cancel out. They can be replaced by a weak 'pseudopotential' and a corresponding smooth pseudowavefunction. Outside the ion core, the pseudofunction behaves as the ordainary function does. Thus, this approach greatly simplifies the calculation of wavefunctions outside the cores, as the use of perturbation theory is possible. To zero order in the pseudopotential, the pseudofunction is a plane wave. To first order, the pseudofunction is perturbed by the pseudopotential. The expression for the true wavefunction inside a core is obtained by orthogonalising the pseudofunction to the core states and renormalising. The square of the wavefunction for Fermi surface electrons at the nucleus is calculated, and averaged over ionic positions. This yields ΩP_f. This approach, which is fully described in (17), is not limited to low concentrations in alloys, as is the partial wave approach, but is applicable both to pure metals and concentrated alloys.

This calculation has been made, exact to first order for alkali-alkali metal alloys (18), and has been extended to polyvalent systems by Host and Styles (19). The approach will be briefly described here,

and the computer program for the evaluation of $\sum P_f$ listed in Appendix 2.

The conduction electron wavefunction may be written as

$$\Psi(\underline{r}) = C\left[\phi(\underline{r}) - \sum_{i,a} \langle a|\phi\rangle \psi_a(\underline{r}-\underline{R}_i)\right] \qquad (1\cdot24)$$

where $\phi(\underline{r})$ is the pseudofunction, ψ_a a core function for which 'a' is an abbreviation, and C is a normalisation constant; the sum is taken over all ions and all core states. C is obtained from the normalisation condition, $\langle\Psi|\Psi\rangle = 1$; x and y represent solvent and solute atoms. Now,

$$|\Psi(\underline{r})|^2 = C^2\left[\phi^*(\underline{r})\,\phi(\underline{r}) - 2\,\mathrm{Re}\sum_{i,a}\langle a|\phi\rangle\phi^*(\underline{r})\psi_a(\underline{r}-\underline{R}_i) + \sum_{\substack{i,j\\a,a'}}\langle a|\phi\rangle\langle a'|\phi\rangle^*\psi_a^*(\underline{r}-\underline{R}_i)\psi_{a'}(\underline{r}-\underline{R}_j)\right] \qquad (1\cdot25)$$

where, to zero order in the pseudopotential, $\phi(\underline{r}) = e^{i\underline{k}.\underline{r}}$, and at a particular site, $\underline{R}_s$,

$$|\Psi(\underline{R}_s)|^2 = C^2\left[1 - 2\,\mathrm{Re}\sum_{i,a}\langle a|k\rangle e^{-i\underline{k}.\underline{R}_s}\psi_a(\underline{R}_s-\underline{R}_i) + \sum_{\substack{i,j\\a,a'}}\langle a|k\rangle\langle a'|k\rangle\psi_a(\underline{R}_s-\underline{R}_i)\psi_{a'}^*(\underline{R}_s-\underline{R}_j)\right] \qquad (1\cdot26)$$

Now, $\langle a|k\rangle = \int\psi_a^*(\underline{r}-\underline{R}_i)\,e^{i\underline{k}\cdot\underline{r}}\,d\underline{r} = e^{i\underline{k}\cdot\underline{R}_i}\int\psi_a^*(\underline{r}-\underline{R}_i)e^{i\underline{k}(\underline{r}-\underline{R}_i)}\,d(\underline{r}-\underline{R}_i)$

$= e^{i\underline{k}\cdot\underline{R}_i}\langle a^x|k\rangle$ (same for all ions in pure x).

Then equation 1·26 reduces to

$$|\Psi(\underline{R}_s)|^2 = C^2\left[1 - 2\,\mathrm{Re}\sum_a\langle a^x|k\rangle\psi_a(0) + \sum_{a,a'}\langle a^x|k\rangle\langle a'^x|k\rangle\psi_a(0)\psi_{a'}^*(0)\right]$$

$$= C^2\left[1 - \sum_a\langle a^x|k\rangle\psi_a(0)\right]^2 = C^2\Omega_x^2(k). \quad (\langle a^x|k\rangle,\ \psi_a(0) \text{ both real}).$$

To first order in the pseudopotential,

$$\phi_k(\underline{r}) = e^{i\underline{k}.\underline{r}} + \sum_{k'}\frac{\langle k'|U|k\rangle}{E_k - E_{k'}}e^{i\underline{k}'.\underline{r}} \qquad (1\cdot27)$$

$\phi_k(\underline{r})$ being normaiised to unit volume. Replacing the summation by an integral, introducing $\underline{q}=\underline{k}'-\underline{k}$, and then substituting equation 1·27 into 1·24 yields

$$\Psi(\underline{r}) = C\left[e^{i\underline{k}.\underline{r}} + \int d\underline{q}\, f(\underline{q})e^{i(\underline{k}+\underline{q}).\underline{r}} - \sum_{i,a}\langle a|k\rangle\psi_a(\underline{r}-\underline{R}_i)\right.$$

$$\left. - \sum_{i,a}\langle a|\int d\underline{q}\, f(\underline{q})e^{i(\underline{k}+\underline{q}).\underline{r}}\rangle\psi_a(\underline{r}-\underline{R}_i)\right] \qquad (1\cdot28)$$

where $f(\underline{q}) = \langle k+q|U|k\rangle\ /(E_k - E_{k+q})$

For an x-type atom at R_s, taking the square modulus of 1·28 yields

$$|\psi_x(R_s)|^2 = \Big| C^2 \Big[e^{ik.R_s} - \sum_a e^{ik.R_s} \langle a^x | k \rangle \psi_a(0) + \int dq\, f(q) e^{i(k+q).R_s} - \sum_{i,a} \langle a | f(q) e^{i(k+q).r} \rangle \psi_a(R_s - R_i) \Big] \Big|^2 . \qquad (1\cdot29)$$

Now, as before,

$$\langle a | f(q) e^{i(k+q).r} \rangle = f(q) e^{i(k+q).R_i} \langle a^x | k+q \rangle .$$

Making this substitution, expanding the square modulus, and neglecting terms containing $f(q)^2$ (second order terms),

$$|\psi_x(R_s)|^2 = C^2 \Big[\gamma_x^2(k) + 2\gamma_x(k) \mathrm{Re} \int dq f(q) e^{iq.R_s} \gamma_x(k+q) \Big] \qquad (1\cdot30)$$

In this expression,

$$\int f(q) e^{iq.R_s} \gamma_x(k+q) dq = (1/2\pi)^3 \int dq e^{iq.R_s} \frac{\langle k+q | U | k \rangle}{E_k - E_{k+q}} \gamma_x(k+q).$$

Now $U(r)$ is the sum of the individual ionic potentials;

$U(r) = \sum_i u_i(r - R_i)$, yielding

$$\langle k+q | U | k \rangle = \int dr e^{-i(k+q).r} \sum_i u_i(r-R_i) e^{ik.r} = \sum_i e^{-iq.R_i} \int d(r-R_i) u_i(r-R_i) e^{-iq.(r-R_i)}$$
$$= \sum_i e^{iq.R_i} u_i(q) .$$

Thus, $$\int f(q) e^{iq.R_s} \gamma_x(k+q) dq = (1/2\pi)^3 \int e^{iq.R_s} \frac{\sum_i e^{iq.R_i} u_i(q) \gamma_x(k+q) dq}{E_k - E_{k+q}} . \qquad (1\cdot31)$$

Taking the time average of $\langle |\psi_x(R_s)|^2 \rangle = (1/N_x) \sum_s^x \overline{|\psi_x(R_s)|^2}$

where N_x is the number of x-type (solvent) ions, and the summation is taken over the x ions at the R_s sites. This yields

$$\langle |\psi_x(R_s)|^2 \rangle = C^2 |\gamma_x(k)|^2 + \frac{2C^2 \gamma_x(k)}{(2\pi)^3} \int \frac{1}{N_x} \sum_s^x \sum_i e^{iq.(R_s - R_i)} \frac{u_i(q) \gamma_x(k+q) dq}{E_k - E_{k+q}} . \qquad (1\cdot32)$$

In this expression,

$$\frac{1}{N_x} \sum_s^x \sum_i e^{iq.(R_s - R_i)} u_i(q) = \frac{1}{N_x} \Big[N_x u_x + \sum_s^x \sum_i e^{iq.(R_s - R_i)} u_x + \sum_s^x \sum_i^y e^{iq.(R_s - R_i)} u_y \Big]$$

$$= u_x + c_x \left[I(q) - 1\right] u_x + c_y \left[I(q) - 1\right] u_y$$

assuming $I_{ii}(q) = I_{ij}(q) = I_{jj}(q)$, the partial structure factors are equal. Finally, this yields

$$\langle |\psi_x(R_s)|^2 \rangle_f = C^2 |\psi_x(k)|^2 \left[1 + \frac{2}{(2\pi)^3 \psi_x(k)} \int \frac{u_x(q)\, \psi_x(k+q)\, dq}{E_k - E_{k+q}} \right.$$

$$\left. + \int \frac{\psi_x(k+q)}{E_k - E_{k+q}} \left[I(q) - 1\right] \left[c_x u_x(q) + c_y u_y(q)\right] dq \right] \qquad (1\cdot33)$$

Ignoring a small (18) renormalisation correction,

$$\langle |\psi_x(R_s)|^2 \rangle_f = |\psi_x^{1\text{-OPW}}(R_s)|^2 \left(1 + \Sigma_x(k) + \Delta_{xy}(k, c_y)\right) = \Omega P_f \qquad (1\cdot34)$$

where

$$\Sigma_x(k) = \frac{2}{(2\pi)^3 \psi_x(k)} \int \frac{u_x(q)\, \psi_x(k+q)\, dq}{E_k - E_{k+q}}, \quad \text{and}$$

$$\Delta_{xy}(k, c_y) = \frac{2}{(2\pi)^3 \psi_x(k)} \int \frac{\psi_x(k+q) \left[I(q) - 1\right] \left[c_x u_x(q) - c_y u_y(q)\right]}{E_k - E_{k+q}} dq \qquad (1\cdot35)$$

The first term on the right of equation 1·34 is the contact density for a single orthogonalised plane wave (OPW). The self term, $\Sigma_x(k)$, measures the effect of the ion pseudopotential at R_x on its own Knight shift. The final term, $\Delta_{xy}(k, c_y)$ the distinct term, is a measure of the influence of the ions other than at R_x, in the alloy.

A full listing of the computer program used to evaluate the contact density is given in Appendix 2. However, some important points will be mentioned here. The calculations required in the following chapters will be performed using the numerical core wavefunctions tabulated in (19). In fact, the total core function is written as a product of a radial part (which is integrated numerically) and an angular part (which is integrated explicitly). Other input parameters are listed below.

1·4·3 Input parameters for the calculation of ΩP_f

Fermi wavevector. Free electron values of k_f will be used throughout,

and are calculated using liquid metal density values and valencies, at the melting points. For the alloys, the assumption that density is linear between the pure metal values has been made, except where experimental density results have been obtained. In these cases, the differences resulting from the use of the approximation of linear interpolation are discussed.

Structure factor. The hard sphere structure factors of (15) will be used. In this calculation, the packing fraction will be taken as 0·45 throughout, at the melting point. The temperature dependence of ΩP_f can be calculated from the temperature dependences of the structure factor and density. The latter is obtained from literature values, and is used to calculate the changes in k_f and Ω with temperature. The temperature dependence of the structure factor is found through the behaviour of the packing fraction. This can be derived as follows: the velocity of sound through many liquid metals (20) as a function of temperature yields calculated values for the isothermal compressibility, b. This is, in turn, related to the packing fraction, η, by the expression,

$$n_o b\, kT = \frac{(1+2\eta)^2}{(1-\eta)^4} \qquad (1\cdot36)$$

(where k is Boltzmanns constant). This yields the temperature dependence of η, the melting point value being taken as 0·45, as in the alloy dependence calculations. Use of experimental structure factors is attempted in some cases, and the results compared with those obtained from the model value.

Pseudopotential. A local pseudopotential described by Ashcroft (21) will be used here.

$$V(x) = \frac{-\lambda^2 \cos sx}{x^2 + \lambda^2 f(x)} \qquad (1\cdot37)$$

where $x = q/2k_f$, $\lambda^2 = 1/\pi a_o k_f$, $s = 2k_f R_{core}$, and the Lindhard function

is $f(x) = \frac{1}{2} + \frac{1-x^2}{4x} \ln\left|\frac{1+x}{1-x}\right|$; a_o is the Bohr radius, and V is in units of $2E_f/3$. s determines the location of the first node. Some values of R_{core} are listed by Ashcroft and other authors; some which are not are calculable from the resistivity data of the pure liquid metal. An attempt to take non-locality of the pseudopotential into account, in a simple way, may be made by making R_{core} energy dependent. Perdew, in a private communication to Host (16), has suggested that an expression of the form

$$R_{core} = R^o_{core} \left[1 - \alpha(k_f^2 - k_f^{o\,2})/k_f^{o\,2} \right] \qquad (1\cdot38)$$

be tried, for each ionic species. (The suffix o refers to the pure metal value). The parameter α (and similarly a parameter β for the second alloy component) may be varied for the best fit with experimental K results. Such an approach, whilst an improvement on the simple local V(x), is not strictly a full introduction of non-locality, but is seen as the next step in the development of this calculation.

Wavefunctions. The value of the s-state core wavefunctions at r=0, $R_{ns}(0)$, may be obtained by extrapolating the numerical values (19) to r=0; these values are used in the evaluation of $\Psi_a(0)$ in the $\chi_x(k)$ terms. (For a fuller description of the calculation, see (16)). These particular wavefunctions ignore relativistic effects, and this may cause errors for elements with high atomic numbers, (22).

1·5 Present investigation

The chapters following chapter 2 are all concerned with an investigation of NMR and susceptibility in metallic systems. Chapter 3 deals with some pure metals, chapter 4 with the alloy systems Pb-Bi, Sn-Cd, and Sn-Bi, chosen because in the liquid state the alloys are expected to be atomically random. Chapter 5 deals with dilute lead alloys, the next with the metal-semiconductor transition in VO_2. Chapter 7 is concerned with alloys suspected of more complicated atomic arrangements than those in 4, and

the final chapter the localised moment behaviour in dilute gallium alloys. It is hoped that the unity of approach to these divergent systems will be made clear, and the usefulness of the mutual comparison of NMR and susceptibility evaluated.

References

1) Clogston A.M.,Jaccarino V. and Yafet Y., Phys. Rev., 134A, 651-61, 1964.

2) Angus W.R., Proc. Roy. Soc., 136A, 569-78, 1932.

3) Williams D.E.G., The Magnetic Properties of Matter, p.73, Longmans, London, 1966.

4) Dupree R. and Seymour E.F.W., The Physics and Chemistry of Liquid Metals, (ed. S.Z.Beer), chapter 11, Dekker, New York, 1972.

5) Herring C., Magnetism, (eds. G.T.Rado and H.Suhl), volume 4, Academic Press, New York, 1966.

6) Rice T.M., Phys. Rev., 175, 858-67, 1968.

7) Dupree R. and Geldart D.J., Solid State Comm., 9, 145-9, 1971.

8) Kanazawa H. and Matsudawa N., Progr. Theor. Phys., 23, 433-46, 1960.

9) Kubo R. and Obata Y., J. Phys. Soc. Japan, 11, 547-50, 1956.

10) Andrew E.R., Nuclear Magnetic Resonance, C.U.P., London, 1958.

11) Slichter C.P., Principles of Magnetic Resonance, Harper and Row, New York, 1963.

12) Clogston A.M.,Gossard A.C.,Jaccarino V. and Yafet Y., Phys. Rev. Lett., 9, 262-5, 1962.

13) Jones E.D., Phys. Rev., 137A, 978-82, 1965.

14) Daniel E., J. Phys. Chem. Solids, 10, 174-81, 1959.

15) Ashcroft N.W. and Lekner J., Phys. Rev., 145, 83-90, 1966.

16) Host I.P., Ph. D. thesis, Warwick University, 1972.

17) Faber T.E., Adv. Phys., 16, 637-51, 1967.

18) Perdew J.P. and Wilkins J.W., Solid State Comm., 8, 2041-45, 1970.

19) Herman F. and Skillman S., Atomic Structure Calculations, Prentice-Hall, New York, 1963.

20) Gitis M.B. and Mikhailov I.G., Soviet Physics (Acoustics), 12, 131-43, 1966.

21) Ashcroft N.W., J.Phys. C (Proc.Phys. Soc.), 2, 232-43, 1968.

22) Host I.P. and Styles G.A., J.Magnetic Resonance, 6, 475-87, 1972.

Chapter 2

Experimental Methods

Measurements have been made in various metal and alloy systems of two or more of the following properties: magnetic susceptibility, steady state NMR widths and shifts, nuclear spin relaxation rates using pulsed NMR, and density. Both the steady state and pulsed NMR techniques have been fully described elsewhere and will be discussed only briefly. The apparatus for the measurement of magnetic susceptibility and for density will be more fully described, as will the techniques of sample preparation necessitated by the various properties of different systems.

2·1 Magnetic susceptibility

Magnetic susceptibilities were measured by an adaption of the Faraday technique (1). The apparatus is shown schematically in figure 2·1. In this method, a small (2 g) sample is placed on one arm of a sensitive microbalance in a large, inhomogeneous magnetic field. Then the force on the sample (other than its weight) in the vertical $\underline{Z}$ direction is

$$\underline{F}_{\underline{z}} = m\chi H_{\underline{x}} \cdot \frac{dB_{\underline{x}}}{d\underline{z}} = m\chi \underline{D}, \qquad (2\cdot1)$$

where the $\underline{X}$ direction is that perpendicular to both $\underline{Z}$ and the pole faces of the magnet (figure 2·2); m is the mass of the sample, and χ the mass susceptibility. The pole pieces used were of such a shape that $\underline{D}$ goes through both a positive and a negative extremum as a function of $\underline{Z}$. The original pole piece design aimed at a uniform $\underline{D}$ over the sample volume near the upper maximum, but $\underline{D}$ was found to be sufficiently uniform around the lower maximum also for that to be used for measurement purposes. Consequently as the sample traverses the $\underline{Z}$ direction, symmetrically placed between the pole pieces in the $\underline{X}$ direction, the extra force $\underline{F}_{\underline{z}}$ experienced will show corresponding maxima. The sign of

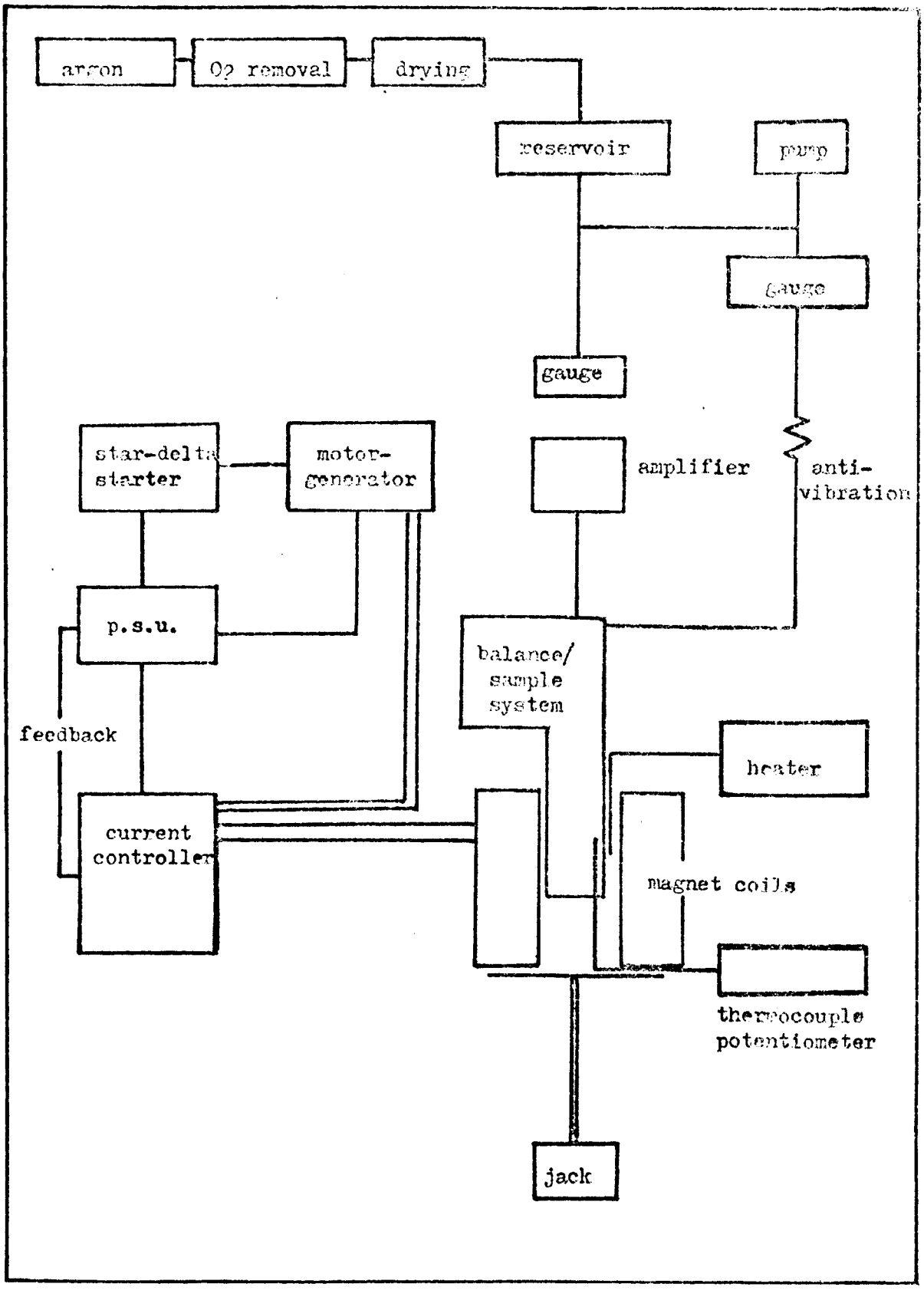

Figure 2·1 Magnetic susceptibility apparatus - Faraday method

these maxima (additions to or subtractions from the weight) will depend upon the sign of χ. Now,

$$(\underline{F}_z)_1 - (\underline{F}_z)_2 = m\chi(\underline{D}_1 - \underline{D}_2) \qquad (2\cdot2)$$

where 1 and 2 refer to the positions of the maxima. Since $(\underline{D}_1 - \underline{D}_2)$ is fixed for a given magnet current, then for two different samples A and B of the same mass, the ratio of the force differences, $(F_1-F_2)_A/(F_1-F_2)_B$, will also be the ratio of the mass susceptibilities. Consequently all the problems involved in evaluating the field gradient accurately are eliminated, by defining all susceptibilities relative to a known standard. The standard chosen was silver metal. This has a reasonably large and well documented susceptibility and is resistant to physical deterioration and chemical attack. The value of χ was taken to be $-2\cdot34 \times 10^{-9}$ m^3kg^{-1},(2). Because the sample moves through the field in the $\underline{Z}$ direction, the problem of positioning the sample in this direction does not arise. The pole pieces are parallel for 150 mm in the $\underline{Y}$ direction (figure 2·2) and so the only critical positioning is involved in placing the sample symmetrically between the poles in the $\underline{X}$ direction. A mirror is fitted to the apparatus to eliminate parallax errors when this adjustment is being made. The magnet current (0-24 A) is maintained by an ac motor/ dc generator and Mullard precision current controller, yielding a current stability of 1 in 10^5. The balance is a Sartorious 4102 electronic microbalance, in which the torque due to the weight is compensated partly by a counterweight and partly by an electromagnetic counter-force which maintains the quartz beam in the null position. The stirrup assembly has diamond pins and sapphire bearings to minimise wear. The balance assembly itself is rigidly mounted on slate planks, which are in turn isolated from two brick pillars by lead sheeting. This system was designed to maximise isolation from spurious vibrations.

The sample is initially approximately counterbalanced with a substance of similar weight and buoyancy (since the range of the balance is limited to 200 mg differences). The extra force due to the magnetic field is read from the balance amplifier output with an accuracy of one microgram. The whole balance and sample assembly is enclosed in an evacuable glass system. This enables measurement to be made under a variety of atmospheres, and removes problems arising from air currents. The sample itself sits in a silica bucket suspended by a platinum hook from a silica fibre attached to the balance. Silica was chosen for the sample holder because its susceptibility is highly reproducible and changes little with temperature; it is resistant to attack by most acids, making it easy to clean. The bottom section of the system is a silica furnace tube (figure 2·3) around which is wound a nichrome wire heating element, supplied by a Roband T112 dc power unit. The furnace is insulated by several layers of Fibrefrax paper. A chromel-alumel thermocouple is situated within 5 mm of the sample. It was determined that the interior temperature gradient was insufficient to cause more than 5 degK error, even at the highest operating temperature (1500 K), from observations of the temperature at which χ changes discontinuously upon melting of some pure metals. The furnace tube assembly is mounted in the magnet gap. The relative motion of the sample and field is achieved by lifting the magnet on a hydraulic jack which is driven by an electric pump. The rate of descent through the positions of maximum $\underline{D}$ is controlled by slowly bleeding hydraulic fluid out of the jack. In practice, the magnet is moved rapidly between these positions and very slowly in their immediate neighbourhoods. The forces at these positions can then be read directly from the balance meter, in micrograms weight.

The balance assembly is connected to an evacuating system (by means

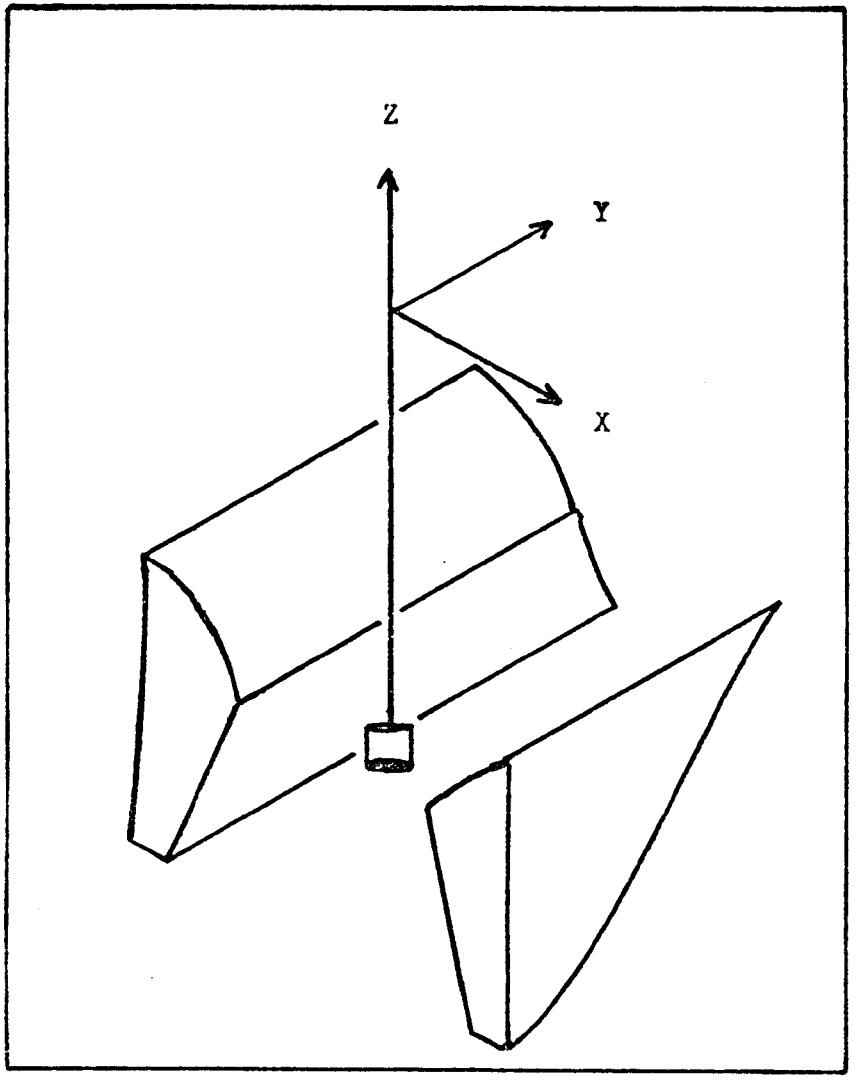

Figure 2.2 Sample suspension

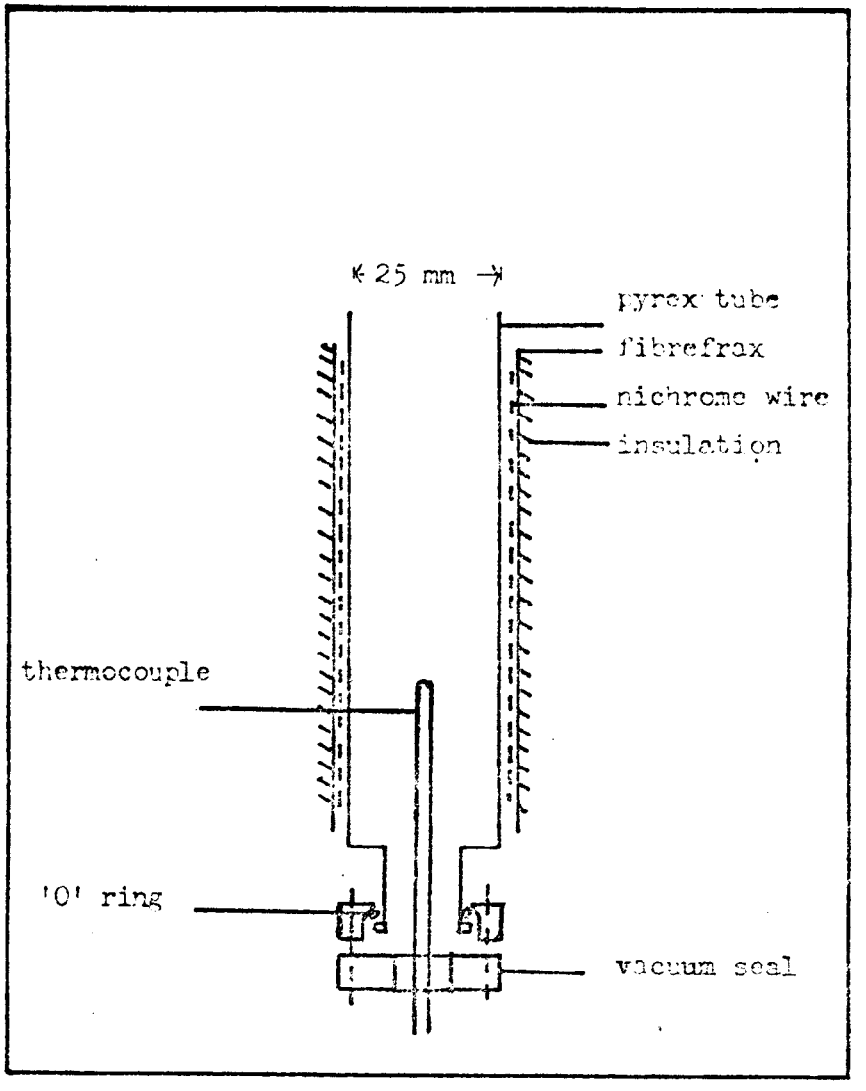

Figure 2.3 Furnace

of anti-vibration bellows) by a large capacity reservoir, designed to increase control of the rate of gas flow into the system. Normally the apparatus was run with an atmosphere of 400 torr of an inert gas (argon or nitrogen), which was first passed through an alkaline pyrogallol solution to remove oxygen traces. Higher pressures were found to cause convection currents at high temperatures disturbing the balance, and running at low pressures of gas or under vacuum sometimes led to evaporation problems. The samples were not sealed. It was necessary to duplicate the run exactly, without the sample, so as to subtract the effect of the sample holder assembly. No way was found of sealing the sample holder while empty, and resealing it full in exactly the same way. Some small differences were bound to be introduced. In fact, nominally identical buckets were found to vary appreciably in mass susceptibility, and since the holder is responsible for a large fraction of the observed force, an appreciable error would have been introduced had sealing been attempted.

All samples and holders were measured over the temperature range used for the sample and also as a function of magnetic field (at one temperature at least). The presence of an inverse field dependence (χ proportioal to B^{-1}) is indicative of ferromagnetic impurities. The value of $\underline{D}$ at which the measurements were made was about 10^7 Nm^{-3}, at a magnet current of 12 A. Samples were discarded for which the intercept of the χ versus B^{-1} curve (corresponding to the value at infinite field) differed from the value of χ at the operating field by more than 1%. The reasons for not operating at the highest field available are that above 15 A the field is no longer linear with current (saturation) and that magnet overheating became a problem in a short time. A voltmeter is used to check on the magnet coil resistance, in order to monitor the temperature.

At least three readings were taken at each temperature and where

possible several samples of a given composition were measured. In the absence of oxidation or evaporation problems, susceptibilities were obtained with a precision of ½% or better.

2·2 Density measurement

There is a wide variety of methods for determining the density of liquid metals. However, two methods are more commonly employed than most. Both of these were attempted for the alloys investigated.

2·2·1 The Archimedean technique

In this method, the upthrust on a sinker when it is immersed in the liquid metal is determined. The effect of surface tension (between the liquid metal and the wire suspending the sinker) can be eliminated by using two different sinker sizes, with the same diameter suspending wire for both. The balance to which the sinker is attached and the sample must both be contained in an evacuable system, containing an inert atmosphere. This was achieved by using a small (1 g) sinker and the microbalance used for the susceptibility measurements. The sinker was made of tungsten carbide, drilled with a spark cutter to accept the tungsten suspension fibre. These materials are both resistant to attack by the metals whose density was under consideration. However, difficulty was experienced in overcoming the surface tension, and the sinker tended to float on the metal. It seems likely that the scale of operation of this technique needs to be larger for success. A larger sinker, and consequently a much larger sample than was available are necessary. After repeated trials this method was abandoned in favour of a pycnometer method.

2·2·2 The pycnometer method

This is probably the simplest technique in principle. It entails filling a known volume with the liquid metal or alloy, and weighing. This technique was employed with success and a diagram of the apparatus

is shown in figure 2·4. A pyrex pycnometer of known internal volume and mass is immersed in the liquid metal under vacuum. Argon is then introduced above the sample, and the pycnometer fills; it is withdrawn, cooled, and weighed (after cleaning any deposit from the outside). Such a technique does not work for metals which expand on freezing, such as bismuth and gallium. The error introduced by the meniscus -which will be different for various concentration alloys- and that due to the expansion of the pyrex were calculated and found to be negligible.

This technique is limited at present to temperatures up to about 830 K, above which pyrex softens. Silica pycnometers proved unsuccessful because the expansion coefficient was so different to that of the metals as to induce strain, causing cracking of the vessel upon cooling. This was found to occur at cooling rates so slow (10 degK per hour) as to make the required experimental time impracticably long. However, the possibilities of using either a stainless steel vessel or one made of an intermediate glass mean that the temperature range can probably be successfully extended up to 1100 K or above. The sample size for this technique is not critical. With a sample of about 10 g, densities were measured to a precision of $\frac{1}{2}\%$.

2·3 Steady state NMR

The apparatus is shown schematically in figure 2·6. A commercially available Varian V.F.16 wide line spectrometer, having a frequency range of 2 - 16 MHz, and utilising the nuclear induction method (3) , is used in conjunction with a 12 inch Varian electromagnet. The magnet is capable of supplying a field of 1·5 T with a homogeneity of 1 part in 10^5. The audio modulated field is swept through the value required for resonance, whilst the frequency is constant. The signal is amplified and demodulated and then displayed on the oscilloscope, or alternatively

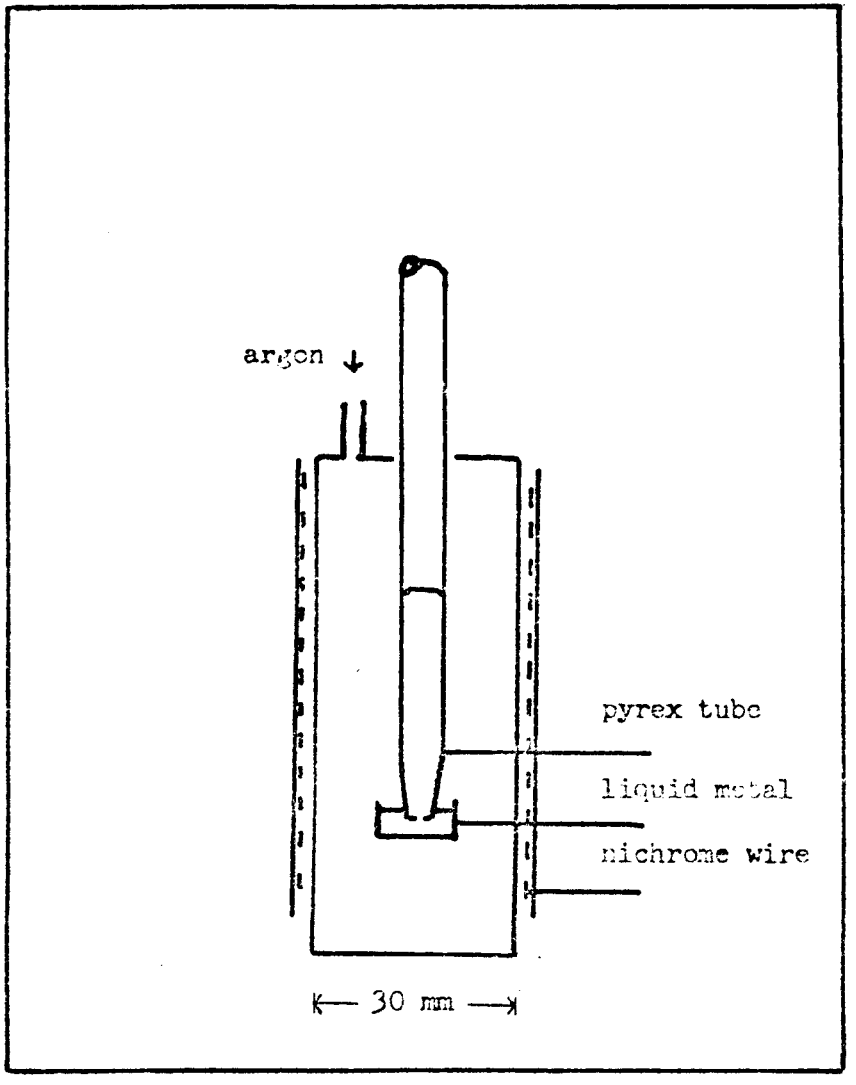

Figure 2.4 · Pycnometer

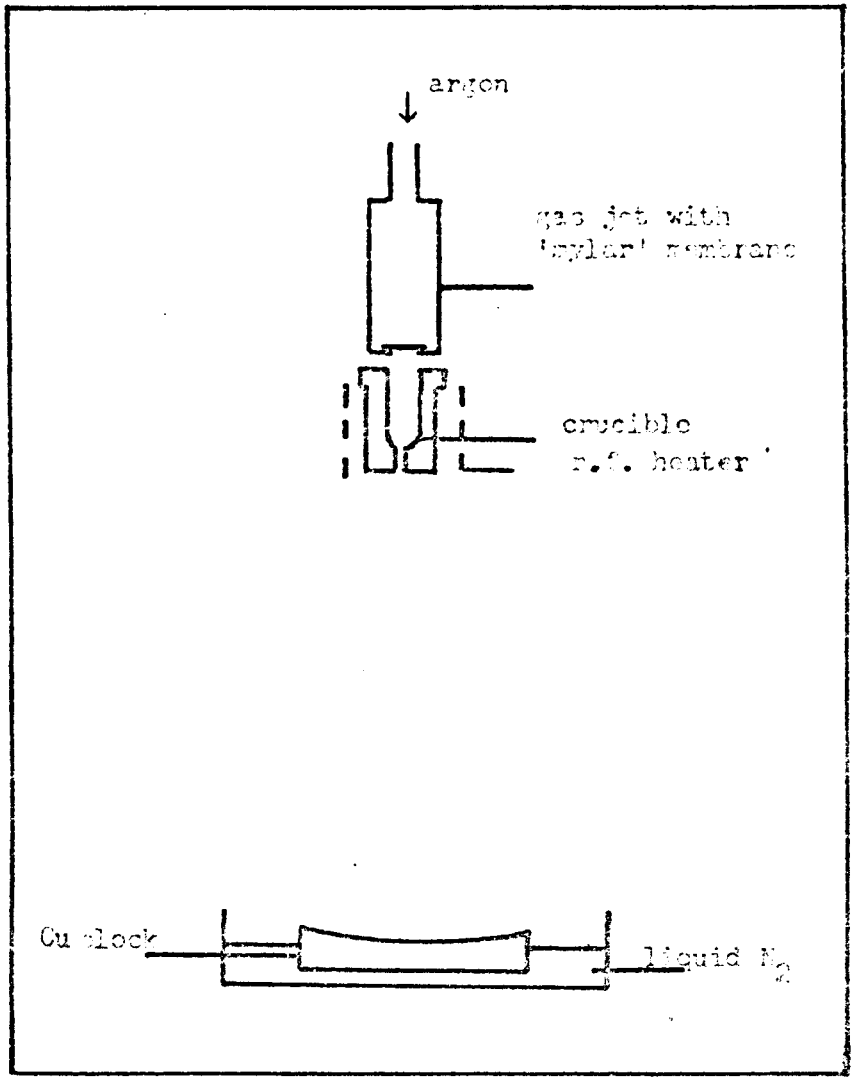

Figure 2.5 'Splat' apparatus

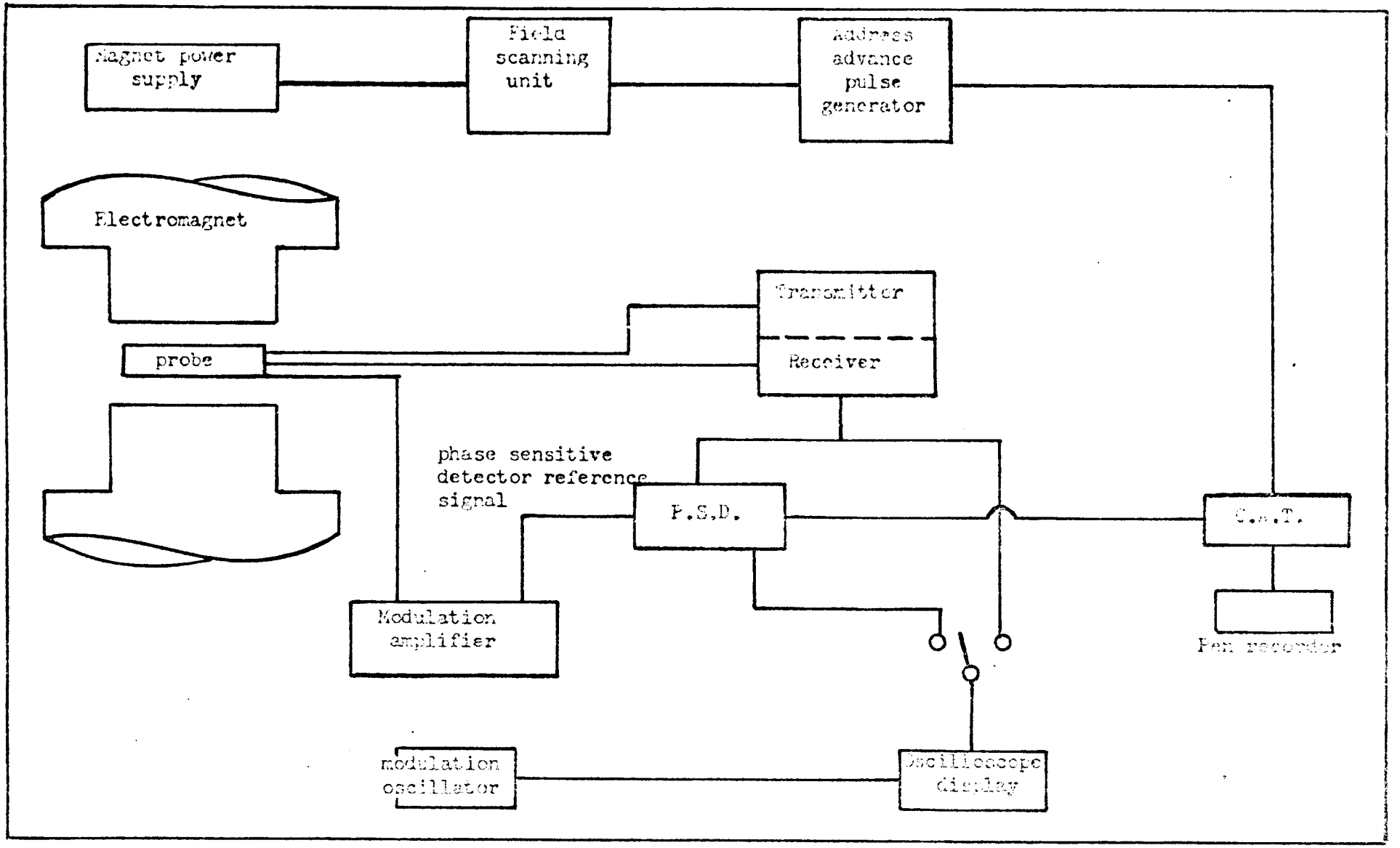

Figure 2.6 The N.M.R. Spectrometer

fed into a phase sensitive detector and pen recorder. The maximum response and sweep times of the instrument limit the sensitivity, and for weak signals a noise averaging device is used. The instrument available was a Northern NS-544 digital memory oscilloscope (Computer of Averaged Transients). The 1 024 storage channels of this instrument are opened in synchronism with the magnetic field sweep. Random noise increases $\sqrt{N}$ times for N sweeps, whereas the signal increases N times. This yields a signal to noise improvement of $\sqrt{N}$. A Venner TSA 3436 counter is used to measure the operating frequency. A subsidiary Watkins-Lound spectrometer is used , the probe in the magnet gap containing a sample of ^2D in heavy water. The gyromagnetic ratio of ^2D is accurately known, and by observing the frequency of the subsidiary spectrometer at resonance, the field value can be ascertained. Usually, two deuteron resonances are superimposed on the signal, at two fields in the neighbourhood of the resonance.

The sample itself (approximately 1500 mm^3) is contained in a pyrex tube. The sample tube is held in a gas flow furnace, similar in design to that described by Schreiber (4). Two compressors are used, one to provide the hot gas flow to the sample, and the other to provide cooling air between the furnace dewar and the probe. The specimen temperature was determined by a Pt/Pt-13% Rh thermocouple located immediately below the sample tube. Experiments have shown that the temperature gradient across the sample does not exceed 5 degK. A chromel-alumel thermocouple monitors the probe temperature, and the maximum attainable temperature of the sample was about 760 K. For the low temperature measurements the furnace assembly is removed and a finger dewar inserted into the probe directly. This dewar is filled with liquid nitrogen, enabling measurements to be taken at 77 K.

2·4 Pulsed NMR

The apparatus used is a commercially available Polaron spectrometer and a Varian 9 inch electromagnet. The sealed sample is placed in a single coil assembly of the probe. The spectrometer has an operating temperature range of 80 K - 800 K and three fixed frequencies, 7,11, and 47 MHz. A sequence of high power r.f. pulses at the Larmor frequency are applied to the coil. The system is designed such that during the pulse the receiver is open circuit as seen from the transmitter; at all other times ,the transmitter is open circuit as seen from the receiver. Hence, the need for only one coil. The receiver output is fed, via a preamplifier, into a r.f. phase sensitive detector, along with a reference signal derived from the free-running oscillator. The detected signal is then fed into a boxcar integrator, and finally a pen recorder output. The apparatus is shown in figure 2·7. The technique used for T_1 (longitudinal relaxation) measurement requires a pulse sequence of $\pi - \tau - \pi/2$. The amplitude of the signal is proportional to M_τ , the longitudinal magnetisation existing at time τ:

$$M_\tau = M_0(1-A \exp(-\tau/T_1)),$$

where A is a constant (ideally equal to 2). The value of M_0 is determined by switching the field on and off resonance. By changing the pulse separation, τ , by stages, values of M can be determined. A graph of $\log_e(M_0-M_\tau)$ against τ yields T_1 from its slope.

2·5 Sample preparation

The alloy samples for magnetic susceptibility and density measurement were prepared in bulk form, by melting together the constituent metals under an inert atmosphere in a pyrex (or silica) mould. The metals used were all of 99·999% purity or better. They were cleaned in acid and dried in ether prior to alloying. The samples were held well above the liquidus temperature (always more than 100 degK above) for several minutes and

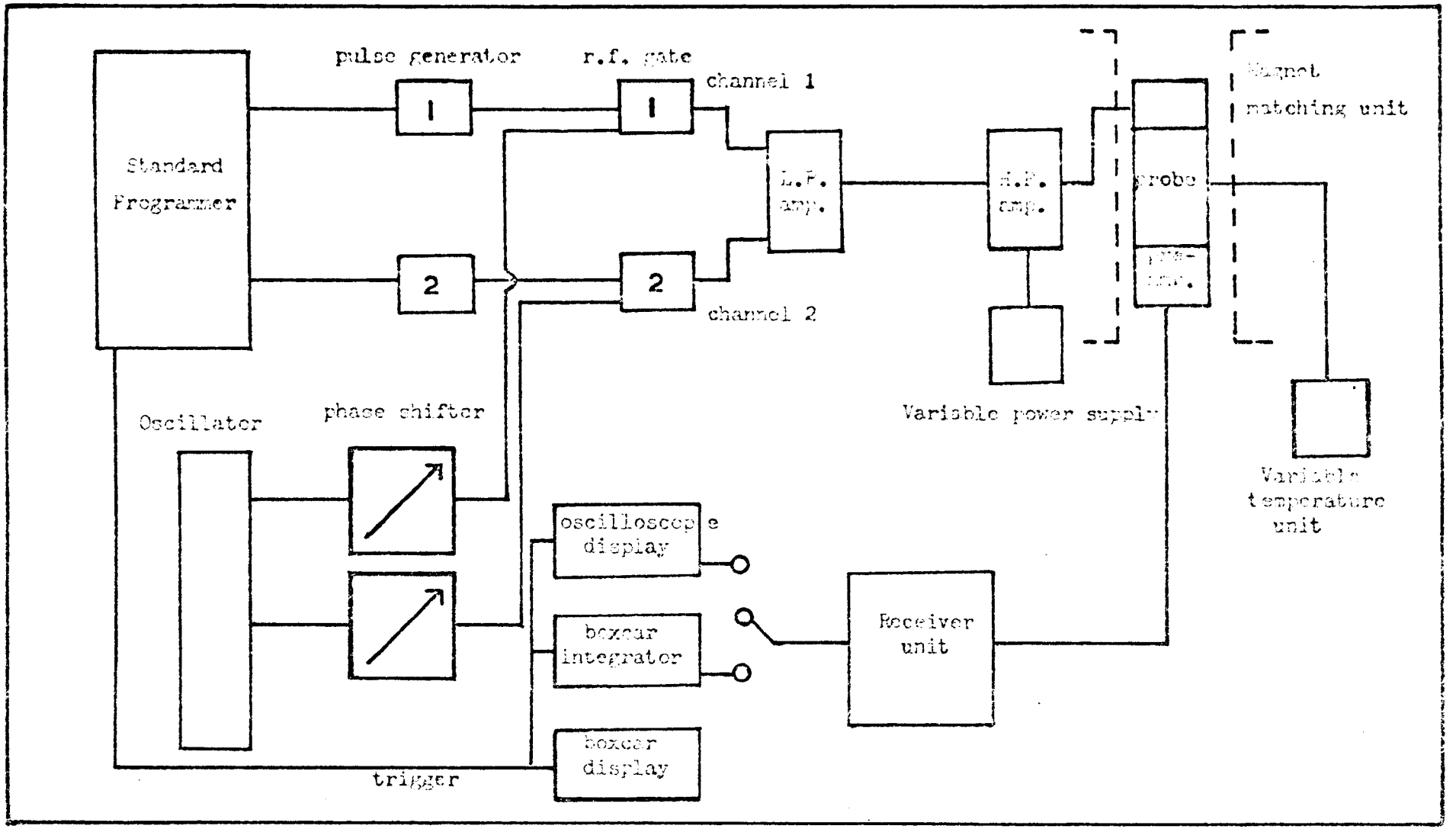

Figure 2.7 Polaron pulse spectrometer

agitated to ensure complete mixing. For the NMR measurements, powdered samples were necessary. In order to facilitate penetration of the r.f. signal, the particle size must be less than the radiofrequency skin depth (generally 10-100 μm). The powders must be prepared this size or less, and mixed with powdered quartz to prevent electrical contact and stop coalescence in the liquid state. The samples were not prepared by filing an ingot. Filing introduces impurities and produces non-spherical particles which do not pack well. Further, phase separation of the bulk may have taken place, leading to inhomogeneities in composition. The metals were formed into an alloy ingot, as above, and this was then swaged down to a long rod of diameter 3/16 inches. This rod was fed into a Metallication M-45 spraying pistol.(This runs on oxypropane fuel and compressed air. The rod is fed into the flame and is dispersed into molten metal droplets, by the compressed air spray. The droplets are quenched in a large supply of cold water. The powder is then washed, dried, and sieved.) For the lead-bismuth and tin-cadmium alloys (which this process was used for) the yield of particles of size less than the relevant skin depth was large in most cases, reaching 90% for some alloys. The method is very fast: a 10 g sample could be sprayed in about 30 s.

For the gallium-manganese and gallium-chromium alloys, this method could not be used , because of the insolubility of the transition metals in gallium in the solid phase. If, however, the powder could be formed from a liquid spray, the insolubility problem would be bypassed. Although the transition metal might separate out locally in each individual particle, the liquid would recover the same degree of homogeneity as the initial liquid bulk. A technique discussed by Host (5) for spraying from the liquid was tried. The molten alloy is tipped out of a pyrex vessel through a nozzle, emerging into a stream of nitrogen gas. This

method proved unsuccessful for these alloys. It was also tried for some lead-bismuth alloys. However, the yield in this case proved to be very low in comparison with the technique of spraying from the solid described earlier.

The method which proved successful for the gallium alloys was the so called "splat" technique. The apparatus is shown schematically in figure 2·5. The liquid alloy is contained in a pyrophyllite crucible, and maintained in a molten state by a r.f. heater. A shock wave is propagated through the sample when a diaphragm situated just above the crucible is burst by high pressure (350 psi) nitrogen gas. This propels the sample through a small hole in the crucible base-a hole too small to allow the escape of the liquid at normal pressures-and onto a copper block maintained at the temperature of liquid nitrogen. The liquid structure is frozen into the solid. This solid, which is in an amorphous and semi-powdered form, is kept at 77 K until it can be powdered with a pestle and mortar, again under liquid nitrogen.

References

1) Kittel C., Introduction to Solid State Physics, p.428, Wiley, New York, 1967.

2) Hellwege K.H., Landolt-Bornstein Zahlenwerte und Funktionen aus Physik, volume 2, p.15, Springer Verlag, Berlin, 1962.

3) Andrew E.R., Nuclear Magnetic Resonance, C.U.P., London, 1958.

4) Schreiber D.S., Rev. sci. Instrum., 35, 1582-3, 1964.

5) Host I.P., Ph.D. thesis, Warwick University, 1972.

Chapter 3

Magnetic properties of pure metals

3·1 Introduction

The procedure explained in chapter 1 for obtaining the electronic contribution from the total susceptibility has been adopted for nine pure metals, listed in table 3·1. The particular choice of metals was governed in part by a wish to test the pseudopotential theory of section 1·4·2 for metals of different valencies, in part to investigate various discrepancies and gaps in the literature, and in part as a basis for the work on alloy systems reported in later chapters. In accordance with the general aim to correlate NMR and magnetic susceptibility, the second part of the chapter is concerned with the behaviour of the Knight shift in some of these metals, as observed from present and some earlier results. The analysis of section 1·3·1 (K and χ with temperature as implicit variable) is not a useful technique in these cases, in view of the small temperature coefficients of susceptibility compared to some transition metals, and it is therefore necessary to use the analysis of section 1·1·3 to deduce χ_p values in order to extract experimental ΩP_fs for comparison with theory.

The direct contact Knight shift has already been defined in terms of the spin susceptibility contribution and the contact density at the nucleus,

$$K_s = (2/3)\chi_p \Omega P_f \quad . \qquad (3·1)$$

Section 3·2 deals with the derivation of the Pauli contribution from experimental susceptibilities; section 3·5 compares the "experimental" ΩP_f values so obtained with theory for six polyvalent metals investigated. Since it will be seen that the χ_p analysis gives consistent results only for the liquid state, the ΩP_f comparison has been made

only for the liquid metals.

A further valuable comparison with theory can be made for the temperature coefficient of the Knight shift, using

$$K_s' = \frac{1}{K_s}\frac{dK}{dT}s = \frac{1}{\Omega P_f}\frac{d(\Omega P_f)}{dT}f + \frac{1}{\chi_p}\frac{d\chi_p}{dT} \qquad (3\cdot2)$$

assuming only small changes with temperature. The theoretical temperature coefficient of ΩP_f is obtained (section 1·4·3) from the temperature dependence of density, k_f, and the structure factor. The temperature coefficient of χ_p can be obtained either from that of χ with an allowance for χ_i and assuming $\chi_p' = \chi_e'$ (χ_p' given by final term in equation 3·2) or from χ_p deduced at one temperature and the expansion coefficient assuming a free electron dependence on volume.

Thus both the above quantities K and K' can be compared with theoretical values. Experimental values for pure tin, cadmium and liquid gallium have been obtained in the present work and values for indium, bismuth and lead taken from (1).

3·2 Susceptibility results

In the expression for the Knight shift, the spin susceptibility χ_p is expressed in volume units. Deriving χ_p from the measured mass susceptibility involves a knowledge of the density. A consistent approach was adopted throughout for the densities used. The values for the density of the solid metal at room temperature, the liquid metal values at the melting point, and the liquid expansion coefficient were all taken from reference (2). The change on melting, yielding the solid density at the melting point (with (2)) and the solid temperature coefficient were taken from (3). These are all summarised in table 3·1. It will be convenient to deal with the liquid metals and the solid metals in turn. Figures 1-7 inclusive show the experimental variations of χ with temperature for

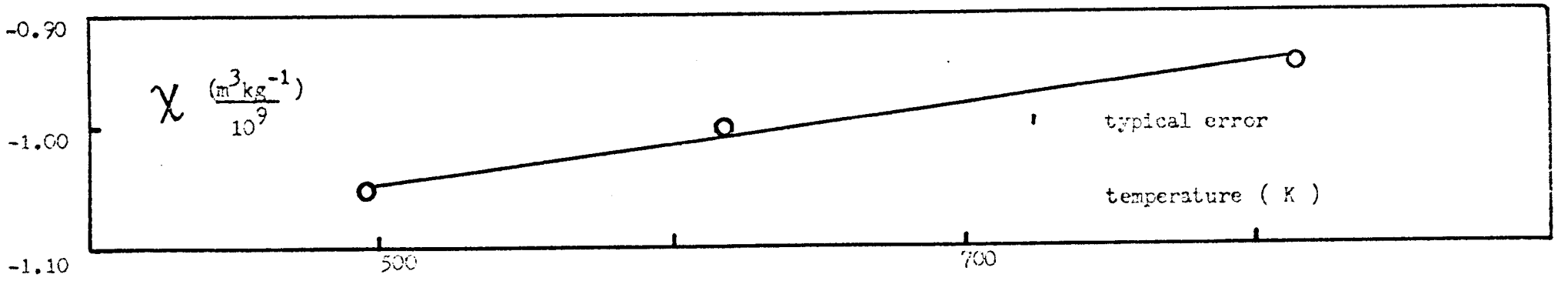

Figure 3.1 Magnetic susceptibility of indium

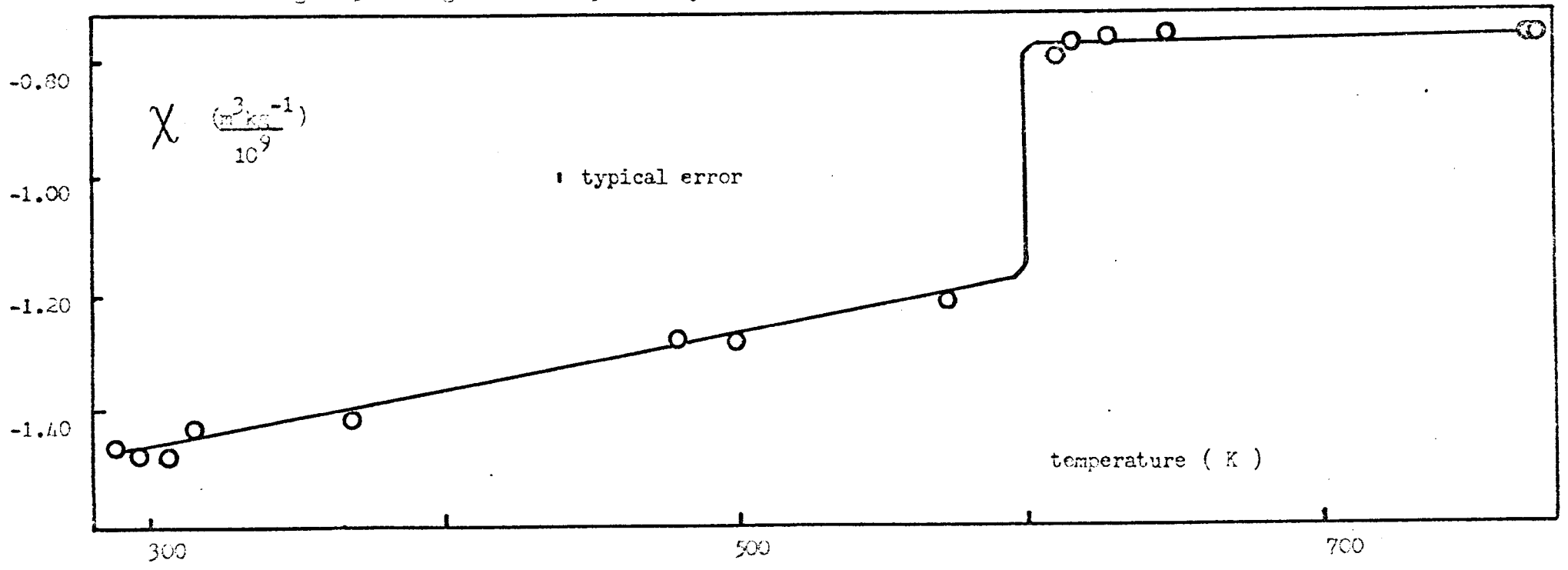

Figure 3.2 Magnetic susceptibility of lead

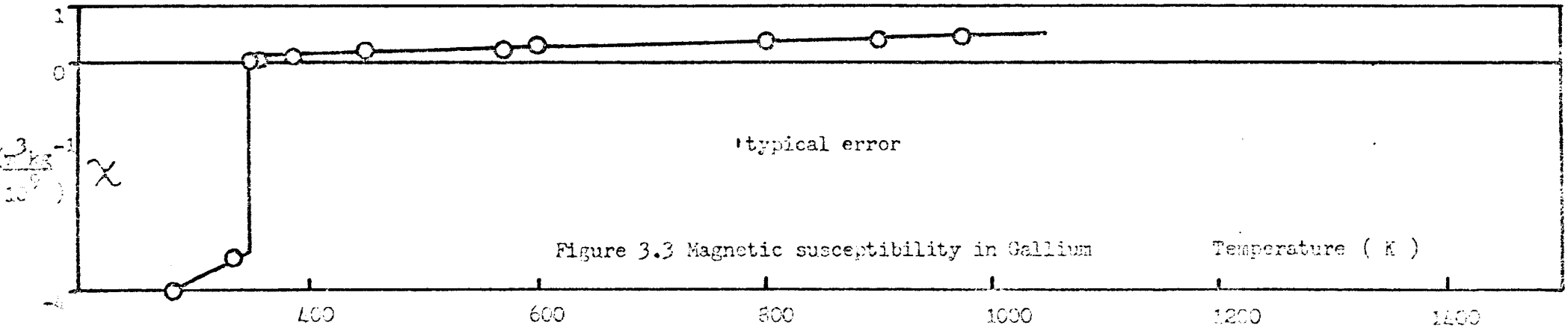

Figure 3.3 Magnetic susceptibility in Gallium

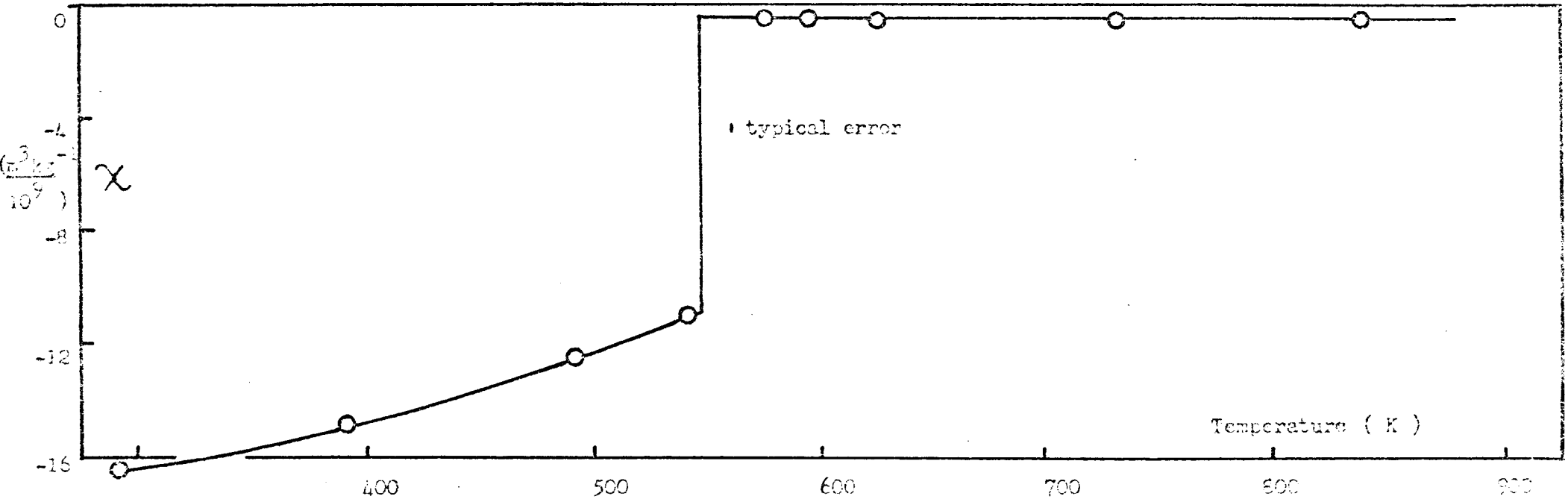

Figure 3.4 Magnetic susceptibility in Bismuth

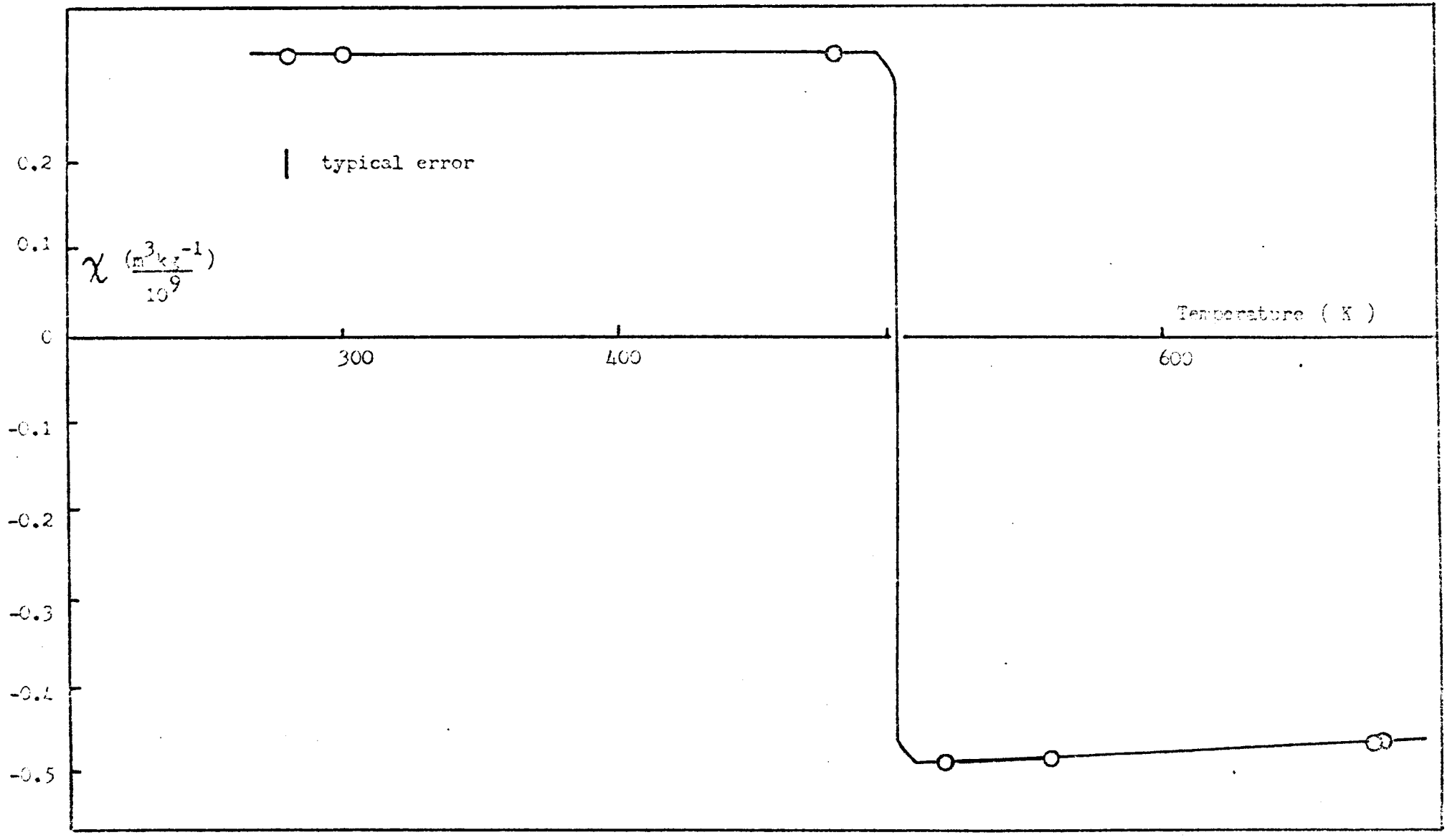

Figure 3.5 Magnetic susceptibility of tin

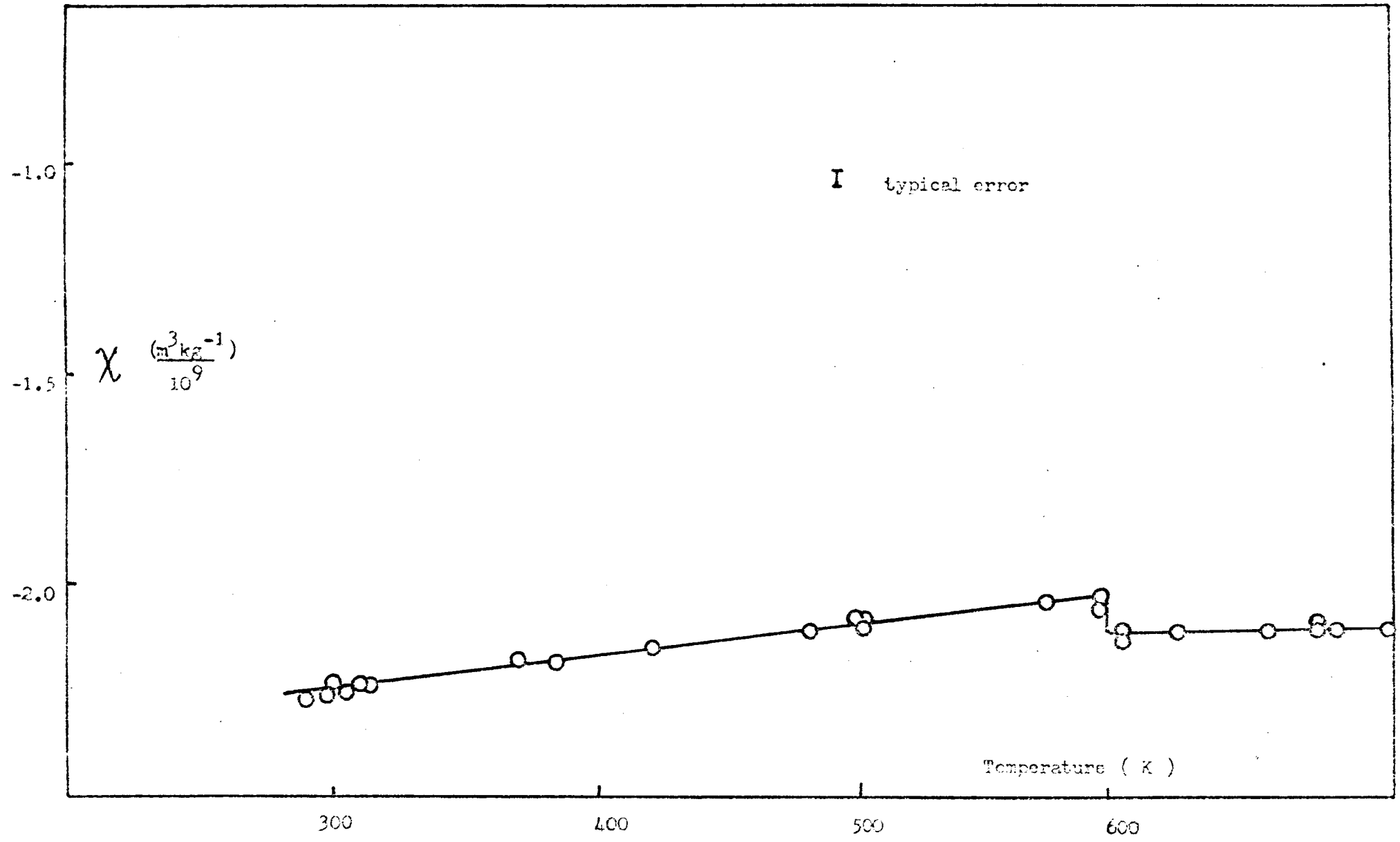

Figure 3.6 Magnetic susceptibility of pure cadmium

Figure 3.7 Magnetic susceptibilities of noble metals

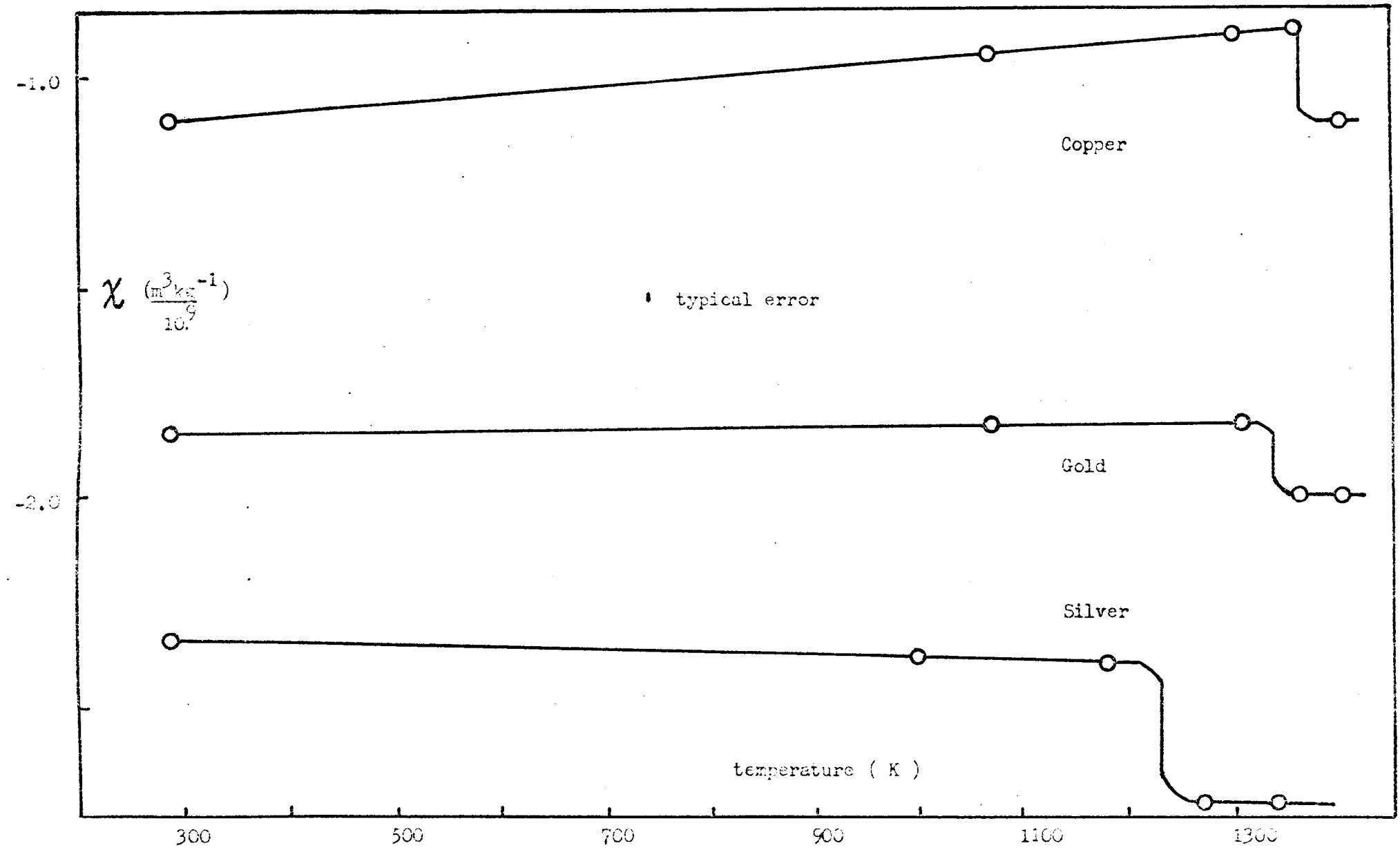

Table 3·1

Densities and expansion coefficients for pure metals

metal	m.pt. (K)	$\rho_{liq}(mp)$ ($kgm^{-3}/10^{-3}$)	$\rho_{sol}(mp)$	$\rho_{sol}(293\ K)$	$-(d\rho/dT)_{liq}$ ($kgm^{-3}K^{-1}/10$)	$-(d\rho/dT)_{sol}$
Ga	303	6·10	5·91	5·97	6·18	2·78
Cd	594	8·02	8·34	8·64	10·76	9·97
In	430	7·03			7·69	
Sn	505	6·96	7·15	7·30	6·80	7·08
Pb	600	10·60	10·98	11·68	12·10	22·88
Bi	544	10·06	9·73	9·80	12·48	12·79
Cu	1356	8·05	8·40	8·96		5·26
Ag	1234	9·30	9·67	10·5		8·82
Au	1340	17·2	$18·1_3$	19·3		11·21

all these metals.

3·2·1 Liquid metals: analysis of results

The assumptions specified in chapter 1 used for obtaining χ_e from χ will be adopted throughout (χ_o is zero, m*=m, and the ionic and electronic terms are independent). In table 3·2 the liquid metal susceptibilities at their respective melting points are summarised. All values are quoted in SI volume units. As can be seen, the predicted and measured values of χ_e are in good agreement for the polyvalent metals and this agreement is marginally better than using the earlier results, quoted by (4). These results for χ_e will be discussed in section 3·3.

3·2·2 Solid metals: analysis of results

The changes in the susceptibilities upon melting, and the values for the solid metals at their melting points are shown in table 3·3.

Table 3.2

Volume susceptibilities of liquid metals at their melting points

metal	χ_{po}^{theo}	χ_{p}^{theo}	$-\chi_{d}^{theo}$	$-\chi_{i}^{theo}$	χ_{e}^{theo}	χ_{e}^{expt}	χ^{expt}	χ^{expt}
	2	3	4	5	6	7	8	9
Ga	1.50	1.99	0.58	1.41	1.41	1.43	0.19	0.023±0.004
Cd	1.23	1.76	0.49	3.04	1.27	1.34	-1.63	-1.700±0.007
In	1.33	1.85	0.52	2.15	1.33	1.40	-0.58	-0.753±0.004
Sn	1.44	1.96	0.55	1.75	1.41	1.41	-0.29	-0.344±0.002
Pb	1.38	1.90	0.54	2.19	1.36	1.36	-0.98	-0.832±0.004
Bi	1.46	1.96	0.56	1.77	1.40	1.22	-0.58	-0.553±0.004
Cu	1.17	1.67	0.48	3.07	1.19	2.19	-1.5	-0.88±0.01
Ag	1.04	1.56	0.41	4.52	1.15	1.95	-3.1	-2.58 "
Au	1.04	1.56	0.41	6.41	1.15	2.96	-5.0	-3.45 "

The values given are $(\chi/10^{-5})$ SI. Column 9 refers to the present work, column 8 from (4), 2 from equation 1.3, 3 from χ_{po} allowing for electron-electron effects, 4 from equation 1.7, 5 from Angus (see chapter 1), 6 from 3 and 4, and 7 from 5 and 9.

Table 3.3

Volume susceptibilities of solid metals at their melting points, and changes on melting

metal	χ^{theo}_{po}	χ^{theo}_{p}	$-\chi^{theo}_{d}$	$-\chi^{theo}_{i}$	χ^{theo}_{e}	χ^{expt}_{e}	χ^{expt}	$\Delta\chi^{expt}$	χ^{expt}	$\Delta\chi^{expt}$
1	2	3	4	5	6	7	8	9	10	11
Ga	1.48	1.96	0.58	1.37	1.38	-0.67	-2.20	2.4	-2.024±0.004	2.065
Cd	1.24	1.77	0.49	3.17	1.28	1.49	-1.95	0.31	-1.678±0.007	0.022
Sn	1.46	1.97	0.55	1.80	1.42	2.04	0.28	-0.57	0.235±0.002	-0.579
Pb	1.40	1.91	0.54	2.25	1.37	0.97	-1.53	0.55	-1.283±0.004	0.451
Bi	1.43	1.94	0.57	1.71	1.37	-8.67	-10.63	10.05	-10.38 ±0.25	9.83
Cu	1.18	1.69	0.48	3.20	1.21	2.46	-0.9	-0.6	-0.74 ±0.01	-0.14
Ag	1.06	1.57	0.41	4.71	1.16	2.40	-2.4	-0.75	-2.31 ±0.01	-0.27
Au	1.06	1.57	0.41	6.77	1.16	3.45	-3.6	-1.4	-3.32 ±0.01	-0.13

The values given are $(\chi/10^{-5})$ SI. Columns 1 - 7 as table 3.2, 8 and 9 from (4), 10 and 11 from present work, with

$$\Delta\chi = \chi_{liq} - \chi_{sol}$$

3·2·3 Temperature coefficients: analysis of results

The behaviour of the pure metal susceptibilities with temperature is summarised in table 3·4. In all cases the electronic susceptibilities are linear with temperature. The values for the solid and liquid states are compared with other literature values and also with the values predicted by a free electron calculation from thermal expansion, due allowance being made for the changes with r_s of the electron-electron enhancement factors. (This last effect contributes about one third as much as does the direct density of states change).

3·3 Discussion

3·3·1 Polyvalent metals

The quite remarkable degree of agreement between the expected and experimentally derived electronic susceptibility for the six polyvalent liquid metals is considered to be a justification of the assumptions made in section 1·1·3, and of the general method adopted. In particular, the results justify the belief that many liquid metals can be accurately described by a free electron model. The implicit assumption that m*=m is validated (see table 3·5). The noble metals (copper, silver and gold) clearly do not fit into this pattern, and will be discussed separately. Further, the value for bismuth, while in slight disagreement, can be explained by assuming m*= 0·93m; the conduction electrons are not completely free of the effects of the ion potential at the melting point. Further evidence for this belief comes from the temperature coefficient of χ, which will be discussed shortly. The picture is more complicated for the solid metals. There are only relatively minor differences between the present results and those quoted in (4). For neither set of experimental values is agreement obtained with the free electron predictions; all the metals require m* = m for the theoretical and experimentally derived

Table 3.4

Temperature coefficients of susceptibility

	solid			liquid		
metal	χ_e' at 293 K	literature	f-e value	χ_e' at m.pt.	literature	f-e value
1	2	3	4	5	6	7
Ga	259±12	279 (11)	-1.2	31.8±6.1	0 (12)	-2.1
Cd	34.2±3.0	26 (8)	-2.3	2.8±3.0	-1 (8)	-2.5
In				3.3±2.5	-2.4 (9)	-2.3
Sn	-9.0±3.0	-7.5 (8)	-2.1	2.0±3.0	0.5 (8)	-2.1
Pb	154±20	145 (8)	-3.2	-6.0±4.0	0.6 (8)	-2.3
Bi	156 "	138 (10)	-0.9	23.3±3.4	60 (10)	-2.5
Cu	1.2±2.0	1.2 (8)	-1.3			
Ag	-10.7±1.8	-12.3 (9)	-2.1			
Au	-4.5±1.2	-16.5 (9)	-1.3			

Columns 2 and 5 are present work; values are $(\chi'/10^{-5})$ SI, where

$$\chi_e' = (1/\chi_e)\,d\chi_e/dT.$$

χ_e values to coincide.

Table 3·5

Implied effective masses at the melting point

metal	solid	liquid
Ga	0·40	1·00
Cd	1·08	1·03
In		1·02
Sn	1·25	1·00
Pb	0·84	1·00
Bi	0·07	0·93
Cu	1·64	1·50
Ag	1·69	1·45
Au	2·33	2·02

In bismuth and gallium, χ_e is found to be negative. Bismuth is known to be a semi-metallic solid, and the open structure of solid gallium may be responsible for tight binding of the electrons.

If m*=m were true for the solid and liquid phases, only small changes would be expected on melting; this is not the case, as is seen by comparing table 3·2 (coloumn 7) and table 3·3 (coloumn 7). The values for m* tabulated are obtained from equations 1·4 and 1·6, matching "experimental" and theoretical χ_e values. The estimates for lead and cadmium are not inconsistent with the low temperature Fermi surface data, (5) and (6) respectively. However, for tin , the Fermi surface data of (7) suggests m* is less than unity, whereas the susceptibility implies a value of 1·25. In all cases the effect of melting is consistent with a reversion of m*/m towards unity; evidently the reversion is not complete for liquid bismuth at the melting point.

The temperature coefficients of χ_e are derived from the observed

variation of total susceptibility and density, the assumption being made that the ionic term (in mass units) does not change. They are compared with the predictions due to thermal expansion. Other literature values are shown for comparison, where available. (The values for bismuth and gallium are over a very restricted range, in the literature). In the liquid phase only lead shows agreement within error with the predicted value. The three metals tin, cadmium, and indium show values which, though they differ in sign, are only different from the expected variation by a small amount in absolute terms. A possible source of error could be a small change in m* with temperature. If m* were to increase by one percent over a range of 100 degK this would be reflected by a net increase in χ_e. The temperature coefficient arising from this process would be of order $+15 \times 10^{-5}$. Clearly, the experimental results are not inconsistent with a value of m* which is greater than 0·995, increasing toward unity at higher temperatures, and thus not inconsistent with the free electron predictions of table 3·2. This type of explanation is almost certainly applicable to liquid bismuth, where m* = 0·93m at the melting point. The large positive value for χ_e' is consistent with an increase of 1 to 2 percent in m* per 100 degK in the liquid. This leaves gallium which shows a similar χ_e' to bismuth, but appears to have a free electron mass already at the melting point. Further, the temperature range covered in the liquid, 1200 degK, would seem to be adequate for any levelling off due to the attainment of the free electron mass to be revealed. No such deviation from linearity is observed, and it seems that an approach of m*/m towards unity will not explain this result. Due to the apparent inapplicability of the free electron approach to solid metals, it is not surprising that in general there is no agreement between prediction and observation for χ_e'. The value for tin is more negative than expected, but it seems unlikely that this results from a

reduction in m* with increasing temperature, because of the Fermi-surface data already discussed. The very large values for bismuth and gallium confirm the failure of free electron ideas in the solid metals. Any real understanding of the values for solid metals requires a full band structure calculation, as has been undertaken (13) for cadmium where the detailed effects of lattice vibrations on the pseudopotential are discussed.

In general it seems that the values for χ_e and χ'_e for the polyvalent metals considered confirm the impression that the free electron approach provides a semi-quantitative explanation for the liquid metals, but that the approach is likely to break down in the case of solid metals.

3·3·2 The noble metals

From the values listed in table 3·2, this approach to the analysis of magnetic susceptibility measurements can be seen to give good agreement with theory for all the liquid metals measured, except the noble metals, where large discrepancies are observed. Following the method of El-Hanany and Zamir (14) for copper, the effects of s-d hybridisation on the density of states at the Fermi level can be estimated for all the noble metals, from a knowledge of the band structure. Such an effect further enhances χ_p and reduces χ_d, yielding a value for m* given by

$$m^*/m = (S/S_f).\ (1/(1-(\frac{V_{sd}}{E_f-E_d})^2)) \qquad (3·3)$$

where the d band is approximated by a single level, E_d, S is the face area of the Fermi sphere, S_f the face area of the equivalent free electron Fermi surface, and V_{sd} the band gap. The assumption is made that $S=S_f$ for gold and silver. Using values of V_{sd} (1·4 eV for Ag, 2·5eV for Au) evaluated from the band structure and E_f-E_d (4·3 eV for Ag, 4·0 eV for Au) from optical measurements, m*/m has been evaluated, yielding values for

χ_p and χ_d shown in table 3·6, along with values derived from the m*/m ratio obtained in (14) for copper.

Table 3·6

Hybridisation effects on χ values of the noble metals

metal	χ_p	χ_d	χ_i	$\chi_{e\text{-liq}}^{expt}$	$\chi_{e\text{-sol}}^{expt}$	χ_e^{theo}
Cu	2·1	0·4	3·1	2·19	2·46	1·7
Ag	1·8	0·4	4·5	1·95	2·40	1·4
Au	2·5	0·3	6·4	2·96	3·45	2·2
1	2	3	4	5	6	7

Column 7 = 2 and 3.

As is apparent from these, the discrepancy is reduced by the introduction of the correction for hybridisation. However, although these results are only an estimation, they imply that the diamagnetic component of the susceptibility is overestimated by 10 percent or more (or that the paramagnetic component is still underestimated). A number of possibilities can be suggested for this, but not quantitatively estimated.

For the noble metals, χ_i is dominated by the contribution from the outer filled d shell. This is readily found to provide 86% of χ_i for copper, 83% for silver, and 82% for gold. Clogston et al (15) have suggested that this contribution may be overestimated by Angus. Slater's rules (section 1·1) state that all electrons in shells lower than the d shell under consideration contribute their full charge to the screening of the nuclear charge. Certainly this cannot underestimate their screening effectiveness; consequently χ_i cannot be overestimated- the better the screening, the larger the distance of outer electrons from the nucleus, and the larger is χ_i .If the rules were modified so that s and p electrons of the same quantum number were assumed to contribute about 0·95 of their charge to screening, then a reduction in χ_i of the required magnitude

would be obtained in each case. This change would certainly affect the noble metals more than other metals, because of the greater significance of their d shell contributions. However, its effect on the polyvalent metals considered in this chapter would be to reduce χ_i by enough to destroy the agreement obtained for χ_e in these cases. It seems likely, therefore, that the core values of Angus are not significantly overestimated, and another source of the discrepancy for the noble metals must be sought. For instance, there may be a paramagnetic orbital component associated with overlapping d sub-bands. This is only one possible suggestion to explain the discrepancy, but clearly the simple approach adopted with success for the polyvalent metals breaks down in the more complicated situation brought about by hybridisation in the noble metals, and close quantitative agreement between theory and experimental predictions is not attainable. For this reason no comparison with Knight shift data will be made for liquid copper. (No measurements are in any case available for liquid silver and gold.)

3·4 Knight shifts: experimental and theoretical results

The experimental values of K obtained for ^{119}Sn, ^{113}Cd and ^{69}Ga in tin, cadmium and gallium respectively are shown in figures 3·8, 3·9 and 8·9; individual values are listed in Appendix 1. Reference compounds were dilute solutions of $SnCl_4$ and cadmium acetate for tin and cadmium respectively and the reference for gallium was taken from the Varian Associates NMR table (5th edition), (10·219 MHz T^{-1}). The linewidths in the liquid states are shown in figures 3·8, 3·9 and 8·8. These all conform to the expected T_1T constant behaviour, where it is assumed that $(T_1)^{-1}$ is proportional to the linewidth. The value of T_1 obtained for liquid gallium at 303 K from the linewidth, 650 s, is in good agreement with actual measurements of T_1, reported in chapter 8.

The values of K and K' in the liquid state at the melting points

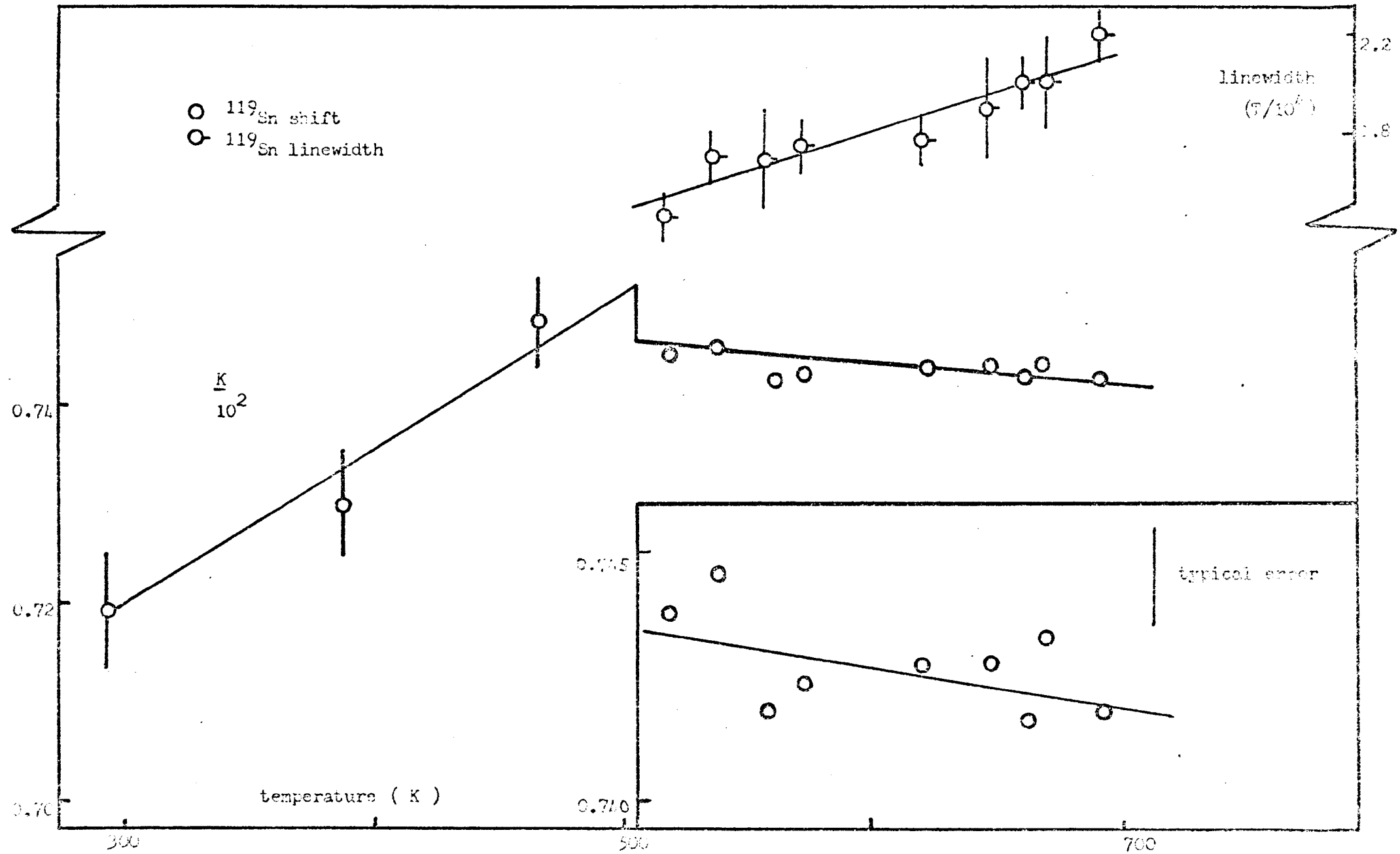

Figure 3.8 ^{119}Sn Knight shift and linewidth in pure tin

Figure 3.9 ^{113}Cd Knight shift and linewidth in pure cadmium

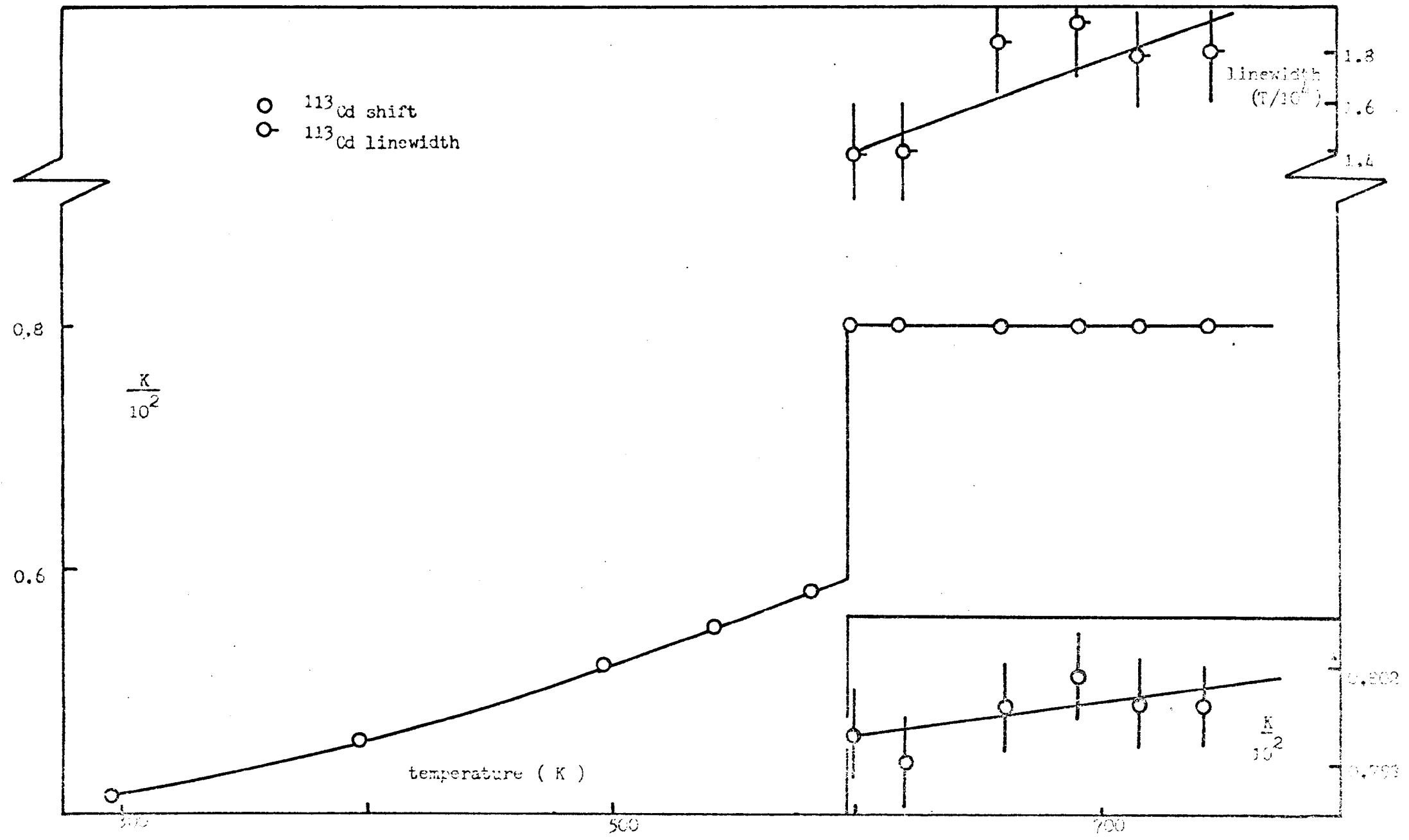

are shown in tables 3·8 and 3·9, column 2, along with values for ^{115}In, ^{207}Pb and ^{209}Bi taken from (1). The new values reported here appear to agree within combined uncertainties with earlier values. K and K' terms calculated as described in section 1·4 (using χ_s from table 3·2, since these give good agreement between χ_e^{expt} and χ_e^{theo}) are given also.

The input parameters for the computer program (Appendix 2) used to calculate ΩP_f are listed in table 3·7. The temperature dependencies of k_f, Ω and η are listed in Appendix 1; $\Omega P_f'$ values are deduced from calculations of ΩP_f at five different temperatures.

Table 3·7

Input parameters for contact density program (in a.u.)

metal	k_f	Ω	R_{core}	$R_{1s}(0)$	$R_{2s}(0)$	$R_{3s}(0)$	$R_{4s}(0)$	$R_{5s}(0)$
Ga	0·884	128·7	1·269	338	105	40·7		
Cd	0·710	165·4	1·406	651	210	91·9	40·5	
In	0·772	192·9	1·323	679	219	97	43	
Sn	0·837	201·6	1·297	696	227	98	45	
Pb	0·833	204·9	1·474	1441	483	230	116	53·5
Bi	0·845	245·3	1·493	1467	492	235	119	55·5

Values of R_{core} are obtained from (16) except for the cadmium term which was taken from (17) and for gallium which was obtained by fitting an Ashcroft form of pseudopotential to one derived from resistivity results (18).

3·5 Discussion of Knight shifts

The fact that the calculated values of K (column 9 of table 3·8) are, on average, about two thirds of the experimental values is probably partly due to the adoption of a simple model potential and partly to the omission of indirect contributions from the theory. The much closer

Table 3·8

Knight shifts of pure liquid metals at their melting points

metal	K^{expt} (%)	χ_E^2	$\frac{1+\Sigma}{\Delta}$	ΩP_f	χ_p	K_s^{opw} (%)	K_s^{theo} (%)
1	2	3	4	5	6	7	8	9
^{69}Ga	0·441	341·5	0·6179	0·0104	214·5	1·99	0·45	0·28
^{113}Cd	0·799	576·2	0·7815	0·0609	413·4	1·76	0·68	0·49
^{115}In	0·786	508·5	0·8308	0·0354	440·4	1·85	0·63	0·54
^{119}Sn	0·743	492·2	0·8010	-0·0816	414·6	1·96	0·65	0·54
^{207}Pb	1·49	1164·3	0·6120	0·0762	799·4	1·90	1·47	1·01
^{209}Bi	1·41	844·4	0·6513	0·0757	613·9	1·96	1·13	0·80

K^{opw} is derived using ΩP_f from the OPW term only, (section 1·4).

Column 7 in units of (1 /10 ^{5}) SI; columns 3,4,5 defined in 1·4·2.

Table 3·9

Temperature coefficients of Knight shifts in pure liquid metals

metal	K'_{expt}	$\Omega P'_f$	χ'_e	χ'_p	K'_{theo} (from 3,4)	K'_{theo} (from 3,5)
1	2	3	4	5	6	7
^{69}Ga	-8·5	-14·6	31·8	-2·3	17·2	-16·9
^{113}Cd	$1·7_6$	5·0	2·8	-2·8	7·8	2·2
^{115}In	-7·7	-4·0	3·3	-2·3	-0·7	-6·3
^{119}Sn	$-1·5_5$	-3·5	2·0	-2·2	-1·5	-5·7
^{207}Pb	-6·7	-6·4	-6·0	-2·3	-12·4	-8·7
^{209}Bi	-9·0	-3·4	23·3	-2·7	19·9	-6·1

All quantities in K^{-1}/ 10 ^{5} ; column 4, "experimental" values from table 3·4; column 5, theoretical values for interacting free electrons deduced as in section 3·2·3.

agreement between experiment and theory found using only the OPW term in the contact density (column 8 of the tables) is almost certainly fortuitous, since this ignores the effect of the pseudopotential altogether. The values in column 8 differ slightly from those found in (1) using a similar method; the present values are to be preferred since they use an improved χ_p and a more rigorous calculation of χ^2_E. The great advantage of the Perdew and Wilkins formulation of the perturbation term due to the pseudopotential $(1+\xi+\Delta)$ is that a first order calculation gives acceptable results in that $\xi+\Delta$ is small compared with unity. This was certainly not always the case with earlier formulations (19) where orthogonalisation was not explicitly included for all components of the pseudofunction (1). The value of ΩP_f is reduced by about one percent and the temperature dependence is reduced in magnitude (to about $-1{\cdot}5 \times 10^{-5}$) when an experimental rather than a hard sphere model structure factor is used for tin. (The structure factor used was obtained by (20).)

However, it seems that although there may be considerable uncertainty in the absolute magnitude, relative changes in the Knight shift with temperature (and concentration) can be predicted with better accuracy. This was also found by Perdew (21) who suggested that the reason lay in the partial cancellation of the electron-ion potential and indirect contributions (both major causes of uncertainty in ΩP_f) from the fractional change, $\delta(\Omega P_f)/\Omega P_f$, upon heating or alloying. Certainly the values for K' (column 7, table 3·9) can be predicted with better accuracy here, and are quite close to the experimental values, particularly if the assumption that χ_p' comes simply from a free electron response to thermal expansion is adopted. (This is also true for liquid bismuth, and appears to contradict the earlier evidence in favour of a changing m*). It is not surprising that this assumption is better than

using "experimental" χ_e' values since these may contain other effects, such as changes in the diamagnetism with temperature, which do not affect χ_p. It is particularly interesting that the theory reproduces the exceptional positive sign of K' for cadmium; this certainly seems to provide strong evidence of the essential correctness of the theory. This positive sign arises in the $\alpha P_f'$ term and is due to the divalent state of cadmium, reflected in k_f. Certainly if k_f for indium is changed so as to correspond to a divalent or a tetravalent state, the resulting temperature coefficients for "pseudo-indium" are very close to the values obtained for cadmium and tin respectively (5·9 and -3·1 in the units of table 3·9). This indicates that k_f is the dominant factor in determining the temperature coefficient, the main effect being observed in the $1+\xi$ term (although present in the others).

It is worth making two final notes about Knight shift calculations. Jena et al (22) have recently carried out a calculation for liquid cadmium, using a formulation which is in principle similar to that of Faber (19), arriving at a value for the shift close to that found in the present work. With the same χ_p enhancement factor as used here, and ignoring indirect effects, it is 0·52 percent (see table 3·8). The values for all the metals were obtained using the free interacting χ_ps of section 3·2, since these gave excellent agreement with the χ_e values derived from experiment and theory. It is equally possible to use an "experimental" χ_p (i.e. $\chi_e^{expt} + \frac{m}{m^*}\chi_d$). This causes negligible differences except for bismuth where K_s^{theo} becomes 0·74 percent.

Finally, the NMR of tin and cadmium show anisotropic lines in the solid, which reflect the non-cubic environment. The values of the enhancements of the Korringa products are 1·08 and 1·16 for tin and cadmium respectively; these are similar to results found for many other

metals (4) and are believed to be due to electron-electron enhancement effects. There is a similar (1·21) enhancement for gallium. The NMR of these metals is further discussed in the respective alloy chapters.

References

1) Heighway J. and Seymour E.F.W., Phys. kondens. Materie, 13, 1-8, 1971.

2) Smithells C.J., Metals Reference Book, p.688, Butterworths, London, 1967.

3) Wilson J.R., Metall. Rev., 10, 381-590, 1965.

4) Dupree R. and Seymour E.F.W., The Physics and Chemistry of Liquid Metals, (ed. S.Z. Beer), chapter 11, Dekker, New York, 1972.

5) Anderson J.R. and Gold A.V., Phys. Rev., 139A, 1459-81, 1965.

6) Stark R.W. and Falicov L.M., Phys. Rev. Lett., 19, 795-98, 1967.

7) Weiss G., Phys. Rev., 149, 504-18, 1966.

8) Collings E.W., Phys. kondens. Materie, 8, 284-304, 1969.

9) Hellwege K.H., Landolt Bornstein Zahlenwerte und Funktionen aus Physik, volume 2, p.15, Springer Verlag, Berlin, 1962.

10) Nachtrieb N.H., J. Phys. Chem., 66, 1163-7, 1962.

11) Marchand A., Comptus Rendus, 241, 468-70, 1955.

12) Wachtel E. and Nier K.J., Z. Metallkunde, 56, 779-89, 1965.

13) Katsuki S. and Tsuji M., J. Phys. Soc. Japan, 20, 1136-45, 1965.

14) El-Hanany U. and Zamir D., Phys. Rev., 5B, 30-40, 1972.

15) Clogston A.M.,Jaccarino V. and Yafet Y., Phys. Rev., 134A, 651-61, 1964.

16) Ashcroft N.W. and Langreth P.C., Phys. Rev., 159, 500-10, 1967.

17) Tomlinson J.L., Phys. Rev., 187, 341-45, 1969.

18) Cohen M.L. and Heine V., Solid State Physics, 24, 38-249, 1970.

19) Faber T.E., Adv. Phys., 16, 637-51, 1967.

20) North D.M.,Enderby J.E. and Egelstaff P.A., J. Phys. C, 2, 1075-87, 1968.

21) Perdew J.P., Ph. D. thesis, Cornell University, 1971.

22) Jena P.,Das T.P.,Gaspari G.D. and Halder N.C., Phys. Rev., 3B, 2158-68, 1971.

Chapter 4

Knight shifts and susceptibilities across some complete alloy systems

4·1 Introduction

The correlation of experimentally derived spin susceptibilities with experimental Knight shifts is pursued in this chapter, where binary alloys of several polyvalent metals are considered. It is intended to extend the successful calculation of the temperature coefficient of K in pure metals (section 3·4) to the concentration dependence in alloys. Furthermore, the behaviour of the Korringa product (section 1·2) in simple alloy systems is studied. In treatments of systems in which quadrupolar interactions or partial localisation of conduction electrons occur, it is generally assumed that the Korringa relation would have been obeyed in the absence of these effects. It is not obvious that this must be so with the changing electron density, upon alloying. Tin and cadmium both have isotopes with spin quantum number, I, equal to $\frac{1}{2}$, and consequently for which no quadrupolar contributions are possible. Both metals have convenient melting points, are neighbours in the periodic table, and do not form intermetallic compounds with each other, (1). The experimental variations of the ^{113}Cd and ^{119}Sn Knight shifts in Sn-Cd alloys have been compared with the theoretical expectations in both solid and liquid alloy phases, and with the information available from the phase diagram for the system (1) shown in figure 4·1. For this, experimental observations of the ^{113}Cd and ^{119}Sn Knight shifts and linewidths, density, and magnetic susceptibility were made.

Further, earlier experimental results of the ^{207}Pb and ^{209}Bi Knight shifts in liquid lead-bismuth alloys (2) have been correlated with the susceptibility and pseudopotential-approach contact density changes (in order to gauge the success of this method for heavy elements) in the same

way as for the tin-cadmium alloys; the approach is explained in section 1·3·4. Finally, experimental variations of ^{209}Bi and ^{119}Sn in the liquid tin-bismuth system (3) are treated in the same way, in order to compare the behaviour of one element in two distinct systems, and because of the strong similarities of the behaviour of the Knight shifts in this system and Pb-Bi.

4·2 Tin-cadmium system: experimental results and discussion

4·2·1 Density : experimental results

In order to obtain χ_p in the by now familiar expression

$$K_s = (2/3)\chi_p \Omega P_f \qquad (4·1)$$

it is necessary to know the density of the metal, since χ_p (in volume units) must be derived from χ (in mass units) as for the pure metals of chapter 3. Measured values of the densities of alloys are not available in the literature for many binary systems. The assumption that Vegard's law is applicable may or may not be true.(This states that the density of an alloy is given by a linear interpolation in concentration between the pure metal values.) For systems which have been investigated, the law was only sometimes found to be obeyed. Consequently the densities of some alloys of these two metals were measured, by the pycnometer technique described in section 2·2·2. The results are shown in figure 4·2 and Appendix 1. The maximum deviation from the linearly interpolated density is 2 percent, indicating that Vegard's law is not greatly in error for this system.

4·2·2 Magnetic susceptibility: experimental results

χ in these alloys was investigated as a function of both concentration and temperature in the solid and liquid phases. The results are plotted isothermally across the system at 293 K and 618 K in figures 4·3 and 4·4 respectively and the detailed measurements given in Appendix 1. The

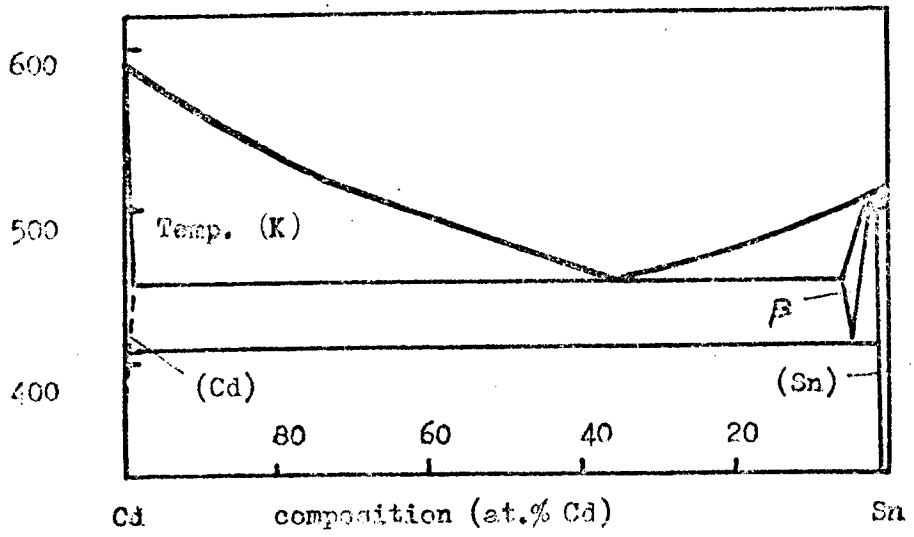

Figure 4.1
Phase diagram
for Sn-Cd system

Figure 4.2
Density of Sn-Cd alloys at 618 K

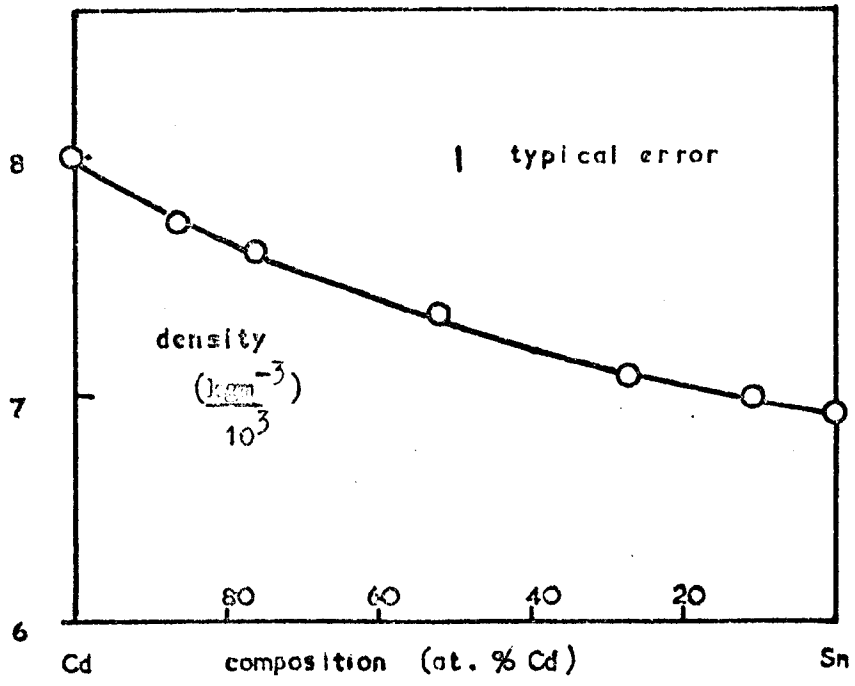

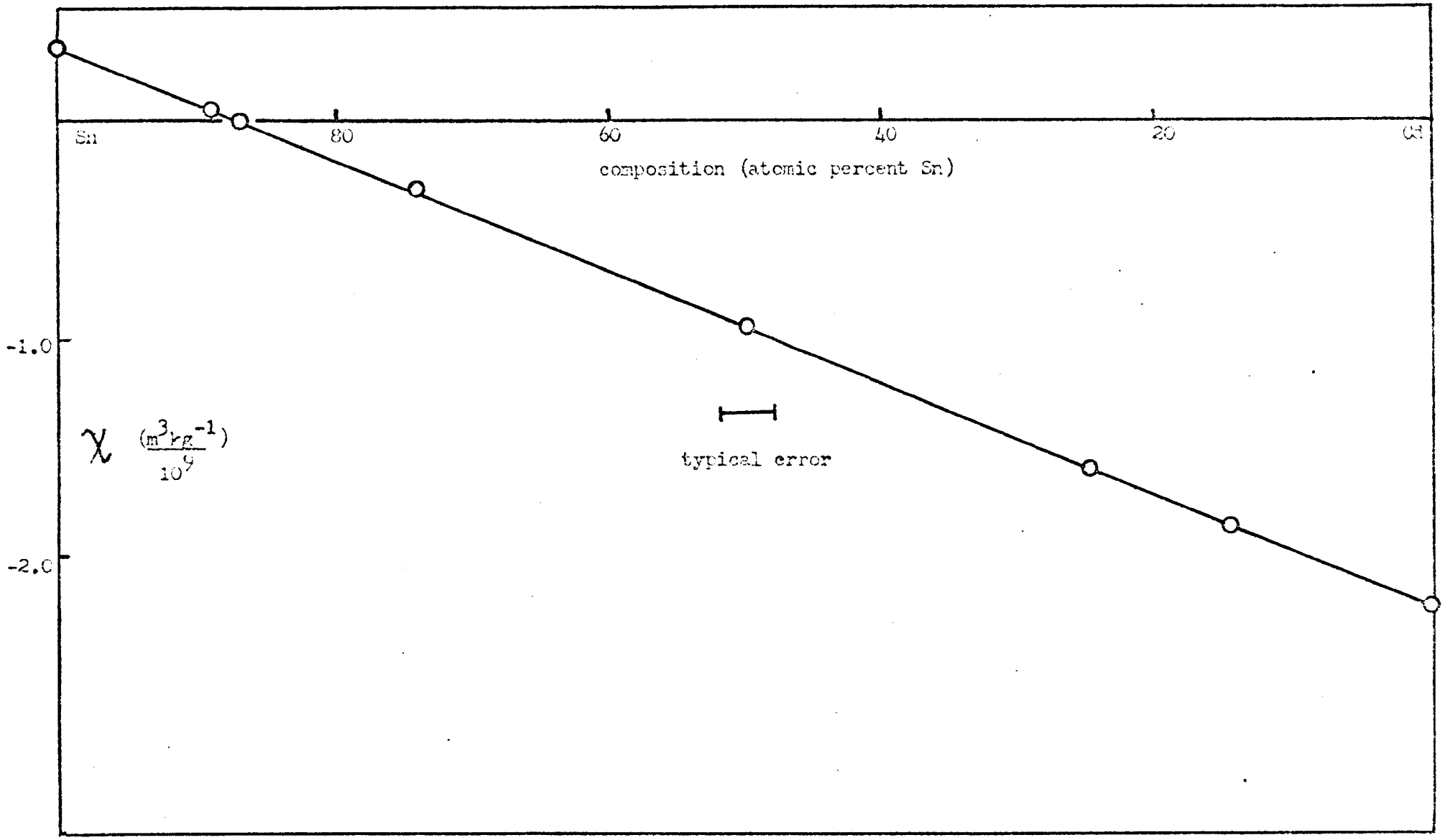

Figure 4.3 Magnetic susceptibility of Sn-Cd alloys at 298 K

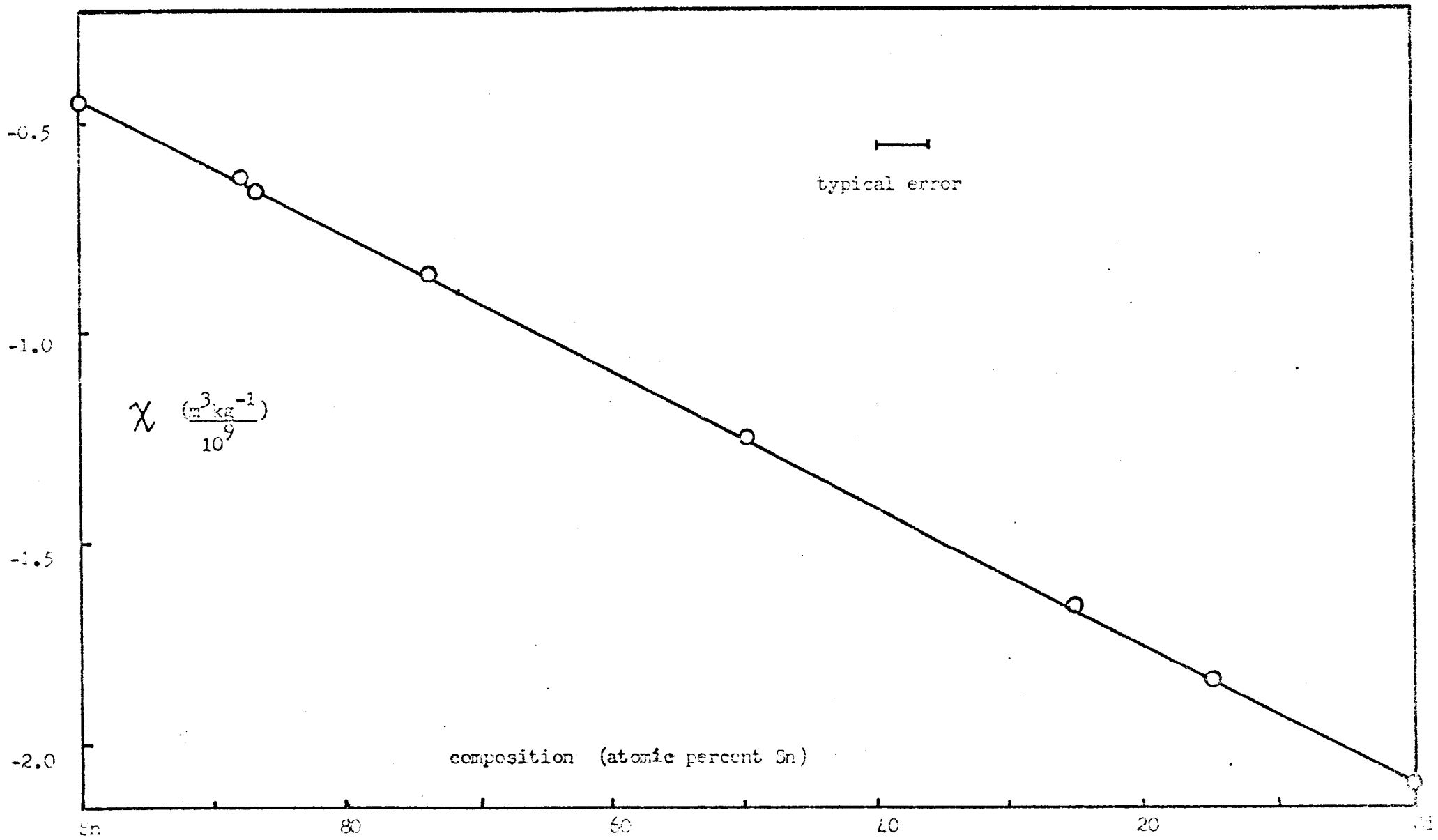

Figure 4.4 Susceptibility of Sn-Cd alloys at 618 K

temperature dependence of susceptibility is non-linear in the solid phase, showing a marked decrease in χ between about 380 K and the liquidus. The phase diagram (figure 4·1) leads one to expect some such changes. In the liquid the susceptibility increases linearly with temperature; the temperature coefficient $(1/\chi)(d\chi/dT)$ appears to vary linearly between the two pure metal values, as shown in figure 4·5.

4·2·3 NMR: experimental results

Both the ^{113}Cd and ^{119}Sn Knight shifts were measured with concentration and at different temperatures in the alloys. Similarly, linewidth measurements were made in the liquid phase. The results for these quantities in the two pure metals have already been given in section 3·5. The results for the alloys are best presented graphically (with detailed results in Appendix 1). Figures 4·6, 4·7, and 4·8 show the change in K with concentration for the liquid alloys at 618 K, ΔK/K with concentration for the solid alloys at 293 K, and the liquid alloy linewidth with concentration at 618 K, respectively, for the ^{119}Sn resonance. Figures 4·9, 4·7, and 4·8 show the same quantities at the same temperatures for the ^{113}Cd resonance.

The temperature variations of both widths and shifts in the alloys were not found to be any different from their behaviour in the pure metals; that is, although both quantities were affected by alloying, the change of the resonance line position and increase of width with temperature were similar to the pure metal behaviour.

4·2·4 Magnetic susceptibility: discussion

The behaviour of χ in the solid phase at room temperature is compatible with the information available on the system from figure 1. The linear dependence of χ on concentration is as expected for a solid which will be a mixture of almost pure tin and almost pure cadmium phases.

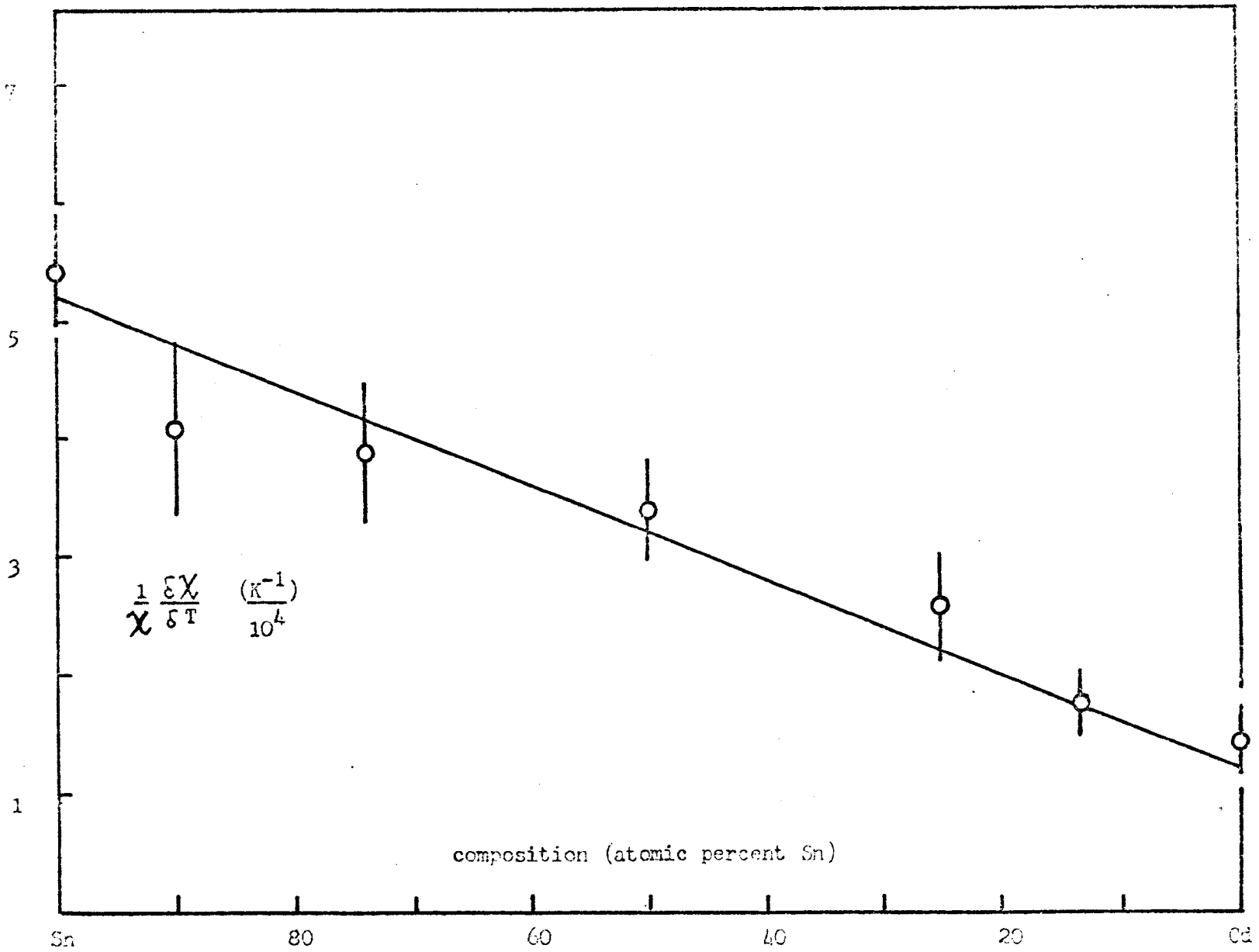

Figure 4.5 Temperature coefficient of susceptibility in Sn-Cd alloys at 673 K

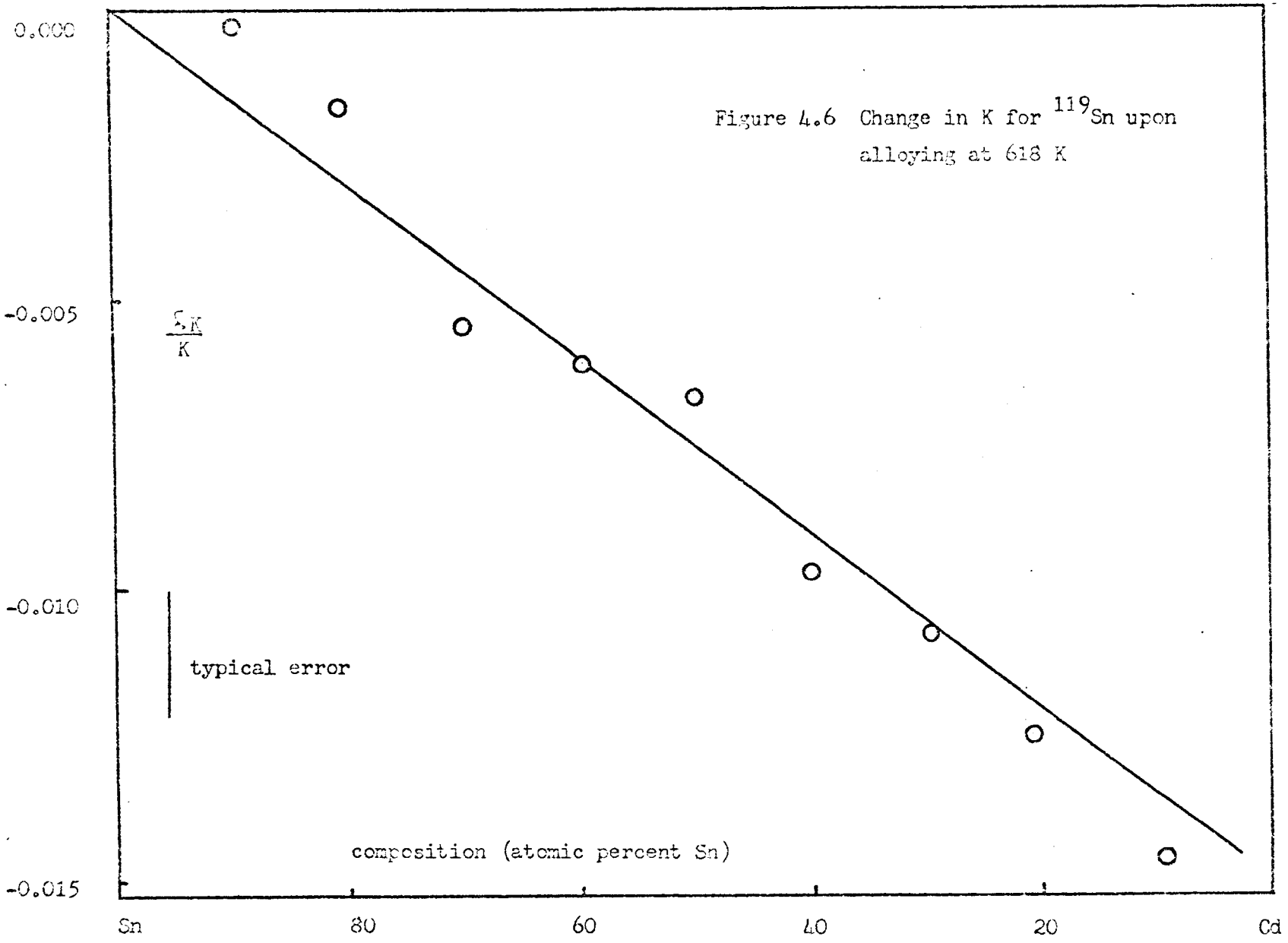

Figure 4.6 Change in K for ^{119}Sn upon alloying at 618 K

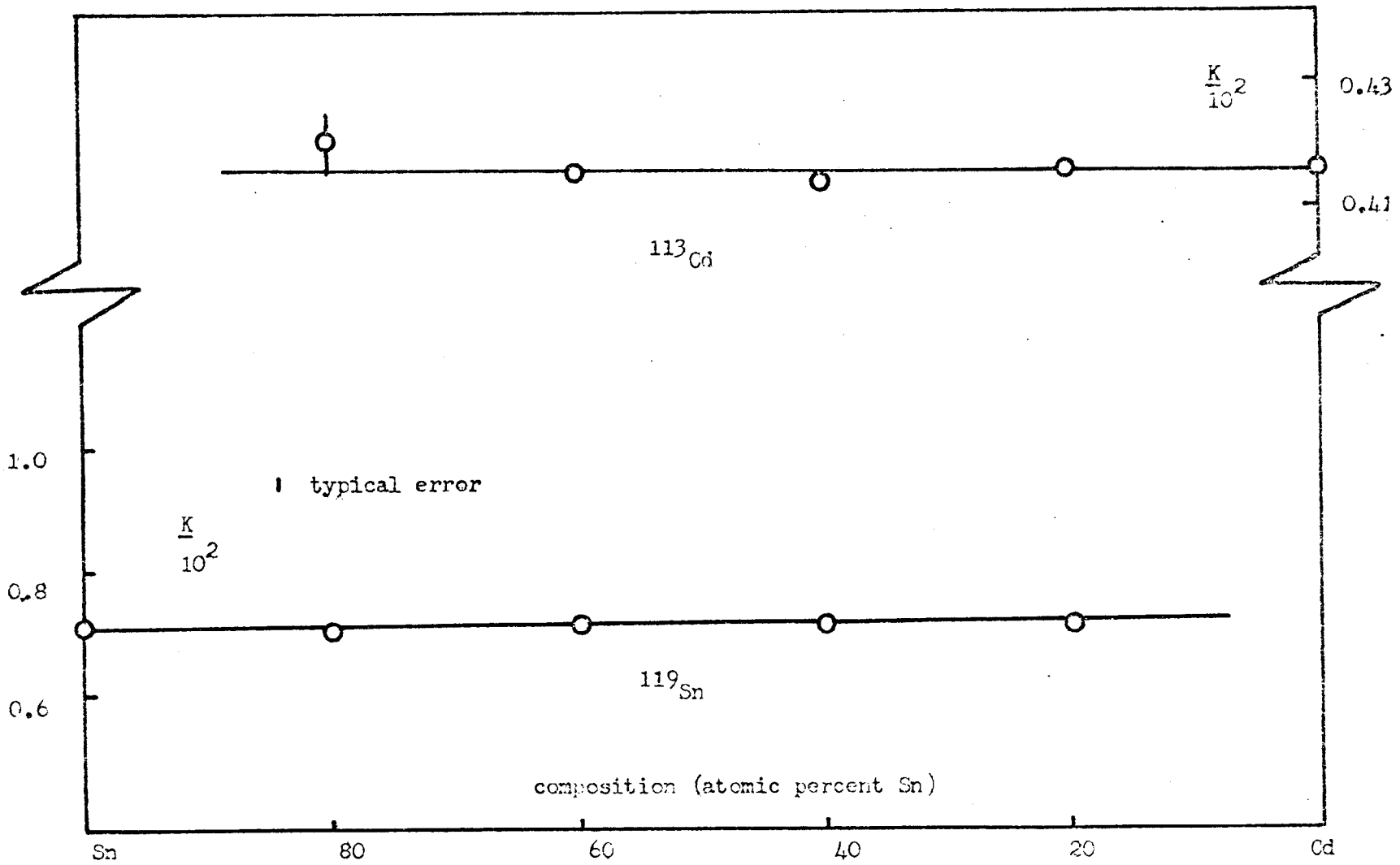

Figure 4.7 Knight shifts at 293 K for ^{113}Cd and ^{119}Sn in Sn-Cd alloys

Figure 48 ^{113}Cd and ^{119}Sn linewidths in Sn Cd alloys at 618 K

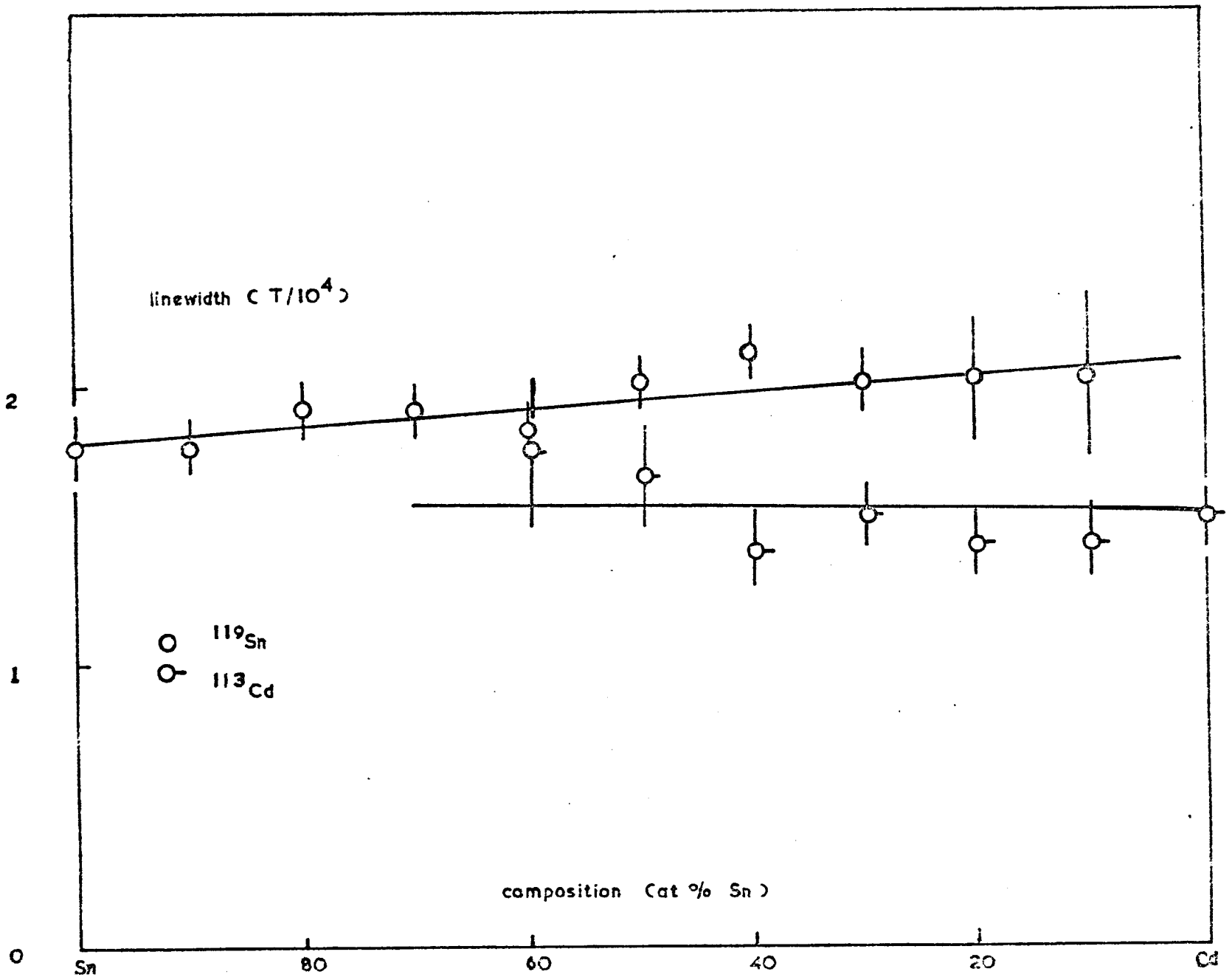

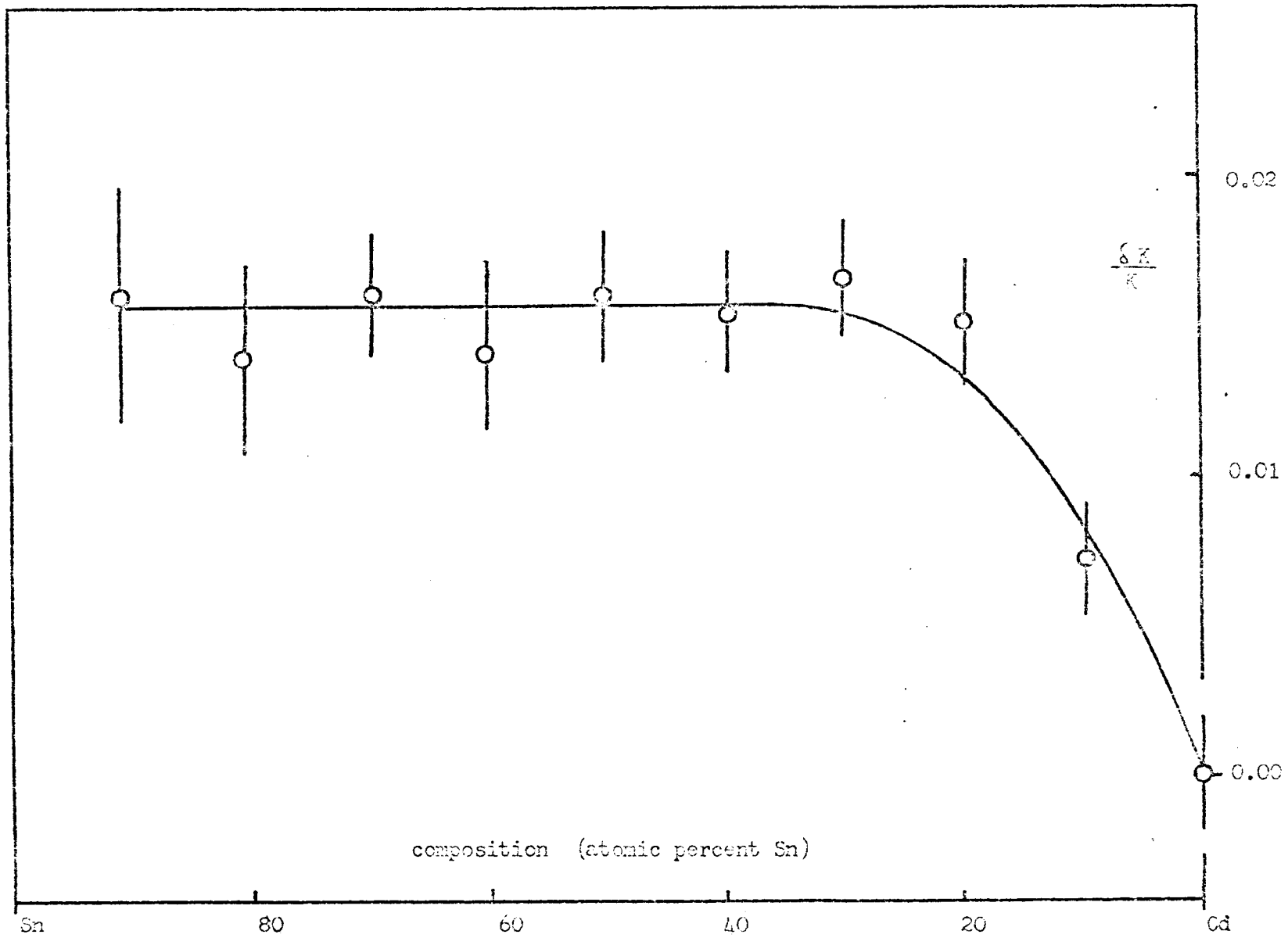

Figure 4.9 Change in K for ^{113}Cd upon alloying in Sn-Cd system at 610 K

In the liquid alloys (figure 4·4) this linear dependence still exists, the susceptibility varying smoothly between the two pure metals, as expected if all of the valence electrons form part of the conduction band, none being used for any sort of molecular bonding.

The susceptibility is analysed in terms of χ_e and χ_i as discussed in section 1·1. The assumption is made that χ_i is a weighted sum of the pure metal core values. This is an approximation, since χ_i can be expected to be affected by the electronic environment to some extent. However, it must be remembered that there will be some uncertainty in the absolute magnitude of χ_i for the pure metals. These values are calculated ones, found by assuming that the cores (of valence indicated by the column of the metal in the periodic table) and the conduction electrons are independent. Further, the linearity of χ with composition would appear to lend support to the view that χ_i cannot be behaving markedly differently in the alloys. Thus, the approximation is believed adequate. χ_e^{expt} (in volume units) is obtained from the measured χ (in mass units) and the measured density. It is shown in figure 4·10. The change in χ_e^{expt}, which varies smoothly between the values for the pure liquid metals, is 4 percent. The values of χ_p, the spin susceptibility consistent with the χ_es, vary smoothly between the pure metals also. Now,

$$\chi_p = (m/m^*)\chi_d^{theo} + \chi_e^{expt} \quad \text{(see table 3·2)},$$

where m* and the enhancement of χ_{do} vary linearly between the pure metal values at the approriate temperature. (These two corrections are small, so that the assumption of linearity is not of great importance.) χ_p is also shown in figure 4·10. The value for $(1/\chi_p)(d\chi_p/dc_p)$ in table 4·3 is derived from this result. The linear behaviour of the temperature coefficient (figure 4·5) in the liquid underlines the simple behaviour of these alloys.

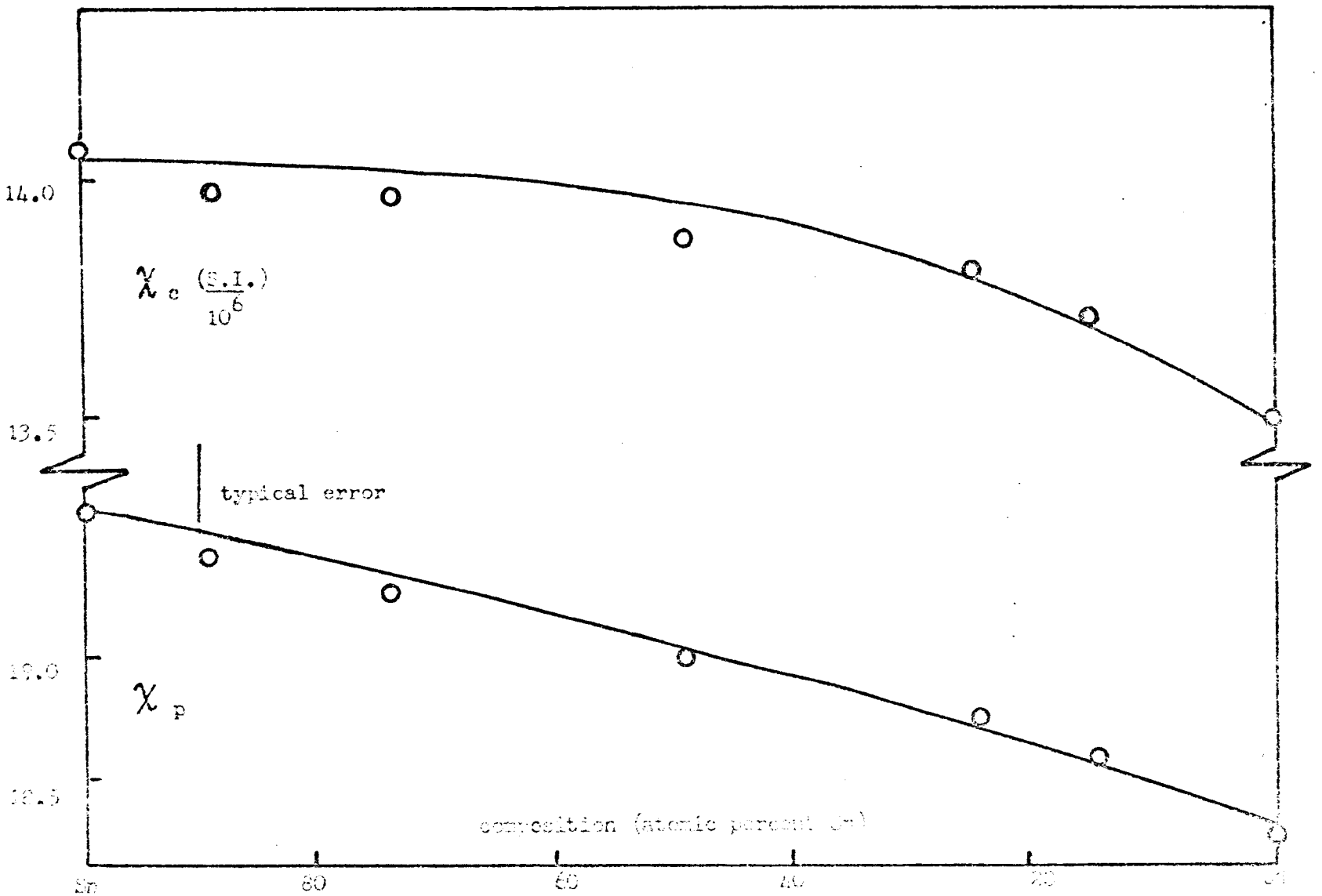

Figure 7.10 Derived electronic and spin susceptibilities in Sn-[illegible]

4·2·5 NMR: discussion

The behaviour of the ^{113}Cd and ^{119}Sn shifts in the solid alloys are also consistent with the existence of almost pure tin and cadmium phases. The resonance signals weaken in intensity with decreasing metal concentration, but the position of the line does not alter. Above 406 K (figure 4·1) the ^{119}Sn signal disappears (reappearing in the liquid), but the ^{113}Cd signal remains. This phenomenon must be due to the presence of the β-phase, which removes most of the tin from its almost pure phase; it appears that equilibrium is reached within the timescale of the experiment. It should be noted that for both metals the resonance signals are anisotropic in the solid, and the centre for the purposes of defining the Knight shift is taken as the crossover point of the derivative of the absorption signal.

The main point of interest here as far as the NMR is concerned is the behaviour of the ^{113}Cd and ^{119}Sn resonance signals in the liquid alloys. As can be seen from figure 4·6, the ^{119}Sn shift changes linearly by about 2 percent. Fron figure 4·9, the change for the ^{113}Cd resonance, in the same direction, is about the same size but is distinctly non-linear, with a large initial slope. These results should be compared with the χ data, which also shows only small changes on alloying. The comparisons with predicted changes in ΔP_f will be made in section 4·2·6. The linewidth data (figure 4·8) yield values for the longitudinal spin-lattice relaxation times, T_1, as described in section 1·2·1 (with the assumption that $T_1=T_2$; direct pulse measurements of T_1 were not found possible). From this, the Korringa product and its enhancement by electron-electron interactions can be evaluated, assuming only direct contact terms are important. This was done for the two pure metals in section 3·5. For ^{119}Sn, the Korringa product $K_s^2T_1T$ appears to decrease upon alloying, changing by (-12 ± 10) percent across the whole composition range. Since

the size of the observed change is of the same order as the experimental error, it is probably true that no significant change takes place. Certainly, for the ^{113}Cd resonance the Korringa product does not change upon alloying. Thus, for this system at least the Korringa relation holds for the alloys equally well as for the pure metals.

4·2·6 Contact density: partial wave analysis

Comparison of expected and measured values of the Knight shifts in the alloys can be made if the change in $|\psi_f|^2$ with concentration can be obtained. Following either the method of partial wave analysis (or phase shift analysis) or the pseudopotential approach ,both described in section 1·4, values of this quantity can be evaluated.

The phase shift method relies on calculated Blandin and Daniel coefficients (4) and phase shifts derived from model potentials. The method of calculating the coefficients was explained in section 1·4·1 (using a hard sphere model structure factor), and the values obtained for tin and cadmium are shown in table 4·1.

Table 4·1

Blandin-Daniel coefficients

host	A_0	A_1	A_2	A_3	B_0	B_1	B_2	B_3
tin	-0·06	-0·02	0·80	1·79	-0·07	0·26	-0·33	-0·47
cadmium	-0·22	1·23	-3·03	-0·25	0·20	-0·46	-0·36	2·75

The calculation of the phase shifts will now be considered, using two different model potentials.

Square well potential. This is the simpler of the two models considered. It has been adequately described elsewhere (4). The Schroedinger equation is solved both inside and outside a spherically symmetric square well potential, which has a radius equal to that of the solute ion it is

representing. From the analytic solutions in terms of partial waves, for the incident and scattered electron wavefunctions, the phase shifts δ_l (where l refers to the lth partial wave) are determined by matching the electron wavefunctions at the potential boundary. The depth of the well is varied until the δ_ls satisfy the Friedel sum rule (5),

$$Z' = \frac{2}{\pi} \sum_l (2l+1)\, \delta_l(k_f) \qquad (4\cdot2)$$

where Z' is the effective charge on the impurity modified by volume dilation ($Z' = Z_F - Z_E(\Omega_F/\Omega_E)$, E is solvent, F is solute). This rule arises because the total screening charge below the Fermi level must equal Z'.

Screened free atom potential. This model has been fully described by Host (6). Briefly, the self consistent atomic potentials of Herman and Skillman (7) are used for the impurity, together with a variable parameter X which adjusts the height of the potential. Essentially, X provides the screening shell at a distance $r = R_T$ from the centre of the ion, since the model potential meets the bottom of the conduction band, cb at R_T. At this point it is terminated. The Schroedinger equations are solved as before, matching wavefunctions at R_T. The parameter X is varied until the Friedel sum rule is satisfied as above. This model potential is shown schematically here, and the values for the phase shifts derived from the two models are shown in table 4·2, those of $(1/\Omega P_{f_E})(d(\Omega P_{f_E})/dc_F)$, $c_F \to 0$, in table 4·3. The comparison with the observed Knight shifts can be made by using the expression

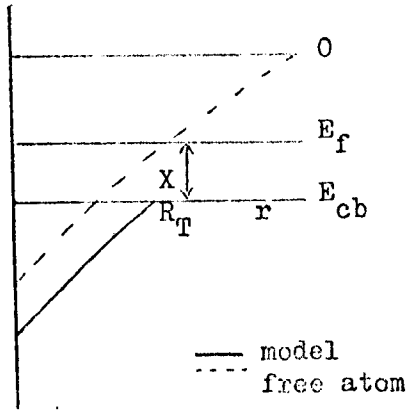

$$\Gamma_{theo} = \frac{1}{K_s}\frac{dK_s}{dc}\Big|_F^E = \frac{1}{\chi_p}\frac{\chi}{dc_F^p} + \frac{1}{\Omega P_{fE}}\frac{d(\Omega P_{f}}{dc_F}\Big|^E \qquad (4\cdot3)$$

for the initial values, where E is the solvent host, F is the impurity. It is seen from table 4·3 that the more sophisticated approach of the screened free atom potential yields closer agreement with the experimental results; the simpler approach gives the correct sign, but the wrong order of magnitude. So far the discussion has been concerned with the change in the solvent shift. A similar analysis is possible for the rate of change of the solute shift (extrapolated to the neighbourhood of zero concentration). The results should be numerically the same as for the solvent shift. Phase shift analysis cannot account for different rates of solute and solvent shift changes at the same point in the concentration range.

Table 4·2

Phase shifts

system (host underlined)		δ_0	δ_1	δ_2	δ_3	Z'
Cd in Sn	(SW)	-0·7410	-0·2965	-0·0645	-0·0075	-1·280
	(SFA)	-0·7371	-0·1511	-0·1657		-1·285
Sn in Cd	(SW)	0·3275	0·3768	0·1565	0·0263	1·560
	(SFA)	0·6185	0·6341	0·0091		1·634

SW = square well potential

SFA = screened free atom potential

Table 4·3

Partial wave analysis results for effect of alloying on K for ^{119}Sn and ^{113}Cd

signal 1	Γ_{expt} 2	χ^1_p 3	ΩP^1_{fE} 4	Γ_{theo} 5
^{119}Sn	-0·015 (0)	-0·07	0·07 [-0·04]	0 [-0·11]
^{113}Cd	0·12 (0·015)	0·07	0·10 [-0·08]	0·17 [0·02]

Figures in square brackets refer to S.W. results; column 5 is obtained from column 4 + column 3; figures in brackets in column 2 are for the other signal at the same concentration; χ^1_p and ΩP^1_{fE} are 2 nd and 3 rd terms of equation 4.3.

4·2·7 Contact density: the pseudopotential approach

This method has been fully described in section 1·4. The input parameters are listed in table 4·4. These are slightly different to

Table 4·4

Input parameters at 618 K (in a.u.)

metal	k_f	Ω	R_{core}	R_{1s}	R_{2s}	R_{3s}	R_{4s}
tin	0·834	203·6	1·297	696	227	98	45
cadmium	0·710	165·4	1·406	651	210	92	40·5

the values used in the pure metal chapter, since the calculation was performed for a constant temperature 618 K in the present case, not at the metal melting points. The assumptions of the model pseudopotentials and structure factors, and that the packing fraction is 0·45 throughout, are as described in section 1·4.

The values obtained for the changes in ΩP_f with concentration, across the entire range are shown in figures 4·11 and 4·12 for ^{119}Sn and ^{113}Cd respectively. It is perhaps worth repeating at this point that the pseudopotential approach yields changes across the whole range, unlike the partial wave approach, which gives only initial values. The changes in ΩP_f are, in both cases, larger than expected from the experimental K and derived χ_p results, but are of the correct sign, overall. The experimentally derived changes are also shown in these figures. As explained in section 1·4, an attempt to improve agreement can be made by making R_{core} energy dependent.(This does not strictly introduce full non-locality.) When this is done with values of α =0·25, β =0·05 (tin as host), the results for ΩP_f are in good agreement with experiment (figures 4·11 and 4·12 again). These values of α and β represent only very small changes (a few percent) in R_{core} over the concentration range. Thus R_{core} values are quite critical in determining ΩP_f. (The values of α and β are of course reversed when cadmium is host.)

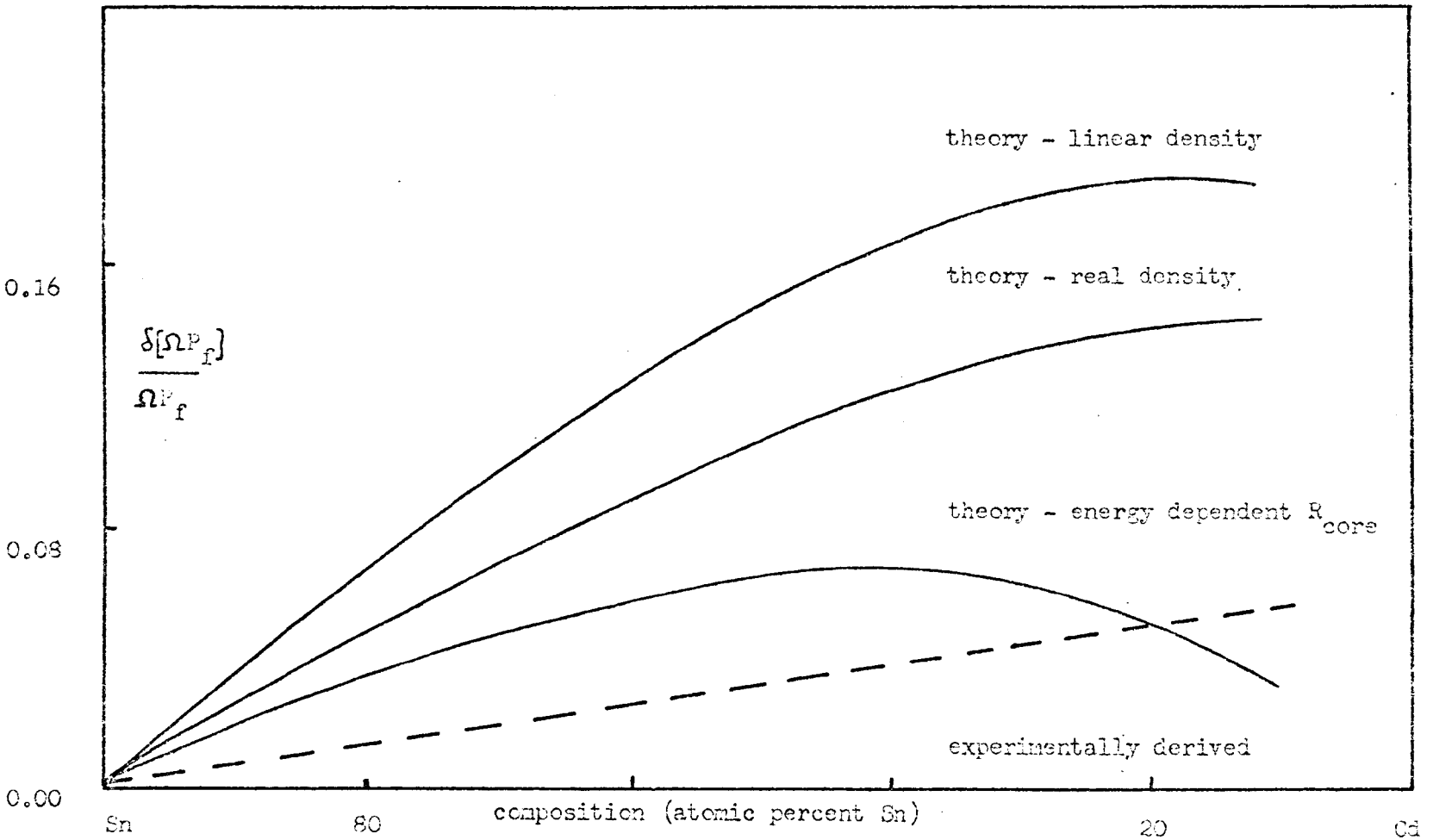

Figure 4.11 Contact densities for ^{119}Sn in Sn - Cd alloys at 618 K

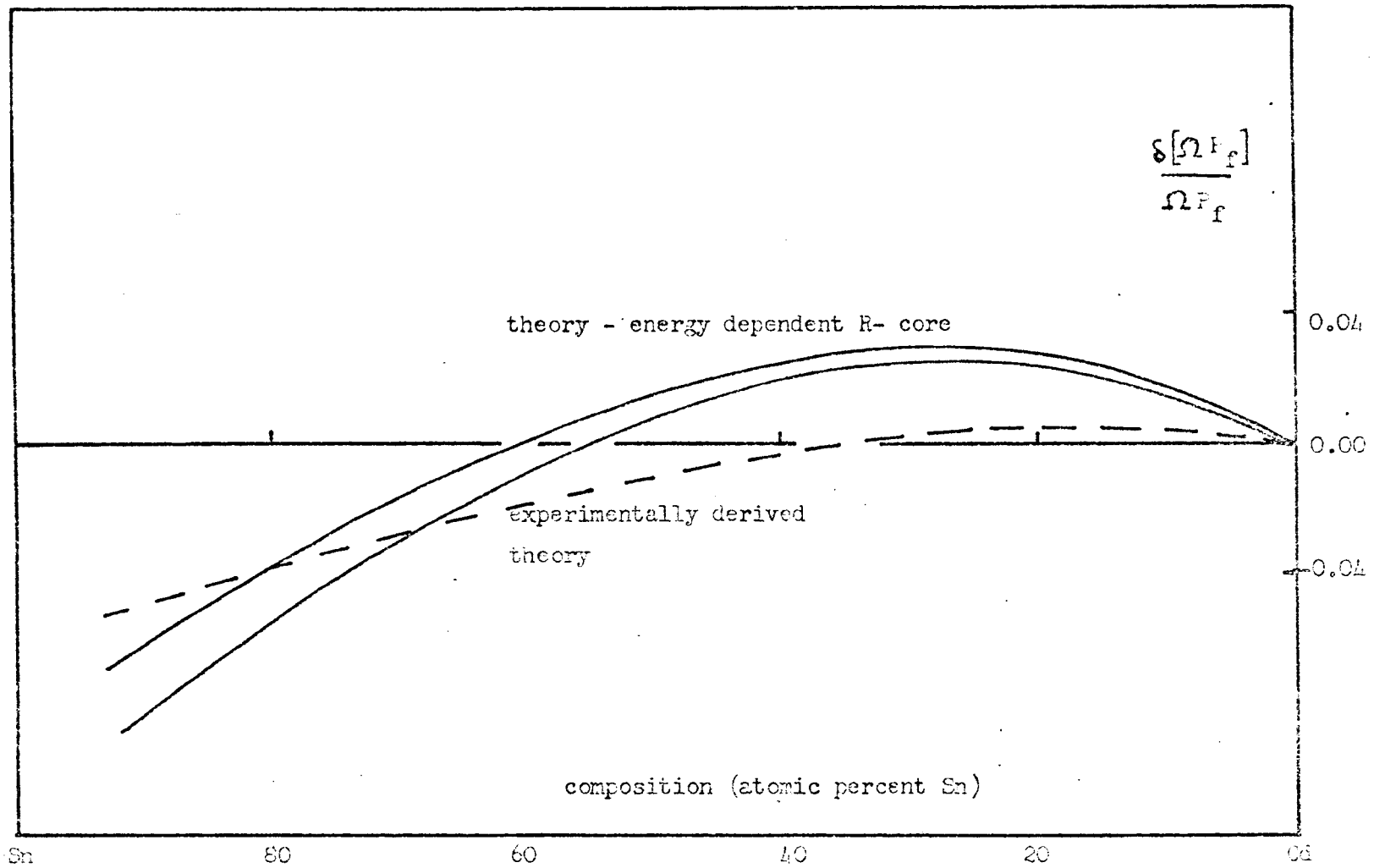

Figure 4.12 Contact densities for ^{113}Cd in Sn - Cd alloys at 618 K

Values of the energy dependence of R_{core} have been obtained from the thermopower for the alkali metals (8) which are similar in magnitude and sign to those above. It is considered that an attempt to obtain a value from the thermopower of tin (and of cadmium) would be of interest. Such an approach is under consideration (G.A.Styles: private communication). It should also be noted that the values of α and β obtained in the present work were found to be virtually independent of each other.

That a non-local pseudopotential is necessary for cadmium at least has been shown (9). Figure 4·13 shows the R_{core} concentration dependencies derived. These results clearly imply that for both tin and cadmium, a more sophisticated non-local pseudopotential is required to describe the values fully. The effect of using real densities, rather than linearly interpolated atomic volumes, can be studied by modifying the computer program accordingly. This was attempted for ^{119}Sn, using the values of density given in figure 4·2. The results only marginally affect the ΔP_f variations found (figure 4·11). Unlike the case of pure tin (section 3·5), use of an experimental structure factor is not possible, since the partial structure factors are not known in these alloys.

To summarise, it appears that both the pseudopotential approach and the method of partial waves yield reasonably good agreement with the experimental results for the changes in the ^{113}Cd and ^{119}Sn Knight shifts upon alloying in this system. The agreement for the pseudopotential method confirms the expectation of section 3·5, that this method is better for fractional changes in K than for its absolute magnitude.

4·3 Lead-bismuth system: results and discussion

4·3·1 Experimental results

The magnetic susceptibilities of alloys of lead and bismuth were measured isothermally in the liquid at 623 K (figure 4·15). A linear

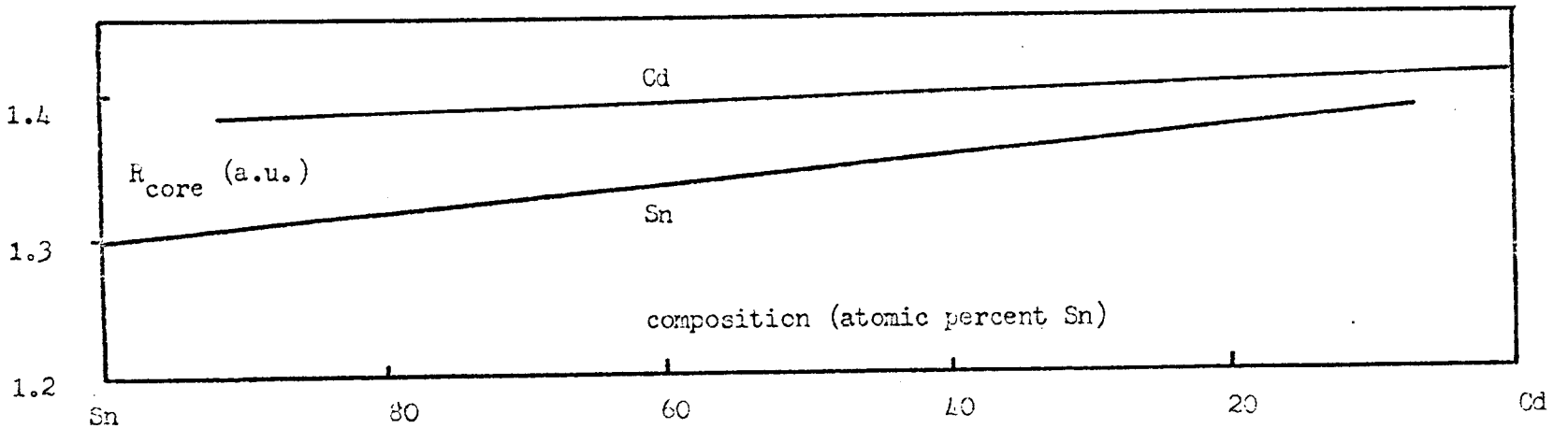

Figure 4.13 R_{core} variations in tin-cadmium alloys at 618 K

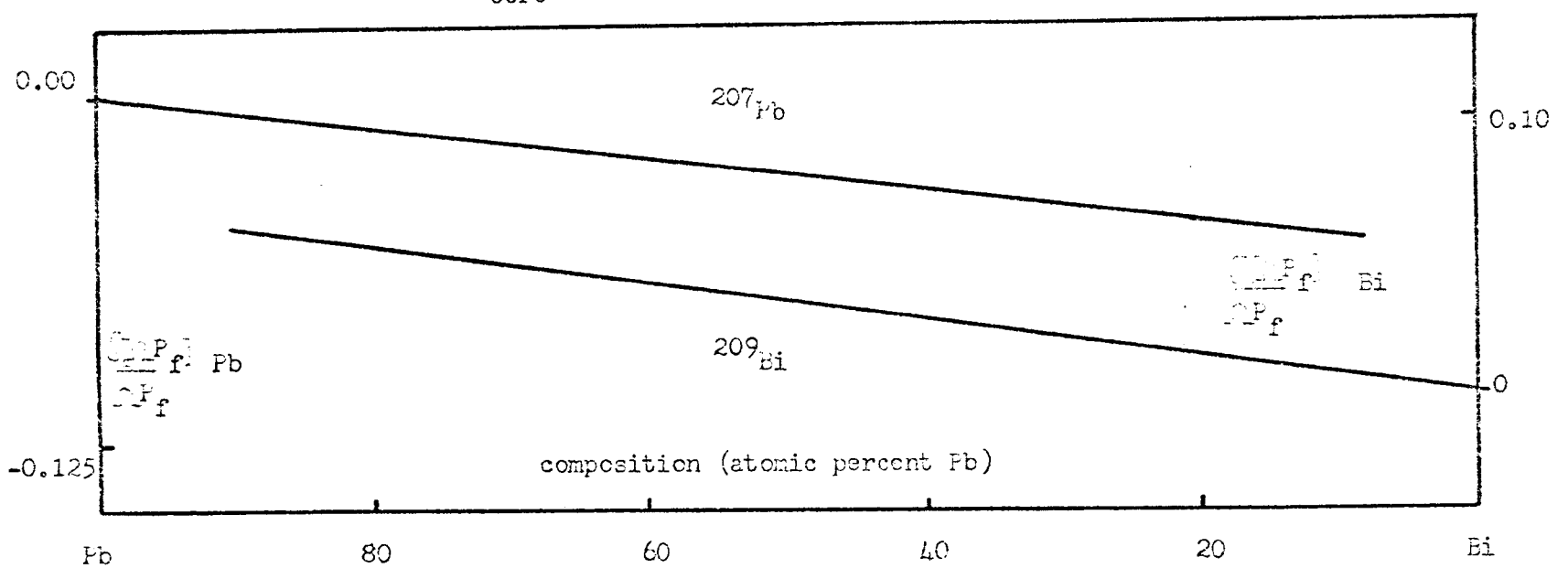

Figure 4.14 Contact density variations in Pb -Bi alloys at 553 K

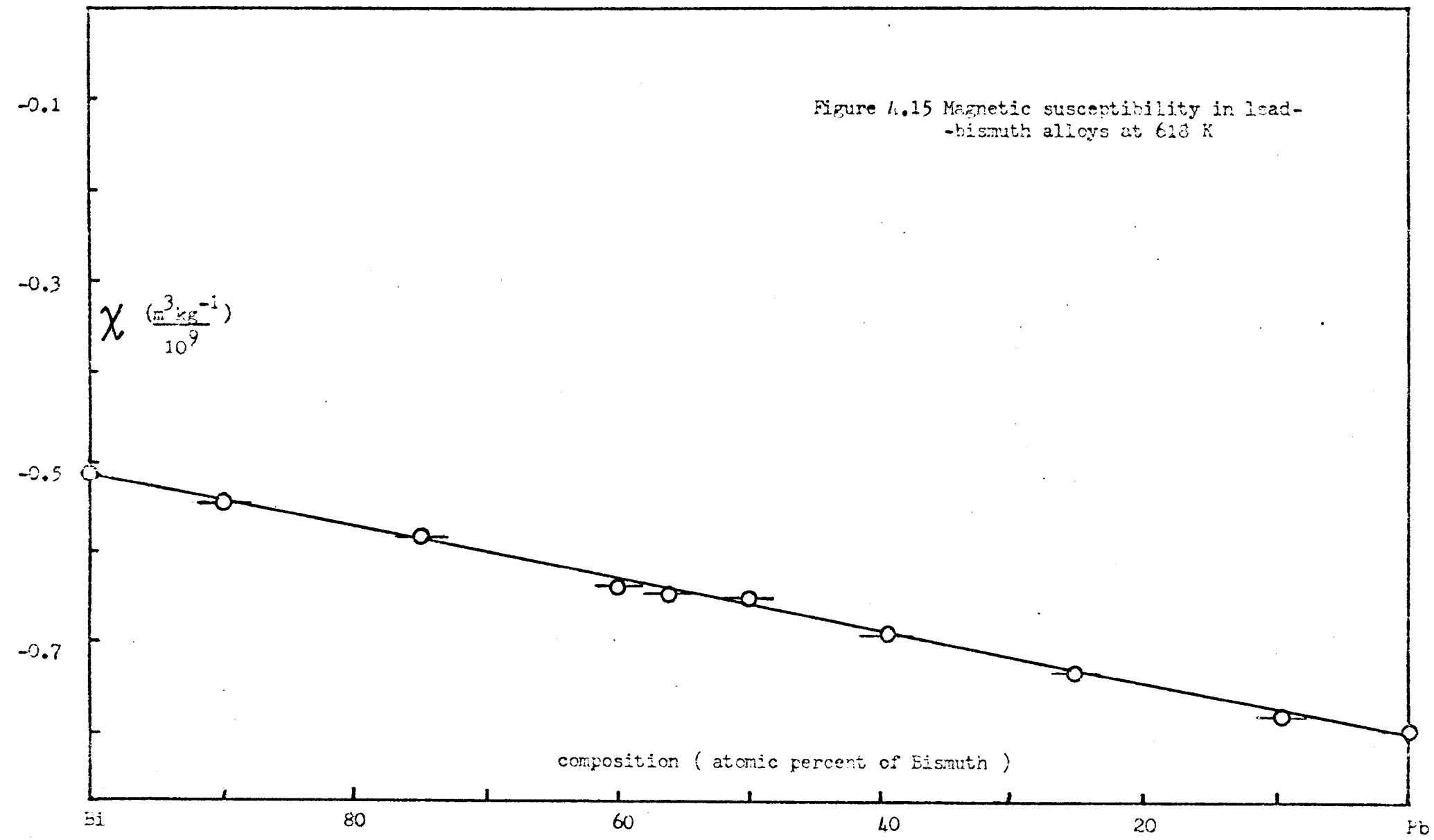

Figure 4.15 Magnetic susceptibility in lead--bismuth alloys at 613 K

variation between the pure metal values was observed. As in section 4·2, these results were analysed to yield the change in χ_p across the range, using the linear interpolation of densities discussed earlier which was found experimentally to be closely followed in these alloys by Kleppa (10). χ_p varies linearly by 5 percent across the system (table 4·6)

4·3·2 Discussion

Heighway (2) has studied the behaviour of both the ^{207}Pb and ^{209}Bi Knight shifts as a function of concentration in this system. Table 4·6 summarises these experimental results together with the deduced χ_p variation and calculated ΩP_f variation. For this last purpose the pseudopotential approach was again adopted, with the relevant computer program input parameters listed in table 4·5, and the ΩP_f variations obtained shown in figure 4·14. (A partial wave analysis is reserved for the next chapter where a variety of dilute lead alloys is discussed).

Table 4·5

Input parameters at 623 K (in a.u.)

metal	k_f	Ω	R_{core}	R_{1s}	R_{2s}	R_{3s}	R_{4s}	R_{5s}
lead	0·833	204·9	1·474	1441	483	230	116	53·5
bismuth	0·843	247·0	1·493	1467	492	235	119	55·5

It should be noted again perhaps that χ_p^1 is derived from m* values (from comparing experimentally derived and theoretical χ_es) and from temperature coefficients, obtained in section 3·2. These are slightly different to the χ_e variations, because slightly different values of m* are obtained for the two pure metals; (χ_p^1 is defined in table 4·6.)

As can be seen from table 4·6, the experimental and expected values for neither shift agree, even as to sign. A possible cause of this may lie in the use of non-relativistic wavefunctions. Certainly, when agreement

is sought by use of the α and β factors, the values required are 10 (for lead) and 16 (for bismuth), this latter value being the best fit, but still not close to experiment.

Table 4·6

Knight shift changes for ^{207}Pb and ^{209}Bi

resonance	K^1	χ_p^1	ΩP_{fE}^1	columns (3+4):K^1 theo
1	2	3	4	5
^{207}Pb	0·2*	-0·05	-0·05 (0·28)	-0·10 (0·23)
^{209}Bi	-0·12	0·05	0·06 (-0·09)	0·11 (-0·03)

*measured only as far as $c_F = 0{\cdot}7$; values in brackets include α and β factors; $K^1 = (K_E(c_F=1)-K_E(c_F=0))/K_E(c_F=0)$, similarly for χ_p^1 and ΩP_{fE}^1.

The use of relativistic wavefunctions may well affect column 4 of table 4·6 significantly since both lead and bismuth are metals of high atomic number, for which the relativistic effects will be appreciable (11). In view of this possibility, it was decided to carry out calculations on tin-bismuth alloys which behave experimentally like lead-bismuth alloys (2) and where one might expect relativistic errors to show up for bismuth but not for tin. It is worth noting that the results for the pseudopotential method do not compare favourably with the results of the partial wave analysis adopted in the next chapter for dilute lead-bismuth alloys.

4·4 Tin-bismuth alloys

The magnetic susceptibility across this liquid alloy system has not been measured in the present work, but in view of the behaviour in the other two systems, and the behaviour of other simple metals observed (section 3·2), it would be very surprising if the assumption of linear variation of χ between the pure liquid metals were to be greatly in error. The input parameters for the pseudopotential approach computer

program at the chosen temperature of 558 K are shown in table 4·7, and the values obtained for the contact densities given in table 4·8.

Table 4·7

Input parameters at 558 K (in a.u.)

metal	k_f	Ω	R_{core}	R_{1s}	R_{2s}	R_{3s}	R_{4s}	R_{5s}
tin	0·835	202·6	1·297	696	227	98	45	
bismuth	0·845	245·3	1·493	1467	492	235	119	55·5

The ^{209}Bi and ^{119}Sn Knight shifts have been observed in this system at 558 K (3). These results are shown in table 4·8 along with the theoretical results of the present work.

Table 4·8

Knight shift changes for ^{119}Sn and ^{209}Bi

resonance	K^1	χ_p^1	ΩP_{fE}^1	columns(3+4): K^1 theo
1	2	3	4	5
^{119}Sn	0·10	-0·07	0·00 (0·17)	-0·07 (0·10)
^{209}Bi	-0·16	0·07	0·00 (-0·15)	0·07 (-0·08)

The values in brackets are obtained when values of α of 6 (for tin) and 15 (for bismuth) are used. These values, like those in lead-bismuth, are extremely large and again imply that relativistic effects are present. This , however, should not be the case for tin, and a full explanation of the poor agreement for these last two systems may involve relativistic effects, a poor pseudopotential, or may lie in the assumed distribution functions. (In the tin-bismuth system, it is possible that χ may be non-linear as a function of concentration.)

For the simple tin-cadmium system,however, it is found that both the pseudopotential and partial wave methods give reasonably good agreement with experiment.

References

1) Hanson M., Constitution of Binary Alloys, McGraw Hill, New York, 1958.

2) Heighway J., Ph. D. thesis, Warwick University, 1969.

3) Setty D.L.R. and Mungawadi B.D., Phys. Letters, 35A, 11-12, 1971.

4) Blandin A. and Daniel E., J. Phys. Chem. Solids, 10, 126-37, 1959.

5) Friedel J., Adv. Phys., 3, 466-567, 1954.

6) Host I.P., Ph. D. thesis, Warwick University, 1972.

7) Herman F. and Skillman S., Atomic Structure Calculations, Prentice Hall, New York, 1963.

8) Ashcroft N.W., J. Phys. C (Proc. Phys. Soc.), 2, 232-43, 1968.

9) Kasowski R.V. and Falicov L.M., Phys. Rev. Lett., 22, 1001-3, 1969.

10) Kleppa O.J., J. Phys. Chem., 59, 175-80, 1955.

11) Mahanti S.D. and Das T.P., Phys. Rev., 3B, 1599-1610, 1971.

Chapter 5

Magnetic properties of dilute lead alloys

5·1 Introduction

In this chapter, the temperature and concentration dependencies of the ^{207}Pb Knight shift and linewidth, and magnetic susceptibility are investigated for alloys of lead with bismuth and thallium; the ^{207}Pb shift and width in lead-indium is also investigated. The following atomic compositions were used:

Pb - 18%Bi, Pb - 20%Tl, and Pb - 15%In.

The study of the ^{207}Pb shift in these alloys as a function of temperature was made by Heighway (1). These results have been verified and extended in the present work. Knight shifts, linewidths, and susceptibility will be dealt with separately below, and then in terms of the partial wave approach, discussed in section 1·4·1. Thus, for solute F, and lead as host,

$$\frac{1}{\Omega P_f}\frac{d\,\Omega P_f}{d\,c_F} = \sum_{l=0} (A_l \sin^2\delta_l + B_l \sin 2\delta_l) \qquad (5\cdot1)$$

where $A_l = (2l+1) \int (n_l^2(kr) - j_l^2(kr))\, P(\underline{r})\, d^3\underline{r}$,

$B_l = -(2l+1) \int n_l(kr)\, j_l(kr)\, P(\underline{r})\, d^3\underline{r}$.

While the concentrations chosen can hardly be said to be very dilute, as required by equation 5·1, it was shown by Heighway and Seymour (2) that the change in K produced by these solutes is proportional to concentration up to at least 20 atomic percent, so that it is reasonable to compare the experimental results with the theoretical expression. Furthermore, the largest possible effect of concentration is obtained, the limit being set by solid solubility considerations.

5·2 Experimental results

5·2·1 ^{207}Pb linewidth

All results quoted (for width, K, and χ) are the mean of at least

four measurements. In the present work, the ^{207}Pb linewidth was investigated in pure lead as a function of temperature from 77 K to 642 K, and as a function of magnetic field at 293 K. The results are in agreement with those of (1), as can be seen from figure 5·1, although there is some disagreement over the exact temperature dependence in the solid. No field dependence of the width was observed. The situation is different in the alloys; considering each in turn:

Pb - 20%Tl. The values obtained at room temperature and above were in satisfactory agreement with those of (1). Both sets are shown in figure 5·2. The width showed little change on cooling to 77 K. There was a small field dependence; the width at 293 K was reduced by 200±150 μT at a field of 0·66 T, compared to its value at 1·3 T (the field at which the temperature dependencies were investigated).

Pb - 18%Bi. As figure 5·2 shows, although the present results confirm the narrowing with increasing temperature observed by (1), the room temperature width is much smaller. The width was found to be field dependent in both cases. The width at 0·66 T is less by 170±170 μT for the present work, whereas it was found to be 400±300 μT less, when the specimen used by (1) was checked.

Pb - 15%In. This particular alloy was studied only at 77 K and 293 K. The results are tabulated below.

Table 5·1

Linewidths in the lead-indium alloy

Conditions	293 K, 1·3 T,	293 K, 0·66 T,	77 K, 1·3 T.
Width (μT)	880±40	750±50*	760±40

*Snodgrass and Bennett (3) obtained a width of 1000 μT at a field of 0·7 T, at this temperature for a similar alloy.

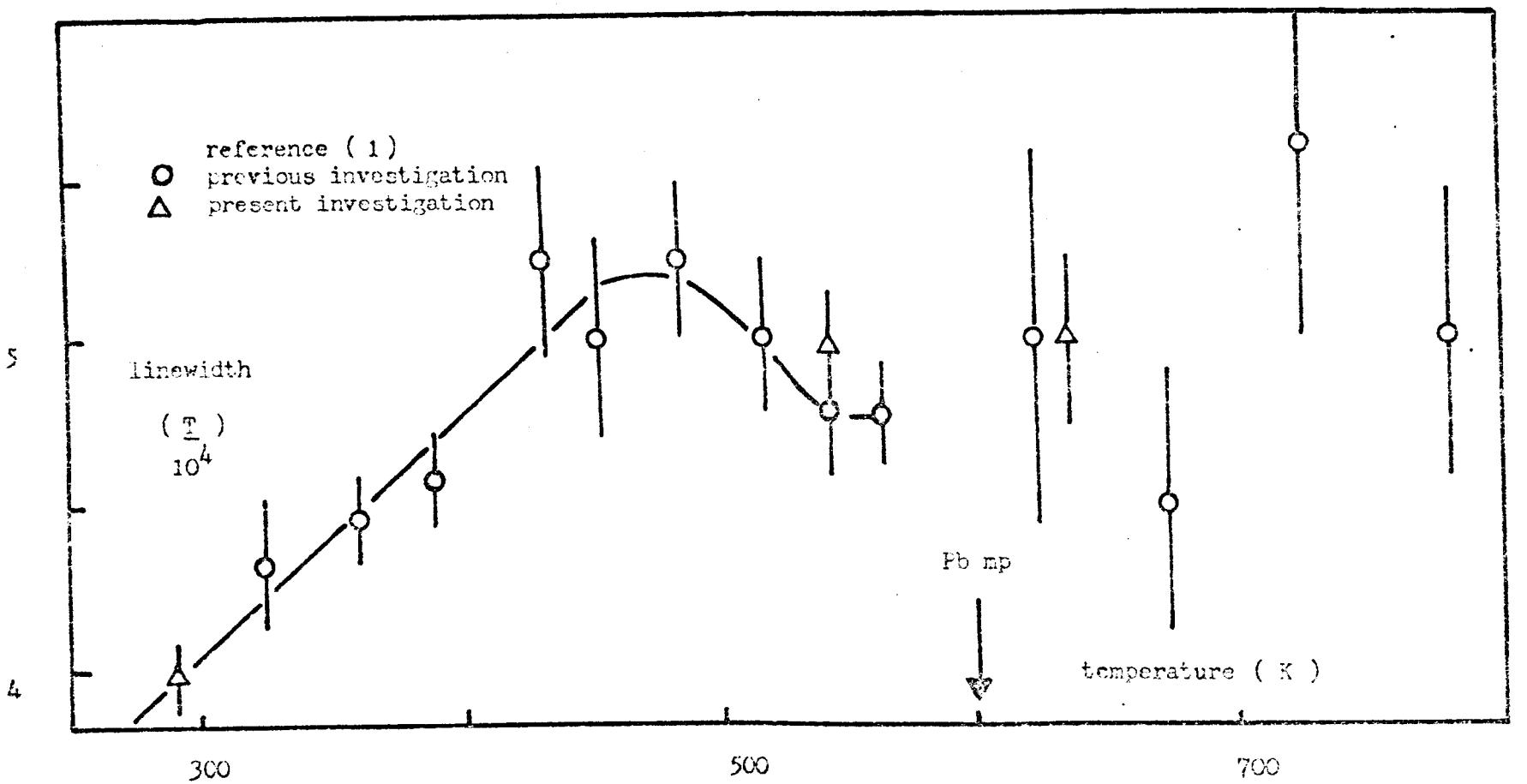

Figure 5.1 ^{207}Pb linewith with temperature

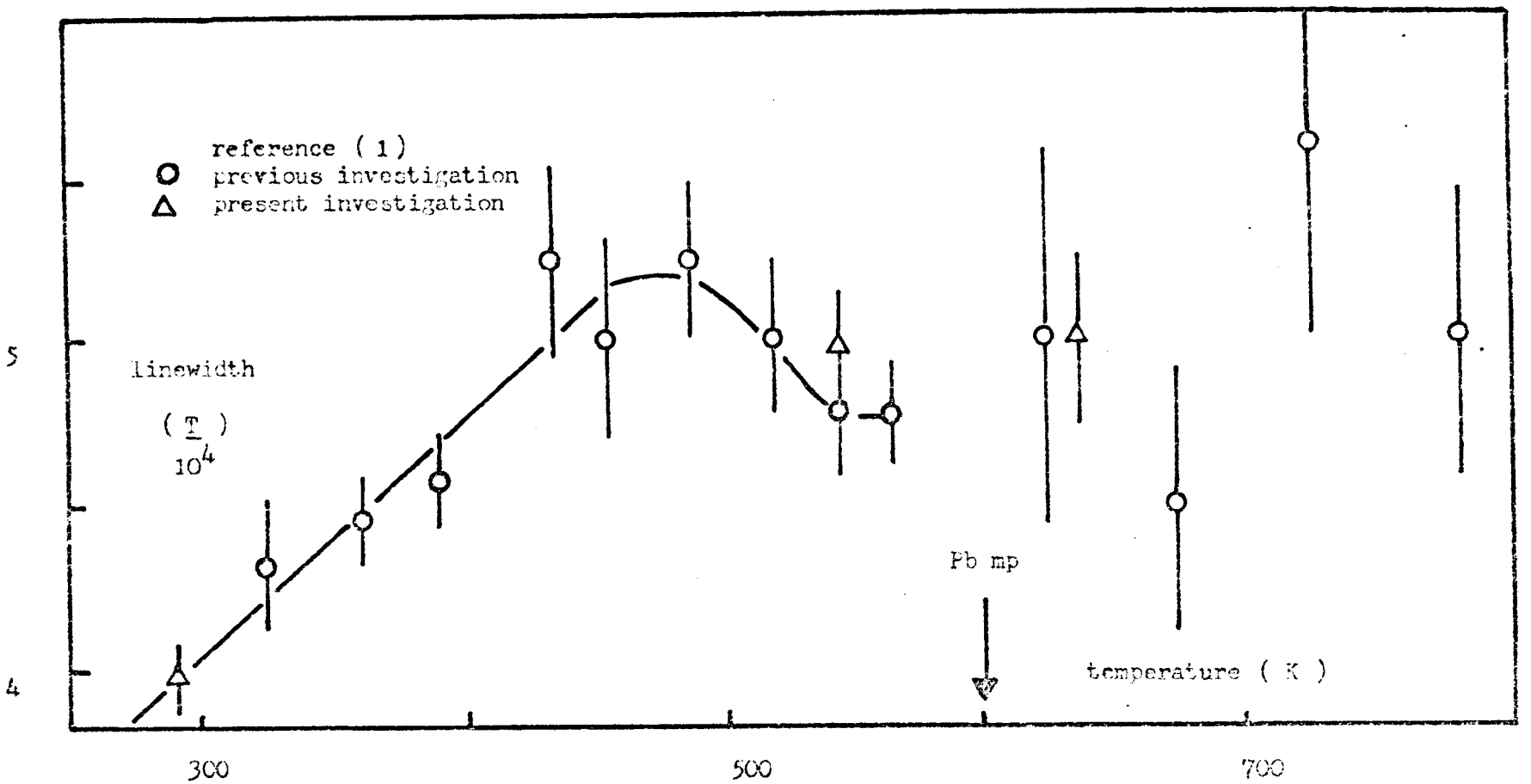

Figure 5.1 ^{207}Pb linewith with temperature

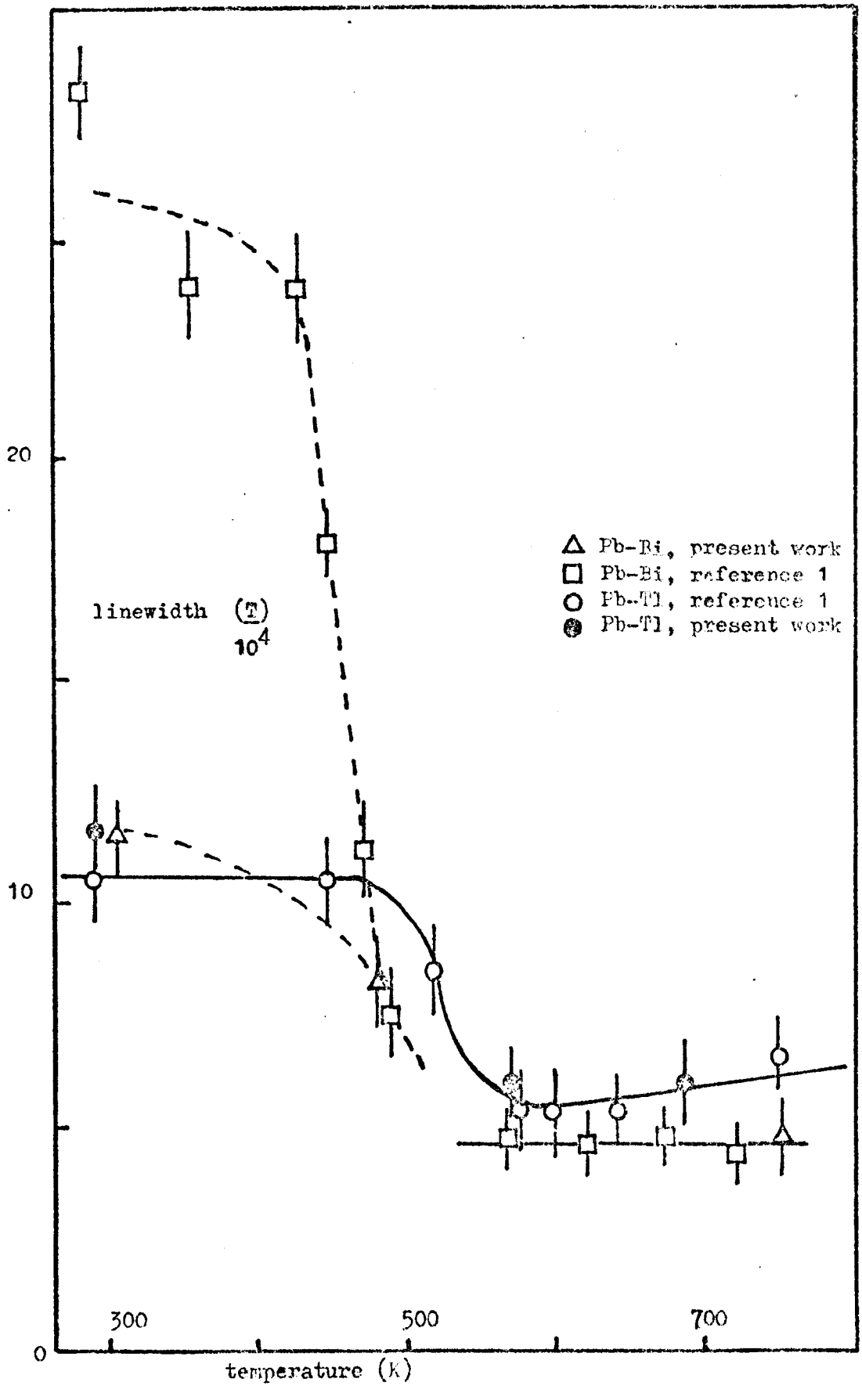

Figure 5·2 Linewidths in lead alloys; present work and previous experimental data

Again, small field and temperature dependencies were observed. It should be noted that no asymmetry of the lines, or deviation from Lorentzian shape, was detected for any of the samples.

5·2·2 The ^{207}Pb Knight shift

One of the main aims of this investigation was to extend the knowledge of the behaviour of the ^{207}Pb shift with temperature down to 77 K, in order to clarify the dependence of Γ ($=K^{-1}\, dK/dc_F$ where c_F is the concentration of solute) with temperature, in these alloys. The results are summarised in rows 4 and 5 of tables 5·2 and 5·3, and figure 5·3. In the solid alloys Γ was found to be independent of temperature up to about 300 K, as previously observed for ^{207}Pb in lead-indium alloys by (3), but becomes temperature dependent between this region and the solidus temperature, the range of line narrowing. The measurements of the pure lead shift were in agreement with those of (1) and the low temperature extrapolation of these, and consequently all values quoted for Γ are defined relative to these particular measurements. In the liquid, Γ again becomes temperature-independent (figure 5·3).

Table 5·2

Temperature coefficients of χ_e and the ^{207}Pb shift, in lead and alloys

1. Sample	Pb - 20% Tl	Pb	Pb - 18% Bi	Pb - 15% In
2. χ_e' (solid)	1100±200	1500±200	1100±200	
3. χ_e' (liquid)	-110± 90	-60± 40	-120± 80	
4. K' (solid, below 300 K)	76± 6	76± 4	75± 9	76± 20
5. K' (liquid)	-95± 12	-76± 9	-92± 7	

All values in units of $(K^{-1}/10^{6})$; $\chi_e' = (1/\chi_{eo})\, d\chi_e/dT$, where the suffix o refers to 300 K for solids and 625 K for liquids; similarly for K'.

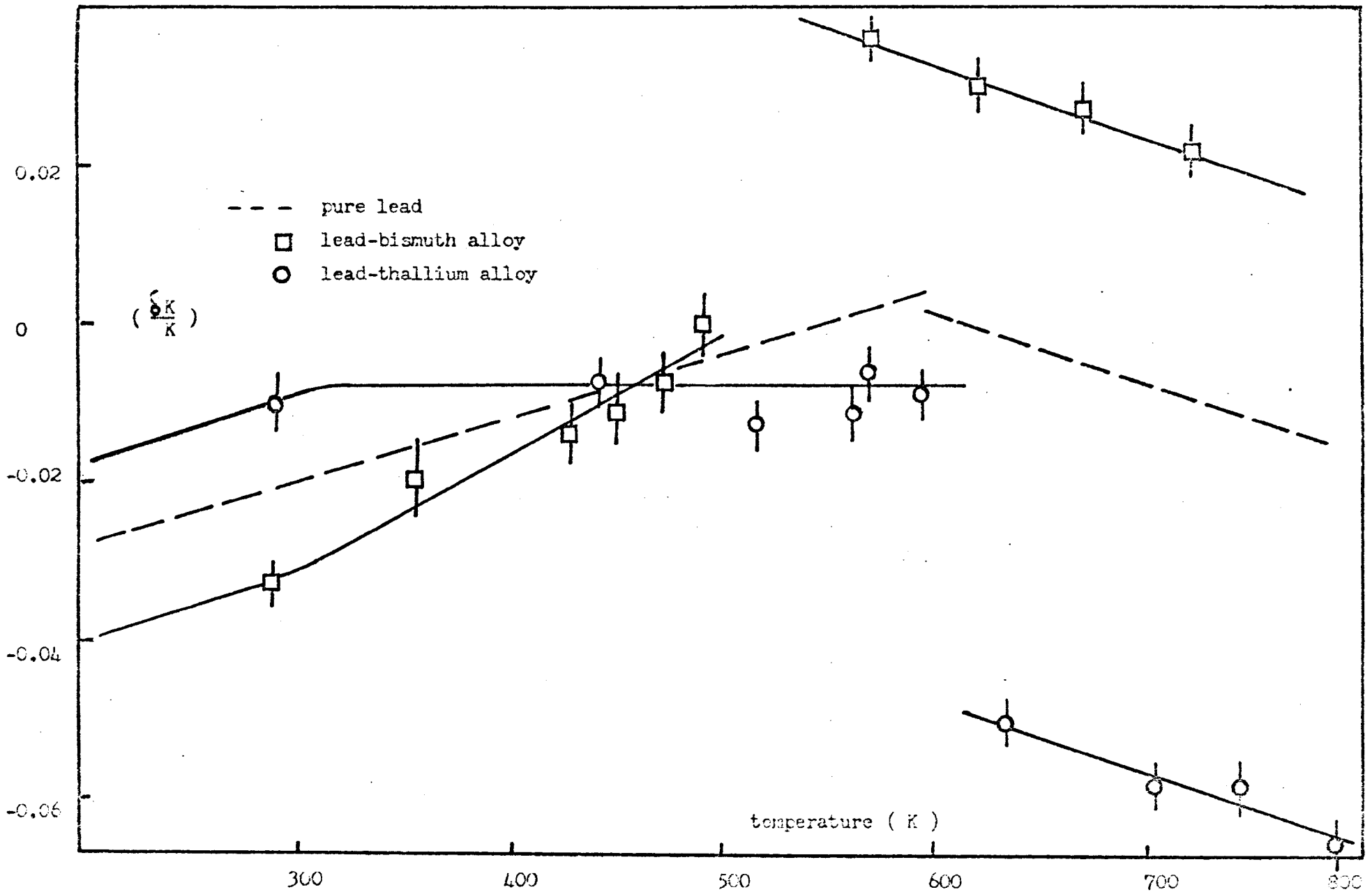

Figure 5.3 ^{207}Pb Knight shift changes in alloys

5·2·3 Magnetic susceptibility

Measurements of the susceptibility were made for the bismuth and thallium alloys in the solid and liquid phases (figure 5·4). The behaviour of χ for pure lead has already been discussed (section 3·2). The assumption that Vegard's law is obeyed (linear interpolation of liquid alloy densities) is made for the lead-thallium alloy, measured densities being available for the lead- bismuth system (4), and pure metal values taken from the literature (5).

Table 5·3

Experimental concentration coefficients of ^{207}Pb shift and χ_e

1. Solute ,F.	Bismuth	Thallium	Indium
2. $(\chi_e^{-1} d\chi_e/dc_F)_{sol.}$	2·0±0·4	1·4±0·4	
3. $(\chi_e^{-1} d\chi_e/dc_F)_{liq.}$	-0·06±0·04*	-0·10±0·03	
4. $\Gamma(^{207}Pb)_{sol.}$	$-0·06\pm0·01_5$	$0·06\pm0·01_5$	0·03±0·02
5. $\Gamma(^{207}Pb)_{liq.}$	$0·16\pm0·00_5$	-0·24±0·01	

* this value compares favourably with that of section 4·3, for χ_p^1.

The solid coefficients are all defined at 300 K, the liquid values at 625 K.

5·3 Discussion

5·3·1 Analysis of the ^{207}Pb linewidth

In polycrystalline lead there are three main contributions to the linewidth: direct and indirect magnetic interactions between the nuclear spins, and the spin-lattice relaxation process.Lead has spin quantum number, $I=\frac{1}{2}$, and a cubic structure in the solid, so there are no quadrupolar or anisotropic contributions to the lineshape. Now, the shape and width of the absorption line at room temperature have been analysed (3). The contribution of the nuclear dipolar interaction , calculated from the Van Vleck formula for the second moment (6), is 35 μT. The

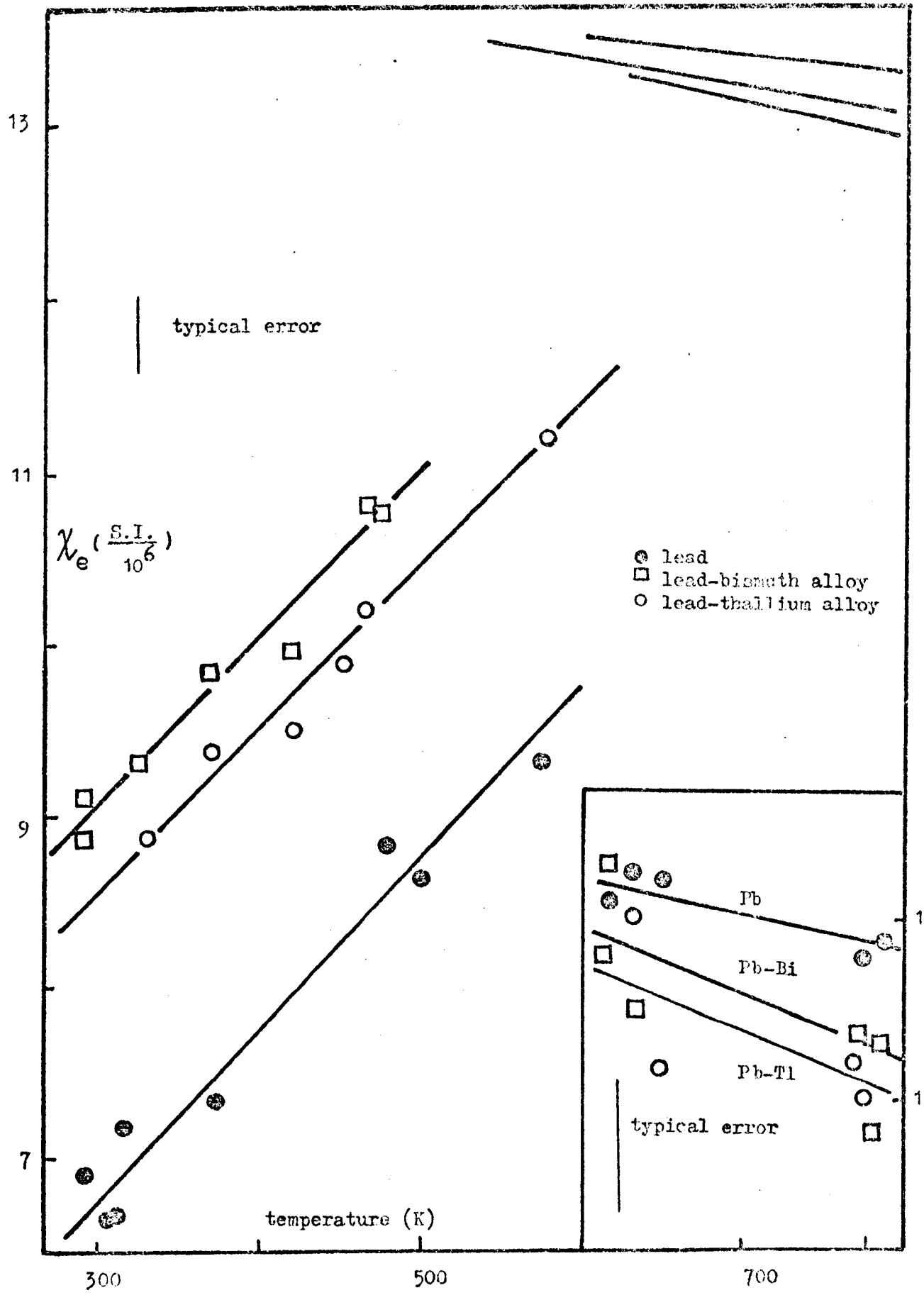

Figure 5·4 Electronic susceptibility in lead , Pb-18%Bi, and Pb-20%Tl

contribution from the pseudodipolar coupling was estimated as 300 μT. Since there is only one magnetic isotope, indirect exchange does not further broaden the line (section 1.2). The spin-lattice relaxation term (obtained either from the Korringa relation or by extrapolation of the low temperature pulse measurements of T_1 of Asayama and Itoh (7)) gives 220 μT. The observed increase in width up to about 450 K is consistent with the proportionality of relaxation rate with temperature expected for a process dependent upon conduction electrons. Narrowing of the line, observed at about 500 K, is attributable to motional narrowing (8) of the classical and pseudodipolar contributions by self diffusion. The residual width is close to that expected from the spin-lattice relaxation contribution (410±30 μT). Furthermore, Heighway (1), calculated the correlation time for diffusive motion from the linewidth, yielding a value for the coefficient of self diffusion, D, at 550 K, which is in satisfactory agreement with the radiotracer measurements (9) of this quantity.

Snodgrass and Bennett (3) have also discussed the main properties of the ^{207}Pb linewidth at room temperature in solid solutions. Their conclusion was that the rapid increase in width with solute concentration is primarily due to pseudodipolar interactions and indirect exchange between the solute and lead nuclei. Another contribution comes from anisotropic Knight shift broadening, this term being field-dependent. The values found in the present work are in qualitative agreement with their observations, though the field dependent widths are smaller here, and in the case of the bismuth alloy, smaller than found by Heighway. This raises the possibility of inhomogeneities of composition in the earlier specimens, producing inhomogeneous Knight shift broadening. The effects of the anisotropic shift and the indirect interactions are motionally narrowed, as for pure lead, near 500 K. The residual widths

are comparable to pure lead, and are as expected from the observed Knight shifts and the Korringa relation.

5·3·2 Discussion of the ^{207}Pb shift

The changes in Γ around the narrowing temperature are unexpected. In order to obtain further information about this phenomenon, a measurement of relative intensities of the signal was made for the lead-thallium alloy, both above (573 K) and below (293 K) the narrowing temperature. After allowing for the direct effect of temperature, there was found to be no difference in intensity, within an experimental uncertainty of 10%. The expectation that in the lower temperature case some nuclei might have their resonances shifted due to the particular arrangements of near neighbour impurities, so that the centre of the observed resonance is not the true mean position, might have explained the behaviour of Γ. However, it would be revealed by an increase in intensity at higher temperatures, which is not observed.But, if in the case of the low temperature lattice, the resonances of a small fraction of the nuclei are displaced well out into or beyond the wings of the observed resonance by interactions with the screening electron clouds around the solute ions, the results may be explained. Motional narrowing gives a true line centre, causing Γ to appear to change in this region. Since hyperfine interactions increase with increasing atomic number, such an effect will be more marked for lead than most other solvents. A calculation for a theoretical estimate of Γ for the liquid alloys will be presented shortly (section 5·3·4), after the discussion of the magnetic susceptibility.

5·3·3 Analysis and discussion of χ data

The assumption that χ_i varies linearly with concentration between the pure metal values is made here, as in section 4·2. Hence, χ_p the quantity of interest, is extracted from χ following the procedure

already explained in earlier chapters. The variations of χ_e, the electronic susceptibility, with temperature and composition are shown in tables 5·2 and 5·3, and figure 5·4. The value of χ_e obtained is in excellent agreement with the value expected for liquid lead, assuming $m^* = m$. The experimental value for χ_e for solid lead is not consistent with this assumption. The observed increase on melting represents a 40% increase in χ_e. The volume change accounts for only 3·5%. As explained in section 3·3, the susceptibility could be understood assuming a value of $m^* = 0·84m$ at the melting point. There remains the difficulty, however, that the Knight shift change obtained (1) on melting is very small. This suggests that the susceptibility change comes mainly from a decrease in the magnitude of the diamagnetic contribution, rather than any substantial increase in χ_p. This would require a conduction electron diamagnetic susceptibility in the solid of about twice the free electron value.

The observed temperature coefficient for pure lead is consistent with free electron behaviour in the liquid, but not the solid (see table 3·4). The value in the liquid is in agreement with that predicted from expansion, within experimental error. In the solid, the observed value is an order of magnitude larger, and of the opposite sign. Again, this is inconsistent with the value of K' in the solid (but not the liquid), without either an unusually large counterbalancing temperature coefficient of D_f, or a large coefficient of the diamagnetic contribution to χ_e. This conformity to free electron behaviour in the liquid but not the solid is expected, from the observed behaviour of other pure metals (section 3·3).

For the liquid alloys, χ_c changes little with composition (table 5·3). For the bismuth alloy, the experimental value of $(\chi_c^{-1} d\chi_c / dc_F)$ is negative, and in agreement with the value obtained across the whole

system (section 4·3). However, the free electron prediction is +0·07. This departure from free electron behaviour is presumably connected with the deduction, from pure metal results, that m^*/m is 0·93 in liquid bismuth at the melting point. It would be expected as a related result that χ_e' for the alloy should be less negative than for pure lead, because of the increased positive temperature coefficient in bismuth, as m^* tends toward m in the liquid. However, such an effect could be masked by the experimental uncertainties. For the thallium alloy, the observed $(\chi_e^{-1} d\chi_e / dc_p)$ is not in contradiction with the free electron prediction of -0·06. For both liquid alloys, a substantial part of the observed values must arise from changes in ΩP_f. In the solid, the picture is more complicated; the addition of small amounts of bismuth or thallium cause much larger changes in χ_e, both of the same sign. The changes in K', on the other hand, are small and of opposite signs, which suggests that the changes in χ_e with composition-as with temperature-are not predominantly due to χ_p. Thus, the solid data point inescapably to the inapplicability of the free electron model, whereas in the liquid there are only mild deviations from free electron behaviour.

5·3·4 The contact density changes

Now, the variations of K and χ_e are compared with the calculated variation of ΩP_f, using equation 5·1 and equation 1·10 , defining K. Values of the constants A_1 and B_1 in equation 5·1 were calculated from the experimental radial distribution function of Kaplow et al (10), for the temperature of 625 K. Values obtained for the model hard sphere radial distribution function of Ashcroft and Lekner (11), which is a reasonable match to the experimental curve, were consistently of the same sign, but smaller in magnitude by a factor of 1½ to 2. The experimental values are shown in table 5·4, together with the values for solid lead calculated by Snodgrass and quoted by Rigney and Flynn (12). The method

used to calculate the phase shifts, δ_l, in this case was as follows. The values of δ_l were obtained from the solute valency, using an effective solute charge modified by Blatt (13), and the Friedel sum rule, (14); p-wave scattering alone was assumed. That is, saturation of the s-content of the solute cell assumed, and d and higher partial waves neglected. The resulting predictions for $(\Omega P_f)^{-1} d\Omega P_f/dc_F$ are shown in table 5·5, column 4. The effects of the χ_p variations are added and the predictions for the total Γ are taken as

$$\frac{1}{\Omega P_f}\frac{d(\Omega P_f)}{dc_F} + \frac{1}{\chi_e}\frac{d\chi_e}{dc_F} \quad ,$$

since, on a free electron approach,

$$\frac{1}{\chi_e}\frac{d\chi_e}{dc_F} = \frac{1}{\chi_p}\frac{d\chi_p}{dc_F}.$$

(This assumption is considered valid for dilute liquid lead alloys, in view of the conclusions of section 5·3·3).

Table 5·4

Blandin-Daniel coefficients calculated for lead (using experimental F(r) in liquid

	A_0	B_0	A_1	B_1	A_2	B_2
Solid	0·04	-0·24	-0·67	0·70	2·29	-0·73
Liquid	-0·04	-0·20	-0·23	0·50	1·69	-0·70

Table 5·5

Phase shift results for Γ of ^{207}Pb in lead-thallium and lead-bismuth solute ; effective charge; δ_1; $(\Omega P_f)^{-1} d\Omega P_f/dc_F$; $\chi_p^{-1} d\chi_p/dc_F$; Γ_{theo}; Γ_{expt};

Thallium	-1·16	-0·61	-0·54	-0·10	-0·64	-0·24
Bismuth	0·22	0·12	0·12	-0·06	0·06	0·16

As can be seen, the theoretical values are of the correct sign and order of magnitude. The value for bismuth as solute is much better than that given by the pseudopotential approach adopted earlier for the Pb-Bi system

(section 4·3·2), although the Perdew and Wilkins approach is not limited to low concentrations, and would appear to involve less unsophisticated assumptions. The experimental Γ values in the solid are smaller by a factor of about 3 or 4. As it happens, the theoretical values of Γ are governed mainly by the coefficient, B_1. Since this is larger in the solid, (table 5·4), the difference between theory and experiment in the solid alloys is an order of magnitude greater than in the liquid, again emphasising the inadequacy of free electron considerations for solid lead and its alloys. A discussion of χ_p in the solid would involve a treatment of the magnetism of overlapping bands; a treatment of K would, in addition, require a knowledge of the fractional s-character of the states at the Fermi level in the overlapping bands. However, the free electron approach gives reasonable results in both liquid lead and its alloys.

References

1) Heighway J., Ph. D. thesis, Warwick University, 1969.

2) Heighway J. and Seymour E.F.W., Phys. Lett., 29A, 282-3, 1969.

3) Snodgrass R.J. and Bennett L.H., Phys. Rev., 134A, 1294-5, 1964.

4) Kleppa O.J., J.Phys. Chem., 59, 175-80, 1955.

5) Smithells C.J., Metals Reference Book, p.688, Butterworths, London, 1967.

6) Slichter C.P., Principles of Magnetic Resonance, Harper and Row, New York, 1963.

7) Asayama K. and Itoh J., J.Phys. Soc. Japan, 17, 1065, 1962.

8) Kittel C., Introduction to Solid State Physics, p.518, Wiley, New York, 1967.

9) Nachtrieb N.H., Adv. Phys., 16, 309-23, 1967.

10) Kaplow R.L., Strong S., and Averbach B.L., Phys. Rev., 138A, 1336-45, 1965.

11) Ashcroft N.W. and Lekner J., Phys. Rev., 145, 83-90, 1966.

12) Rigney D.A. and Flynn C.P., Phil. Mag., 15, 1213-20, 1967.

13) Blatt F.J., Phys. Rev., 108, 285-90, 1957.

14) Blandin A. and Daniel E., J.Phys. Chem. Solids, 10, 126-37, 1959.

Chapter 6

The semiconductor-metal transition in VO_2

6·1 Introduction

Vanadium dioxide, VO_2 , and other oxides of vanadium (e.g. V_2O_3) undergo reversible semiconductor-metal transitions; the temperature of this change for VO_2 is 341 K, (T_t). The low temperature phase is monoclinic in structure, and the transition involves both crystallographic (to a rutile structure) and magnetic changes. The electrical conductivity is observed (1) to increase by four orders of magnitude at T_t, from 10 $ohm^{-1}m^{-1}$ in the semiconducting region to 10^5 $ohm^{-1}m^{-1}$ in the metallic state. All these oxides are insulators in their ground states, in contradiction to the band theory of solids. It was decided to investigate the magnetic properties of VO_2 in order to attempt to compare these with the current theoretical model predictions, both above and below the transition.

The general technique of comparing Knight shifts and magnetic susceptibilities, developed in chapter 1, will again be used, but in a different fashion to its use in pure metals and alloys. The orbital and spin contributions to both these quantities will be estimated through a procedure which involves the temperature dependencies of these terms, (section 1·3·1). Once estimated, the relevance of their values in terms of the band structure of VO_2 will be discussed.

In order to explain the procedure fully, it is necessary to consider the various possible contributions to the susceptibility, in this particular system.

$$\chi(T) = \chi_i^{dia} + \chi_i^{vv} + \chi_d^{dia}(T) + \chi_d^{spin}(T) + \chi_o \qquad (6·1)$$

The analysis depends entirely on the ability to recognise which components are temperature dependent, and which are not. Considering these contributions in turn :

χ_i^{dia}. This is the ion core contribution, calculated for one V^{5+} and two O^{2-} ions from the free ion values of Angus (2).

χ_i^{vv}. This term arises from the departure from spherical symmetry of the ion cores, associated with the covalency of the vanadium-oxygen bonding. It is a paramagnetic Van Vleck-type term (section 1·1).

$\chi_d^{dia}(T)$. This is the conduction electron diamagnetic part. It should be noted that since V^{4+} has a $3d^1$ configuration, there is no s-term in the conduction electron susceptibility.

$\chi_d^{spin}(T)$. This is related to the last term, through the equation,

$$\frac{\chi_d^{dia}}{\chi_d^{spin}} = \frac{1}{3}(m/m^*)^2. \qquad (6\cdot2)$$

Since there is good evidence (1) that $m^* >> m$ the free electron mass, the diamagnetic term is quite negligible. Thus,

$$\chi_d(T) = \chi_d^{spin}(T).$$

The reason for the temperature dependence of the conduction electron term is as follows. $\chi_d(T)$ involves an average of the density of states, D(E), over a range kT at the Fermi level (where k is Boltzmanns constant). The d bands are quite narrow, and the width of their structure is of the same order as kT. This has the effect of introducing a strong temperature dependence into χ_d.

χ_o. The orbital contribution is known as the Kubo-Obata (3) term. It is the analogue, for itinerant electrons moving in an orbitally degenerate d band, of the Van Vleck paramagnetism. In fact, the orbital magnetic moment is normally quenched by the crystalline electric field; upon application of a magnetic field there is an admixture of higher energy unoccupied levels into the occupied levels in the d sub-bands, unquenching part of the moment. This term is essentially temperature-independent,

since all the d electrons contribute, unlike the situation in the case of $\chi_d(T)$, where only those in the vicinity of the Fermi surface are involved in thermal excitation. Thus, equation 6·1 may be rewritten as

$$\chi(T) = \chi_i + \chi_o + \chi_d(T). \qquad (6·3)$$

The Knight shift can be expressed in terms of a core polarisation term, $K_{cp}(T)$, and an orbital term, K_o, each proportional to the corresponding susceptibility term, $\chi_d(T)$ and χ_o respectively.

$$K(T) = K_{cp}(T) + K_o$$
$$= \alpha' \chi_d(T) + \chi_o \beta' \qquad (6·4)$$

Rather unusually, there is no direct contact contribution, because of the absence of s conduction electrons. This enables the shift to be separated into one identifiable temperature dependent term, and one identifiable temperature independent term.

The core polarisation term arises from the fact that the d electrons perturb core s wavefunctions differently, depending on whether the d spin is parallel or anti-parallel to the s spin (section 1·2). Consequently, the electron density at the nucleus is not the same for the two paired s electrons, leading to a net magnetic field, arising from non-cancellation of the contact interactions. α' is not easy to calculate theoretically, but an experimental study of the temperature variations of K(T) and $\chi(T)$ can be expected to yield a value for α' since

$$\alpha' = \frac{dK/dT}{d\chi/dT} \qquad (6·5)$$

Now,

$$\beta' = (2/N) \langle r^{-3} \rangle \qquad (6·6)$$

where N is Avogadro's number, and $\langle r^{-3} \rangle$ represents an average over a unit cell of the d conduction electron - vanadium nucleus separation, r. This expression assumes that the radial parts of the wavefunctions of the d

sub-bands are the same, and neglects a small long range contribution to this shift. It may be approximated by calculating $\langle r^{-3} \rangle$ for the $3d^1$ electron in a V^{4+} ion. Once χ_i and ρ' are known, a plot of K against χ with temperature as an implicit variable, may be used to yield values for ρ', $\chi_d(T)$, and χ_o (as well as $K_{cp}(T)$ and K_o), following the procedure used for some transition metals (4) and for another oxide of vanadium (5). This technique is applicable of course only if K and χ are both appreciably temperature dependent.

6·2 Experimental results

Measurements of both K and χ in the range 290-480 K were obtained for a powdered sample of VO_2, prepared by heating a mixture of V_2O_3 and V_2O_5 in the appropriate proportions under vacuum at 1070 K. All susceptibility measurements quoted are for the powder, but anisotropic susceptibility measurements on a small single crystal gave excellent agreement with these at all temperatures, thus:

$$\frac{2\chi_{\parallel} + \chi_{\perp}}{3}_{\text{crystal}} = 0{\cdot}998\,\chi_{\text{powder}},$$

where $\parallel$ and $\perp$ refer to the axes of the crystal.

In the semiconducting region below T_t the susceptibility is paramagnetic and independent of temperature, (table 6·1). Detailed NMR observations were not made below the transition; the derivative of the absorption line shows many but not all of the features described by Umeda et al (6), who explained their results in terms of a second order quadrupole effect, a traceless chemical shift,(anisotropic), and an isotropic shift of 0·28±02 %. The position and width of the present observed line (figure 6·3) did not vary with temperature.

At T_t χ changes discontinuously and decreases linearly with further increase of temperature (figure 6·1). The result of a set of 12 observations

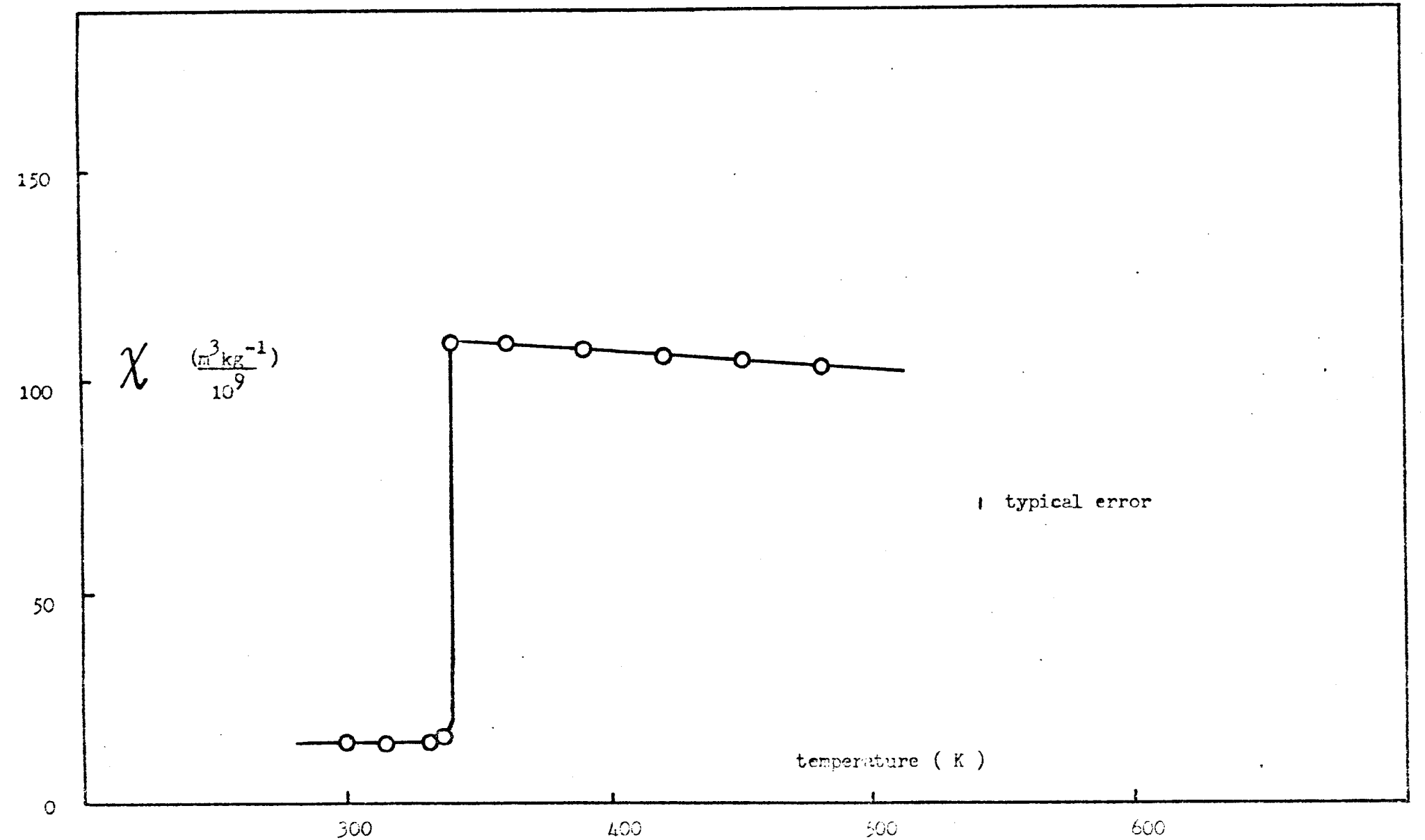

Figure 6.1 Magnetic susceptibility in VO_2

in the range 341-478 K is given in table 6·1. The Knight shift becomes negative at T_t , and then changes linearly with temperature (figure 6·2). The results quoted are derived from six observations in a similar temperature range. The resonance line (figure 6·3) is quite closely Lorentzian in shape, with no sign of the structure visible below the transition. The peak to peak derivative width decreases as the field increases, being (3·0±0·2) mT at 0·8 T and (1·8±0·1) mT at 1·4 T.

6·3 Discussion

The observed data are analysed in terms of equations 6·3 and 6·4. The ionic susceptibility was taken to be the observed (7) paramagnetic susceptibility of iso-structural titanium dioxide, TiO_2 , which has no itinerant d electrons. (Titanium is next to vanadium in the periodic table and the Angus value for the free ion susceptibility is close to that for the value for vanadium).The value found was $(0{\cdot}84\pm0{\cdot}02) \times 10^{-9}$ m^3kg^{-1}.

Table 6·1

source	semiconducting phase	metallic phase			
	χ_{ion} ($m^3kg^{-1}/10^9$) ;	χ_{spin} ($m^3kg^{-1}/10^9$);	$\frac{d\chi}{dT}$ ($m^3kg^{-1}K^{-1}/10^3$);	K (%);	$\frac{dK}{dT}$ ($K^{-1}/10^6$) ;
present work	15·17 ± 0·10	111·2 ± 0·3	-4·30 ±0·11	-0·391 ±0·007	4·60 ±0·10
ref. (8)	12·6	105·7			
ref. (9)	10·1	100·5	-4·1		
ref. (10)	11·9	99·3	-4		
ref. (11)				-0·38±0·02 at 373 K	

Clearly this is only a small fraction of the total susceptibility in the metallic state. There is some uncertainty in assigning a value to χ_{spin} because of the effects of covalency (if present) on $\langle r^{-3} \rangle$ .For an electron in a free $3d^1$ ion, V^{4+}, using the value of $\langle r^{-3} \rangle$ given by Rado and Suhl

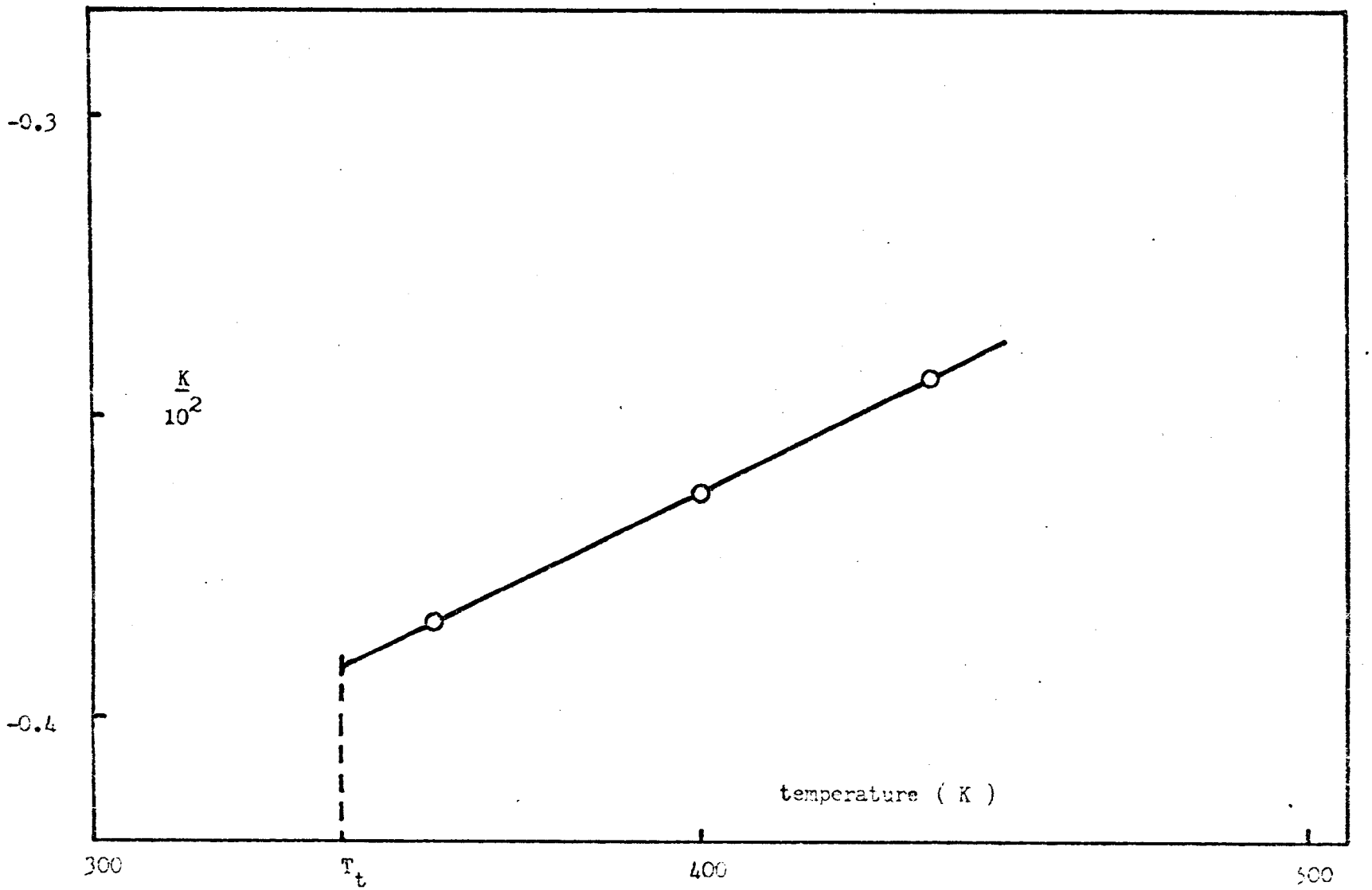

Figure 6.2 Knight shift in metallic VO_2

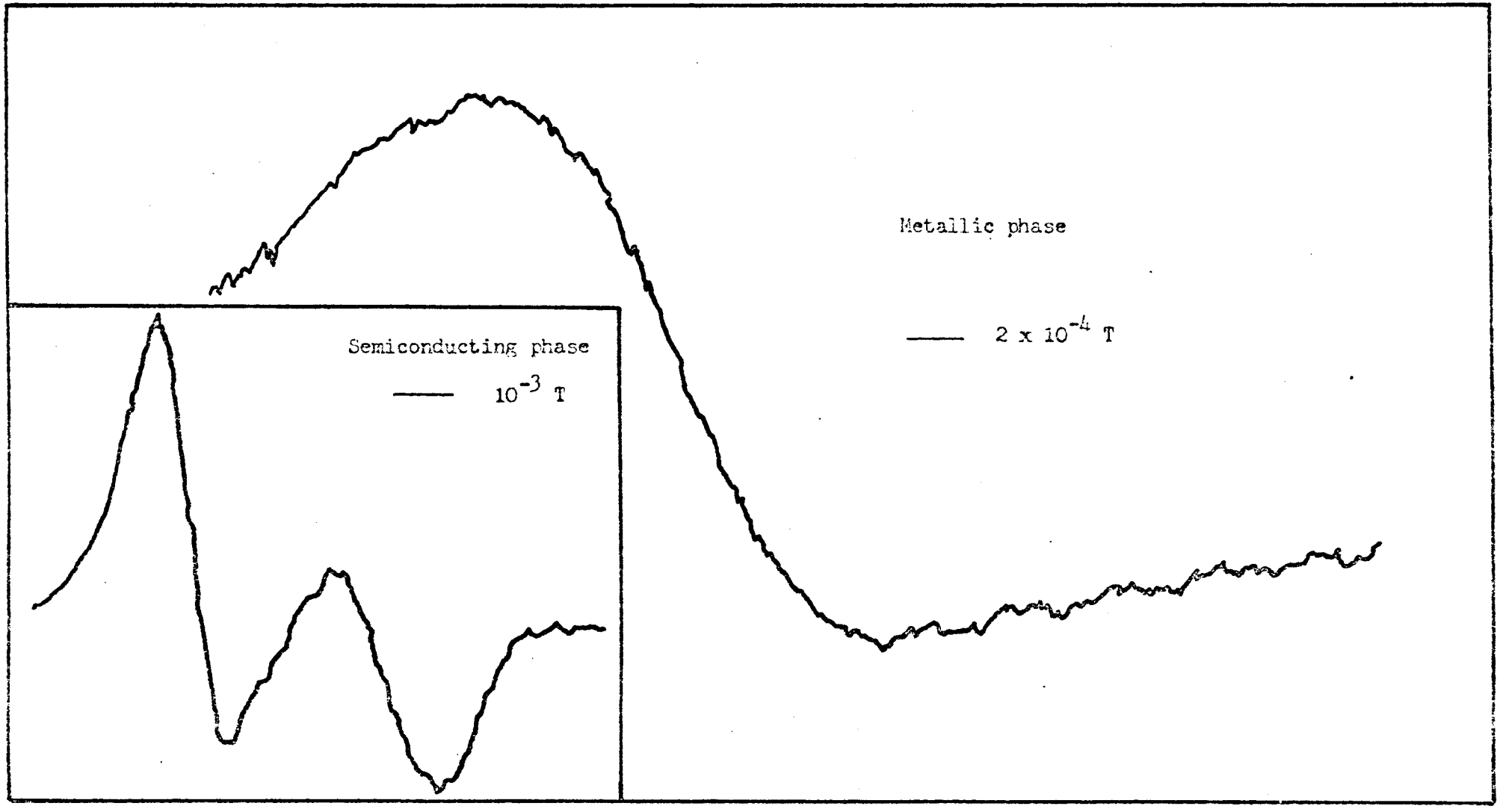

Figure 6.3 Experimental lineshape derivatives in VO_2

(12), $\beta' = 5{\cdot}38 \times 10^5 \text{kgm}^{-3}$; for a V^{4+} ion in a rutile type crystal, Shimizu (13) calculates a smaller value of $\langle r^{-3} \rangle$, assuming 30% covalency. This yields $\beta' = 3{\cdot}77 \times 10^5$ kgm^{-3}. The experimental results give a value for α' from equation 6·5 of $-(1{\cdot}07 \pm 0{\cdot}04) \times 10^5$ kgm^{-3}. This may be compared with the corresponding quantities for pure vanadium metal, $-(1{\cdot}32 \pm 0{\cdot}20) \times 10^5$ kgm^{-3} (14), and for V_2O_3, $-(1{\cdot}65) \times 10^5$ kgm^{-3}(5).

In figure 6·4 the experimental K - χ curve (a - b) is extrapolated to meet a line drawn from χ_i with slope β'. The projections of the two segments onto the susceptibility axis then give χ_o and $\chi_d(T)$, in accordance with equation 6·4. As can be seen, this has been done for both values of β' with the following two alternative sets of results for the metallic phase.

For $\beta' = 5{\cdot}38 \times 10^5$ kgm^{-3}, indicated by 1 in figure 6·4,

$\chi_o = (12{\cdot}2 \pm 0{\cdot}6) \times 10^{-9}$ m^{3}kg^{-1}, $\chi_o / \chi_d = 0{\cdot}124 \pm 0{\cdot}006$,

$K_o = (0{\cdot}66 \pm 0{\cdot}04)$ %, $K_{cp} = -(1{\cdot}05 \pm 0{\cdot}04)$ %.

For $\beta' = 3{\cdot}77 \times 10^5$ kgm^{-3}, indicated by 2 in the figure,

$\chi_o = (16{\cdot}3 \pm 0{\cdot}8) \times 10^{-9}$ m^{3}kg^{-1}, $\chi_o / \chi_d = 0{\cdot}173 \pm 0{\cdot}009$,

$K_o = (0{\cdot}61 \pm 0{\cdot}04)$ %, $K_{cp} = -(1{\cdot}00 \pm 0{\cdot}04)$ %.

In principle, since both the orbital and spin interactions with the nucleus give rise to spin-lattice relaxation, a choice between the derived sets of values of χ_o and χ_d should be possible, by measuring the V^{51} spin-lattice relaxation time, T_1, in VO_2. Attempts were made to measure this directly, but they were unsuccessful. The failure was attributed to the shortness of T_1 (the apparatus has a "dead time" of approximately 10-15 μs). However an approximate check can be made through the linewidth. This contains several contributions in addition to that arising from T_1 processes (section 1·2). The combined effect of the anisotropic Knight shift and electric quadrupole interaction (both of which quantities are

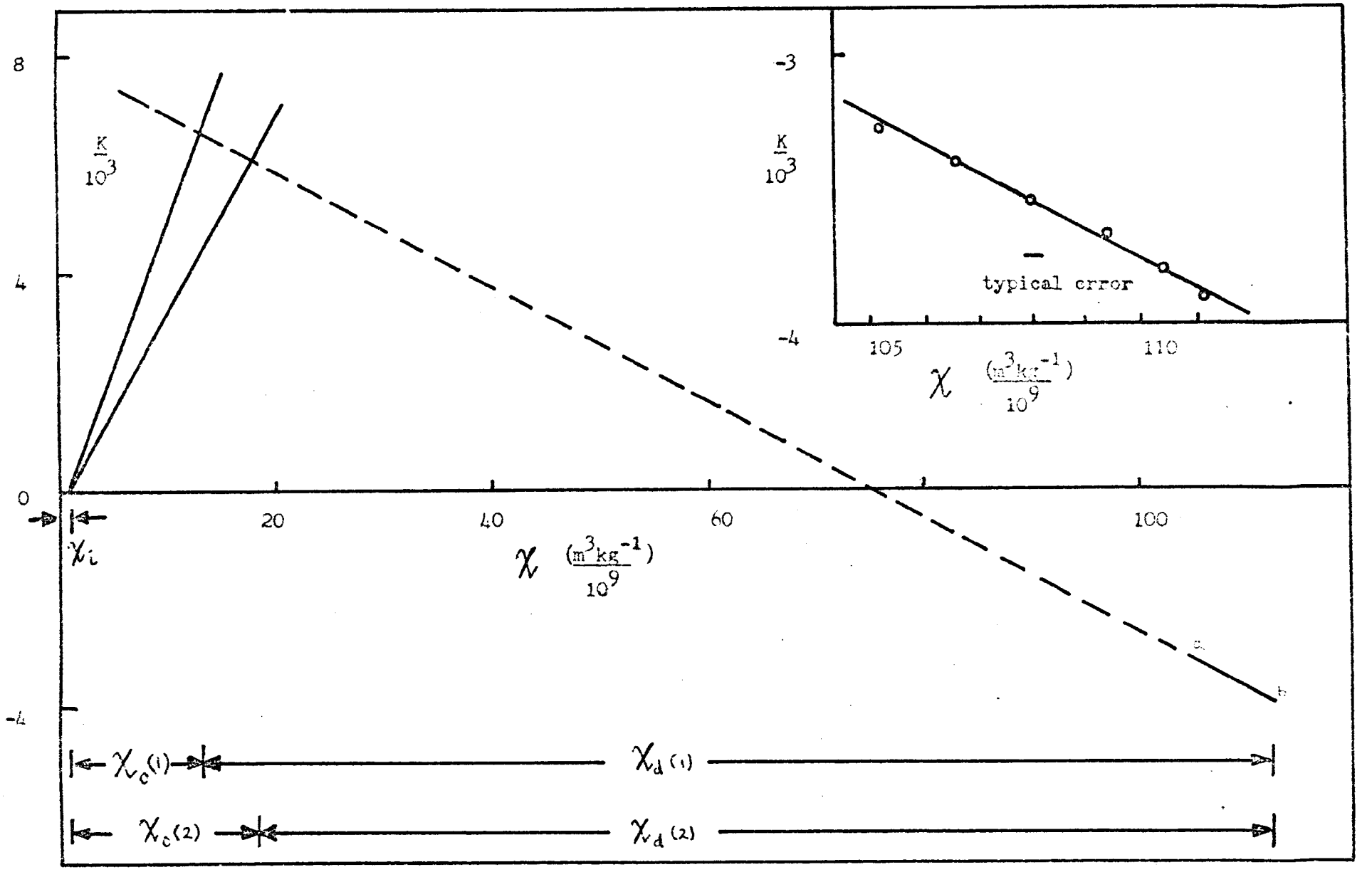

Figure 6.4 Susceptibility-Knight shift correlation in VO_2

known at 373 K from the single crystal data of (6)) leaves the central $\frac{1}{2} \rightarrow -\frac{1}{2}$ transition with a complex lineshape for a powdered sample, as discussed by Baugher et al (15). Using the data of (6), the line at 0·8 T should show two singularities separated by 2·2 mT, flanked by shoulders with an overall separation of 2·8 mT (figure 6·5a). At 1·4 T one singularity, flanked by shoulders separated by 4·3 mT, is expected (figure 6·5b). The lineshapes are similar to the third and sixth diagrams of figure 2 of (15). Also in figure 6·5, the effect of folding the predicted curves with a 2 mT Lorentzian line is shown. The singularities have more influence on the resultant width than the shoulders. The shape and width are both consistent with the experimentally observed lines. Since the nuclear dipole-dipole interaction contributes only 0·4 mT, the bulk of the 2 mT broadening must come from T_1 effects. Now the core polarisation contribution to the relaxation rate can be conveniently estimated from K_{cp} (16) through

$$(1/T_1)_{cp} = \left(\frac{4\pi kT}{h}\right)\left(\frac{\gamma_n}{\gamma_e}\right)^2 K_{cp}^2 \left(\frac{1}{3} f^2 + \frac{1}{2}(1-f)^2\right) \qquad (6\cdot7)$$

where k is Boltzmann's constant, γ_e and γ_n the gyromagnetic ratio for s electrons and for the nucleus respectively, and f is the fractional t_{2g} charecter of the d electrons at the Fermi surface. Here f is 3/5. The expression yields 0·15 ms for $(T_1)_{cp}$ in the temperature range investigated, from the experimentally derived value of K_{cp}. There is no similar "Korringa-type" relation for $(T_1)_o$ and K_o, since K_o is not related to $D(E_f)$, whereas $(T_1)_o$ is. However, $(T_1)_o$ can be deduced from $(T_1)_{cp}$ using $(T_1)_o/(T_1)_{cp} = \frac{1}{2}(\alpha'/\beta')^2$, since both relaxation rates are related to the respective hyperfine fields, H_o and H_{cp}; these are in turn related to α' and β' (16). The factor of $\frac{1}{2}$ arises from the particular choice of f = 3/5. The result is 3 μs or 6 μs, corresponding to the two values of β' considered above. These correspond to line broadening of 6 mT and 3 mT respectively. It is clear that the orbital relaxation process

Figure 6.5 ^{51}V metallic phase lineshapes (all to same scale)

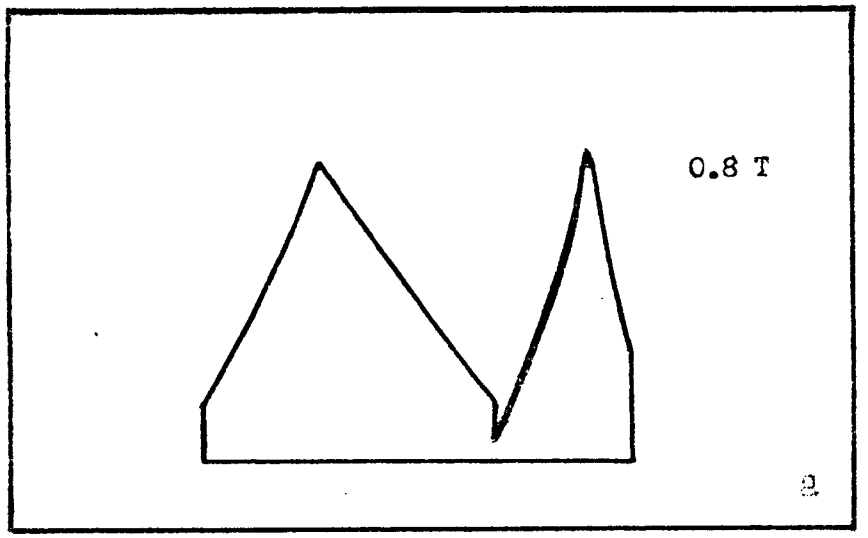

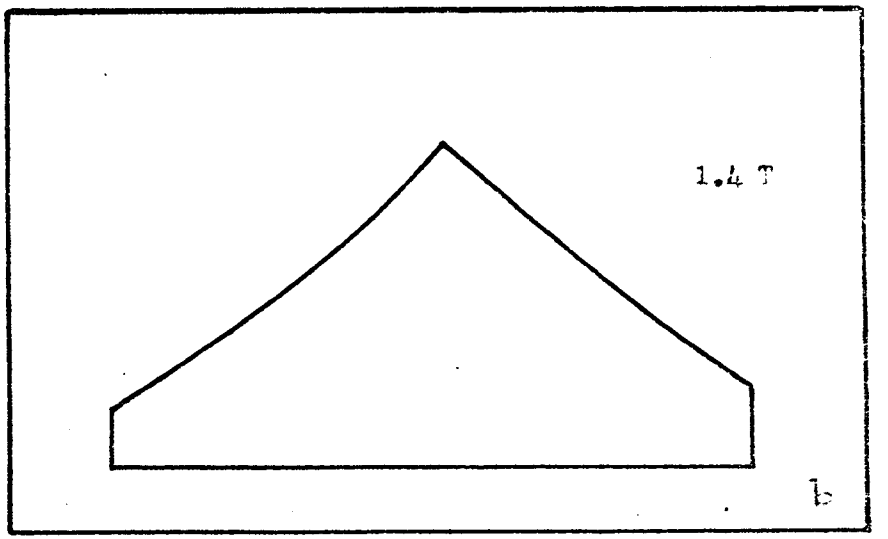

Theoretical lineshapes from quadropolar interactions

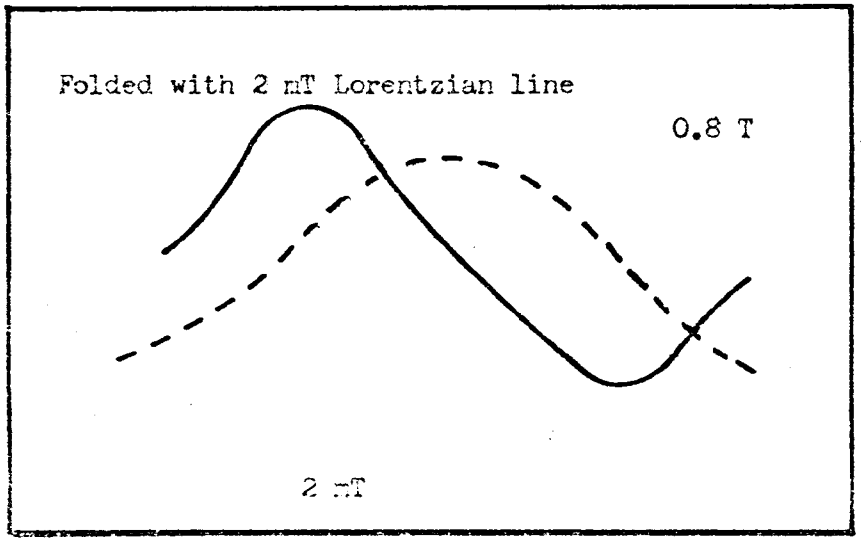

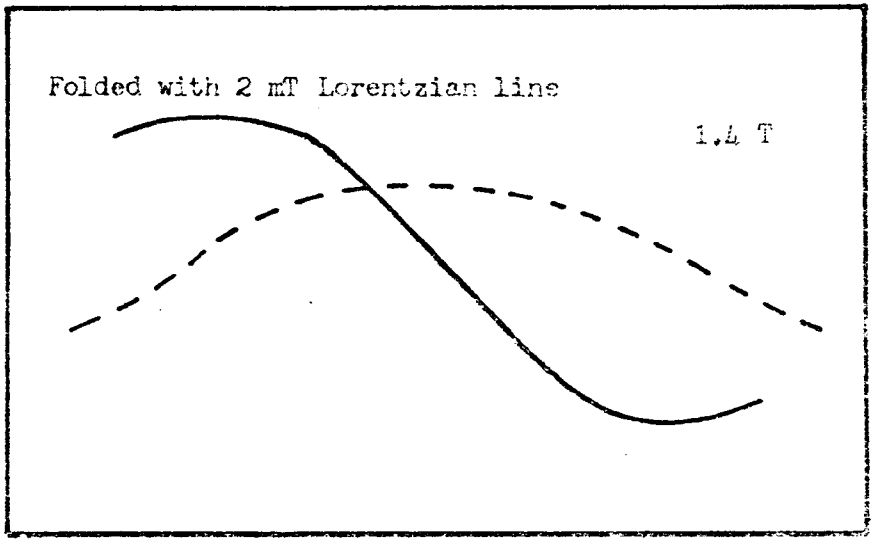

Resultant lineshapes and derivatives

dominates, as it does in pure vanadium (17). However, in that case, $(T_1)_o$ is about 50 times longer than the second value quoted above, which could arise from a density of states at the Fermi level about 7 times smaller than in VO_2. The value for $D(E_f)$ for d states deduced from the value obtained for χ_d is 16 $eV^{-1}molecule^{-1}$; this quantity in pure vanadium is 2 $eV^{-1}atom^{-1}$ (13). This is independent evidence for $(T_1)_o$ = 6 μs in VO_2, which amount also gives a reasonable fit to the linewidth data. Thus, the value derived from the estimate of $\langle r^{-3} \rangle$, including covalency effects, can be regarded as a satisfactory fit to the total NMR data, and the χ_o and K_o obtained using this β' are taken to be the correct ones.

It is of interest to compare the values of χ_o and K_o with the observed susceptibility and shift below T_t (where K_{cp} and χ_d are zero). If the degree of covalency were unchanged by the transition, $K_o(T > T_t)$ would equal the observed $K(T < T_t)$, and $\chi_o(T > T_t)$ would equal $\chi(T < T_t)$ minus the same χ_i as used above the transition temperature. However, the increased lattice distortion below T_t is likely to increase the degree of covalency, thus ensuring that χ_i is positive and decreasing β'. This means that $\chi_o(T < T_t)$ is certainly less than the total susceptibility, 15·17 x 10^{-9} m^3kg^{-1}, and hence must be less than $\chi_o(T > T_t)$, 16·3 x 10^{-9} m^3kg^{-1}. Consequently $K(T < T_t)$ must be expected to be less than $K_o(T > T_t)$ on two counts (since $K_o = \beta' \times \chi_o$); the experimental values (0·28 % and 0·61 % respectively) confirm this prediction.

6·4 The band structure of VO_2

Attention is now turned to the insight which can be obtained from the above data, together with other existing data on the band structure of VO_2 which is clearly important in understanding the nature of the transition. Considering each phase in turn:

$T > T_t$. The existence and magnitude of χ_o imply that the electronic

processes responsible for the charecteristic properties of VO_2 take place in at least two partially overlapping bands, containing Bloch states between which the orbital angular momentum operator has non-zero matrix elements. (Orbital degeneracy is necessary for the existence of χ_o). Models requiring isolated d bands , such as that due to Adler and Brooks (18) are eliminated since the energy denominator in the expression for χ_o (19) is large, causing χ_o to be too small. (Hence the requirement for partially overlapping bands). As conjectured by Goodenough (20), it seems likely that the bands involved are the $d_{x^2-y^2}$ sub-band and an anti-bonding band, $(d_{zx}:p_x)_\pi^*$, associated with π-overlap between cation d_{zx} and anion p_x orbitals (see figure 6·6). The existence of such hybridisation is certainly consistent with the use of the value of $\langle r^{-3} \rangle$ appropriate to about 30 % covalency. Assuming that these two sub-bands are parallel across the Brillouin zone and overlap by 50 %, Hyland and Hearn (21) have calculated that the observed χ_o indicates a vertical gap of about 0·45 eV, a value comparable to that inferred from optical absorption data (22) and to that given in (1) for the separation between the $d_{x^2-y^2}$ and d_{zx} levels of an isolated V^{4+} ion in an orthorhombic electric field, namely 0·43 eV; this latter value should correspond to the vertical gap at the zone centre. The same, and other (23), optical data imply an overall $(d_{x^2-y^2})$ bandwidth of about 1·5 eV, whence it follows (figure 6·6) that the bottom of the upper band must lie at least below the centre of the lower band. The resulting energy spectrum is thus consistent with the existence of a semi-metallic state in VO_2 for $T > T_t$, in which the density of states at the Fermi level is about 16 $eV^{-1}molecule^{-1}$.

$\underline{T < T_t}$. The valence band is the bonding portion of the $d_{x^2-y^2}$ band which splits off to a lower energy following the establishment of alternatively long and short cation separations along the tetragonal c-axis (1) on cooling through T_t. In this way a gap appears in the energy spectrum

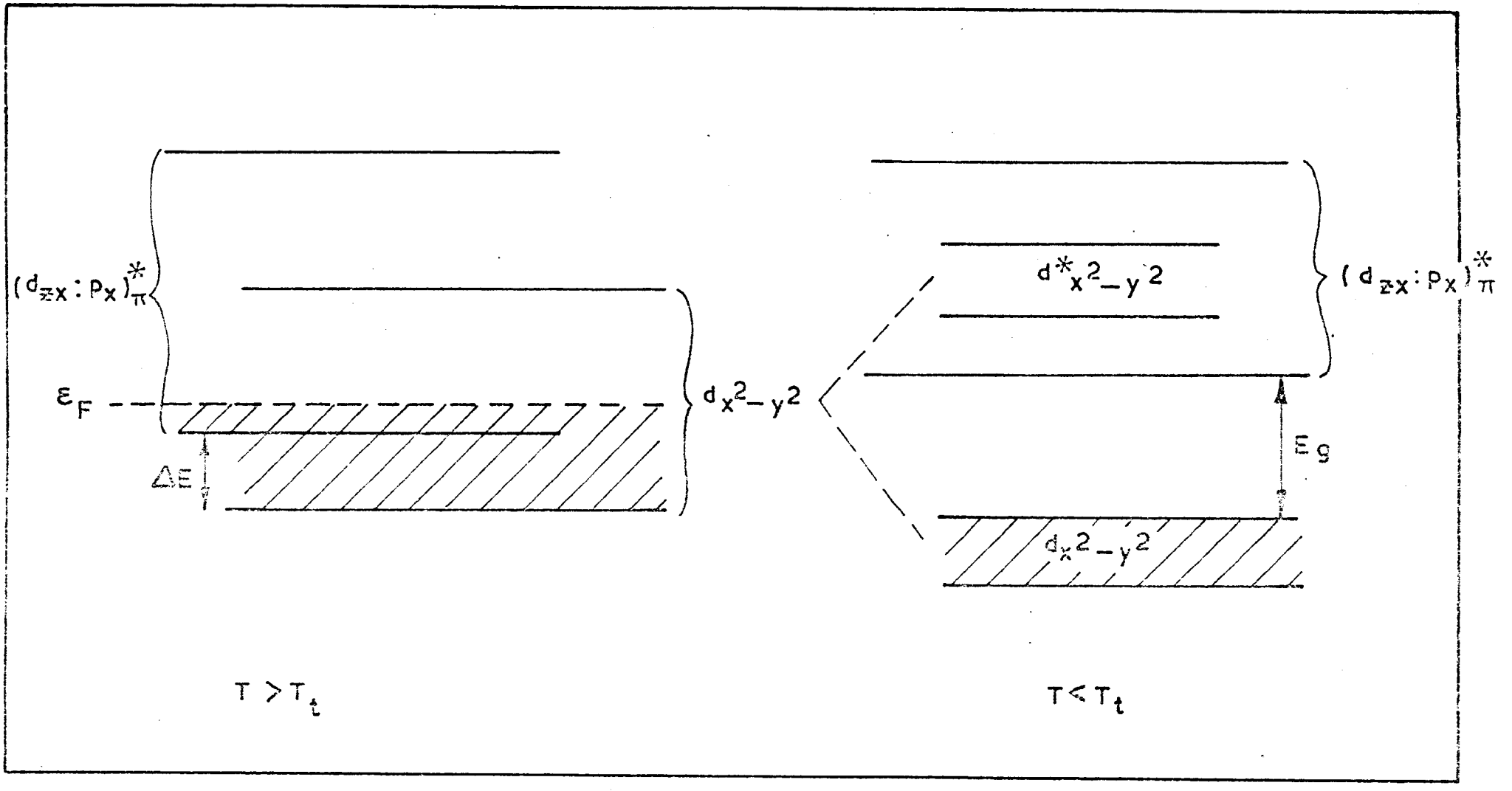

Figure 6.6 Band structure of VO_2

of the system, which separates this bonding band from the $(d_{zx}:p_x)_{\pi}^*$ anti-bonding band which still contains the anti-bonding portion of the $d_{x^2-y^2}$ band; according to Hyland (24) this anti-bonding $[d^*_{x^2-y^2}, (d_{zx}:p_x)_{\pi}^*]$ complex constitutes the conduction band. The depopulation of the $(d_{zx}:p_x)_{\pi}^*$ band at T_t increases the covalency of the system (since $(d_{zx}:p_x)_{\pi}^*$ is an anti-bonding band) and this in turn leads to a de-stabilisation of the $[d^*_{x^2-y^2}, (d_{zx}:p_x)_{\pi}^*]$ complex, enhancing the gap which originated initially from the c-axis cation-cation bonding (25).

As mentioned earlier the observed susceptibility in this phase is

$$\chi = \chi_i^{dia} + \chi_i^{vv} + \chi_o .$$

Optical data (22) reveal that the gap associated with the vertical transitions between the valence and conduction bands, from which transitions χ_o arises, lies between 0·4 and 0·5 eV. (Approximately of the same magnitude as the vertical gap for $T > T_t$). On the basis of Hearn's (21) calculation, the valence band is no longer parallel to the conduction band, for $T < T_t$, whence the calculated value for χ_o is slightly reduced from its value for $T > T_t$, in agreement with the experimental deduction.

References

1) Hyland G.J., J.Phys. C,(Proc.Phys.Soc.),1, 189-207, 1968.

2) Angus W.R., Proc.Roy.Soc., 136A, 569-78, 1932.

3) Kubo R. and Obata Y., J.Phys.Soc. Japan, 11, 547-50, 1956.

4) Clogston A.M.,Gossard A.C.,Jaccarino V. and Yafet Y., Phys.Rev.Lett., 9, 262-65, 1962.

5) Jones E.D., Phys.Rev., 137A, 978-82, 1965.

6) Umeda J.,Kusumoto H . and Narita K., J.Phys.Soc.Japan, 21S, 619-21, 1966.

7) Senftle F.E.,Pankey T. and Grant F.A., Phys.Rev., 120, 820-25, 1960.

8) Guggenheim H.J. and Berglund C.N., Phys.Rev., 185, 1022-33, 1969.

9) Hill G.J. and Martin R.H., Phys.Letters, 27A, 34-5, 1968.

10) Kosuge K., J.Phys.Soc.Japan, 22, 551-57, 1967.

11) Umeda J.,Kusumoto H.,Narita K. and Yamada E., J.Chem.Phys., 42, 1458-59, 1969.

12) Rado G.T. and Suhl H., Magnetism, vol. IIA, p.291, Academic Press, London, 1967.

13) Shimizu T., J.Phys.Soc.Japan, 18, 1192-1203, 1963.
23, 848-56, 1967.

14) Drain L.E., Proc.Phys.Soc., 83, 755-62, 1964.

15) Baugher J.F.,Taylor P.C.,Oja T. and Bray P.J., J.Chem.Phys., 50, 4914-25, 1969.

16) Jaccarino V., Proc.Int.School of Physics Enrico Fermi, Course 37, p.335, Academic Press, London, 1967.

17) Yafet Y. and Jaccarino V., Phys.Rev., 133A, 1630-37, 1964.

18) Adler D. and Brooks H., Proc. 1st.Conf.of Solids at High Pressures, Academic Press, London, 1965.

19) White R.W., Quantum Theory of Magnetism, p.86, McGraw-Hill, New York, 1970.

20) Goodenough J.B., Magnetism and the Chemical Bond, Interscience,New York, 1963.

21) Hearn C.J., To be published.

22) Verleur H.W.,Barker A.S. and Berglund C.N., Phys.Rev., 172, 788-98, 1968.

23) Mokerov V.G. and Rakov A.V., Soviet Physics(Solid State), 11, 150-52, 1969.

24) Ford C.J.,Segel S.L.,Seymour E.F.W. and Hyland G.J., Phys.kondens. Materie, 14, 111-18, 1972.

25) Goodenough J.B., Progr.Solid State Chem., 5, 351-57, 1971.

Chapter 7

Magnetic susceptibility and Knight shifts in more complicated alloys

7·1 Introduction

Recent investigations have been made of the NMR properties in alloy systems in which the possibility of non-random atomic arrangements in the liquid phases had been suggested ((1) and (2)). Measurements of the magnetic susceptibility were therefore undertaken in these systems in order to provide further information of their electronic structures (and atomic arrangements), and also to enable correlations with these Knight shift measurements to be made.

7·2 Noble metal alloys

Existing x-ray diffraction and electrical resistivity data suggest the possibility of intermetallic compound formation in liquid alloys of the noble metals with indium, and with tin (1). The magnetic susceptibility of some of these alloys has been investigated as a function of temperature and concentration. The systems chosen were

1) liquid copper-indium, gold-indium, and silver-indium alloys, and
2) gold-tin alloys in both the solid and liquid phases.

7·2·1 Experimental results

The results for the total mass susceptibility are shown in figures 7·1 and 7·2, along with the pure noble metal values of section 3·2. As can be seen, all the noble metal-indium alloys have similar maxima in the diamagnetic susceptibility at about thirty atomic percent of indium, whether plotted isothermally or following the liquidus. The possibility of a similar maxima in the gold-tin system at between 85 and 90 atomic percent gold cannot be ruled out at 773 K. (The temperature coefficient of susceptibility of liquid gold-Appendix 1-is small, and the value for gold considered "supercooled" to 773K would be very close to the point plotted). The results

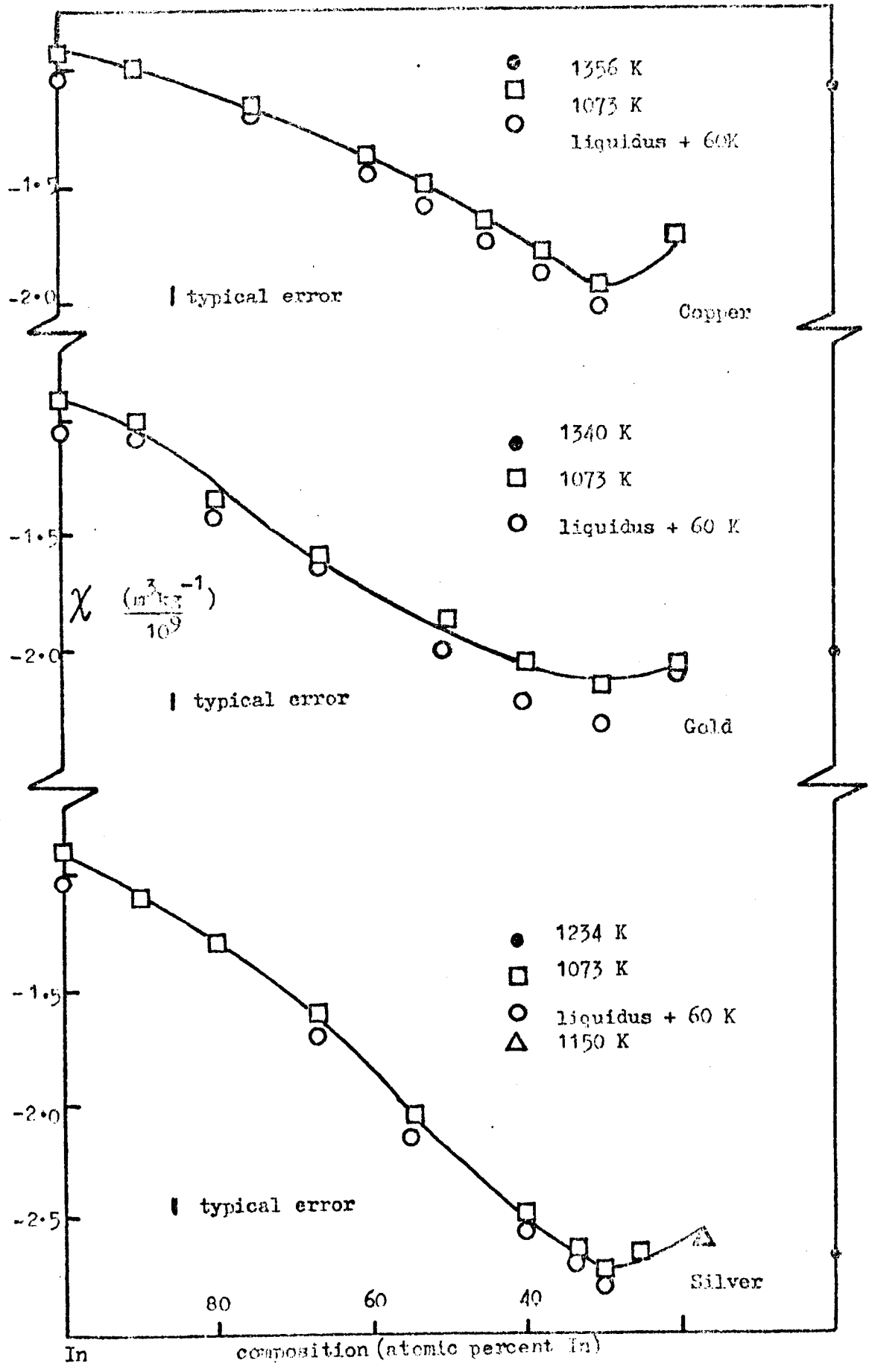

Figure 7·1 Magnetic susceptibility for some liquid noble metal-indium alloys

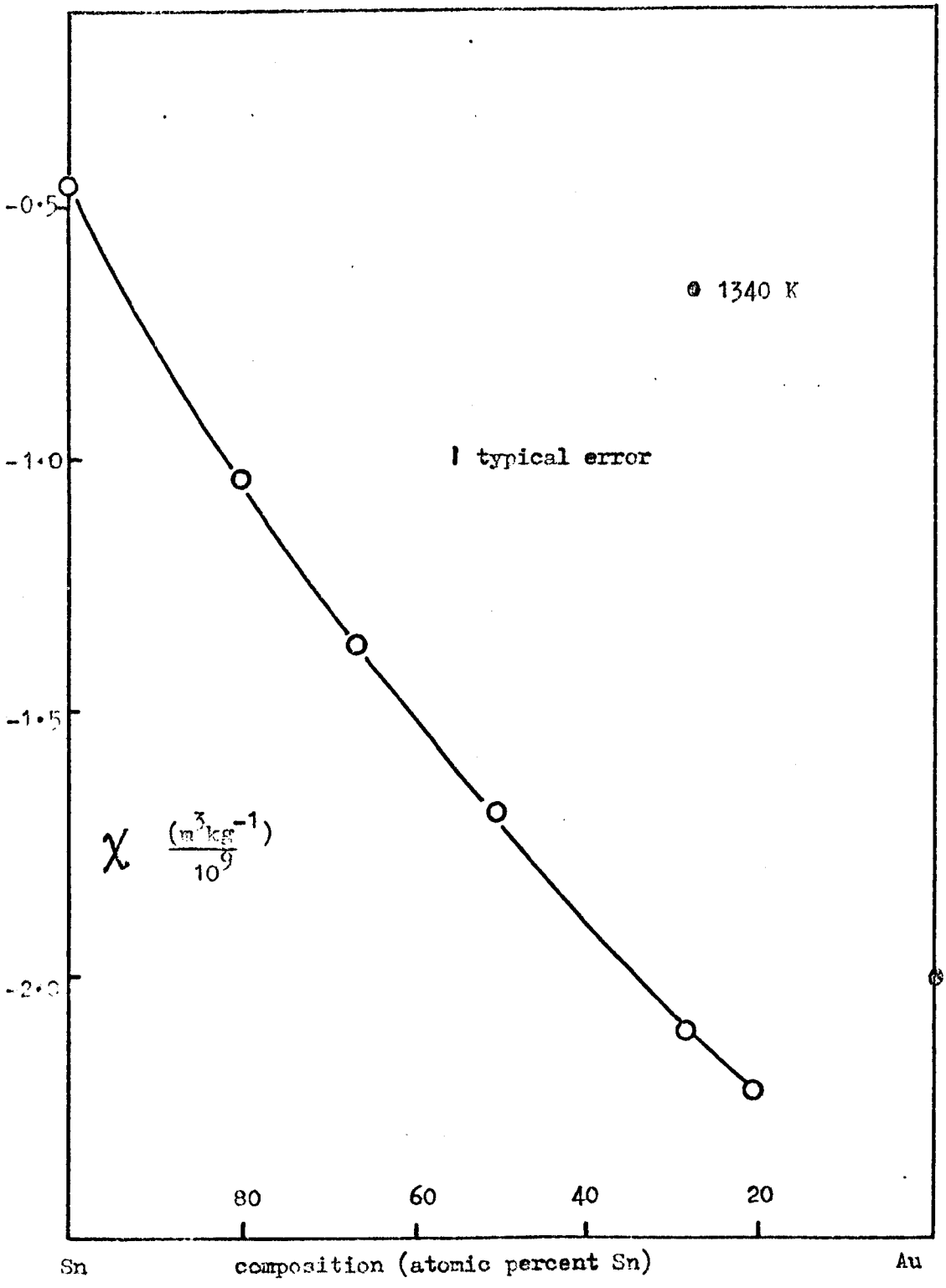

Figure 7·2 Magnetic susceptibility of Sn-Au alloys at 773 K

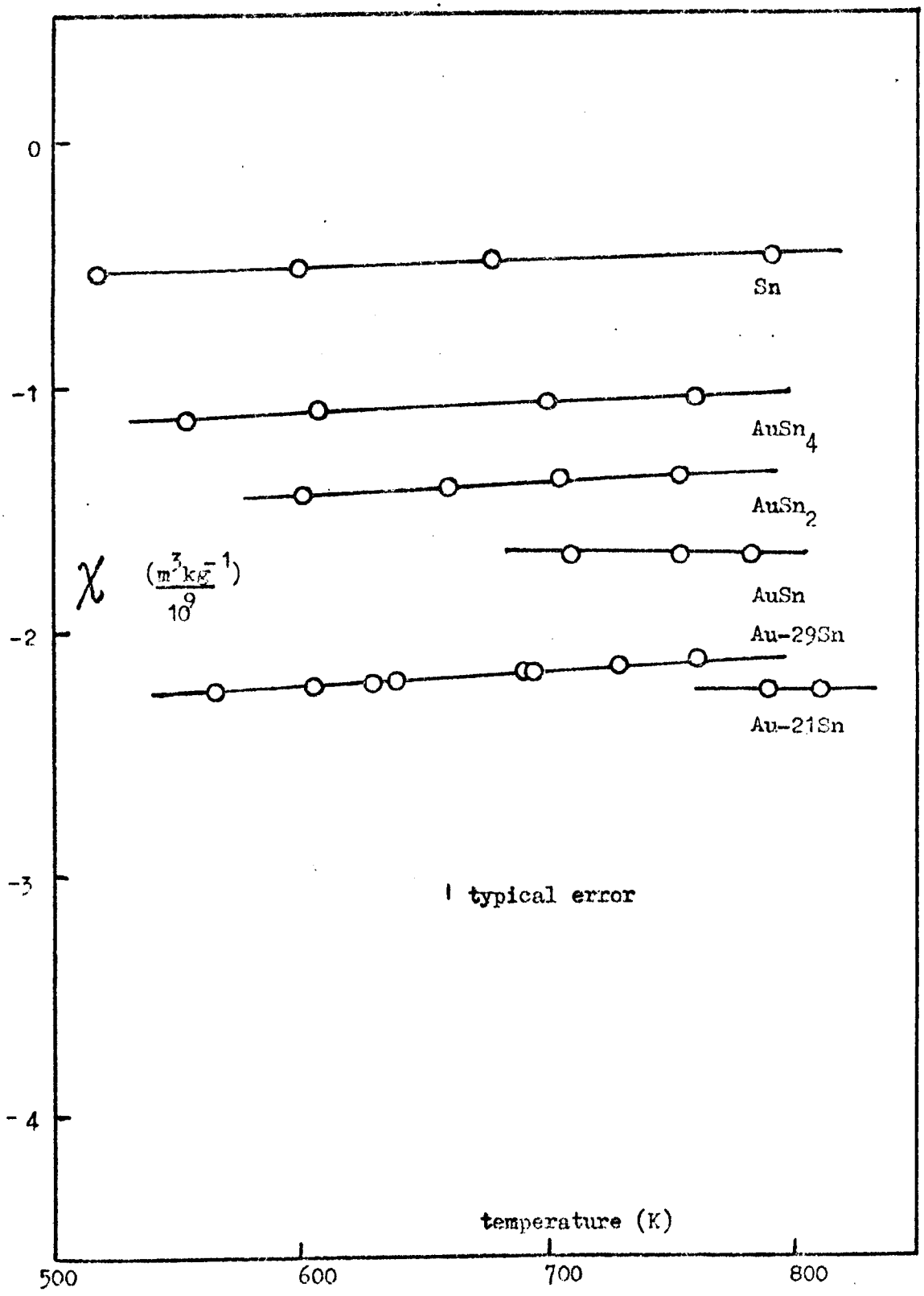

Figure 7·3 Magnetic susceptibilities of some liquid Au-Sn alloys

for χ_m in the liquid phase are shown in figure 7·3; the full experimental data is listed in Appendix 1.

7·2·2 Discussion of susceptibility data

All the systems appear to exhibit a negative maximum ~~diamagnetism at the measuring temperatures~~ in the mass susceptibility. This should be contrasted with the linear behaviour in the simple alloys investigated in Chapter 4, and is consistent with a reduction of the conduction electron paramagnetism, associated with some kind of bond formation. (It is simpler to consider mass susceptibility than the more appropriate volume electronic susceptibility if compound formation is considered likely, since under these conditions assumptions about the ionic terms and interpolated densities would be difficult to justify.) Moreover, from the measured temperature dependencies of χ_m, it is found that as the temperature increases these maxima gradually disappear, in keeping with the suggestion that order is retained from the solid, being slowly lost due to thermal fluctuations. However, none of the maxima occurred at compositions suspected of bond formation (Au_3Sn, $AuIn_2$, $CuIn_2$, $AgIn_2$) and furthermore the NMR evidence of (1) does not lend support to the idea either. Accordingly, since the evidence for liquid atomic ordering is weak, it was decided to look for other possible explanations in terms of random alloy behaviour i.e. as in earlier chapters. The results were analysed at the temperatures at which the Knight shift data were obtained, and also extrapolated to 1363 K, a temperature at which all the noble metals themselves are liquid. Assuming random behaviour, linear interpolations of alloy densities and of ion-core diamagnetism between the pure metal values were made, and the volume electronic susceptibility obtained, as explained in section 1·1. The results of such an analysis are shown in figures 7·4 - 7·6. As expected, χ_e is everywhere paramagnetic. There is a minimum corresponding to the maximum diamagnetism in χ_m, in the copper-indium and silver-indium alloys at 1073 K. The very

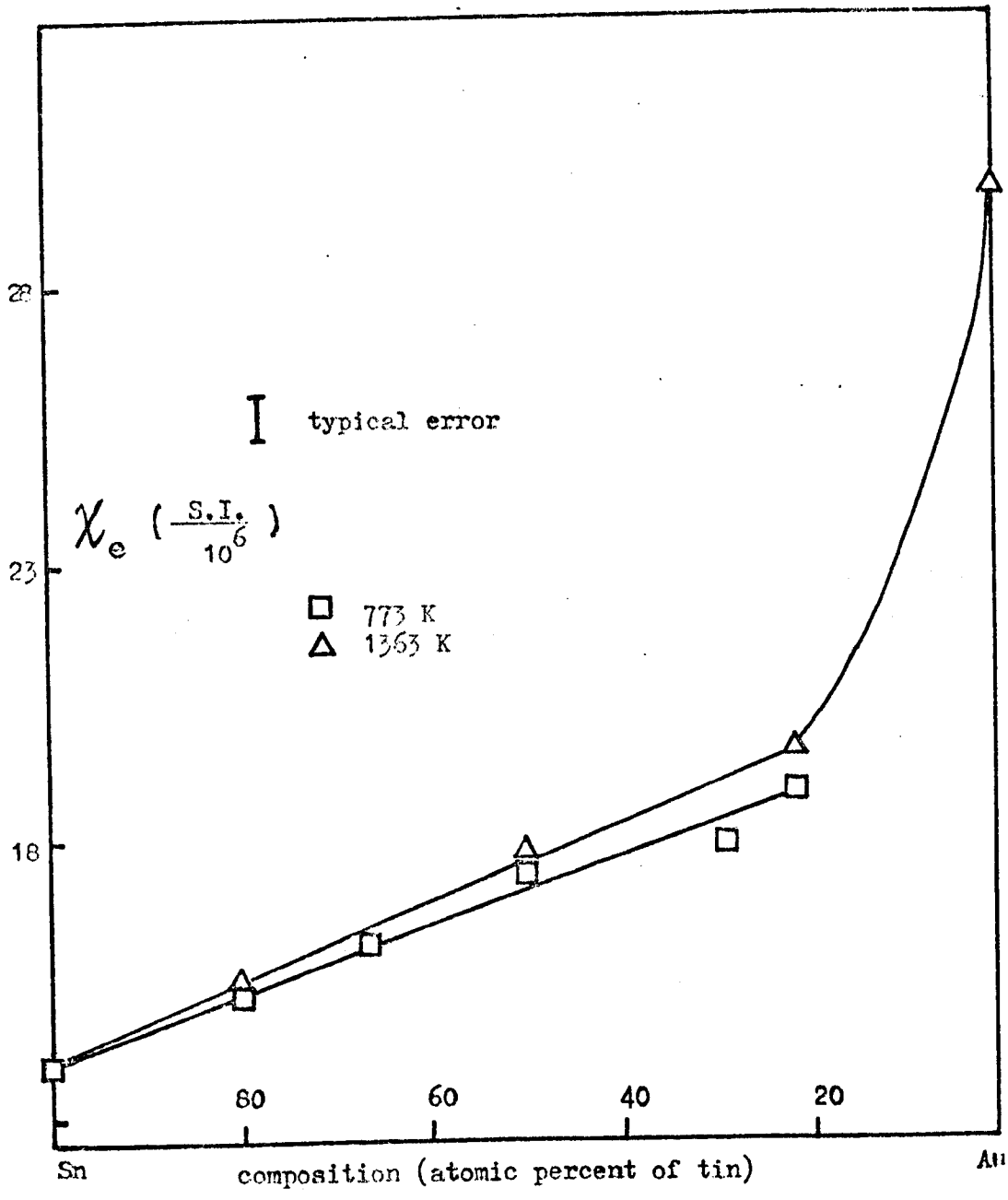

Figure 7·4 Electronic susceptibility of liquid Sn-Au alloys

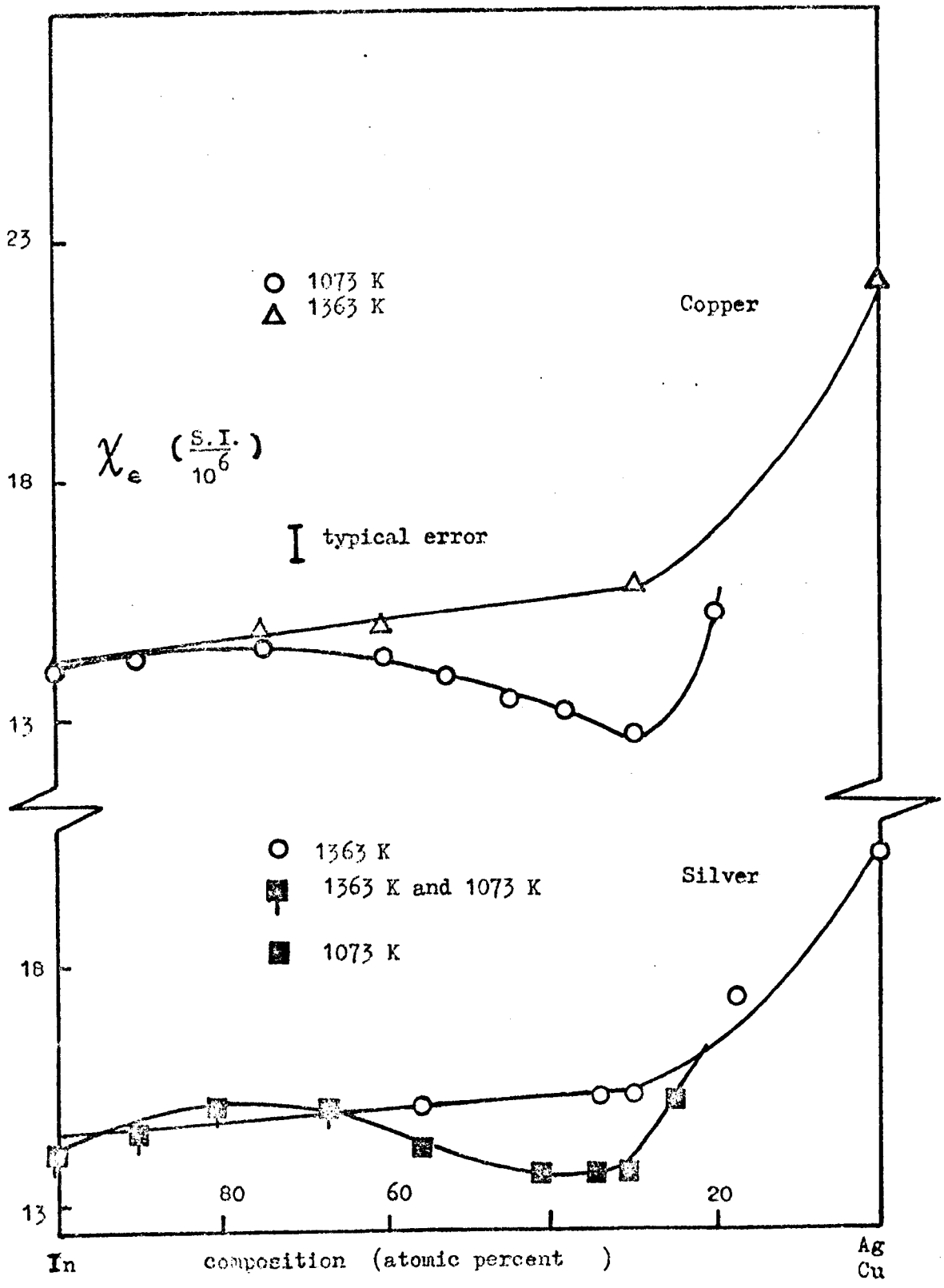

Figure 7·5 Electronic susceptibility of liquid In-Ag and In-Cu alloys

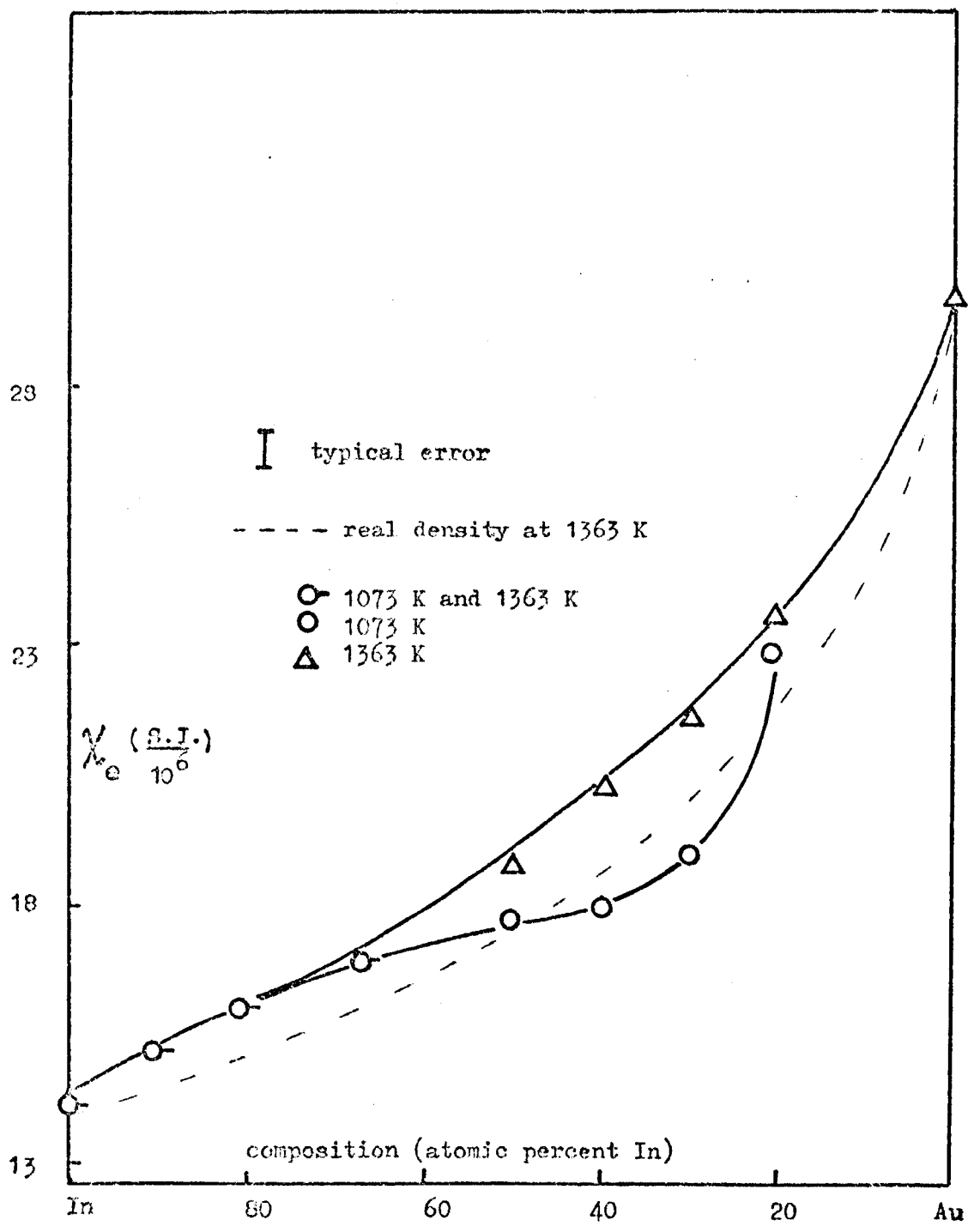

Figure 7·6 Electronic susceptibility in In-Au alloys

large increase in χ_e near the noble metal end of the concentration range is mirrored in the very large fractional increase in the ^{63}Cu shift observed by (1) in this region.(Copper was the only noble metal for which a resonance was observed.) The minima disappear at higher temperatures in both systems. No minima are observed for either of the gold alloys. The assumption of linear behaviour of the density with alloy composition is undoubtably an approximation. Bramall (private communication) has recently measured the density across the gold-indium system, up to 1363 K (figure 7·7). The values of χ_e deduced using these densities are shown in figure 7·6. The approximation appears to make little difference to the behaviour of χ_e, but causes a maximum error of about ten percent in χ_e in the middle of the concentration range.

The main problem in analysing the results arises from the complications associated with the noble metal susceptibilities already discussed in section 3·3·2. The approach adopted in section 4·2·4 for alloys, deducing χ_p from χ_e by subtracting a calculated χ_d value, is likely to be inaccurate since it ignores the effects of s-d hybridisation which are particularly important near the noble metal end. However, even with this qualification, an attempt to give a possible explanation for the minimum occurring in χ_e (and presumably χ_p) in the silver-indium and copper-indium systems can be made. As discussed in section 3·3·2, the s-d hybridisation leads to an enhancement of the density of states in the noble metal. In the alloy this enhancement decreases faster than the simple free electron increase of the density of states with increasing indium concentration, ignoring for the moment the electron-electron enhancement (which will be similar for both pure metals). These opposing effects may yield initial slopes of χ_p with concentration which are negative at both pure metal ends, with a minimum somewhere near the noble metal end (where the s-d enhancement has effectively vanished). For the gold alloys

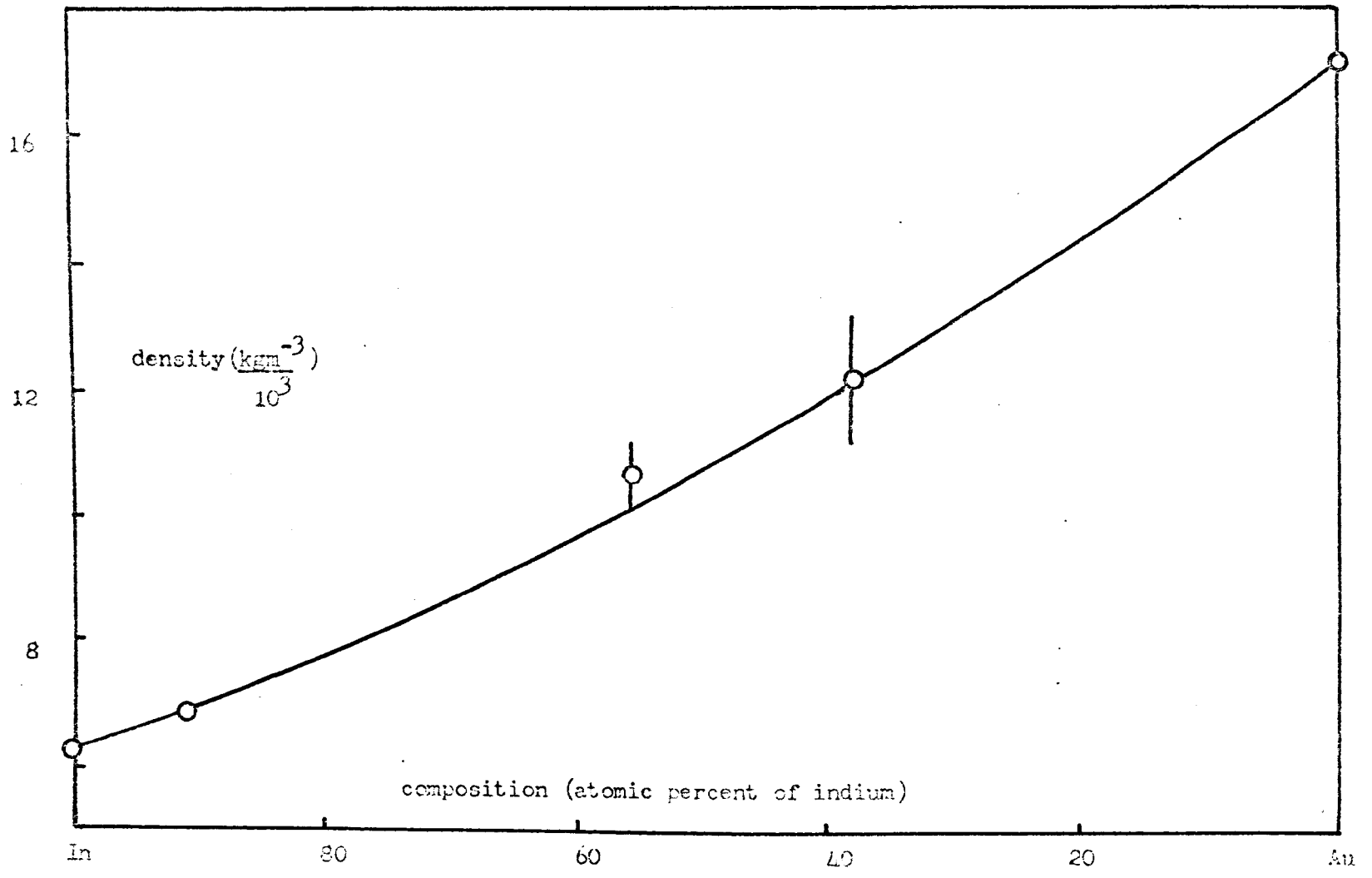

Figure 7.7 Density of In-Au alloys at 1363 K

this effect may be masked, there being a much larger change in χ_e across the concentration range. This approach does not explain the disappearance of the minimum with temperature, nor the apparent small maximum in χ_c near indium. It is clear, however, that s-d hybridisation effects will be present. The problem of comparing experimental Knight shifts and susceptibilities will now be considered.

7·2·3 Discussion of P_f: the partial wave approach

Table 7·1 shows the experimental Knight shift changes, Γ_{expt}, and the calculated initial changes in ΩP_f, obtained by (1). These latter values were obtained from a partial wave analysis, using a screened free atom potential. From the general expression for the direct contribution to K, (equation 1·10) the initial slope is just the sum of the initial values, $(1/\Omega P_{fE})(d(\Omega P_{fE})/dc_F)$ and $(1/\chi_p)(d\chi_p/dc_F)$, E and F refering to the solvent and solute respectively. The difficulties in obtaining the last term are by now apparent. The values from χ_e^{expt} ($\chi_e^{expt} + \chi_d$, ignoring the unknown m* correction to χ_d-see section 4·2·4-which will only reduce an already small term) are shown in table 7·1, column 3. They are all positive. Another way of estimating this quantity is from the expected changes in the electron/atom ratio and electron-electron enhancement, thus for free electrons,

$$\frac{1}{\chi_p}\frac{d\chi_p}{dc_F}(fe) = \frac{1}{3}\left(Z_F - \frac{Z_E}{\Omega}\right)\frac{d\Omega}{dc_F} + \frac{1}{\epsilon_E}\frac{d\epsilon_E}{dc_F} \qquad (7·1)$$

where the first two terms on the right of equation 7·1 cover the change in χ_{po} due to changes in the valency and atomic volume upon alloying, and ϵ_E is the electron-electron enhancement factor for pure metal E. The change in this last term is very small, and the assumption of linearity of ϵ with concentration can be made. This expression comes from the definition of χ_p for free interacting electrons. Since free electron behaviour of liquid indium and tin is expected (section 3·3·1) such an analysis may be useful. The values of the coefficient obtained are shown

in table 7·1, column 4. These are all small negative numbers and as can be seen give a better fit with experimental K values. This is not surprising and reinforces the belief that the simple analysis of χ' adopted with success in other systems, yielding χ_p, does not work for noble metals and their alloys. Furthermore, it must be remembered that the measured density (in the Au-In system) caused a further small change in the initial slope of χ_p. There is thus considerable uncertainty in this quantity although it is clear that it gives a smaller contribution than $(1/\Omega P_{f_E})(d(\Omega P_{f_E})/dc_F)$ in all these systems.

Table 7·1

Contributions to Γ in noble metal alloys

system solvent	system solute	χ_p^1	$\chi_p^1(fc)$	ΩP_{fE}^1	$\Gamma^{theo}_{(3+5)}$	$\Gamma^{theo}_{(4+5)}$	Γ_{expt}
1	2	3	4	5	6	7	8
tin	gold (773 K)	0·35	-0·04	0·17	0·52	0·13	0·28
indium	gold (1073 K)	0·45	-0·03	0·24	0·69	0·21	0·28
indium	silver "	0·19	-0·04	0·20	0·39	0·16	0·22
indium	copper "	0·13	-0·02	0·15	0·28	0·13	0·11

$\chi_p^1 = \frac{1}{\chi_p}\frac{d\chi_p}{dc_F}$, and similarly for $\chi_p^1(fe)$ and ΩP_{fE}^1.

7·2·4 Discussion of P_f: the pseudopotential approach

Host (1) has also calculated the expected variations in ΩP_f with concentration across the whole alloy range, using the pseudopotential approach discussed in section 1·4·2. Unlike the phase shift method, this is not limited to very small concentrations, and it seems clear that there will be less uncertainty in the total change in χ_p than in its initial slope. The values for χ_p (from $\chi_e^{expt} + \chi_d$) and ΩP_f for the alloys can then be multiplied to obtain estimates for the variation in K across the whole range, and the results compared with the experimental values at the measuring temperatures (see figures 7·8 and 7·9). The

Figure 7.8 Knight shift variation in liquid indium alloys at 1073 K

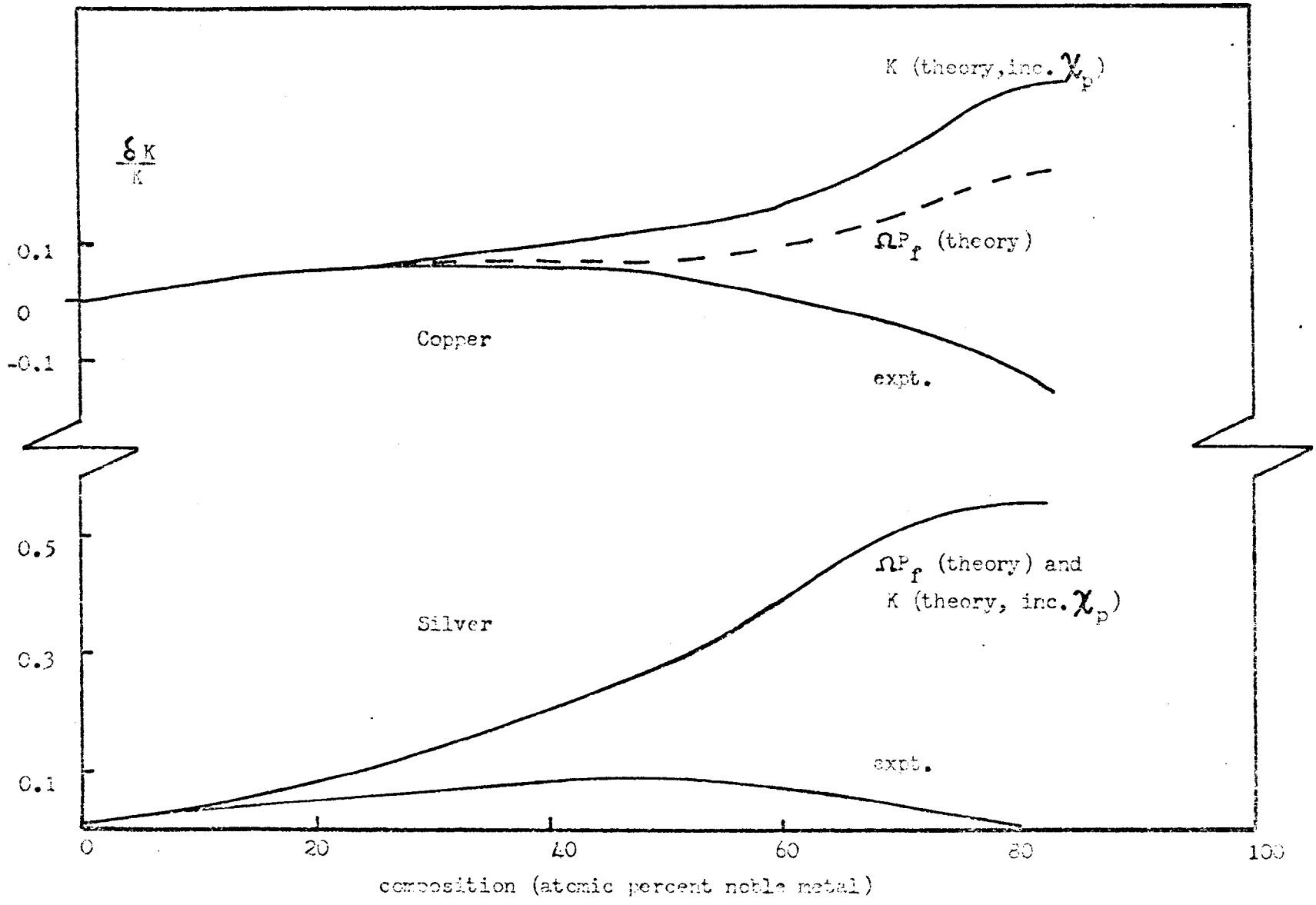

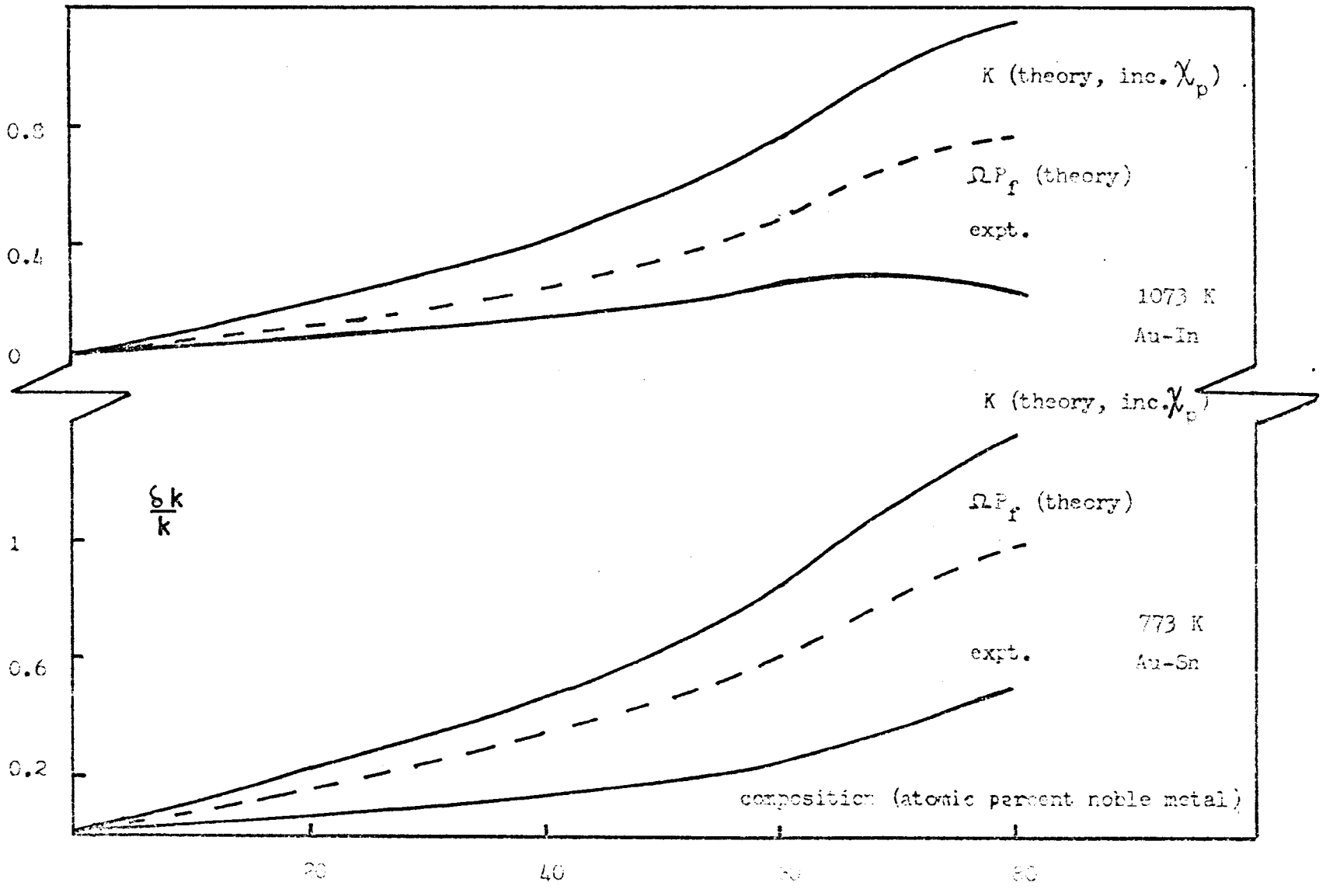

Figure 7.9 Knight shift variations in some liquid gold alloys

main contributions come from the ΔP_f changes. Comparison with experiment shows that the general trend in K is adequately described but that the quantitative change is too large in all cases. The assumption of linearity of atomic volume (only slightly different to linearity of density in these cases) also affects the values of the Fermi wavevector used in the calculation. This is certainly one source of error. The actual values of the Knight shifts of ^{115}In and ^{119}Sn are both larger than predicted by this calculation (69 % of K_{expt} for ^{115}In, 74 % for ^{119}Sn).

7·2·5 Conclusion

It is clear that both the pseudopotential and phase shift approaches meet with limited success in describing the experimental variations of the Knight shifts in these alloy systems, but many necessary approximations and simplifications limit the procedures to a semi-quantitive fit. No firm evidence for non-random atomic behaviour in the liquid phase was found for any system.

7·3 Thallium-tellurium alloys

7·3·1 Introduction

Marked maxima have been observed in the Hall coefficient and resistivity for liquid $TeTl_2$ alloys, as discussed by Brown et al (2) whose NMR study of this liquid alloy system was supplemented by the present author by an investigation of χ.

7·3·2 Experimental results

The magnetic susceptibility of tellurium was measured at 750 K and that of four alloys with thallium was studied as a function of temperature in the range 650-1000 K. The results are summarised in figure 7·10. The large error for Te arose from its high evaporation rate at the measuring temperatures. The full results are tabulated in Appendix 1.

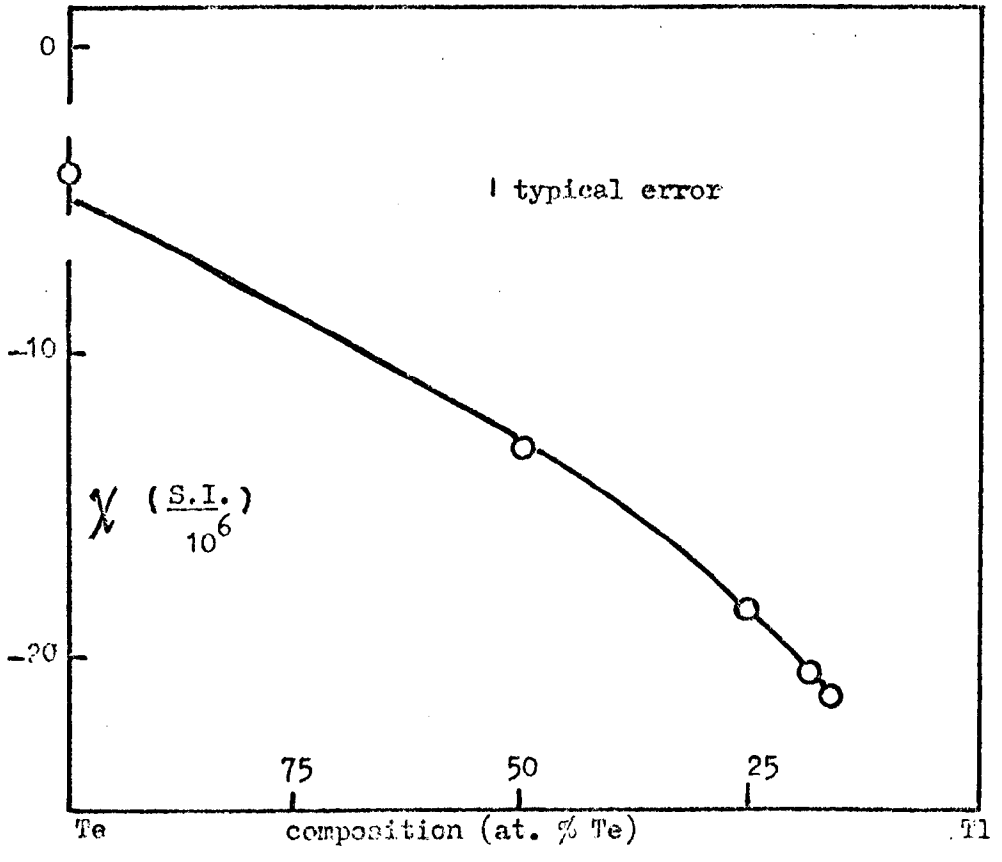

Figure 7·10 Magnetic susceptibilities of Te-Tl alloys at 773 K

7·3·3 Discussion

These results have been compared with the Knight shift variations with temperature and concentration by (2). For these particular alloys, which are semiconductors, it is not a straightforward matter to subtract the ion core diamagnetism. However, an estimation of χ_e from the measured susceptibility was attempted by the following procedure. The electrical conductivity, σ', is proportional to the square of the density of states in these alloys (3). Now, χ_e (in mass units) is proportional to $D(E_f)$. Hence,

$$\frac{1}{\sigma'}\frac{d\sigma'}{dT} = \frac{2}{\chi_e}\frac{d\chi_e}{dT} \qquad (7·2)$$

Also in mass units, the ionic term in χ is independent of temperature, so $d\chi_e/dT$ is equal to $d\chi/dT$. From the measured σ' data (3), values of χ_e can be deduced using $d\chi/dT$ for the various alloys. In this way χ_e at 800 K was found to decrease from $2·1 \times 10^{-9}$ m^3kg^{-1} for $Te_{60}Tl_{40}$ to $0·2_5 \times 10^{-9}$ m^3kg^{-1} for $Te_{36}Tl_{64}$ and $0·1_3 \times 10^{-9}$ m^3kg^{-1} for $Te_{34}Tl_{66}$. The volume susceptibilities were calculated from the known densities of these alloys (4). These give 15, 2·5, and 1·3 ($\times 10^{-6}$) respectively, in SI units. Thus, by comparison with typical metal values (13×10^{-6} SI), it is seen that the susceptibility data confirm a rapid decrease in $D(E_f)$ as the composition $TeTl_2$ is approached. Neglecting any possible orbital contribution to the susceptibility,

$$K = Y\chi_p \qquad (7·3)$$

where Y involves the electron density at the nucleus, and will be large for a large s charecter of the conduction electrons. Comparisons of the temperature coefficients of the observed shift and χ_p (assuming $\chi_p = 3\chi_e/2$, and obtaining χ_e as previously explained) yield values for Y which are large (comparable with the values for the pure metals in the tellurium row of the periodic table).

It was thus concluded in (2) that the conduction electron density

at the ^{125}Te nucleus changes little on alloying with thallium, and the variations of Knight shift and susceptibility both with concentration and with temperature are due principally to changes occurring in the density of states at the Fermi surface. The large shift which the authors observed in $TeTl_2$, where the density of states is small and consequently the conduction electron contribution is small, is interpreted as being a chemical shift having its origin in bonding electrons. They say that this strongly suggests that molecular groups of the form $TeTl_2$ exist in the liquid.

References

1) Host I.P., Ph.D. thesis, University of Warwick, 1972.

2) Brown D.,Moore D.S. and Seymour E.F.W., Phil. Mag., 23, 1249-59, 1971.

3) Enderby J.E. and Simmons C.J., Phil. Mag., 20, 125-34, 1969.

4) Kanda F.A., USAEC Report NYO-2731/8, 1967.

Chapter 8

Local moment formation in gallium alloys

8·1 Introduction

Magnetic moments in free transition metal ions arise from the incompletely filled d shells present. If such an ion is dissolved in a non-magnetic metallic host (such as one of the metals considered in chapter 3) the d levels broaden due to the interactions with the surrounding conduction electrons, becoming resonance states since they lie within the conduction band of the host. If the coupling with these electrons of the host is large compared to to the interactions between the d electrons of the impurity, the magnetic moment vanishes. This is the case if the host has a large density of states at the Fermi level, and also for impurities for which the d levels of both spin directions are either nearly empty or nearly full, and also for impurity levels which are far removed from the Fermi level. Friedel (1) has discussed this behaviour in terms of a "virtual bound state"; this state consists of the conduction band and the localised moment (most of the impurity electron wavefunction is localised near the transition metal ion) modified by a weak perturbational exchange coupling between them. Kondo (2) has suggested that below a characteristic temperature T_K this state collapses to a "quasi bound state", in which the moment is counterbalanced by a cloud of spin polarisation arising from the same s-d interaction which gives rise to the virtual bound state. Friedel has formulated an approximate criterion for the conditions necessary for localised moment formation (section 8·3·3).

This criterion leads to the prediction that localised moments will not occur in liquid gallium alloys, with any of the first series transition metals as impurity. Earlier work (3) on gallium-manganese alloys had suggested that a moment existed, and consequently it was decided to investigate some systems with gallium as the host. By introducing various

transition metal impurities into a host matrix the parameters, such as p, the number of d electrons, can be varied and some insight may be gained of local moment formation. One easily identifiable characteristic of local moments is the behaviour of their magnetic susceptibility, which varies inversely with temperature (section 1·1·4). In the present work the net susceptibility $\Delta\chi$ (after subtraction of the host component) of some transition metals in liquid gallium was measured. The atomic concentration of the impurity was kept at , or below, about one percent, so as to minimise the complications which would arise from impurity-impurity interactions at higher concentrations. The behaviour of the host Knight shift, linewidth, and longitudinal spin-lattice relaxation time were also investigated in alloys of gallium with manganese and gallium with chromium. These quantities may yield information about the localised state, including an estimate of its lifetime. Further, the susceptibility and NMR data may be considered together, as in earlier chapters; such an approach might yield a self-consistent picture of the localised moment system. This will be discussed fully in section 8·3. The overall data for gallium-manganese alloys will be considered, and values for the characteristic temperature, θ, the lifetime of the state, and the conduction electron-local moment coupling constant, J, (4) derived. The results will be compared with those of the copper-manganese system (5) and those of the aluminium-manganese system (6), (local moment forming and not, respectively).

8·2 Experimental results

8·2·1 Magnetic susceptibility

All the metals used here were of 99·999 percent purity or better, as in earlier chapters. The net magnetic susceptibility of several concentrations of manganese in gallium was derived from total susceptibility measurements. The results are summarised in figure 8·1; they were obtained at temperatures between 1200 K and the liquidus, below which point the

manganese is lost from solution. (All the impurities considered are insoluble in gallium in the solid phase). This linear behaviour of reciprocal net susceptibility with temperature is characteristic of local moments, and the results will be analysed in terms of a Curie-Weiss law in section 8·3.

Figure 8·2 shows the experimentally derived results obtained for the several gallium-chromium alloys investigated, plotted in a similar fashion; again, linearity is observed. There is more uncertainty in the intercept on the temperature axis ,however, because of the shallow slope and limited temperature range. The range was limited at the upper end by evaporation of the gallium and at the lower end by the liquidus. These results will be analysed in the same way as those of Ga-Mn.

Further, the behaviour of $\Delta\chi$ as a function of impurity concentration and temperature was studied in dilute gallium-iron and gallium-copper alloys (figures 8·3 and 8·4). In these systems, $\Delta\chi$ was found to be small and virtually temperature independent, showing a slight increase with temperature. It is apparent that these two systems do not show local moment formation. (The figures show the total χ.)

Figures 8·5 and 8·6 show the net susceptibility as a function of concentration for the gallium-manganese and gallium-chromium systems respectively, at an isotherm in the liquid phase. As can be seen, there is no difficulty in dissolving the impurity, the additional susceptibility varying linearly with concentration.It is worth pointing out that in these alloys

$$\chi_{Ga\text{-}Mn} > c_{Ga}\,\chi_{Ga} + c_{Mn}\,\chi_{Mn} \qquad (8\cdot1)$$

where c is the atomic concentration. Finally, the original χ data for all these systems is listed in Appendix 1.

In order to investigate the NMR of the gallium host in these two

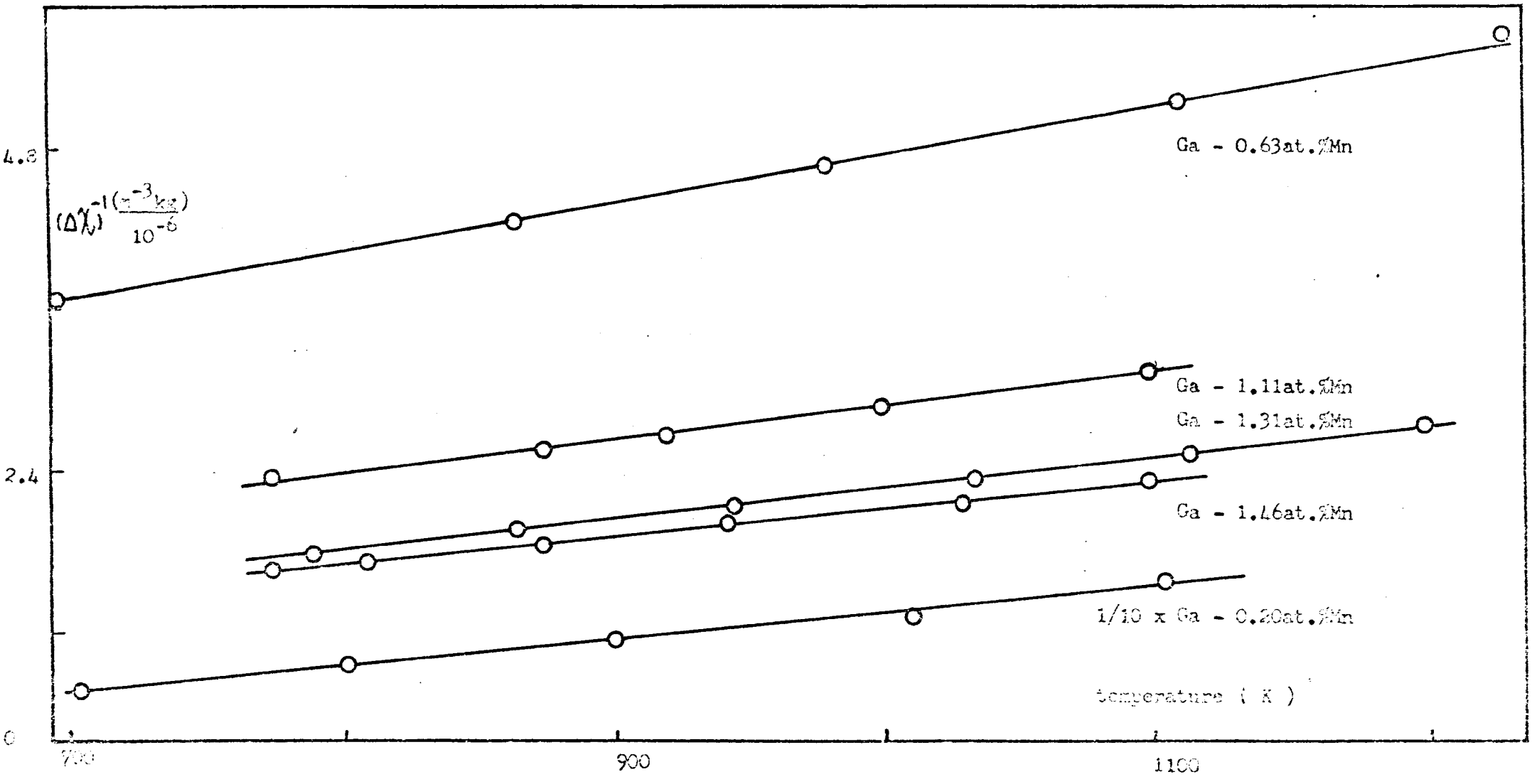

Figure 8.1 Reciprocal net susceptibilities for some gallium-manganese alloys

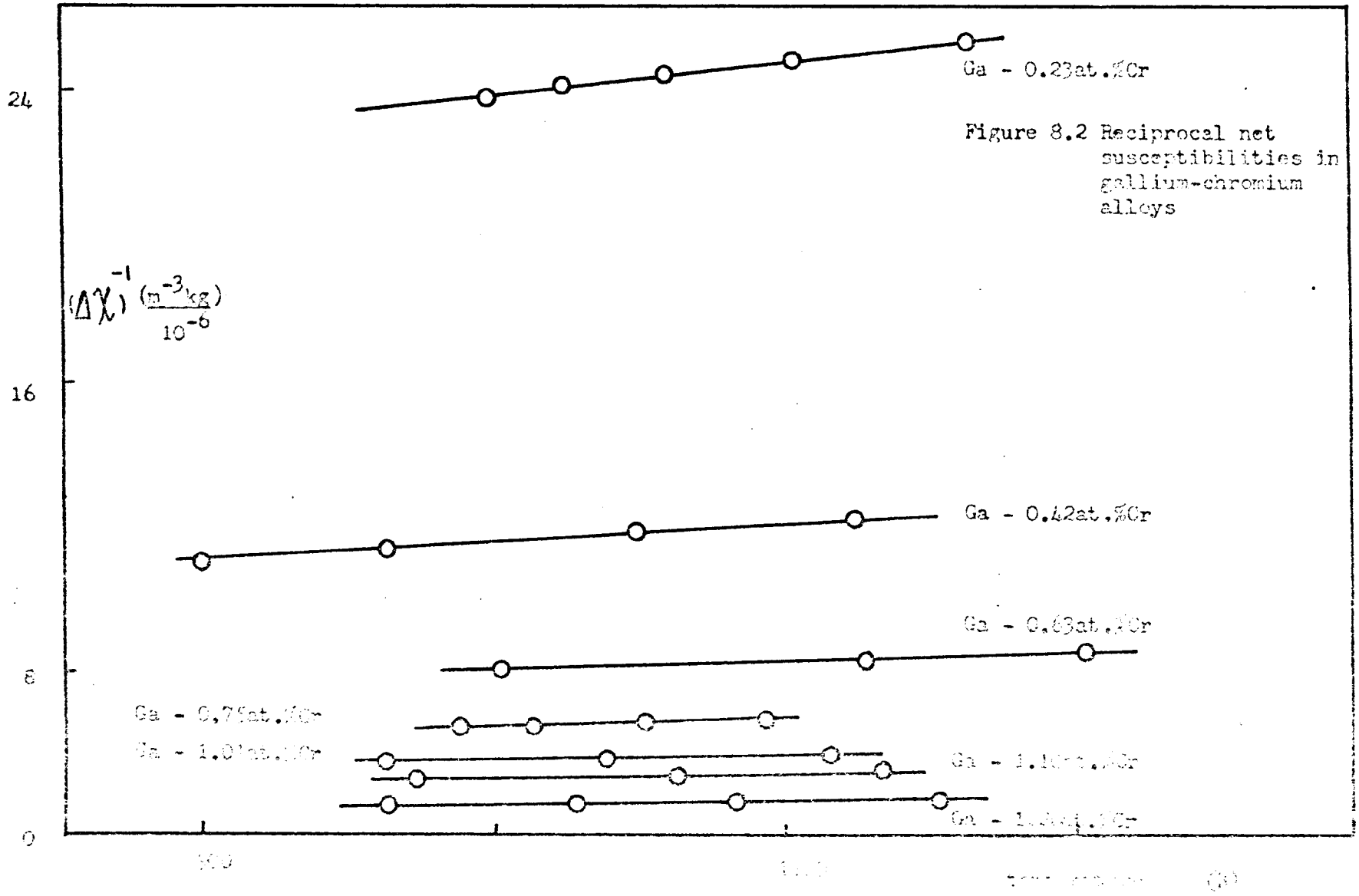

Figure 8.2 Reciprocal net susceptibilities in gallium-chromium alloys

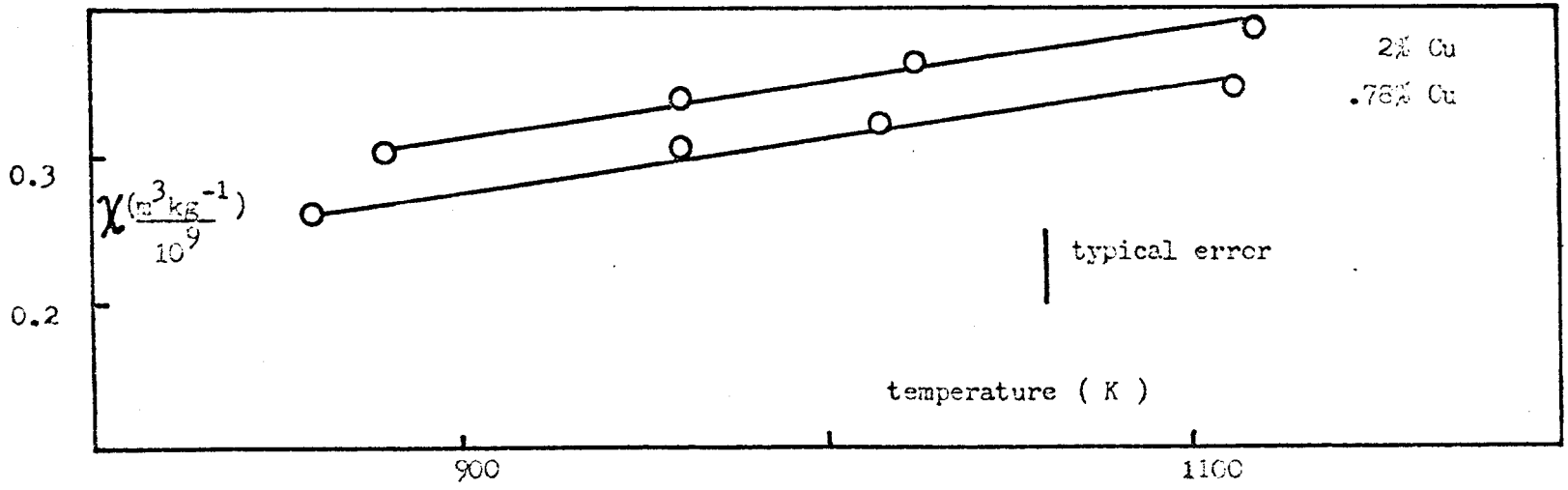

Figure 8.3 Magnetic susceptibility in gallium-copper alloys

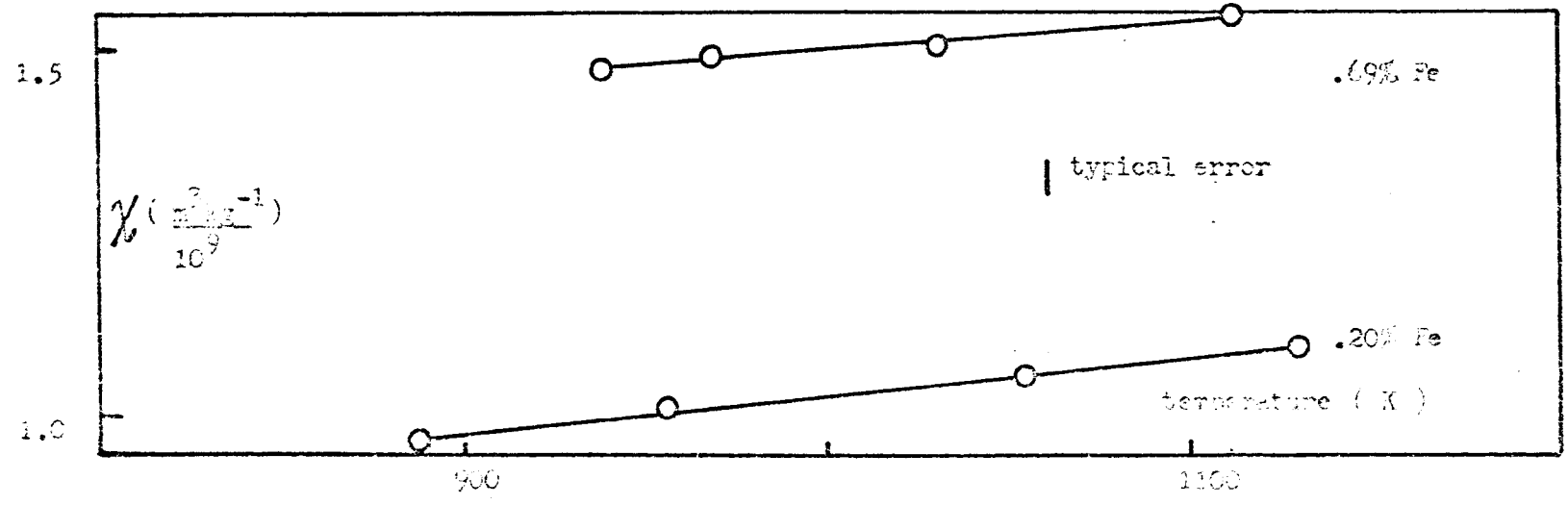

Figure 8.4 Magnetic susceptibility in gallium-iron alloys

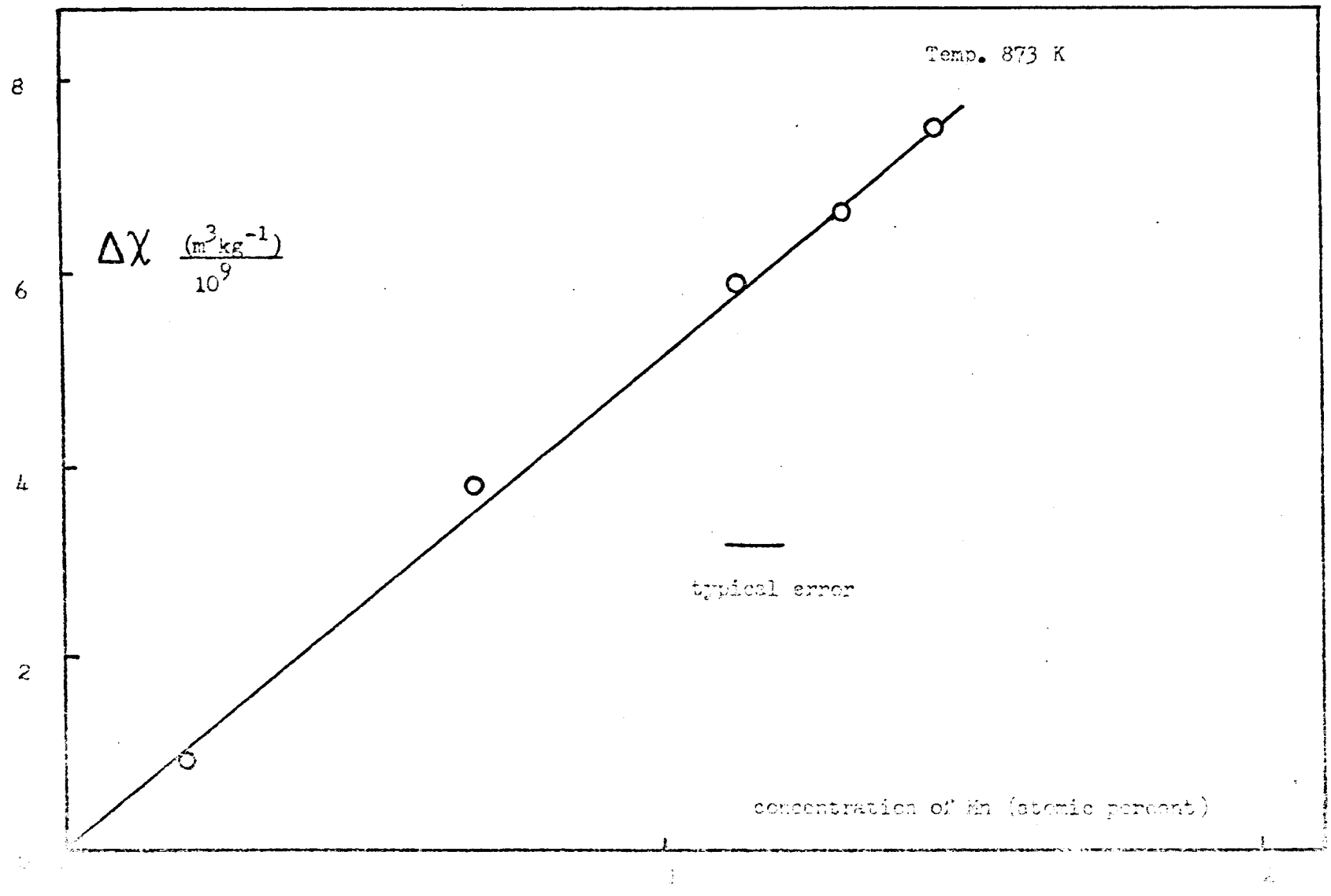

Figure 3.5 Additional susceptibility in gallium-manganese alloys

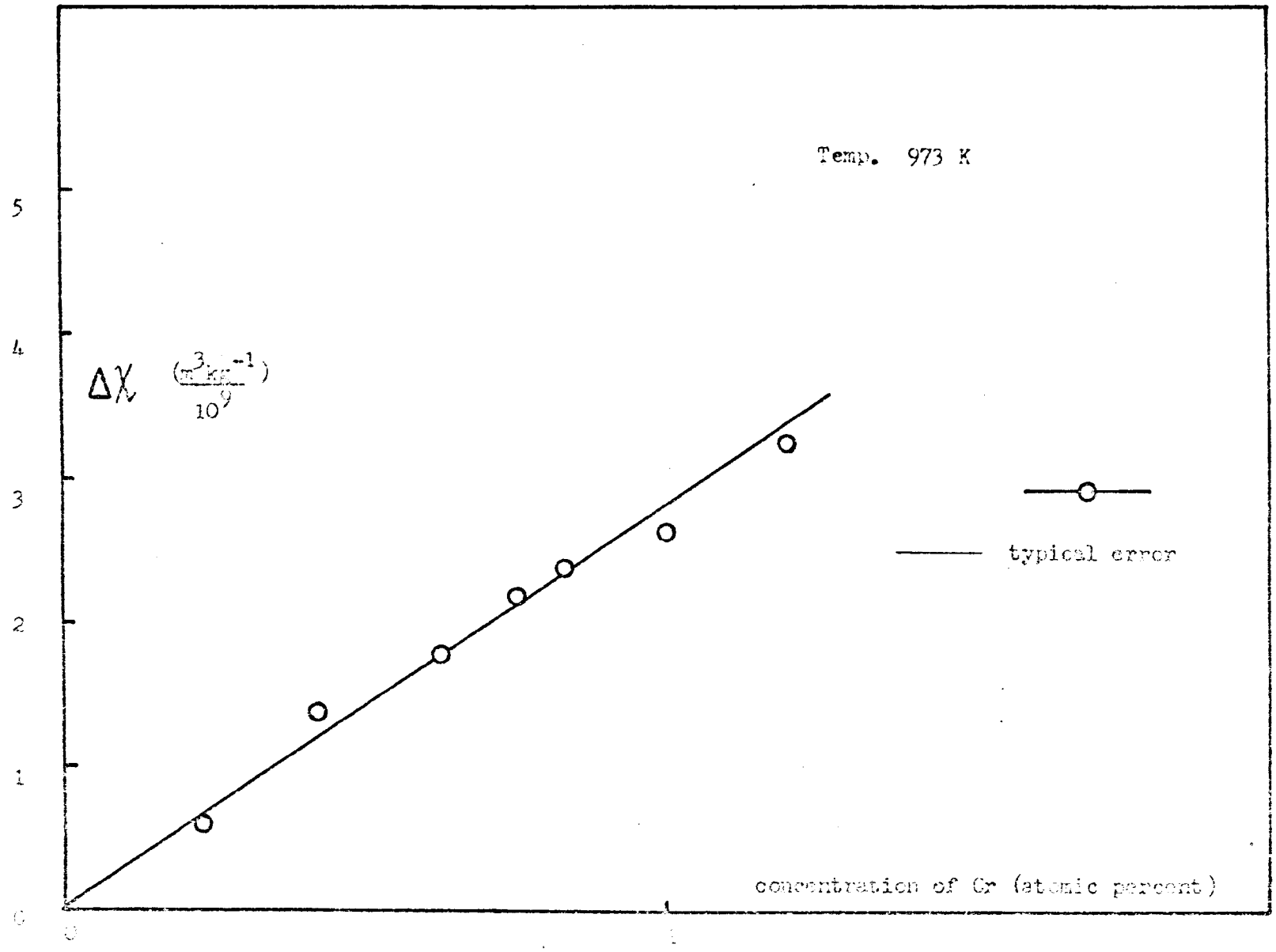

Figure 8.6 Additional susceptibility in palladium-chromium alloys

local moment systems (section 8·2·2) powdered samples are required, because of skin depth problems. The difficulty of obtaining powdered alloys in systems in which the impurity is insoluble in the solid host has already been fully discussed (section 2·5). In order to check upon the constitution and homogeneity of the powders produced by the technique described, their magnetic susceptibilities were measured (figure 8·7). These results show the characteristic behaviour and magnitude of the net susceptibility observed in the bulk samples, but obtained down to much lower temperatures, presumably the result of supercooling. It should be noted ,however, that a few samples showed a discontinuous change in $(\Delta\chi)^{-1}$, the intercept on the temperature axis becoming more positive for the lower temperature segment. Both segments of the line exhibited linear behaviour. This phenomenon remains unexplained. No sample showed any sign of ferromagnetic impurities. Any insolubility, arising from an end of supercooling, would be expected to reduce $\Delta\chi$ (equation 8·1), leading to a more negative intercept, the opposite to the observed behaviour. The host NMR in these anomolous samples has also been investigated (section 8·2·2). It is worth stressing that the Curie-Weiss behaviour of the susceptibility persisted down to room temperature in the powdered alloys. This phenomenon proved invaluable in the study of the host NMR; since the available upper limit in temperature was 780 K, this supercooling vastly increased the measuring range.

8·2·2 ^{69}Ga NMR data

The ^{69}Ga Knight shift, linewidth, and spin-lattice relaxation time were studied in liquid gallium (section 3·4) and some gallium-manganese alloys. The results are summarised in figures 8·8 and 8·9; figure 8·9 shows that there is an additional positive shift of the resonance in these alloys. The value of Γ, $(1/K)(dK/dc_{Mn})$, is 0·5±0·2; its temperature variation, or lack of it, is uncertain. The linewidth shows an increase of about 10 percent in these alloys and is consistent with the behaviour of T_1, which is shorter

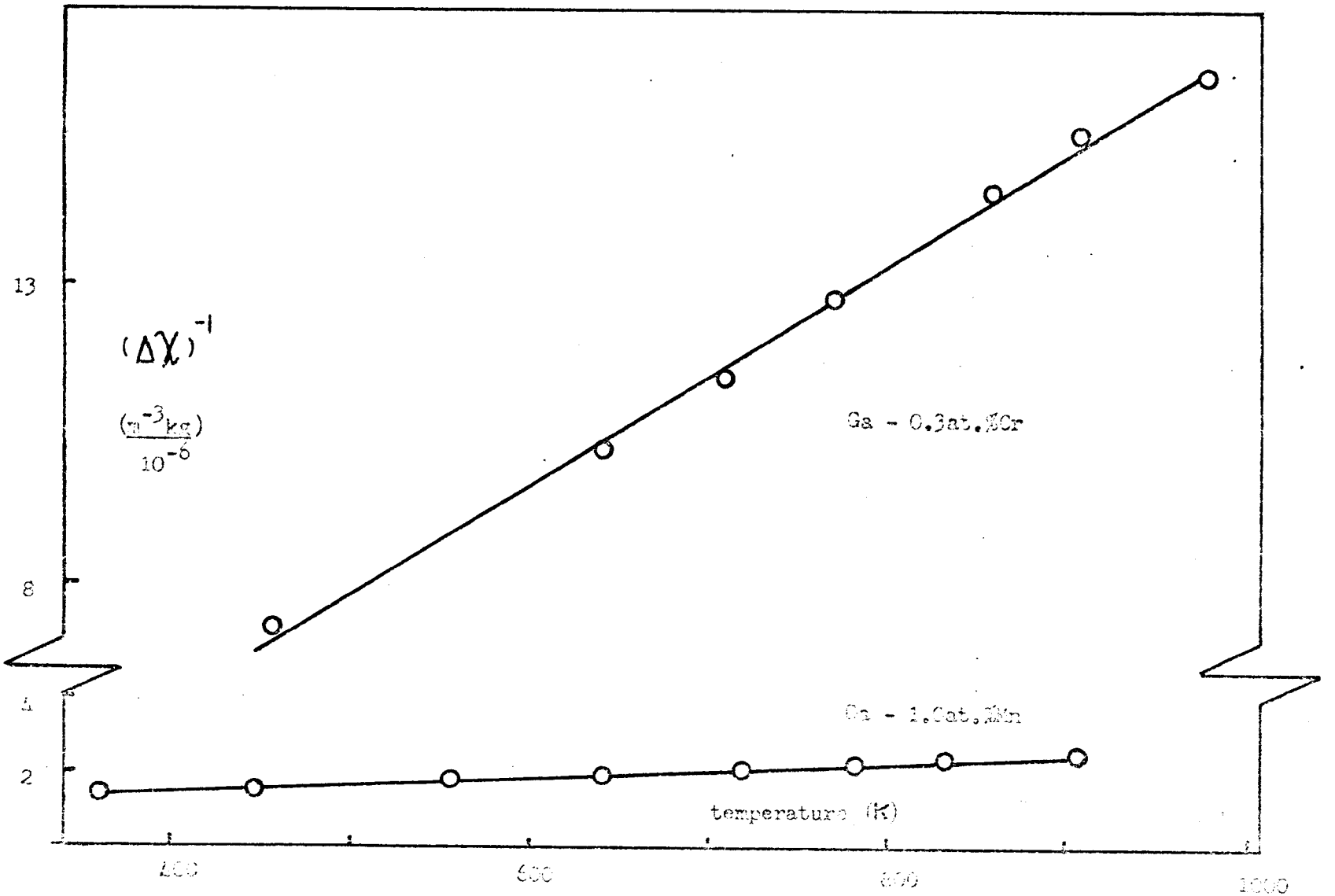

Figure 8.7 Reciprocal mol susceptibility in powdered samples

in the alloys becoming closer to the value for pure gallium at high temperatures, (figure 8·8). The samples which had shown anomolous behaviour in the magnetic susceptibility did not exhibit any significant differences from the others in the NMR data.

Similar behaviour of the shift and width was observed in the gallium-chromium system (figures 8·9 and 8·8 respectively). The Γ obtained is $0{\cdot}6 \pm 0{\cdot}4$, and the linewidth increase is similar to that in gallium-manganese. Because of the small concentrations used, the observed shifts were all very small, but were obtained in sufficient number to be convincing proof of a real positive shift.

All these results will be discussed in comparison with the behaviour of impurities which do not possess localised moments, as a contrast, and in relation to the magnetic susceptibility, in accordance with the general approach adopted in earlier chapters. It should be mentioned that a search was conducted for the ^{55}Mn resonance, in the more concentrated alloys; it was not observed. This failure is probably attributable to broadening of the resonance; the signal intensity was believed enough to ensure observation if this were not the case, and the search was conducted over a range of 0·1 T, enough to cover a Knight shift of ± 5 percent. The ^{69}Ga resonance signals were observed in samples which were preheated to 1100 K and were obtained at temperatures between 300 K and 780 K. In some cases the highest observation temperature available was above the liquidus of the alloy, in others, not. No changes in Γ were observed at the liquidus for those samples for which measurement above it were possible, apparently vindicating the view that supercooling is occuring below the liquidus, rather than any precipitation of the impurity.

8·3 Discussion

8·3·1 Magnetic susceptibility

A study of the other metals of the first transition series in liquid

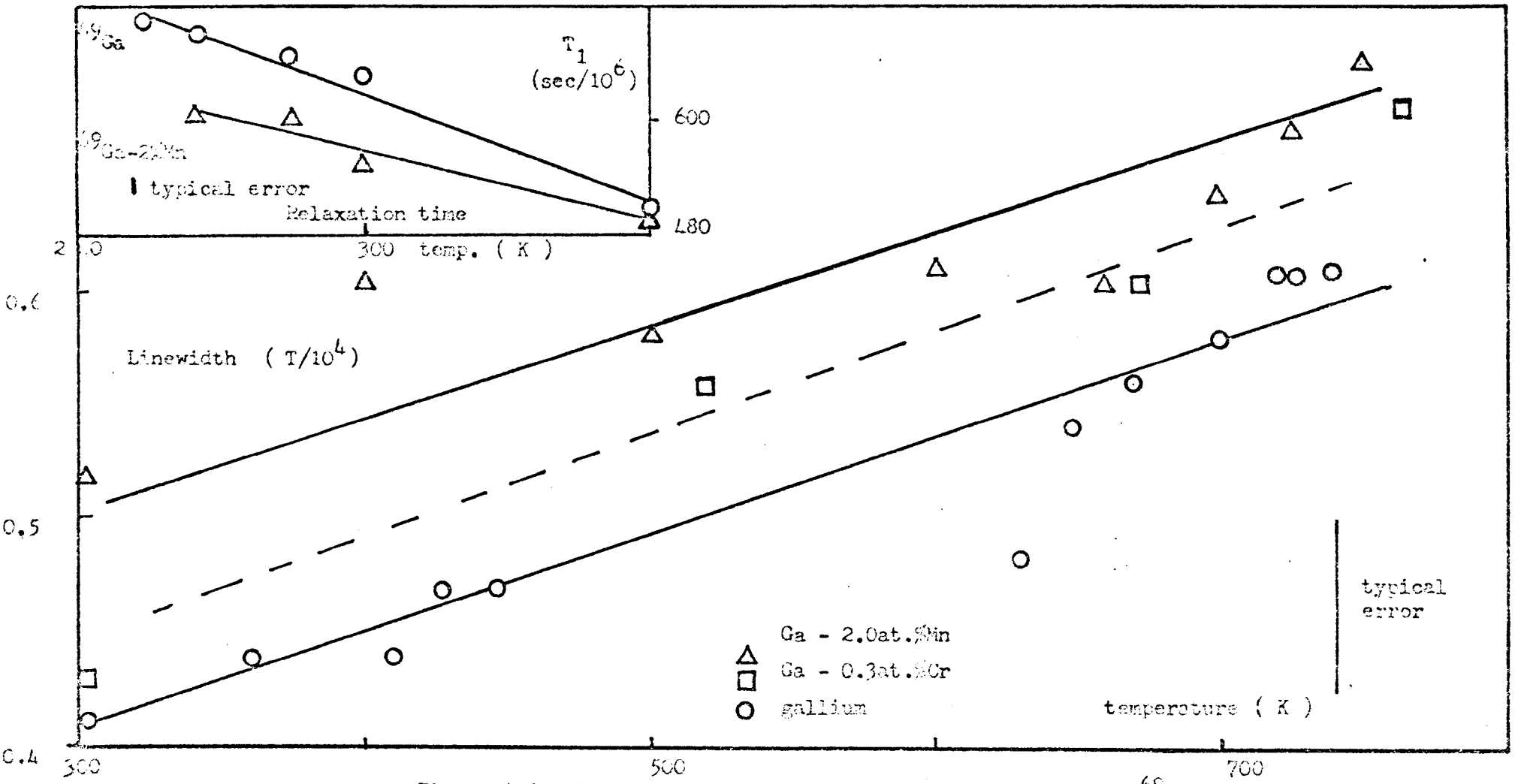

Figure 8.8 Linewidth and spin lattice relaxation times for ^{69}Ga

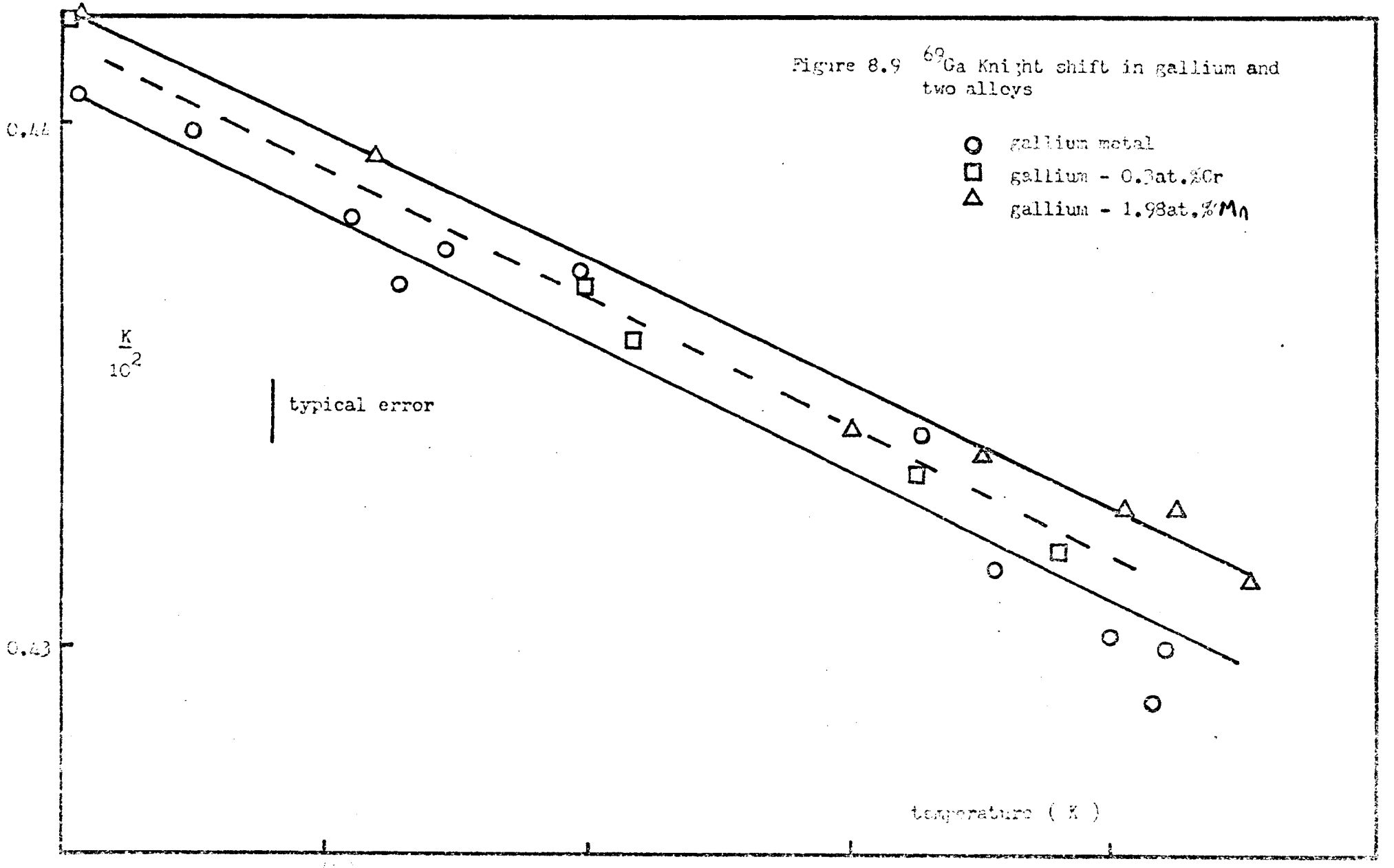

Figure 8.9 ^{69}Ga Knight shift in gallium and two alloys

gallium has recently been made (P.L.Caswell: private communication). Figure 8·10 summarises $\Delta\chi$ for one atomic percent of impurity in gallium at 1173 K, for this transition series. This shows a distinct peak at manganese, the metal with the largest unpaired spin. This is the result expected, with manganese and chromium having the largest effective number of Bohr magnetons, and being the only metals forming local moments. These two will be discussed more fully.

Gallium-manganese alloys. These show a distinct Curie-Weiss type of behaviour, with a concentration-independent moment, $p_{eff}\,\mu_B$, and intercept, θ, where

$$\left(\frac{\Delta\chi}{4\pi \times 10^{-3}}\right) = \frac{c_i \cdot N\, p_{eff}^2\, \mu_B^2}{3k(T+\theta)} \quad \text{(per mole, SI)}. \qquad (8\cdot2)$$

where N is Avogadro's number, μ_B the Bohr magneton, k Boltzmann's constant, and c_i the concentration of impurity atoms. The value of the moment ($5\cdot9 \pm 0\cdot5\,\mu_B$) is not inconsistent with the amount expected for manganese, which has a free ion spin quantum number, 5/2. The measuring range of temperature was above θ (600 ± 40 K), the range for which linearity of $(\Delta\chi)^{-1}$ with temperature is expected from the Curie-Weiss law. It can safely be concluded that manganese in gallium possesses a localised moment, the susceptibility of which follows equation 8·2, neglecting impurity-impurity effects.

Gallium-chromium alloys. The analysis conducted in an similar manner to that for gallium-manganese yielded values for θ and p_{eff} (table 8·1) which are concentration dependent. Further, the intercept was so large for most concentrations considered that it was outside the temperature range from which the intercept was derived. More explicitly, θ is derived from extrapolating the linear results in the measuring range back to zero on the χ-axis. The value obtained for θ was above the measuring range, yet linear behaviour of $(\Delta\chi)^{-1}$ is only expected above θ. Clearly, this analysis is inconsistent. Moreover, the value for p_{eff} (approximately

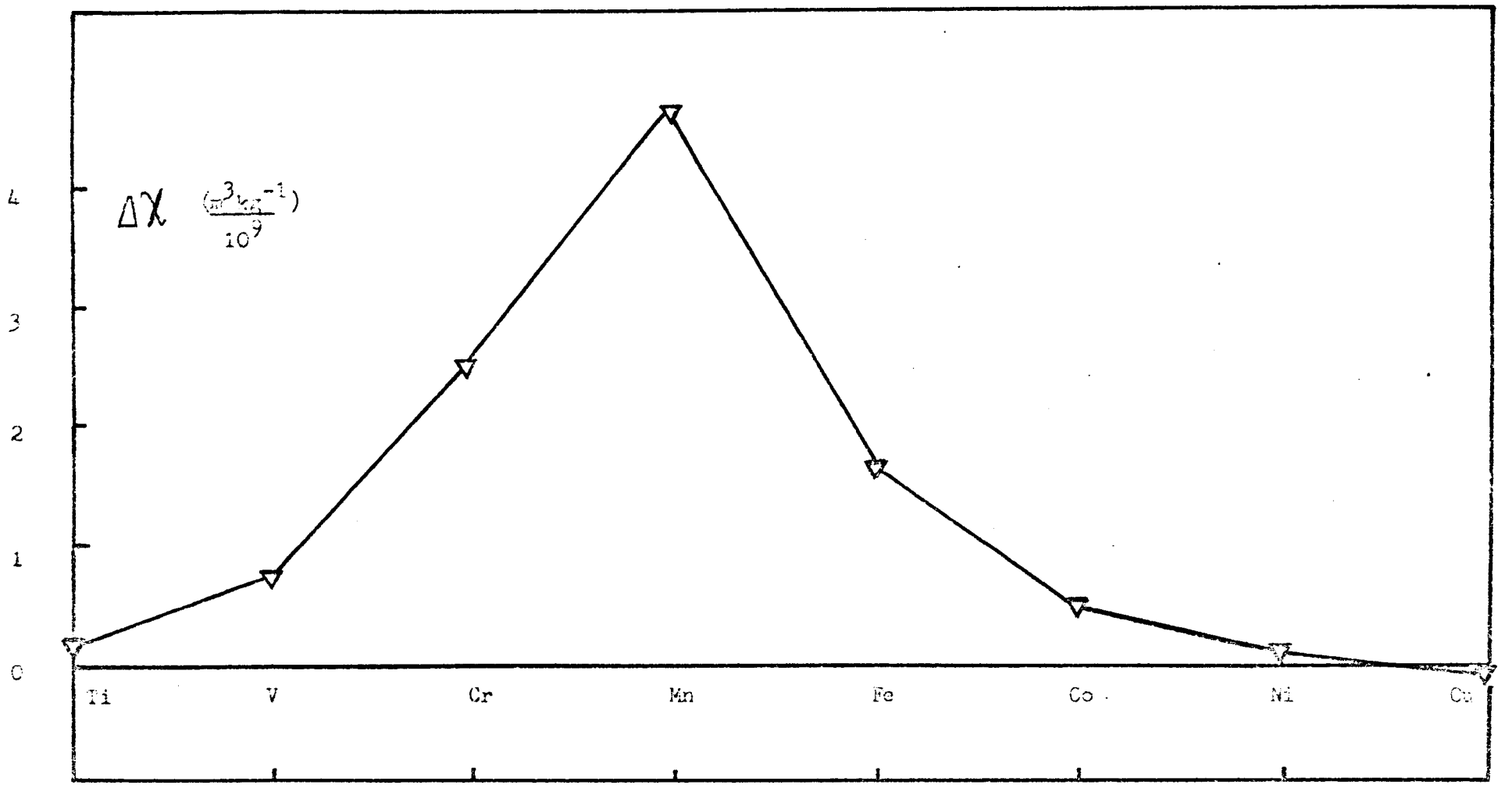

Figure 8.10 Additional susceptibility of 1 percent transition metal in gallium at 1173 K

$7\mu_B$ for one atomic percent of impurity) is larger than can be expected from the spin quantum number for chromium. Both of these results point clearly to the inapplicability of the simple Curie-Weiss law to the gallium-chromium system, at the temperatures measured. Several alternative formulae for $\Delta\chi$ in this ambiguous region can be considered (see, for instance, (7) and (8)), but as it is possible to fit the susceptibility results to a large variety of formulae over such a limited temperature range, such an approach will be of dubious value. A possible explanation of these results may be that impurity-impurity effects wipe out the local moment (i.e. a single chromium ion has a moment, two neighbouring ones do not). This would explain the behaviour of θ with concentration, the intercept value of about 80 K (figure 8·11) being the value of θ for a single chromium ion. If impurity-impurity effects were present, however, $\Delta\chi$ against concentration would not be linear, but would be parabolic with a downward curvature. Figure 8·6 does not appear to show this, although the one point off the straight line, previously believed to be a concentation error (not all the chromium in solution), must be seen in a new light in view of this possibility. It does seem clear ,however, that gallium-chromium is on the borderline for local moment formation.

Table 8·1

The Curie-Weiss parameters in Ga-Cr and Ga-Mn

system	θ (K)	$d\theta/dc_i$ (K)	p_{eff}	dp_{eff}/dc_i
1	2	3	4	5
gallium-manganese	600±40	-	5·9±0·5	-
gallium-chromium	80±300	-3×10^5	4·2±0·4	3×10^2

Columns 2 and 4 are for $c_i = 0$; the moment, $\mu = p_{eff}\ \mu_B$.

8·3·2 NMR and susceptibility

The introduction of a monovalent impurity into a trivalent host typically causes a positive fractional change Γ in the host Knight shift

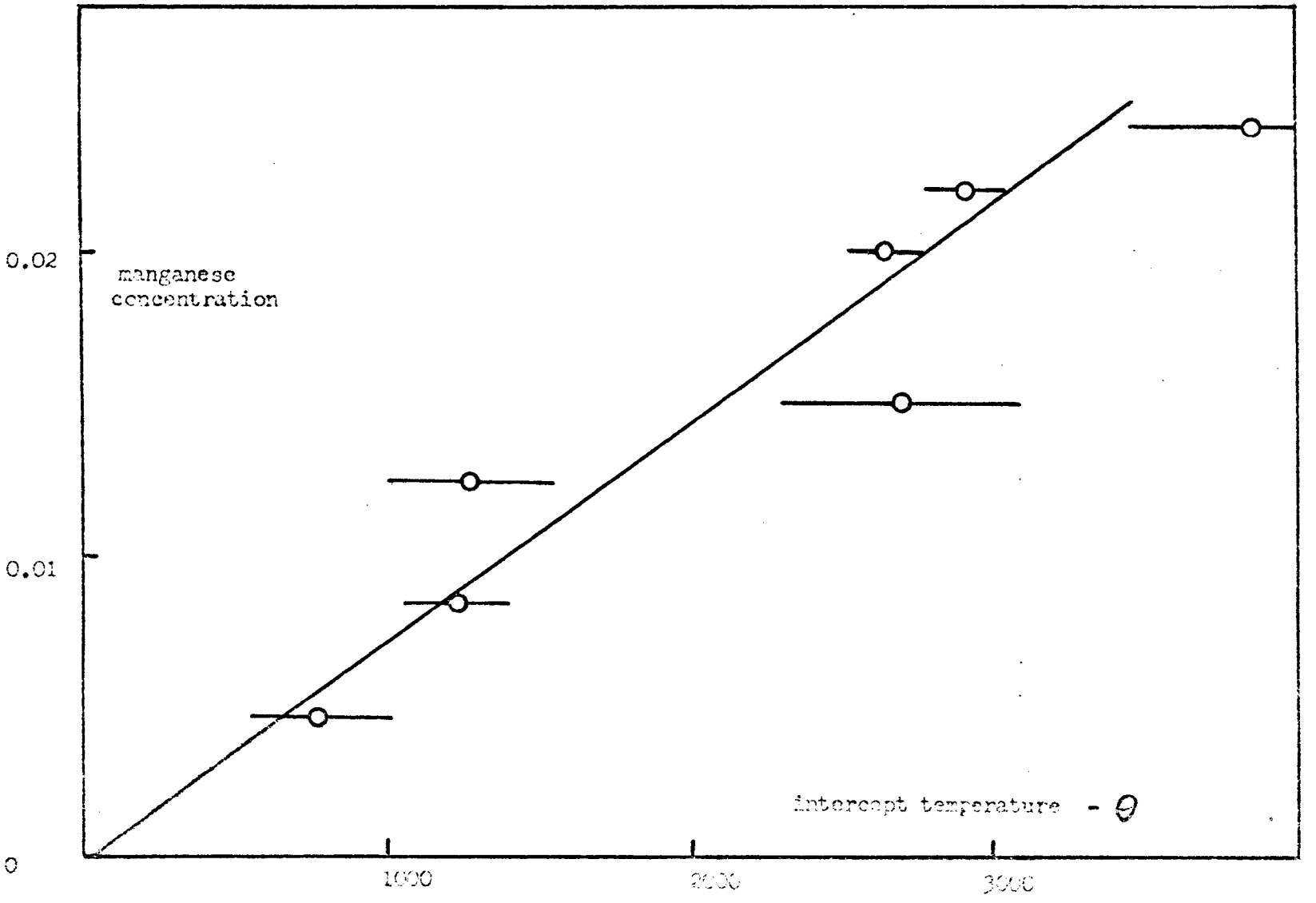

Figure 3.11 Curie-Weiss intercept in gallium-manganese alloys

of about 0·2 across the concentration range (see for example table 7·1). However, the change in the paramagnetic electronic susceptibility with concentration is very large; $(1/\chi_p)(d(\chi)/dc_i)$ is approximately 27 (where χ_p refers to the spin susceptibility of gallium given in section 3·2). Clearly this change is not reflected in the Knight shift change in the gallium-manganese system. Presumably this means that the effect of the moment is itself localised within the immediate neighbourhood of the impurity. However, the moment does have an effect since Γ is larger than would be expected from simple valency considerations.

The relaxation data suggest that the presence of the localised magnetic moment contributes another relaxation mechanism, shortening T_1; at higher temperatures this mechanism is apparently less effective, T_1 approaching the value for pure liquid gallium. This contribution will be discussed in section 8·3·3.

8·3·3 Comparison with theory

The presence of a local moment in gallium-manganese and gallium-chromium alloys is in contradiction to the (admittedly approximate) condition for local moment formation of Friedel:

$$p \cdot \Delta E > W \qquad (8·3)$$

where p is the number of electrons or holes (depending on whether there are less than or more than five electrons) in the d shell, W is the effective width of the virtual bound state, related to E_f^{host}, and ΔE is the difference in energy between a pair of electrons on the moment of parallel and antiparallel states. This rule leads to a predicted impurity versus host Fermi level curve which has a peak at manganese (8). Even so, gallium as host should be outside the local moment region that this curve delineates. The Al-Mn system does not form local moments (6), but aluminium has virtually the same density of states as gallium, and it is surprising that it obeys

the criterion whereas gallium does not. The Al-Mn system has been described (9) as a localised spin fluctuation. Crudely, its moment is too short-lived to be effective. Daybell and Steyert (7) show that the coupling constant between the moment and the conduction electrons may be estimated from the density of states and the characteristic temperature ($T_K = T_f \exp -(|JD(E_f)|)^{-1}$). This yields J=1·0 eV for Ga-Mn. In Al-Mn J is not known with any certainty, but one estimate (A.Nareth:private communication) puts it at 5·2 eV. This would explain the reason why no moment appears in aluminium-manganese, the weaker coupling allowing moment formation in gallium-manganese. In the copper-manganese system (strongly moment forming) J is 0·6 eV (7); J is related to ΔE (equation 8·3), the bigger is J, the smaller is ΔE. Now, the relaxation rate due to the moment, $(1/T_1)_{lm}$, is simply related to the local field caused by the moment, and a correlation time which will be charecteristic of either diffusion or the lifetime of the moment, depending upon which is shorter. If these two times are labelled τ_d and τ_e respectively, two conditions may be considered.

1) $\tau_d > \tau_e$. Here the moment is short lived, and the gallium sees an averaged (over space and time) local field:

$$\bar{H} = c_i \nu H_{loc} \cdot \frac{\mu H_a}{3kT} = c_i \Gamma_K H_a \qquad (8\cdot4)$$

where ν is the number of nearest neighbours (assumed to be 10), H_a the applied field, and H_{loc} the instantaneous local field at the nuclear site, assumed to be negligible further away. This yields

$$\nu H_{loc} = \Gamma_K \frac{3kT}{\mu} \qquad (8\cdot5)$$

and further

$$\left[\frac{1}{T_1}\right]_{lm} = \frac{2}{3} \gamma_n^2 c_i \nu (H_{loc} \cdot \frac{\mu H_a}{3kT})^2 \tau_d \qquad (8\cdot6)$$

from (5), with $\omega_o \tau_d < 1$.

2) $\tau_e > \tau_d$. Here the moment is long lived and the gallium nuclei see an instantaneous local field, the diffusion rate being the governing time, thus

$$\left[\frac{1}{T_1}\right]_{in} = \frac{2}{3}\gamma_n^2 c_i \nu H_{loc}^2 \tau_d \qquad (8\cdot7)$$

again with $\omega_o \tau_d \ll 1$.

From measurements of the relaxation in the gallium-manganese system (obtaining H_{loc} from equation 8·5) and estimates of τ_d from diffusion and viscosity data (10) of 10^{-11} s, it was found that condition 2 is obeyed, condition 1 being several orders of magnitude out. This shows that $\tau_e > 10^{-11}$ s. No field dependence was attempted because of signal intensity problems, but another way of distinguishing between the two conditions comes from the different temperature dependencies of T_1 predicted. However, the difference was found to be insufficient to enable a decisive choice to be made experimentally, and thus confirm (or contradict) the above conclusion that diffusion governs this relaxation rate.

A similar approach to the linewidth data of the Cu-Mn (5) and Al-Mn (6) systems yields the result that $\tau_e > 10^{-12}$ s in both cases, but the uncertainty, particularly for the Al-Mn system, is very large. Values of H_{loc} derived from equation 8·5 were about 0·1, 1·5, and 5·8 T for gallium, aluminium and copper hosts respectively. Moreover, an estimate of H_{loc} for gallium-manganese from the susceptibility data, putting H_{loc} equal to $(5\cdot9\ \mu_B/r^3)$ with r as the nearest neighbour distance, also gives $H_{loc} \simeq 0\cdot1$ T.

Unfortunately no relaxation data are available for the copper-manganese and aluminium-manganese systems, so it is not possible to say anything conclusive about lifetimes in strong, weak and non-local moment systems, but it appears that a localised moment exists in the gallium-manganese system and has a lifetime longer than 10^{-11} s.

References

1) Friedel J., Nuovo Cim. (Suppl,2), 7, 287-311, 1958.

2) Kondo J., Progr. Theoret. Phys., 32, 575-84, 1965.

3) Wachtel E. and Nier K.J., Z. Metallkunde, 56, 779-89, 1965.

4) Heeger A.J., Sol. Stat. Phys., 23, 283-411, 1969.

5) Gardner J.A.and Flynn C.P., Phil. Mag., 15, 1233-54, 1967.

6) Flynn C.P., Rigney D.A. and Gardner J.A., Phil. Mag., 15, 1255-73, 1967.

7) Daybell M.D. and Steyert W.A., Phys. Rev., 167, 536-44, 1968.

8) Tamaki S., J. Phys. Soc. Japan, 22, 865-8, 1967.

9) Caplin A.D. and Rizzuto C., Phys. Rev. Lett., 21, 746-8, 1968.

10) Wilson J.R., Met. Rev., 10, 381-590, 1965.

Conclusion

With the exception of the noble metals which must be expained in terms of s-d hybridisation, the susceptibility of the liquid metals can be well understood in terms of free electron theory. No such analysis works for any of the solid metals considered. The calculation of the Knight shifts depends upon a reliable knowledge of the spin susceptibility of the conduction electrons. Values derived for the absolute magnitude of the shift in the liquid metals show disappointing agreement with experiment (being about 70 percent of the measured quantity in all cases) but the far better agreement for the temperature coefficients supports the view that the cause lies in the relatively poor pseudopotential and neglect of indirect contributions to the shift. The fractional change with composition in the tin-cadmium system (in which the Korringa product was found to be constant upon alloying) is also quite well represented by this technique. The agreement is poor,however, for alloys of very heavy metals. This also is seen as a limitation of the input data rather than of the method. In systems suspected of liquid atomic ordering (some containing the troublesome noble metals) the analysis of the susceptibility data is more difficult, and the comparison of shift and susceptibility of limited success, although some confirmation (or denial) of ordering is possible. No direct comparison is of use in the local moment (Ga-Cr and Ga-Mn) systems, but some correlations can be made indirectly (in the calculation of the local magnetic field, for example).

The only solid in which the approach is applied with success is vanadium dioxide, for which the mutual temperature dependence enables a spin-orbit division of both the shift and susceptibility, and predictions about the band structure in the metallic and semiconducting phases,to be made. The general approach of comparing NMR and susceptibility data proves to be valuable in simple (and under certain circumstances more complicated) systems.

Table 9·1 Magnetic susceptibilities of pure metals

metal	temperature (K)	χ ($m^3kg^{-1}/10^9$)	metal	temperature (K)	χ ($m^3kg^{-1}/10^9$)
gallium	77±5	−4·08±0·04	tin	293±5	0·335±0·002
"	293 "	−3·46 "	"	303 "	0·335 "
"	303 "	0·036±0·001	"	481 "	0·329 "
"	325 "	0·062 "	"	518 "	−0·496 "
"	375 "	0·108 "	"	566 "	−0·482 "
"	383 "	0·109 "	"	673 "	−0·454 "
"	448 "	0·196 "	"	678 "	−0·455 "
"	493 "	0·178 "	"	908 "	−0·403 "
"	568 "	0·217 "			
"	603 "	0·284 "	lead	291 "	−1·461±0·015
"	798 "	0·342 "	"	298 "	−1·482 "
"	903 "	0·403 "	"	308 "	−1·483 "
"	973 "	0·412 "	"	318 "	−1·438 "
			"	372 "	−1·416 "
bismuth	293 "	−16·64±0·10	"	480 "	−1·269 "
"	393 "	−14·77 "	"	499 "	−1·286 "
"	493 "	−12·44 "	"	573 "	−1·213 "
"	538 "	−11·06 "	"	613 "	−0·804±0·006
"	573 "	−0·53±0·01	"	618 "	−0·775 "
"	593 "	−0·532±0·004	"	631 "	−0·770 "
"	623 "	−0·530 "	"	650 "	−0·767 "
"	733 "	−0·464 "	"	773 "	−0·764 "
"	840 "	−0·417 "	"	784 "	−0·769 "
silver	293 "	−2·337±0·009	copper	293 "	−1·098±0·006
"	293 "	−2·34±0·01	"	295 "	−1·098 "
"	1003 "	−2·39 "	"	1073 "	−0·930 "
"	1183 "	−2·40 "	"	1293 "	−0·897 "
"	1283 "	−2·75 "	"	1453 "	−1·093 "
"	1323 "	−2·74 "	"	1453 "	−1·093 "

Table 9·1 (continued)

metal	temperature (K)	χ ($m^3 kg^{-1}/10^9$)	metal	temperature (K)	χ ($m^3 kg^{-1}/10^9$)
cadmium	293±5	−2·251±0·020	cadmium	653±5	−2·116±0·020
"	298 "	−2·285 "	"	673 "	−2·077 "
"	297 "	−2·212 "	"	681 "	−2·109 "
"	308 "	−2·232 "	"	707 "	−2·101 "
"	313 "	−2·224 "			
"	368 "	−2·179 "	gold	293±5	−1·85±0·01
"	383 "	−2·192 "	"	293 "	−1·85 "
"	418 "	−2·145 "	"	1073 "	−1·82 "
"	483 "	−2·108 "	"	1298 "	−1·82 "
"	499 "	−2·081 "	"	1363 "	−2·00 "
"	503 "	−2·091 "	"	1403 "	−2·00 "
"	575 "	−2·050 "			
"	593 "	−2·065 "	indium	498±5	−1·05±0·01
"	603 "	−2·130 "	"	618 "	−1·00 "
"	603 "	−2·111 "	"	815 "	$-0{\cdot}94_9$ "
"	618 "	−2·122 "			

Table 9·2 Knight shifts and linewidths in pure metals

metal	temperature (K)	Knight shift (%)	linewidth ($T/10^4$)
gallium	303±5	0·4405±0·0005	0·41±0·05
"	348 "	0·4398 "	0·44 "
"	411 "	0·4382 "	0·44 "
"	427 "	0·4368 "	0·47 "
"	443 "	0·4376 "	0·47 "
"	496 "	0·4373 "	0·58 "
"	628 "	0·4343 "	0·48 "
"	646 "	0·4315 "	0·54 "
"	653 "	0·4312 "	0·56 "
"	699 "	0·4303 "	0·58 "
"	713 "	0·4290 "	0·61 "
"	723 "	0·4300 "	0·61 "
"	738 "	0·4267 "	0·61 "

Table 9·2 (continued)

metal	temperature (K)	Knight shift (%)	linewidth ($T/10^4$)
tin	293±5	0·7193±0·0010	2·6±0·3
"	383 "	0·7293 "	2·8 "
"	468 "	0·7485 "	3·4 "
"	505 "	0·7530 "	3·4 "
"	505 "	0·7430 "	1·5±0·1
"	518 "	0·7438 "	1·46±0·10
"	537 "	0·7446 "	1·70 "
"	560 "	0·7418 "	1·7±0·2
"	572 "	0·7424 "	1·75±0·10
"	618 "	0·7428 "	1·9±0·2
"	648 "	0·7428 "	1·77±0·10
"	661 "	0·7419 "	2·03±0·10
"	669 "	0·7433 "	2·0±0·2
"	689 "	0·7418 "	2·23±0·20
cadmium	293 "	0·4175 "	1·39±0·10
"	393 "	0·4617 "	1·40 "
"	493 "	0·5232 "	1·78 "
"	539 "	0·5552 "	1·72 "
"	577 "	0·5826 "	-
"	595 "	0·7991 "	1·39±0·10
"	618 "	0·7981 "	1·40 "
"	658 "	0·8004 "	1·85 "
"	689 "	0·8017 "	1·92 "
"	713 "	0·8004 "	1·77 "
"	739 "	0·8004 "	1·8±0·2

Table 9·3 Contact densities for pure metals

Tin					Cadmium				
temp. (K)	KF (a.u.)	omega (a.u.)	eta	dens.	temp. (K)	KF (a.u.)	omega (a.u.)	eta	dens.
505	·837	201·6	·45	414·60	594	·710	165·4	·45	413·36
605	·834	203·6	·428	413·22	694	·706	167·7	·432	415·82
705	·832	205·6	·406	411·06	794	·704	169·9	·415	417·79
905	·826	209·8	·362	408·10	994	·697	174·7	·380	421·84
1105	·820	214·2	·318	404·38	1194	·690	180·0	·345	428·01

Table 9·3 (continued)

Indium

temp.	KF	omega	eta	dens.
430	·772	192·9	·45	440·43
530	·769	194·8	·432	438·47
630	·767	197·1	·414	436·73
830	·760	201·8	·378	434·89
1030	·755	206·4	·342	431·78

Bismuth

temp.	KF	omega	eta	dens.
544	·845	245·3	·45	613·87
644	·842	248·2	·431	611·96
744	·838	251·5	·412	609·74
944	·831	258·1	·374	606·10
1144	·824	265·2	·336	601·15

Gallium

temp.	KF	omega	eta	dens.
303	·884	128·7	·45	214·54
403	·880	130·2	·425	211·23
503	·877	131·9	·399	208·00
703	·870	134·6	·348	202·04
903	·860	137·1	·297	197·89

Lead

temp.	KF	omega	eta	dens.
600	·833	204·9	·45	797·74
700	·830	207·2	·431	789·86
800	·826	209·6	·412	783·64
1000	·821	214·5	·374	768·53

Table 9·4 Contact densities for "pseudo"-indium

temp.	KF	omega	eta	dens.	temp.	KF	omega	eta	dens.
430	·675	192·9	·45	503·25	430	·850	192·9	·45	395·4
530	·672	194·8	·432	504·9	530	·846	194·8	·432	394·8
630	·670	197·1	·414	506·65	630	·844	197·1	·414	392·7
830	·663	201·8	·378	514·4	830	·837	201·8	·378	390·1
1030	·658	206·4	·342	521·1	1030	·830	206·4	·342	388·0

Table 9·5 Density of tin-cadmium alloys at 618K

alloy composition	density ($kgm^{-3}/10^3$)
Sn	6·89±0·03
Sn - 11 at.% Cd	6·99 "
Sn - 26 at.% Cd	7·08 "
Sn - 52 at.% Cd	7·32 "
Sn - 76 at.% Cd	7·60 "
Sn - 86 at.% Cd	7·74 "
Cd	8·03 "

Table 9·6 Magnetic susceptibilities of tin-cadmium alloys

composition (at.%)	temperature (K)	$-\chi$ ($m^3kg^{-1}/10^9$)	composition (at.%)	temperature (K)	$-\chi$ ($m^3kg^{-1}/10^9$)
Sn - 11Cd	663±5	-0·650±0·003	Sn - 52Cd	673±5	-1·235±0·005
"	566 "	-0·674 "	"	571 "	-1·278 "
"	463 "	-0·256 "	"	484 "	-1·316 "
"	432 "	-0·108±0·001	"	443 "	-0·955 "
"	397 "	+0·075 "	"	345 "	-0·901 "
"	298 "	+0·064 "	"	305 "	-0·917 "
Sn - 13Cd	673 "	-0·671±0·003	"	288 "	-0·929 "
"	293 "	+0·023±0·001	Sn - 76Cd	649 "	-1·636 "
Sn - 26Cd	663 "	-0·858±0·003	"	519 "	-1·691 "
"	573 "	-0·887 "	"	473 "	-1·713 "
"	533 "	-0·901 "	"	453 "	-1·725 "
"	486 "	-0·886 "	"	371 "	-1·547 "
"	433 "	-0·401±0·002	"	295 "	-1·592 "
"	372 "	-0·260 "	Sn - 86Cd	660 "	-1·811 "
"	298 "	-0·274 "	"	553 "	-1·837 "
			"	493 "	-1·859 "
			"	413 "	-1·836 "
			"	366 "	-1·803 "
			"	288 "	-1·852 "

Table 9·7 NMR data for ^{119}Sn in tin-cadmium alloys

composition (at.%)	temperature (K)	Knight shift (%)	linewidth ($T/10^4$)
Sn90 - Cd	544±5	0·7451±0·0010	1·70±0·10
"	618 "	0·7425 "	1·77 "
Sn80 - Cd	293 "	0·719±0·001	2·6±0·2
"	323 "	0·717 "	2·9 "
"	373 "	0·728 "	3·3 "
"	513 "	0·7442±0·0010	1·52±0·10
"	618 "	0·7415 "	1·92 "
"	669 "	0·7433 "	1·98 "
Sn70 - Cd	515 "	0·7379 "	1·60 "
"	618 "	0·7385 "	1·91 "

Table 9·7 (continued)

composition (at.%)	temperature (K)	Knight shift (%)	linewidth ($T/10^4$)
Sn60 - Cd	293±5	0·714±0·001	2·9±0·2
"	323 "	0·714 "	3·6 "
"	383 "	0·725 "	3·6 "
"	517 "	0·7401±0·0010	1·59±0·10
"	618 "	0·7381 "	1·83 "
"	663 "	0·7381 "	2·03 "
"	693 "	0·7369 "	2·7±0·4
Sn50 - Cd	523 "	0·7391 "	1·58±0·10
"	618 "	0·7377 "	2·02 "
Sn40 - Cd	293 "	0·714±0·001	3·6±0·2
"	375 "	0·722 "	4·4±0·4
"	395 "	0·724 "	3·9±0·2
"	543 "	0·7371±0·0010	2·03±0·10
"	618 "	0·7354 "	2·10 "
"	680 "	0·7343 "	2·5±0·2
Sn30 - Cd	565 "	0·7379 "	2·1 "
"	618 "	0·7345 "	2·6 "
Sn20 - Cd	293 "	0·714±0·001	3·6 "
"	377 "	0·720 "	3·9 "
"	586 "	0·7361±0·0010	2·2 "
"	618 "	0·7334 "	2·6 "
Sn10 - Cd	620 "	0·7318 "	2·1±0·4

Table 9·8 NMR data for ^{113}Cd in tin-cadmium alloys

composition (at.%)	temperature (K)	Knight shift (%)	linewidth ($T/10^4$)
Cd90 - Sn	618±5	0·8049±0·0010	1·37±0·10
"	675 "	0·8097 "	1·95 "
Cd80 - Sn	293 "	0·417±0·001	1·26 "
"	349 "	0·439 "	-
"	399 "	0·462 "	1·43 "
"	424 "	0·478 "	1·56 "
"	573 "	0·8123±0·0010	1·32 "
"	618 "	0·8114 "	1·34 "
"	689 "	0·8154 "	1·76 "

Table 9·8 (continued)

composition (at.%)	temperature (K)	Knight shift (%)	linewidth ($T/10^4$)
Cd70 - Sn	559±5	0·8126±0·0010	1·32±0·10
"	618 "	0·8125 "	1·46 "
Cd60 - Sn	293 "	0·415±0·001	1·50 "
"	353 "	0·441 "	1·25 "
"	412 "	0·470 "	1·2±0·2
"	540 "	0·8107±0·0010	1·2 "
"	618 "	0·8115 "	1·32±0·10
"	686 "	0·8115 "	1·68 "
Cd50 - Sn	525 "	0·8108 "	1·15 "
"	618 "	0·8119 "	1·60 "
Cd40 - Sn	293 "	0·417±0·001	1·65 "
"	404 "	0·467 "	-
"	526 "	0·8081±0·0010	1·48 "
"	619 "	0·8101 "	1·71 "
"	689 "	0·8089 "	1·76 "
Cd30 - Sn	522 "	0·809±0·001	-
"	618 "	0·8119±0·0020	-
Cd20 - Sn	293 "	0·423±0·002	-
"	514 "	0·805±0·005	-
"	618 "	0·8102±0·0020	-

Table 9·9 Contact densities at host metal nuclei

metal	system (at.%)	OPW term	dens.	metal	system (at.%)	OPW term	dens.
^{119}Sn	Sn	493·9	413·8	^{113}Cd	Cd	576·2	413·3
	Sn90-Cd	509·5	428·2		Cd90-Sn	563·1	422·6
	Sn80-Cd	524·5	442·4		Cd80-Sn	550·0	426·2
	Sn70-Cd	538·9	454·4		Cd70-Sn	536·7	425·7
	Sn60-Cd	552·9	465·7		Cd60-Sn	523·3	422·2
	Sn50-Cd	566·5	476·3		Cd50-Sn	509·6	416·9
	Sn40-Cd	579·8	483·9		Cd40-Sn	495·5	408·8
	Sn30-Cd	592·8	489·4		Cd30-Sn	481·1	401·6
	Sn20-Cd	605·7	491·3		Cd20-Sn	466·2	394·9
	Sn10-Cd	618·5	488·7		Cd10-Sn	450·8	378·5

Table 9·9 (continued)

metal	system (at.%)	OPW term	dens.	metal	system (at.%)	OPW term	dens.
^{207}Pb	Pb	1164·3	799·4	^{209}Bi	Bi	844·4	613·9
	Pb90-Bi	1156·7	796·0		Bi90-Pb	849·2	618·6
	Pb80-Bi	1149·4	792·4		Bi80-Pb	854·0	622·5
	Pb70-Bi	1142·3	787·3		Bi70-Pb	858·9	626·4
	Pb60-Bi	1135·4	782·8		Bi60-Pb	863·9	630·0
	Pb50-Bi	1128·7	777·1		Bi50-Pb	869·1	633·3
	Pb40-Bi	1122·1	773·0		Bi40-Pb	874·4	638·0
	Pb30-Bi	1115·7	768·6		Bi30-Pb	879·8	641·7
	Pb20-Bi	1109·5	763·7		Bi20-Pb	885·4	645·9
	Pb10-Bi	1103·4	758·9		Bi10-Pb	891·1	648·9
^{119}Sn	Sn90-Bi	492·7	415·3	^{209}Bi	Bi90-Sn	845·6	614·3
	Sn80-Bi	491·4	415·5		Bi80-Sn	846·8	615·3
	Sn70-Bi	490·6	415·8		Bi70-Sn	848·0	615·3
	Sn60-Bi	490·2	414·9		Bi60-Sn	849·2	615·2
	Sn50-Bi	489·6	415·8		Bi50-Sn	850·4	615·0
	Sn40-Bi	488·9	415·6		Bi40-Sn	851·6	614·8
	Sn30-Bi	488·3	415·4		Bi30-Sn	852·8	613·9
	Sn20-Bi	487·7	415·2		Bi20-Sn	853·9	612·9
	Sn10-Bi	487·0	414·3		Bi10-Sn	855·1	612·1

Table 9·10 Contact density values with non-zero alpha and beta (see also 9·21)

metal	system	dens.	metal	system	dens.
^{119}Sn	Sn90-Cd	423·6	^{119}Sn	Sn90-Bi	417·6
α =0·2	Sn80-Cd	433·4	α =2·0	Sn80-Bi	420·0
β =0·1	Sn70-Cd	439·4	β =0	Sn70-Bi	422·6
	Sn60-Cd	444·8		Sn60-Bi	424·9
	Sn50-Cd	449·6		Sn50-Bi	427·2
	Sn40-Cd	450·9		Sn40-Bi	429·5
	Sn30-Cd	450·2		Sn30-Bi	431·8
	Sn20-Cd	446·2		Sn20-Bi	434·1
	Sn10-Cd	438·1		Sn10-Bi	436·0
^{113}Cd	Cd90-Sn	424·3	^{209}Bi	Bi90-Sn	614·3
α =0·1	Cd80-Sn	430·0	α =0	Bi80-Sn	615·3
β =0·2	Cd70-Sn	431·7	β =2·0	Bi70-Sn	615·3
	Cd60-Sn	430·3		Bi60-Sn	615·2
	Cd50-Sn	427·0		Bi50-Sn	615·0
	Cd40-Sn	420·5		Bi40-Sn	614·8

Table 9·10 (continued)

metal	system	dens.	metal	system	dens.
^{113}Cd	Cd30-Sn	414·0	^{209}Bi	Bi30-Sn	613·9
	Cd20-Sn	407·8		Bi20-Sn	612·9
	Cd10-Sn	394·4		Bi10-Sn	612·1

Table 9·11

Contact dens. with zero density

alloy	dens.
Sn	413·3
Sn90-Cd	422·2
Sn80-Cd	432·1
Sn70-Cd	441·8
Sn60-Cd	450·7
Sn50-Cd	459·0
Sn40-Cd	465·6
Sn30-Cd	470·2
Sn20-Cd	473·4
Sn10-Cd	474·3

Table 9·12

Magnetic susceptibility at 625 K

alloy	susceptibility ($m^3kg^{-1}/10^9$)
Bi	-0·510±0·003
Bi90-Pb	-0·535 "
Bi75-Pb	-0·591 "
Bi60-Pb	-0·636 "
Bi56-Pb	-0·646 "
Bi50-Pb	-0·660 "
Bi39-Pb	-0·694 "
Bi25-Pb	-0·737 "
Bi10-Pb	-0·784 "
Pb	-0·789 "

Table 9·13 Susceptibility of dilute lead alloys

system	temperature (K)	susceptibility ($m^3kg^{-1}/10^9$)	system	temperature (K)	susceptibility ($m^3kg^{-1}/10^9$)
Pb-18%Bi	778±5	-0·821±0·004	Pb-20%Tl	776±5	-0·756±0·004
	622 "	-0·852 "		623 "	-0·756 "
	579 "	-1·118 "		473 "	-1·030 "
	463 "	-1·218 "		372 "	-1·131 "
	368 "	-1·304 "		778 "	-0·721 "
	773 "	-0·881 "		613 "	-0·748 "
	649 "	-0·901 "		421 "	-1·126 "
	450 "	-1·257 "		322 "	-1·190 "
	329 "	-1·365 "		787 "	-0·728 "
				616 "	-0·697 "
				467 "	-1·022 "
				293 "	-1·240 "
				293 "	-1·203 "

Table 9·14 Knight shifts of ^{207}Pb

system	shift (%)	temp. (K)	shift (%)	temp. (K)	shift (%)	temp. (K)
Pb	1·181±·008	77±5	1·210±·008	293±5	1·221±·009	813±5
	1·225 "	919 "				
Pb-18bi	1·178 "	77 "	1·210 "	293 "	1·228 "	748 "

Table 9·14 (continued)

system	shift (%)	temp. (K)	shift (%)	temp. (K)	shift (%)	temp. (K)
Pb-18Bi	1·278±·009	853±5	1·178*±·009	77±5	1·202*±·009	293±5
Pb-20Tl	1·198 "	77 "	1·213 "	293 "	1·222 "	838 "
	1·287 "	948 "				
Pb-15In	1.186 "	77 "	1·231 "	293 "		

* sample used by J.H.(reference 5.1)

Table 9·15 Magnetic susceptibility and ^{51}V Knight shift in VO_2

temperature (K)	K (%)	susceptibility ($m^3kg^{-1}/10^9$)
293±5		15·17±0·10
315 "		15·13 "
335 "		15·63 "
340 "		42·21 "
342 "		111·2±0·2
356 "	0·384±0·003	
363 "		110·5 "
393 "		109·5 "
400 "	0·364 "	
423 "		108·1 "
438 "	0·345 "	
453 "		106·7 "
478 "		105·3 "

Table 9·16 Magnetic susceptibilities of noble metal alloys

system (at.%)	temperature (K)	susceptibility ($m^3kg^{-1}/10^9$)	system (at.%)	temperature (K)	susceptibility ($m^3kg^{-1}/10^9$)
Ag-17In	1150±5	-2·61±0·04	Cu-20In	1073±5	-1·72±0·03
Ag-25In	1073 "	-2·68 "	Cu-30In	1073 "	-1·94 "
Ag-30In	1073 "	-2·74 "	"	993 "	-2·04±0·04
"	990 "	-2·80 "	Cu-37½In	1073 "	-1·78 "
Ag-33⅓In	1073 "	-2·65 "	"	992 "	-1·88 "
"	991 "	-2·71 "	Cu-45In	1073 "	-1·66 "
Ag-40In	1073 "	-2·49 "	"	962 "	-1·76 "
"	895 "	-2·56 "	Cu-52½In	1073 "	-1·51 "

Table 9·16 (continued)

system (at.%)	temperature (K)	susceptibility ($m^3kg^{-1}/10^9$)	system (at.%)	temperature (K)	susceptibility ($m^3kg^{-1}/10^9$)
Ag-55In	1073±5	-2·06±0·04	Cu-52½In	950±5	-1·58±0·04
"	798 "	-2·16 "	Cu-60In	1073 "	-1·38 "
Ag-66In	1073 "	-1·62 "	"	923 "	-1·45 "
"	733 "	-1·71 "	Cu-75In	1073 "	-1·17 "
Ag-80In	1073 "	-1·31 "	"	873 "	-1·19 "
Ag-90In	1073 "	-1·11 "	Cu-90In	1073 "	-1·00 "
Au-20In	1073 "	-2·10±0·03	Au-50Sn	712 "	-1·68±0·02
"	1033 "	-2·10 "	"	754 "	-1·67 "
Au-30In	1073 "	-2·19 "	"	783 "	-1·67 "
"	823 "	-2·38 "	Au-29Sn	567 "	-2·22±0·03
Au-40In	1073 "	-2·09 "	"	605 "	-2·21 "
"	713 "	-2·27 "	"	629 "	-2·20 "
Au-50In	1073 "	-1·91 "	"	638 "	-2·19 "
"	833 "	-2·02 "	"	690 "	-2·15 "
Au-66In	1073 "	-1·62 "	"	694 "	-2·15 "
"	877 "	-1·67 "	"	730 "	-2·14 "
Au-80In	1073 "	-1·37±0·02	"	767 "	-2·11 "
"	816 "	-1·43 "	Au-80Sn	553 "	-1·11±0·02
Au-90In	1073 "	-1·14 "	"	612 "	-1·08 "
"	731 "	-1·21 "	"	699 "	-1·06 "
			"	759 "	-1·03 "
			Au-66Sn	601 "	-1·42 "
			"	659 "	-1·39 "
			"	705 "	-1·37 "
			"	754 "	-1·36 "
			Au-21Sn	789 "	-2·24 "
				811 "	-2·22 "

Table 9·17 Susceptibility of thallium-tellurium alloys

system (at.%)	temperature (K)	susceptibility ($m^3kg^{-1}/10^9$)	system (at.%)	temperature (k)	susceptibility ($m^3kg^{-1}/10^9$)
Te	751±5	-0·84±0·03	Te34-Tl	683±5	-2·70±0·02
"	773 "	-0·73 "	"	711 "	-2·67 "
Te60-Tl	673 "	-2·09±0·02	"	745 "	-2·62 "
"	773 "	-1·85 "	"	816 "	-2·51 "
"	823 "	-1·78 "	"	876 "	-2·47 "
Te40-Tl	723 "	-2·37 "	"	979 "	-2·41 "
"	773 "	-2·32 "	"	800 "	-2·60 "

Table 9·17 (continued)

system (at.%)	temperature (K)	susceptibility ($m^3kg^{-1}/10^9$)	system (at.%)	temperature (K)	susceptibility ($m^3kg^{-1}/10^9$)
Te40-Tl	873±5	-2·28±0·02	Te34-Tl	856±5	-2·54±0·02
Te36-Tl	693 "	-2·56 "	"	933 "	-2·48 "
"	773 "	-2·53 "	"	981 "	-2·47 "
"	843 "	-2·49 "			

Table 9·18 Magnetic susceptibility of gallium alloys

system (at.%)	temperature (K)	susceptibility ($m^3kg^{-1}/10^9$)	system (at.%)	temperature (K)	susceptibility ($m^3kg^{-1}/10^9$)
Ga-0·67Mn	1230±5	3·676±0·019	Ga-1·11Mn	1098±5	5·504±0·026
"	1090 "	3·912 "	"	998 "	5·802 "
"	978 "	4·144 "	"	918 "	6·068 "
"	863 "	4·369 "	"	873 "	6·203 "
"	695 "	4·766 "	"	773 "	6·523 "
"	536 "	0·204 "	"	687 "	5·958 "
			"	663 "	3·013 "
Ga-1·31Mn	1198 "	6·090±0·034	Ga-0·2Mn	1203 "	1·211±0·007
"	1113 "	6·360 "	"	1103 "	1·253 "
"	1033 "	6·627 "	"	1010 "	1·312 "
"	940 "	6·967 "	"	899 "	1·333 "
"	863 "	7·267 "	"	800 "	1·372 "
"	788 "	7·545 "	"	703 "	1·410 "
"	643 "	2·602 "	"	613 "	0·567 "
Ga-1·46Mn	1098 "	6·699±0·037	Ga-0·69Fe	1113 "	1·558±0·008
"	1028 "	6·961 "	"	1028 "	1·507 "
"	941 "	7·320 "	"	968 "	1·494 "
"	873 "	7·556 "	"	938 "	1·472 "
"	808 "	7·774 "			
"	773 "	7·883 "	Ga-0·26Fe	1129 "	1·096 "
"	741 "	7·982 "	"	1054 "	1·061 "
"	710 "	4·373 "	"	956 "	1·017 "
"	656 "	1·777 "	"	887 "	0·970 "
			"	824 "	0·598 "
Ga-0·75Cu	1118 "	0·385±0·003	Ga-2·09Cu	1113 "	0·348±0·002
"	1023 "	0·364 "	"	1015 "	0·324 "
"	956 "	0·339 "	"	958 "	0·308 "
"	878 "	0·305 "	"	862 "	0·262 "
"	799 "	0·234 "	"	698 "	0·190 "

Table 9·18 (continued)

system (at.%)	temperature (K)	susceptibility ($m^3kg^{-1}/10^9$)
Ga-1·01Cr	1135±5	3·001±0·015
"	1063 "	3·021 "
"	964 "	3·049 "
"	908 "	3·040 "
Ga-0·42Cr	1125 "	1·669±0·009
"	1048 "	1·666 "
"	968 "	1·690 "
"	900 "	1·700 "
"	853 "	1·519 "
Ga-0·85Cr	1093 "	2·874±0·014
"	1043 "	2·866 "
"	1003 "	2·859 "
"	963 "	2·859 "
Ga-0·69Fe	1113 "	1·558±0·009
"	1028 "	1·507 "
"	968 "	1·494 "
"	938 "	1·472 "
Ga-0·25Cr powder	978 "	1·39±0·01
	901 "	1·42 "
"	850 "	1·46 "
"	763 "	1·56 "
"	703 "	1·65 "
"	630 "	1·76 "
"	448 "	2·14 "
Ga-1·0Mn powder	903 "	5·88±0·02
	845 "	6·09 "
"	783 "	6·47 "
"	713 "	6·94 "
"	613 "	7·64 "
"	543 "	8·13 "
"	448 "	8·80 "
"	358 "	9·85 "
Ga-0·8Mn powder	978 "	2·74±0·01
	918 "	2·82 "
"	873 "	2·90 "
	808 "	3·01 "
	725 "	3·19 "
	508 "	3·43 "
	383 "	4·02 "
Ga-1·1Cr	1135±5	3·214±0·015
"	1063 "	3·241 "
"	973 "	3·269 "
"	921 "	3·261 "
Ga-0·63Cr	1203 "	2·140±0·010
"	1130 "	2·161 "
"	1001 "	2·181 "
Ga-1·2Cr	1153 "	3·703±0·017
"	1083 "	3·722 "
"	1029 "	3·744 "
"	968 "	3·756 "
Ga-0·25Cr	1163 "	1·054±0·005
"	1103 "	1·044 "
"	1058 "	1·035 "
"	1023 "	1·030 "
"	958 "	1·025 "
Ga-0·2Mn powder	918 "	1·36±0·01
	853 "	1·38 "
"	758 "	1·42 "
"	656 "	1·55 "
"	573 "	1·63 "
"	498 "	1·73 "
Ga-0·7Mn powder	878 "	1·57 "
	743 "	1·69 "
"	470 "	2·17 "
"	423 "	2·29 "
"	298 "	2·78 "
Ga-2Mn powder	963 "	10·50±0·05
	898 "	10·72 "
"	843 "	11·12 "
"	763 "	11·65 "
"	648 "	12·83 "
"	533 "	14·40 "
"	373 "	16·37 "

Table 9·19 ^{69}Ga NMR data

system (at.%)	temperature (K)	K (%)	linewidth (T/10^4)	system (at.%)	temperature (K)	K (%)	linewidth (T/10^4)
Ga-0·7Mn	756±5	·4295±·0010	·67±·05	Ga-0·25Cr	753±5	·4290±·0010	·67±·05
"	673 "	·4322 "	·60 "	"	673 "	·4316 "	·58 "
"	583 "	·4341 "	·54 "	"	516 "	·4355 "	·55 "
"	512 "	·4360 "	·52 "	"	303 "	·4417 "	·43 "
"	398 "	·4390 "	·50 "	Ga-1 Mn	733 "	·4283 "	·62 "
"	303 "	·4418 "	·46 "	"	623 "	·4347 "	·52 "
"	758 "	·4301 "	·69 "	"	303 "	·4430 "	·45 "
Ga-2 Mn	753 "	·4312 "	·70 "	"	698 "	·4295 "	·67 "
"	703 "	·4325 "	·64 "	"	623 "	·4320 "	·58 "
"	726 "	·4323 "	·67 "	"	693 "	·4314 "	·59 "
"	600 "	·4341 "	·61 "	"	303 "	·4424 "	·48 "
"	399 "	·4392 "	·61 "	"	713 "	·4294 "	·55 "
"	303 "	·4420 "	·52 "	"	618 "	·4332 "	·55 "
"	659 "	·4332 "	·60 "	"	323 "	·4421 "	·44 "
Ga-0·2Mn	743 "	·4281 "	·70 "	Ga-·25Cr	623 "	·4332 "	·55 "
"	680 "	·4303 "	·61 "	"	500 "	·4370 "	·48 "
"	656 "	·4317 "	·58 "	"	303 "	·4421 "	·41 "
"	543 "	·4370 "	·56 "	Ga-·2Mn	733 "	·4281 "	·56 "
"	493 "	·4370 "	·50 "	"	625 "	·4322 "	·53 "
"	363 "	·4408 "	·44 "	"	698 "	·4281 "	·62 "
"	303 "	·4421 "	·39 "	"	644 "	·4314 "	·56 "
"	681 "	·4309 "	·55 "	"	313 "	·4415 "	·41 "
"	621 "	·4345 "	·51 "	Ga-·3Mn	703 "	·4297 "	·62 "
				"	635 "	·4329 "	·59 "
				"	573 "	·4345 "	·44 "
				"	448 "	·4370 "	·50 "
				"	348 "	·4408 "	·42 "

Table 9·20 ^{69}Ga relaxation data

system(at.%)	T_1(ms)	temp.(K)	system(at.%)	T_1(ms)	temp.(K)
Ga	0·52±0·01	398±5	Ga-2Mn	0·49±0·02	398±5
"	0·65 "	303 "	"	0·55 "	303 "
"	0·67±0·02	273 "	"	0·61 "	273 "
"	0·69 "	243 "	"	0·61 "	243 "
"	0·70 "	223 "			

Table 9·21 Contact densities with non-zero alpha and beta

metal	system	dens.	metal	system	dens.
^{119}Sn	Sn90-Cd	425·8	^{113}Cd	Cd90-Sn	422·9
	Sn80-Cd	435·0		Cd80-Sn	427·4
α =0·25	Sn70-Cd	440·2	α =0·05	Cd70-Sn	428·2
β =0·05	Sn60-Cd	444·3	β =0·25	Cd60-Sn	426·1
	Sn50-Cd	447·7		Cd50-Sn	422·0
	Sn40-Cd	447·8		Cd40-Sn	415·0
	Sn30-Cd	445·4		Cd30-Sn	408·0
	Sn20-Cd	439·6		Cd20-Sn	401·7
	Sn10-Cd	429·3		Cd10-Sn	387·0

metal	system	dens.	metal	system	dens.
^{207}Pb	Pb90-Bi	815·4	^{209}Bi	Bi90-Pb	592·7
	Pb80-Bi	836·8		Bi80-Pb	574·9
α =10	Pb70-Bi	859·8	α =16	Bi70-Pb	561·0
β =16	Pb60-Bi	885·0	β =10	Bi60-Pb	549·6
	Pb50-Bi	912·5		Bi50-Pb	543·2
	Pb40-Bi	941·4		Bi40-Pb	540·1
	Pb30-Bi	970·9		Bi30-Pb	541·6
	Pb20-Bi	1000·6		Bi20-Pb	548·8
	Pb10-Bi	1030·4		Bi10-Pb	558·8

metal	system	dens.	metal	system	dens.
^{119}Sn	Sn90-Bi	422·1	^{209}Bi	Bi90-Sn	594·8
	Sn80-Bi	429·5		Bi80-Sn	578·4
α = 6	Sn70-Bi	437·5	α =15	Bi70-Sn	563·1
β =15	Sn60-Bi	445·7	β = 6	Bi60-Sn	550·2
	Sn50-Bi	453·8		Bi50-Sn	539·5
	Sn40-Bi	461·9		Bi40-Sn	531·4
	Sn30-Bi	469·8		Bi30-Sn	524·8
	Sn20-Bi	477·4		Bi20-Sn	521·6
	Sn10-Bi	484·2		Bi10-Sn	521·3

Appendix 2

Contact density computer program

Key to identifiers:

K Number used to set concentration; K=0 (pure solvent), K=11 (pure solute).

K2 k_f^2.

R distance from nucleus (in a.u.), r.

RZERO r starting value of Simpson's rule integration, before conversion to a.u.

BL Overlap integral before it is equated to overlap integral procedure result.

F Simpson's rule interval parameter.

B1-B4 Intermediate sums in Simpson's rule, BLL procedure.

HCON Simpson's rule interval in BLL procedure.

RZEROCON starting value of Simpson's rule integration (in a.u.) in BLL.

COD,CEV Intermediate sums in CO procedure.

X $q/2k_f$.

DELY Interval in y in Simpson's rule in CO procedure.

DELF CO procedure parameter, starting value of interval in y.

DELYA,DELYB starting values for interval in y, used in CO procedure.

Y y, abscissa of y - integration in procedure CO.

KF k_f.

Q q.

Q2 q^2.

K2Q $2k_fq$.

YA,YB Starting values for y in Simpson's rule in CO.

YBR,YAR Ranges of integration for y in Simpson's rule in CO.

CZ,CN First and last terms in Simpson's rule in CO.

KFA k_f for pure element X.

KFB k_f for pure element Y.

OMEGAA,OMEGAB Ionic volumes of pure X and Y.

RCA,RCB Core radii of Ashcroft pseudopotential for X and Y.

PI 3·14159.

WI $1/(\pi k_f)$.

GAMMA $\chi_x(k)$.

TERMA,TERMB Normalisation terms for X and Y elements.

PS,PD Intermediate sums in Simpson's rule integration of self and distinct terms.

H3 Simpson's rule integration interval divided by 3.

SIG Hard sphere diameter.

STR $I(k\sigma) - 1$.

FL $\ln|(1-q/2k_f)/(1+2k_f)|$.

XFL $(q/2k_f)$ times FL.

CAPGAM $\Gamma(k,q)$, the angular integral in the self and distinct terms.

RB,RC Intermediate sums used in evaluation of CAPGAM.

VA,VB Ashcroft potentials for X and Y elements.

GS,GD Self and distinct term integrands in Simpson's rule.

PST,PDT Final sums in Simpson's rule integration of self and distinct terms.

DENS $\chi_x^2(k)/N(c_y) \cdot (1+\xi+\Delta)$.

PF DENS/Ω .

QRA qR^X_{core} .

QRB qR^Y_{core} .

VAL Alloy valence.

N Principal quantum number of core state.

L Angular momentum quantum number of core state.

RAD Abscissa integer for core state.

M Running integer used in integration over q.

KINT k-value integer.

RADZERO Integer representing starting r value in overlap intergral.

C,I Integers used in BLL procedure .

A,B Integers used in CO procedure.

E Integer (1 or 2) representing X or Y element.

NJ1,T Integers used in q-integration.

BLA(E,L,N,KINT) Overlap integral array.

J(L) Bessel function array.

P(E,L,N,RAD) Core state wavefunction array.

CA(K),CB(K) Concentrations of X and Y elements.

OMEGAB(K) Volume per electron.

BETA(K) $N_k(c_y)$, normalisation factor.

OPW(K) $\chi^2_x / N_k(c_y)$.

H(T) Simpson's rule interval, q integrtion.

AJ(T) Starting q values for Simpson's rule q integration.

PT(K) $1 + \xi + \Delta$ for a given concentration.

OMEGAI(K) Average ionic volume at a given concentration.

XS(N) $R_{no}(0)$ for s core functions.

BLK(N) BLL for $K=k_f$, overlap integral.

CON(E) Conversion factor for Herman and Skillman wavefunctions.

NMAX(E) Maximum n value for core functions.

LMAX(E) Maximum l value for core functions.

NRAD(E,L,N) Number of wave function ordinates for a given core state.

NWF(E) Number of core states for given element.

RCAZERO Starting value of RCA .

RCBZERO Starting value of RCB.

ALPHA,BETAR α, β .

ALZERO,BEZERO Starting values of α, β.

DELPHA,DELBETA Intervals in α and β .

U,W Number of integer steps in changing α and β .

```
Perdew and Wilkins calculation of Knight shifts in liquid alloys;
"begin""real" K,R,RZERO,BL,F,B1,B2,B3,B4,HCON,RZEROCON,COD,CEV,CIN,X,
DELY,DELF,Y,KF,K2,Q,Q2,K2Q,YB,YA,YBR,YAR,DELYB,DELYA,CZ,CN,KFA,KFB,
OMEGAA,OMEGAB,RCAZERO,RCBZERO,RCA,RCB,ALPHA,PI,WI,GAMMA,TERMA,TERMB,
PS,PD,H3,SIG,STF,FL,XFL,CAPGAM,RB,RC,VA,VP,GS,GD,PST,PDT,DENS,PF,QRA,
QRB,VAL,BETAR,ALZERO,DELPHA,BETZERO,ALSBTA,BETA;
"comment" Calculates PF in liquid alloys at specific concentrations,
uses Ashcroft and Lekner structure factors,Ashcroft local
pseudopotential and Herman and Skillman core wave functions;
    "real""array" BLA(1:2,0:3,1:5,0:139),J(0:4),P(1:2,0:3,1:5,0:100),
    CA,CB,OMEGAT,BETA,CPW,R,AJ,HJ,FT,CHIAI(1:11),XS,BLK(1:16),CON(1:2);
    "integer" N,L,RAD,M,KINT,RAZERO,I,C,A,B,S,NJ1,T,D,G,U,W,TNUP;
    "integer""array" NMAX(1:2),LMAX(1:2,1:5),NEAR(1:2,0:3,1:5),NAF(1:2);
    "comment" Procedure CO evaluates Q-dependent integral required
    in self and distinct terms;
    "real""procedure" CO(N);
    "integer" N;
    "begin""real""procedure" CINT(YZERO,DELF,S);
        "value" YZERO,DELF,S;
        "real" YZERO,DELF;
        "integer"S;
        "begin" CIN:=0;
            "for" A:=1"step"1"until"7"do"
            "begin" COD:=CEV:=0;
                DELY:=DELF*(10↑A)/10;
                "for"B:=1"step"2"until"9"do"
                "begin" Y:=YZERO+S*DELY*B;
                KINT:=ENTIER(10*SQRT(K2+Q2-K2Q*Y));
                COD:=COD+(BLA(1,0,N,KINT)-BLK(N))/(Y/X-1);
                "end"
                "for"B:=2"step"2"until"8"do"
                "begin"Y:=YZERO+S*DELY*B;
                KINT:=ENTIER(10*SQRT(K2+Q2-K2Q*Y));
                CEV:=CEV+(BLA(1,0,N,KINT)-BLK(N))/(Y/X-1);
                "end";
```

```
            KINT:=ENTIER(10*SQRT(K2+Q2-K2Q*YZERO));
            CZ:=(BLA(1,0,N,KINT)-BLK(N))/(YZERO/X-1);
            YZERO:=YZERO+S*10*DELY;
            KINT:=ENTIER(10*SQRT(K2+Q2-K2Q*YZERO));
            CN:=(BLA(1,0,N,KINT)-BLK(N))/(YZERO/X-1);
            CIN:=CIN+(DELY/3)*(CZ+CN)+(4*DELY/3)*COD+(2*DELY/3)*CIV;
        "end"
        CINT:=CIN;
    "end" of procedure CINT;
    K2:=KF*KF;
    Q2:=Q*Q;
    K2Q:=2*KF*Q;
    "if"X >1 "then"CO:= CINT(1,0.00000018,-1) "else"
    "begin" YB:=X-0.0000002;
            YA:=X+0.0000002;
            YBR:=YB+1; YAR:=1-YA;
            DELYB:=0.00000009*YBR;
            DELYA:=0.00000009*YAR;
            "if"YAR<0.0000002"then" CO:=CINT(YB,DELYB,-1)
            "else" CO:=CINT(YA,DELYA,1)+CINT(YB,DELYB,-1);
    "end";
"end" of procedure CO;
"comment" Procedure S calculates structure factor using current alloy
values of KF and SIGMA. The packing fraction ETA is .45 initially ;
"real""procedure" S(Z,ETA);
"real" Z,ETA;
"begin""real" ZZ,ZZZ,R1,R2,R3,R4,R5,T1,T2,T3;
      "if" Z <0·5 "then" S:=0·025 "else"
      "begin"  ZZ:=Z*Z;  ZZZ:= Z*Z*Z;
      T1:=(1+2*ETA)↑2/(1-ETA)↑4;
      T2:=-6*ETA*(1+ETA/2)↑2/(1-ETA)↑4;
      T3:=1/2*ETA*(1+2*ETA)↑2/(1-ETA)↑4;
      R1:=T1+2*T2+4*T3-24*T3/ZZ;
      R2:=-(T1+T2+T3)*Z+(2*T2+12*T3)/Z-24*T3/ZZZ;
      R3:=-2*T2/Z+24*T3/ZZZ;
      R4:=24*ETA/ZZ;
      R5:=R4*(R1*SIN(Z)+R2*COS(Z)+R3);
      S:=1/(1+R5);
      "end";
"end" of procedure S;
```

```
"comment" Procedure V calculates the pseudopotential using the
appropriate core radius. It is truncated at the second node;
"real""procedure" V(QR);
"real" QR;
"begin""real" DENOM,X2;
      "if" X <0·01"then" V:=-1·0 "else""if" QR>4·71 "then" V:=0·00
"else""begin" X2:=X*X;
              DENOM:=X2+WI*(0·5-0·25*(1-X2)*FL/X);
              V:=-WI*COS(QR)/DENOM;
     "end";
"end" of procedure V;
"real""procedure" BINT(N,L,RAD,E);
"integer"N,L,RAD,E;
"begin""real" XKR;
      XKR:=KF*R;  "if" XKR <0·01 "then" XKR:=0·01;
      J(0):=SIN(XKR)/XKR;
      "if" L>0"then" J(1):=J(0)/XKR-COS(XKR)/XKR;
      "if" L>1"then" J(2):=3*J(1)/XKR-J(0);
      "if" L>2"then" J(3):=5*J(2)/XKR-J(1);
      "if" L>3"then" J(4):=7*J(3)/XKR-J(2);
      BINT:=4*3·14159*R*P(E,L,N,RAD)*J(L);
"end" of procedure BINT;
"real""procedure" BLL(N,L,KF,E);
"real" KF; "integer" N,L,E;
"begin" RZERO:=-0·05;  BL:=0;
              "for" C:=1"step"1"until"(NRAD(E,L,N)-1)"div" 10 "do"
              "begin" F:=0·01*(2↑C)/2;
              B1:=B2:=0;
              RADZERO:=10*(C-1);
              RZERO:=RZERO+5*F;  RCON:=F*CON(E);
              RZEROCON:=RZERO*CON(E);
              "for" I:=1"step"2"until"9"do"
              "begin" RAD:=RADZERO+I;  R:=RZEROCON+RCON*I;
                      B1:=B1+BINT(N,L,RAD,E);
              "end";
              "for" I:=2"step"2"until"8"do"
              "begin" RAD:=RADZERO+I;R:=RZEROCON+RCON*I;
                      B2:=B2+BINT(N,L,RAD,E);
              "end" ;
```

```
                RAD:=RADZERO; R:=RZEROCON;
                B3:=BINT(N,L,RAD,E); RAD:=RADZERO+10;
                R:=RZEROCON+10*HCON; B4:=BINT(N,L,RAD,E);
                BL:=BL+(HCON/3)*(B3+B4)+4*(HCON/3)*B1+2*(HCON/3)*B2;
            "end";
            BLL:=BL;
    "end" of procedure BLL;
    "for"E:=1,2"do"
    "begin""read" CON(E),NWF(E),NMAX(E);
          "for"N:=1"step"1"until"NMAX(E)"do""read"LMAX(E,N);
          "for"N:=1"step"1"until"NWF(E)"do"
          "begin""read"N,L,NRAD(E,L,N);
                "for"RAD:=0"step"1"until"NRAD(E,L,N)-1"do"
                "read" P(E,L,N,RAD);
                "for" KF:=0"step"0·1"until"13·0"do"
                "begin"KINT:=ENTIER(10*(KF+0·0001));
                      BLA(E,L,N,KINT):=BLL(N,L,KF,E);
                "end";
          "end";
    "end";
"for"E:=1,2"do"
"begin""print" ''L' ELEMENT= ',sameline,E;
      "for"N:=1"step"1"until"NMAX(E)"do"
      "begin""print" ''L' N= ',sameline,N;
            "for"L:=0"step"1"until"LMAX(E,N)"do"
            "begin""print" ''L' L= ',sameline,L;
                  "for"KINT:=0"step"1"until"130"do"
                  "print"prefix(''S2''),sameline,freepoint(4),
                  BLA(E,L,N,KINT);
            "end";
      "end";
"end";
      "read"KFB,OMEGAB,RCAZERO,RCBZERO,ALZERO,BEZERO,DELPHA,DELBETA,U,W;
      "print" ''L' KFB=',sameline, freepoint(4),KFB,''S2' OMEGAB= ',
      OMEGAB,''S2' RCAZERO= ',RCAZERO,''S2' RCBZERO= ',RCBZERO,
      ''S2' ALZERO= ',ALZERO,''S2' BEZERO= ',BEZERO,''S2' DELPHA= ',
      DELPHA,''S2' DELBETA= ',DELBETA;
```

```
"for"N:=1"step"1"until"NMAX(1)"do""read"XS(N);
"for"N:=1"step"1"until"NMAX(1)"do""print" ''L' XS= ',sameline,
freepoint(4),XS(N);
"comment" The program now sets up the temperatures and compositions
for which calculations will be performed. The following instruction
must be changed to change these temperatures;
"for"TEMP:=1"do"
"begin""read"KFA,OMEGAA,BETA;
"print" ''L'KFA=',sameline,freepoint(4),KFA,''S2'OMEGAA=',OMEGAA,
        ''S2'BETA=',BETA,''S2'TEMPERATURE=',TEMP;
"for"D:=1"step"1"until"U"do""begin""for"G:=1"step"1"until"V"do"
     "begin"ALPHA:=ALZERO+(D-1)*DELPHA;
            BETAR:=BEZERO+(G-1)*DELBETA;
            PI:=3·14159;
"comment" The next instruction must be changed to change compositions;
            "for"K:=1"step"1"until"10"do"
            "begin"CA(K):=1-0·1*(K-1); CB(K):=1-CA(K);
            OMEGAF(K):=3*PI*PI*(CA(K)/KFA↑3+CB(K)/KFB↑3);
            OMEGAI(K):=CA(K)*OMEGAA+CB(K)*OMEGAB;
            VAL:=(CA(K)*OMEGAA*KFA↑3+CB(K)*OMEGAB*KFB↑3)/(3*PI*PI);
            KF:=(3*PI*PI/OMEGAF(K))↑(1/3);
            WI:=0·31831/KF;  KINT:=ENTIER(10*(KF+0·0001));
            "print" ''L4'CA=',sameline,freepoint(4),CA(K),''S2'KF=',KF;
            RCA:=RCAZERO*(1-ALPHA*(KF*KF-KFA*KFA)/(KFA*KFA));
            RCB:=RCBZERO*(1-BETAR*(KF*KF-KFB*KFB)/(KFB*KFB));
            GAMMA:=1;  TERMA:=0;
            "for"N:=1"step"1"until"NMAX(1)"do"
            "begin"GAMMA:=GAMMA-(1/(4*PI))*XS(N)*BLL(N,0,KF,1);
                   BLK(N):=BLL(N,0,KF,1);
            "for"L:=0"step"1"until"LMAX(1,N)"do"
            TERMA:=TERMA+((2*L+1)/(4*PI))*BLL(N,L,KF,1)↑2;
            "end";
            TERMB:=0;
            "for"N:=1"step"1"until"NMAX(2)"do"
            "begin""for"L:=0"step"1"until"LMAX(2,N)"do"
            TERMB:=TERMB+((2*L+1)/(4*PI))*BLL(N,L,KF,2)↑2;
            "end";
            BETA(K):=1-(CA(K)*TERMA+CB(K)*TERMB)/OMEGAI(K);
            OPW(K):=GAMMA*GAMMA/BETA(K);
  "print"''L' GAMMA= ',sameline,freepoint(4),GAMMA,''S2' BETA= ',
  BETA(K),''S2' OPW= ',OPW(K);
            IS:=1;
```

```
                PD:=0;
                H(1):=H(10):=0·05;H(2):=H(9):=0·025;H(3):=H(8):=0·01;
                H(4):=H(7):=0·00475;H(5):=H(6):=0·00045;H(11):=0·10;
                AJ(1):=0·05;AJ(2):=0·5;AJ(3):=0·9;AJ(4):=0·98;
                AJ(5):=0·999;AJ(6):=1·0001;AJ(7):=1·001;AJ(8):=1·02;
                AJ(9):=1·40;AJ(10):=2·50;AJ(11):=3·40;
                NJ(1):=9;NJ(2):=16;NJ(3):=8;NJ(4):=NJ(7):=4;
                NJ(5):=NJ(6):=2;NJ(8):=38;NJ(9):=44;NJ(10):=18;NJ(11):=26;
        "comment" Program now enters Q-loop.Integration mesh finest
        close to singularity(Q=2*KF);
        "for"T:=1"step"1"until"11"do"
        "begin" NJ1:=NJ(T)+1;   H3:=H(T)/3;
                "for"M:=1"step"1"until"NJ1"do"
                "begin"X:=AJ(T)+(M-1)*H(T);
                        Q:=X*2*KF;QRA:=Q*RCA;QRB:=Q*RCB;
                        SIG:=((16*PI*BETA*VAL)↑(1/3))/KF;
                        STR:=S(Q*SIG,BETA)-1;
                        FL:=LN(ABS((1-X)/(1+X))); XFL:=X*FL;
                        RB:=RC:=0;
                        "for"N:=1"step"1"until"NMAX(1)"do"
                        "begin"RB:=RB+XS(N)*BLK(N);RC:=RC+XS(N)*CO(N);
                        "end";
                CAPGAM:=(XFL*(1-(1/(4*PI))*RB)-(1/(4*PI))*RC)/GAMMA;
                VA:=V(QRA);VB:=V(QRB); GS:=2*CAPGAM*VA;
                GD:=2*CAPGAM*(CA(K)*STR*VA+CB(K)*STR*VB);
                "comment" Integration of self and distinct term integrands
                over Q will now be done using Simpsons Rule;
                "if"M=1"then""goto" FIRST AND LAST;
                "if"M=NJ1"then""goto" FIRST AND LAST;
                "if"M-ENTIER(M/2)*2=0"then""goto"EVEN "else""goto" ODD;
                FIRST AND LAST: PS:=PS+H3*GS; PD:=PD+H3*GD;
                PST:=PS; PDT:=PD; "goto" EXIT;
                EVEN: PS:=PS+4*H3*GS; PD:=PD+4*H3*GD; "goto" EXIT;
                ODD: PS:=PS+2*H3*GS; PD:=PD+2*H3*GD;
                EXIT: PT(K):=PST+PDT;
                "end";  "if"QRA>5·2"and"QRB>5·2 "then""goto" CONTINUE;
        "end";  CONTINUE: DENS:=OFW(K)*PT(K); PT:=DENS/OMEGAI(K);
"print" ''L'ALPHA=',sameline,freepoint(5),ALPHA,''S2'BETAR=',BETAR,''S2'RCA=',
RCA,''S2'RCB=',RCB,''L'SELF TERM=',sameline,freepoint(5),PST,''S2'DISTINCT
TERM=',PDT,''S2'TOTAL TERM=',PT(K),''S2'DENS=',DENS;
                "end" of K-LOOP;
                "end"; "end"; "end";
"end"of program;
```